Mathematical Analysis of Blood Microcirculation with Solute Dispersion and Heat Transfer Aspects

THESIS

Submitted in partial fulfilment of the requirements for the degree of

DOCTOR OF PHILOSOPHY

by

SHAH PALLAV DHANENDRAKUMAR

Under the Supervision of

DR. ASHISH TIWARI

BITS Pilani
Pilani | Dubai | Goa | Hyderabad | Mumbai

BIRLA INSTITUTE OF TECHNOLOGY AND SCIENCE,
PILANI-333031 (RAJASTHAN) INDIA

2023

BIRLA INSTITUTE OF TECHNOLOGY & SCIENCE, PILANI

CERTIFICATE

This is to certify that the thesis titled **"Mathematical Analysis of Blood Microcirculation with Solute Dispersion and Heat Transfer Aspects"** submitted by **Mr. Shah Pallav Dhanendrakumar**, ID No. **2018PHXF0025P** for the award of Ph.D. of the institute embodies original work done by him under my supervision.

Signature of the Supervisor
Name: **DR. ASHISH TIWARI**
Designation: **Associate Professor**

Date: **20 November 2023**

Dedicated

To

My Beloved Family

Acknowledgements

Undertaking this research and writing a thesis has been challenging yet rewarding. I have been fortunate enough to receive support and encouragement from numerous people, without whom this accomplishment would not have been possible. The collective efforts of these individuals have been pivotal in shaping the direction and scope of this work, and I am indebted to their generosity and unwavering commitment to my success.

I am incredibly honored to extend my deepest gratitude to my esteemed supervisor, Dr. Ashish Tiwari, whose invaluable guidance, profound wisdom, and steadfast support have been the driving force behind the realization of this work. His mentorship have been fundamental to this work, providing me with the tools, knowledge, and motivation needed to navigate the complexities of this research journey with greater clarity and purpose. I am genuinely grateful for the depth of his expertise and his unwavering commitment to my intellectual growth as a researcher. I will always be indebted for his invaluable contributions to my research journey.

I would like to express my heartfelt thanks to the members of my Doctoral Advisory Committee (DAC), Prof. Devendra Kumar and Prof. Bhupendra kumar Sharma, for their willingness to lend their expertise and knowledge to this research. Their thoughtful and constructive feedback has helped refine my ideas, sharpen my focus, and develop my analytical skills.

I am obliged to Prof. Balram Dubey, Prof. Bhupendra Kumar Sharma (Ex. HoDs) and Prof. Devendra Kumar, HoD, Department of Mathematics for their humble guidance and support. I would like to acknowledge all the faculty members and research scholars for their valuable support and cooperation during my research work. The memories and friendships that have been established hold a significant place in my heart and will be valued indefinitely. I express my gratitude for your significant contribution to my academic journey.

I would like to thank the Vice-Chancellor, Director, Dean Academic (AGSRD), and Registrar of BITS Pilani for providing me an opportunity to achieve a challenging position in the respective field pertinent to my qualification, which allowed me to use my skills to prove myself worthy.

I express my deepest gratitude to my senior, Dr. Satyendra Singh Chauhan, for his invaluable guidance, encouragement, and advice. I have learned so much from your experiences, expertise, and perspectives, and I am grateful for the time and effort you have devoted to my development. Your willingness to share your knowledge and insights has been a source of inspiration and motivation. On the other hand, my junior fellows (Amit

Saini, Yogesh Kuntal, and Neelima Ghiya) have brought new perspectives and energy to our research discussions, inspiring me to keep pushing the boundaries of my research. I am truly fortunate to have had the opportunity to work with such talented and dedicated individuals, and I am grateful for their support and encouragement.

I would like to extend my gratitude towards Late Dr. S.J. Bhatt, Dr. A.B. Patel, Dr. P.A. Dabhi, Dr. Manish Pandey, Dr. Rakshit Upadhyay, Dr. Savan Patel and Dr. Reshma Sanjhira for their motivation and invaluable support in the beginning of this journey.

I feel incredibly privileged to have friendship of Deepak, Sugandha, Barkha, Komal Deswal, Shivani, Geetika, Sonali, Satpal, Himanshu, Parveen, Komal Bansal, Meghna, Sandeep Bhaisahab, Chandan, Amit and Pritam. I am grateful to you all for having chai pe charcha and creating the lighthearted card cartel. You have created a space where we can unwind, share stories and support each other. Your friendship has added immense joy and warmth to my days, and I am truly grateful for the valuable time we have spent together. I would also like to thank Kapil, Ankit, Umesh, Sanjeev, Gaurav, Mahendra, Yogesh, Shilpa, Sarita, Sonu, and Swati for becoming great colleagues and friends.

I am immensely grateful to my parents (Dhanendrakumar Shah and Shilpa Shah), my brother (Dr. Jainam Shah) and friends (Dr. Rakshit Upadhyay and Dr. Darshna). Their belief in me has been a driving force behind my accomplishments. Completing this work would not have been possible without my beloved wife, Vin's steadfast support, patience, and understanding. Her constant support, affection, and faith in me have been my greatest sources of strength during this challenging journey.

I am indebted to the many individuals who have contributed to this work in various ways. I extend my sincere gratitude to all those who have supported and accompanied me throughout this remarkable endeavor.

Place: BITS Pilani
Date: **20 November 2023**

Shah Pallav Dhanendrakumar
(Department of Mathematics)

"Every new body of discovery is mathematical in form, because there is no other guidance we can have."

- Charles Darwin

Abstract

Blood microcirculation is a crucial process which is vital for oxygenation of tissues and healthy functioning of the cardiovascular system. Maintaining organs' healthy functioning depends on the efficient intricate system of microvessels responsible for transporting oxygen and nutrients to tissues while simultaneously collecting waste. Therefore, it is essential to investigate and understand the mechanisms regulating microcirculation to discover new treatments and improve clinical outcomes. Recent developments in imaging technology allowed to capture exquisitely detailed pictures of microvascular blood flow. However, it can be difficult to interpret these pictures and extract quantitative data on blood flow velocity, flow rate, and other critical characteristics. To better diagnose and track the progress of microcirculatory disorders, quantitative data can be extracted through mathematical analysis. Researchers can simulate many scenarios using mathematical models to determine the most important factors affecting blood flow. The potential of the mathematical study of blood microcirculation through microvessels to improve our knowledge of complicated physiological processes and disease states has gained significant attention in recent years. Mathematical models can also be used to simulate the effects of various drugs on microcirculation and identify the most effective treatment strategies. The limits of existing diagnostic and treatment methods can be uncovered by mathematical analysis, which can inspire the discovery of more effective treatments. The potential applications of this field of research are vast and far-reaching, making it an area of significant interest and importance to researchers and clinicians alike.

The thesis is aimed at investigating the blood microcirculation through suitable mathematical approach and structured into seven chapters, each serving a specific purpose. **Chapter 1** provides an introduction to the research topic of blood microcirculation in the human cardiovascular system. It begins by highlighting the need to study blood microcirculation, as it is critical in maintaining tissue oxygenation and overall cardiovascular health. The next section of the chapter conducts a thorough literature survey to recognize research gaps that should be addressed. This method ensures that the research is well-focused and relevant by establishing clear research objectives for the proposed study. The methodology is discussed in detail to help readers understand the approach that will be followed. Chapter 1 set the foundation for the research by establishing the need for studying blood microcirculation, identifying research gaps, establishing research objectives, outlining the research methodology, and introducing fundamental concepts critical for understanding the research findings.

The microcirculation through microvessels separates the blood into a core fluid rich in

erythrocytes surrounded by plasma fluid devoid of cells. Throughout the thesis, the two-fluid model has been employed to depict blood flow in microvessels accurately. **Chapters 2 and 3** represent the cell-free plasma layer as a Newtonian fluid and the core fluid as a micropolar fluid in which blood particles like RBCs, WBCs, and platelets are suspended, respectively, to account for the micro-structure of erythrocytes. In addition, the thixotropic behavior of blood is investigated by modeling it as a two-fluid, having a Newtonian fluid with constant viscosity modeling the plasma surrounding and the central region having a viscoelastic Herschel-Bulkley fluid with variable viscosity throughout **Chapters 4-6**.

The objective of **Chapter 2** is to examine the influence of the microrotation of erythrocytes, external magnatic field and heat transfer on mechanical quantities of blood microcirculation through the microvessel with thin endothelial glycocalyx-layered microvessels. A Brinkman formulation governs the flow through the thin glycocalyx layer adjacent to the microvessel wall. The heat transfer through EGL and its applications to physiological aspects have also been studied. The equations governing the various flow characteristics are solved analytically. In addition, Fåhræus effect and hematocrit have been investigated. Two boundary conditions have been formulated, representing the termination of erythrocyte spin and no occurrence of couple stress at the micropolar-plasma interface. Compared to the no-spin condition, the relatively strong influence of the no-couple stress condition on Fåhræus effect, flow characteristics, and hematocrit has been observed. Graphical interpretations of the different parametric influences on blood microcirculation have been studied with both boundary conditions.

Chapter 3 considers blood microcirculation under the identical scenario of Chapter 2 with absorbing vessel walls and aims to extend the study to examine the mechanism of the solute dispersion phenomenon. A jump in stress is witnessed at the plasma fluid-EGL interface, which is depicted as an interfacial condition derived by Ochoa-Tapia and Whitaker [1]. Sankarasubramanian and Gill's [2] approach has been employed to acquire asymptotic expressions for the solute dispersion coefficients and mean concentration with the help of analytical temperature and velocity profile. To comprehend certain clinical features of blood microcirculation, the effect of erythrocyte spinning, coupling number, EGL thickness and permeability, thermal conductivity, radiation parameter, and Hartmann number on the solute dispersion coefficients and mean concentration interpreted graphically.

A theoretical attempt has been made in **Chapter 4** to examine the impact of the heat transfer aspect on the flow characteristics of temperature-dependent viscous blood microcirculation through endothelial glycocalyx layered microvessels. The velocity profile through the core of the microvessel is obtained analytically with a linear approximation of the Reynolds viscosity model. The Brinkman-Forchheimer equation governs blood flow through

the endothelium glycocalyx layer to encompass the permeability spectrum. The perturbation technique is employed to solve the Brinkman-Forchheimer governing equation analytically. Singular and regular perturbation problems are encountered for small Darcy numbers (SDN) and large Darcy numbers (LDN), respectively. Analytical solutions acquired for hemodynamical characteristics and exercised for the graphical interpretations regarding the simultaneous impact of Forchheimer number, permeability, viscosity, Grashof number, thermal conductivity, and Richardson number have been discussed in detail. The study observed the addition in resistance proportional to the thickness of the EGL adjacent to the microvessel wall. The study concludes the impact of temperature on flow characteristics and comprehends the importance of studying temperature-dependent viscosity models for devising clinical procedures involving temperature variations.

Delivering drugs to the targeted location or transporting nutrients to needy organs involves the dispersion of solutes through blood microcirculation. The process is believed to be influenced by the varying characteristics of viscosity, heat transfer, and other related factors. The change in temperature during clinical procedures can affect blood viscosity; hence, examining its impact on the drug deliverance process becomes intriguing. **Chapter 5** is motivated toward examining the dispersion of solutes in blood microcirculation through microvessels influenced by temperature-sensitive viscosity and heat transfer. Sankarasubramanian and Gill [2] procedure is exercised to derive asymptotic expressions for coefficients of diffusion and mean concentration influenced by heat transfer and temperature-sensitive viscosity. The fluid model is reduced to its specific cases to validate obtained results regarding the solute dispersion process influenced by temperature-sensitive viscosity. In addition, the dispersion process is accelerated with the dominance of thermal buoyancy forces. The graphical analysis shed light on the solute dispersion process's sensitivity regarding heat transfer and temperature-sensitive viscosity.

The focus of **Chapter 6** is to study the hydrodynamic characteristics of blood microcirculation through a microvessel having EGL adjacent to the absorbing wall with a sophisticated mathematical model. The endothelial glycocalyx layer affects the hydrodynamical properties of plasma in microcirculation due to the absorption of plasma proteins and carbohydrate accumulation ([3], [4]). The equations governing the mathematical model delineating blood microcirculation through microvessel having EGL adjacent to the absorbing wall. Sankarasubramanian and Gill [2] procedure is exercised to obtain asymptotically solve the solute dispersion process. A comparison has been drawn between the generalized model and its reduced specific fluid models for the solute dispersion process. The graphical study interprets the sensitivity of the solute dispersion coefficients regarding EGL thickness, EGL

porosity, plasma layer thickness, and wall absorbing capacity. EGL adjacent to the microvessel wall decreases both convective and axial dispersion in the case of a wall with high reactivity. One notable observation is that a decrease in the porosity of EGL adjacent to the microvessel wall leads to a decrease in the average solute concentration.

Chapter 7 serves as a critical component of the thesis by comprehensively summarizing the key research findings, highlighting the most noteworthy results with physical significance and practical applications. This chapter aims to offer readers a clear and concise understanding of the research, drawing attention to the most relevant and essential aspects. By identifying the research's strengths and weaknesses, readers can better understand the reliability and validity of the findings. By outlining potential challenges and opportunities for further development, the chapter provides a road map for future scope and improvements to the completed research work. By synthesizing all this information in one place, the chapter helps to ensure that the research can be effectively translated into practical applications and future research.

Contents

List of Figures

List of Tables

List of Abbreviations

BCs	Boundary Conditions
BP	Bingham Plastic Fluid
BVP	Boundary value problem
HB	Herschel-Bulkley Fluid
IC	Initial Condition
IVP	Initial Value problems
LDN	Large Darcy number
NCS	No-couple stress condition
NF	Newtonian Fluid
NS	No-spin condition
PL	Power-Law Fluid
PW	Porous region near the vessel Walls
SDN	Small Darcy number
SFM	Single-Fluid Model
TFM	Two-Fluid Model

List of Symbols

$\sim$	Symbolize dimensional quantities
r	Transverse (radial) coordinate
z	Longitudal (axial) coordinate
t	Time coordinate
h_1	Core region thickness
h	Peripheral region thickness
R_1, R_2, R_3	Tube radius in core, Plasma and porous regions, respectively
R_p	Radius of plug core region
w_H	Axial velocity of Herschel-Bulkley fluid in core
w_p	Axial velocity of the fluid in plug core region
w_M	Axial velocity of micro-polar fluid in core
w_N	Axial velocity of Newtonian fluid in plasma region
w_B	Axial velocity in porous region
W_0	Characteristic velocity
n	Fluid behavior parameter (Microscale parameter for Micropolar fluid and power law index for Herschel-Bulkley fluid)
p_H, p_N, p_B	Pressures in core, plasma and porous regions, respectively
p_s	Pressure gradient
q_0	Characteristic pressure gradient
T_H, T_N, T_B	Temperatures in core, plasma and porous regions, respectively
K_H, K_N	Thermal conductivities
K_0	Thermal conductivity ratio
Q_H, Q_N	Constant heat absorptions
Q_s	Rate of fluid flow (volumetric flow rate)
T_w, T_∞	Temperature at wall and ambient temperature, respectively
Gr	Grashof number (free convection parameter)
Re	Reynolds number
Ri	Richardson number (i.e., $Ri = Gr/Re^2$)

F	Forchheimer number
S	Dimensionless parameter defined in Eq.
C_F	Inertial coefficient
k	Permeability of the porous medium (i.e., Darcy number Da)
g	Gravitational force
B	Magnetic field
W	Average (mean) velocity of the fluid
N	Coupling parameter
N_1	Radiation parameter
H	Hartmann number
H_1^2	Magnetic number
Ht	Hematocrit
Fe	Fahraeus effect
H_T	Tube hematocrit
H_D	Discharge hematocrit
K	Viscosity parameter
m	Varying viscosity index
W_{rbc}	Velocity of RBCs
$C_v(r)$	Concentration profile
c_v	Constant in concentration relation
C	Concentration of the solute
C_0	Initial concentration of the solute
C_M	Mean concentration of the solute
J_0, J_1	Bessel functions of order zero and one, respectively
M_0, M_1, M_2	Exchange, convective and axial dispersion coefficients, respectively
Pe	Peclet number
D_m	Constant molecular diffusivity
d	Radius of initial solute distribution
Region- I	Core region $(0 < r \leq R_1)$
Region- II	Plasma region $(R_1 \leq r \leq R_2)$
Region- III	Porous region $(R_2 \leq r \leq 1)$

Greeks letters

ϕ	Azimuthal angle
α	Viscosity index
α_p	Porosity parameter
τ_H	Shear stress of Herschel-Bulkley fluid

τ_N	Shear stress of Newtonian fluid
τ_y	Yield stress
Θ	Dimensionless yield stress
θ	Dimensionless temperature
$\theta_M, \theta_H, \theta_N, \theta_B$	Temperatures in core, plasma and porous regions, respectively
ρ_M, ρ_H, ρ_N	Density of Herschel-Bulkley and Newtonian fluids, respectively
ρ_0	Density ratio
γ_1, γ_2	Mean absorption coefficients
γ_0	Mean absorption coefficients ratio
γ	Coefficient of the volume expansion due to the temperature
τ_w	Shear stress at wall
$\mu(\theta_H)$	Variable viscosity of core fluid
μ_M, μ_H, μ_N	Constant viscosity coefficients of Micro-polar , Herschel-Bulkley and Newtonian fluid, respectively
μ_E	Effective viscosity of the porous medium
λ_1	Viscosity ratio parameter ($\lambda_1^2 = \widetilde{\mu}_E/\widetilde{\mu}_N$)
λ_s	Flow resistance (impedance)
β	Wall absorption parameter
β_S	Stress-jump parameter
δ	Dirac delta function
δ_{ij}	Kronecker delta function
ξ	Variable defined in Eq.
Ω_M	Angular velocity
α_M, α_N	Mean radiation absorption coefficients of micropolar and Newtonian fluids, respectively
σ_M, σ_N	Electrical conductivities of micropolar and Newtonian fluids, respectively
σ_0	Ratio of electrical conductivities
Γ	Material constant
α_k	Roots of transcendental Eq.
κ_M	Rotational viscosity
ϕ_M	Parameter (couple stress)
μ_R	Viscosity ratio (i.e. $\widetilde{\mu}_N/\widetilde{\mu}_M$)

Subscripts

H	Symbolizes for Herschel-Bulkley fluid (for $w_H, \theta_H, \tau_H, Q_H, K_H, \mu_H, \rho_H, p_H$)
M	Micropolar fluid in velocity profile (for $w_M, \theta_M, \tau_M, \alpha_M, K_M, \mu_M, \rho_M, p_M$)

	and mean concentration for concentration profile (for C_M)
N	Symbolizes for Newtonian fluid (for $w_N, \theta_N, Q_N, K_N, \mu_N, \rho_N, p_N$)
E	Effective coefficient of Brinkman region (for μ_E)
B	Symbolizes for porous region (for w_B, p_B)
S	Stress-jump parameter (for β_S)
p	Plug flow value (for w_p, R_p)
s	Steady flow value (for p_s, Q_s, λ_s)
w	Value at vessel wall (for τ_w, T_w)
y	Value at yield stress (for τ_y)

Chapter 1

Introduction

The cardiovascular diseases triggered by an abnormal blood circulation in arteries account for the majority of untimely deaths in developed countries. The improvement in such scenario requires a deep understanding of blood circulation in human cardiovascular system for advancement of clinical diagnosis and treatment procedures.

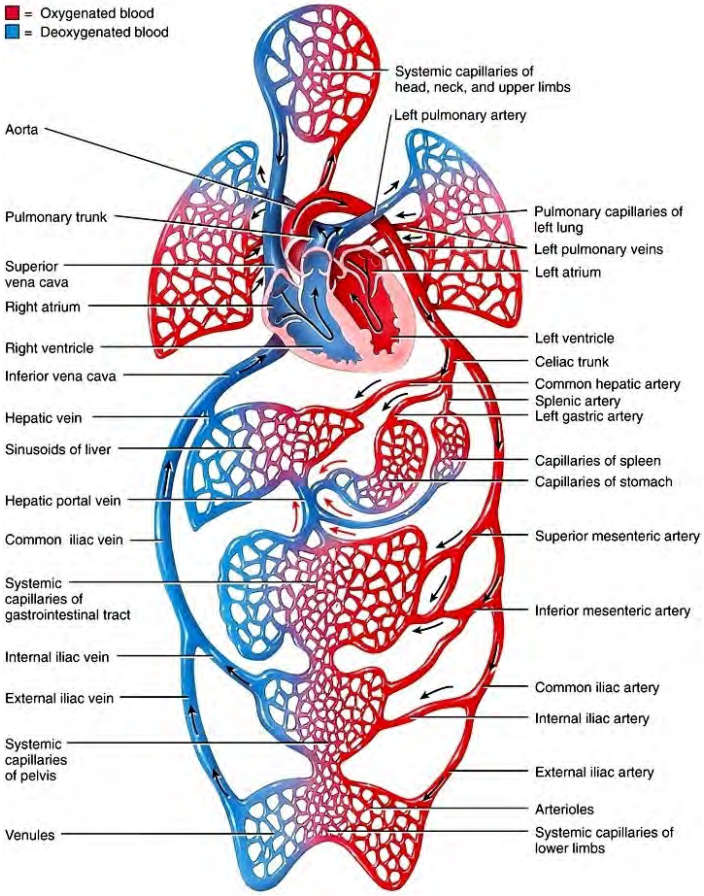

Figure 1.1: Systematic Blood Circulatory Route [5]

The systematic conception of blood circulation in the human cardiovascular system based on evidence provided by William Harvey, opens the window of opportunity for future scholars to study modern physiology. Blood travels through a systematic circulatory route as shown in Figure 1.1 and reach to specific organs in the body [5]. While in circulation through capillary bed, blood performs two essential operations of transport and exchange. Each cell of the human body has particular immunological and nutritional requirements, which are taken care by blood in continuous motion.

The capillary bed (Figure 1.2:(a)) is a unique interweaving structure of microvessels (capillaries) being $200 \pm 250\ \mu m$ long and having a diameter of $8\mu m$ to $10\mu m$ (Figure 1.2:(b)). At the capillary

bed, the cells attain direct access to blood. Throughout the body, capillaries function as part of a capillary bed, a network of 10–100 capillaries. Thin-walled exchange microvessels, known as capillaries (Figure 1.2:(c)), primarily facilitate the exchange of substances between the blood and interstitial fluid. Throughout the body, capillaries function as part of a capillary bed, a network of 10–100 capillaries. Capillaries are present close to nearly all cells throughout the body, although their density depends upon the metabolic demands of the specific tissue they supply. Tissues with high metabolic demands, such as muscles, the brain, the liver, the kidneys, and the nervous system, possess abundant capillary networks to facilitate the delivery of oxygen and nutrients (Figure 1.2:(d)). Compared to the diameter of red blood cells, the diameter of such microvessels is either smaller or approximately equal.

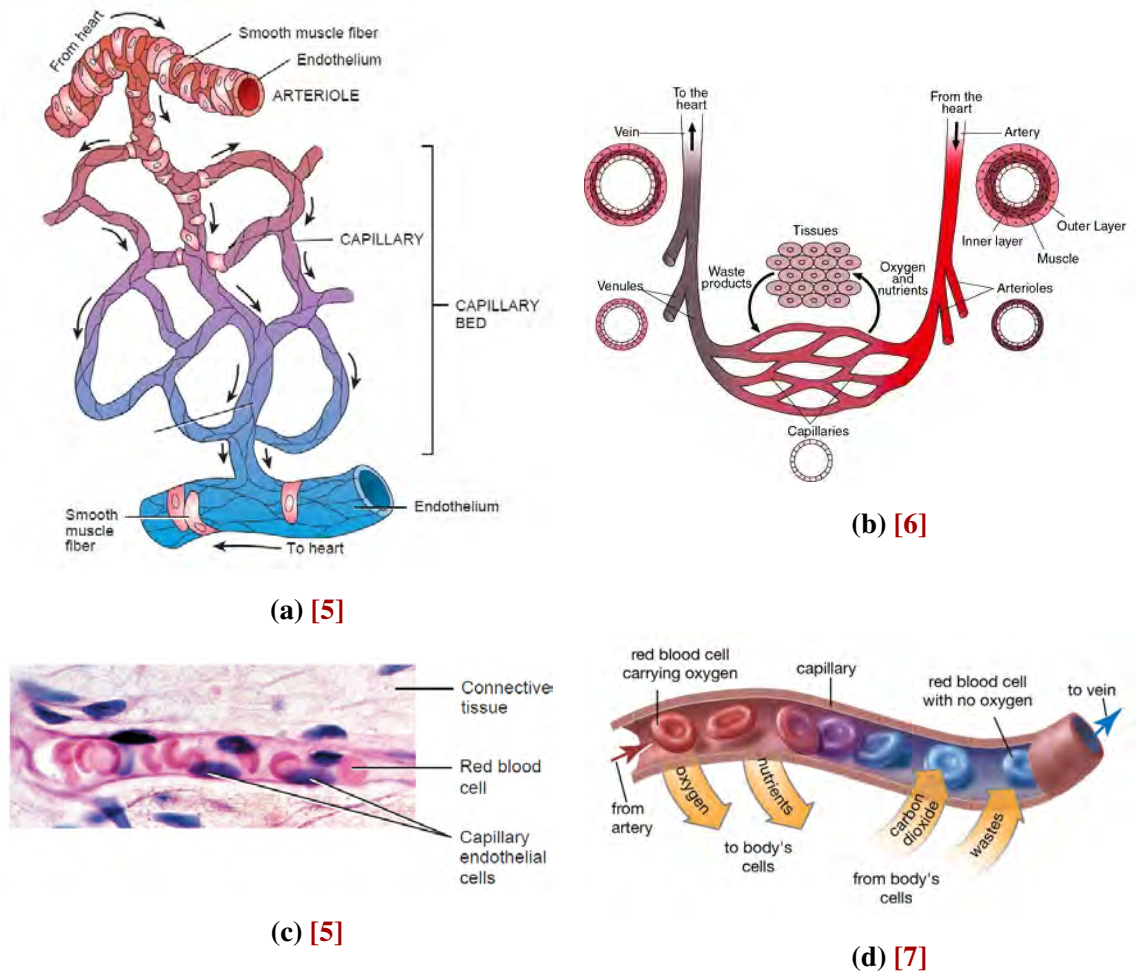

(a) [5] **(b)** [6]

(c) [5] **(d)** [7]

Figure 1.2: Blood microcirculation (a) Capillary bed, (b) Diameter of capillary, (c)Red blood cells passing through capillaries and (e) Oxygen transport phenomena in capillary

Vital organs of the human body, like the brain, lungs, and kidneys, are equipped with a highly dense network of microvessels to deal with the tremendous requirement of nutrient exchange. Therefore, studying the mechanical aspects of micro-circulation in microvessels

is of immense importance to understanding the mechanism of life-threatening diseases and inventing or improving the clinical diagnosis and treatment procedure.

The branch of fluid dynamics examining the mechanical aspect of physiological flow is known as bio-mechanics. Bio-mechanics can empower researchers with laws of physics to express the fluid flow in terms of a mathematical expressions and the effects of mechanical parameters on the behaviour of fluid flow could be analyzed through these expressions. In mathematics, there are customarily two approaches namely analytical and numerical to solve a problem governing the real life phenomenon. The solution gained through analytical approach is exact and guarantee the accurate prediction regarding qualitative behaviour of real life phenomenon in contrast to the solution achieved through numerical approach. However, in practice numerical techniques are exercised for practical purposes as most of the time to get analytical solution is either impossible or quite difficult. In 1828, Jean Poiseuille's work [8] marked the beginning of the study of mechanics of the blood flow and contributed to the circulation through small vessels. Blood circulation through microvessels is termed by Fung [9] as micro-circulation. The current chapter accommodates the documentation of required concepts with a detailed literature review to identify the gap in existing research work, establish objectives for the proposed work and devise a methodology to achieve established objectives.

1.1 The Microcirculation

1.1.1 Blood Components in Microcirculation

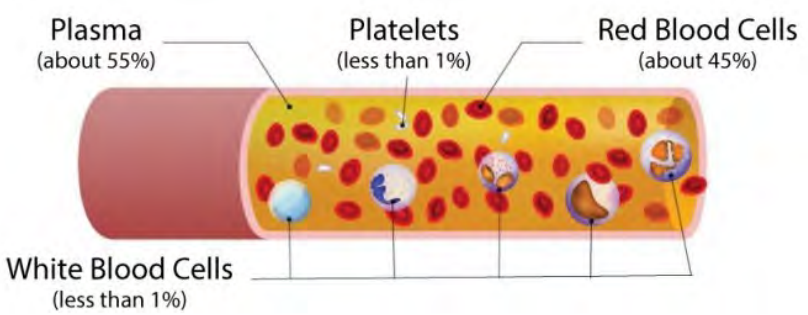

Figure 1.3: Blood Components [10]

The term "microcirculation" describes the process by which the body's tissues receive and release oxygen, nutrients, and wastes via the body's tiny blood vessels (such as arterioles, capillaries, and venules). Several different components of microcirculatory blood are responsible for keeping tissues healthy and functioning correctly.

1. The most numerous blood cells, which are about 99% of the cellular components of blood, known as red blood cells (RBCs), transport oxygen from the lungs to the body's tissues and remove carbon dioxide. About $40-45\%$ of the total blood volume comprises RBCs. In the microcirculation, the proportion of RBCs may be slightly lower due to their larger size than other blood components, making it difficult for them to pass through narrow capillaries. RBCs must be highly deformable to pass through the tight confines of microcapillaries on their way to the tissues. RBCs emit vasodilators and vasoconstrictors, which help to control blood flow and blood pressure, respectively.

2. White blood cells (WBCs) are part of the immune system and defend the body against infections and foreign substances. WBCs comprise a small percentage of the total blood volume, typically less than 1%. WBCs can move through the walls of blood vessels and into surrounding tissues to fight infections.

3. Platelets, which are cellular fragments in the form of a disc, contribute to blood coagulation. Platelets are also present in small numbers in the microcirculation, typically less than 1% of the total blood volume. They can bind to injured blood vessel walls in the microcirculation and secrete clotting factors to avoid excessive bleeding.

4. Plasma, the blood's liquid component containing the remaining 1% of the cellular components, comprises proteins, electrolytes, hormones, and nutrients. Plasma aids in the transportation of nutrients, waste materials, and other substances throughout the body and plays a part in regulating blood pressure and pH balance. Plasma comprises approximately $55-60\%$ of the total blood volume.

Vasoactive chemicals like nitric oxide and endothelin are released, and smooth muscle cells in the walls of arterioles contract and relax to control blood flow in the microcirculation. Red blood cells (RBCs) can influence blood flow via rheological factors, including viscosity and shear stress. The microcirculation system relies heavily on the blood and its many components to function and stay healthy.

1.1.2 Structure of Microvessels in Microcirculation

Microcirculation includes small blood vessels such as arterioles, capillaries, and venules, which have distinct structural features that allow them to perform their specialized functions in exchanging gases, nutrients, and waste products between the blood and surrounding tissues. Here is a brief description of the structure of these microvessels:

1.1.2.1 Arterioles

Arterioles are small blood vessels that connect larger arteries to capillaries. They have a muscular wall composed of smooth muscle cells, which can contract or relax to regulate blood flow to the capillaries. Arterioles also have a layer of endothelial cells lining their inner surface, which provides a barrier between blood and the surrounding tissue.

1.1.2.2 Capillaries

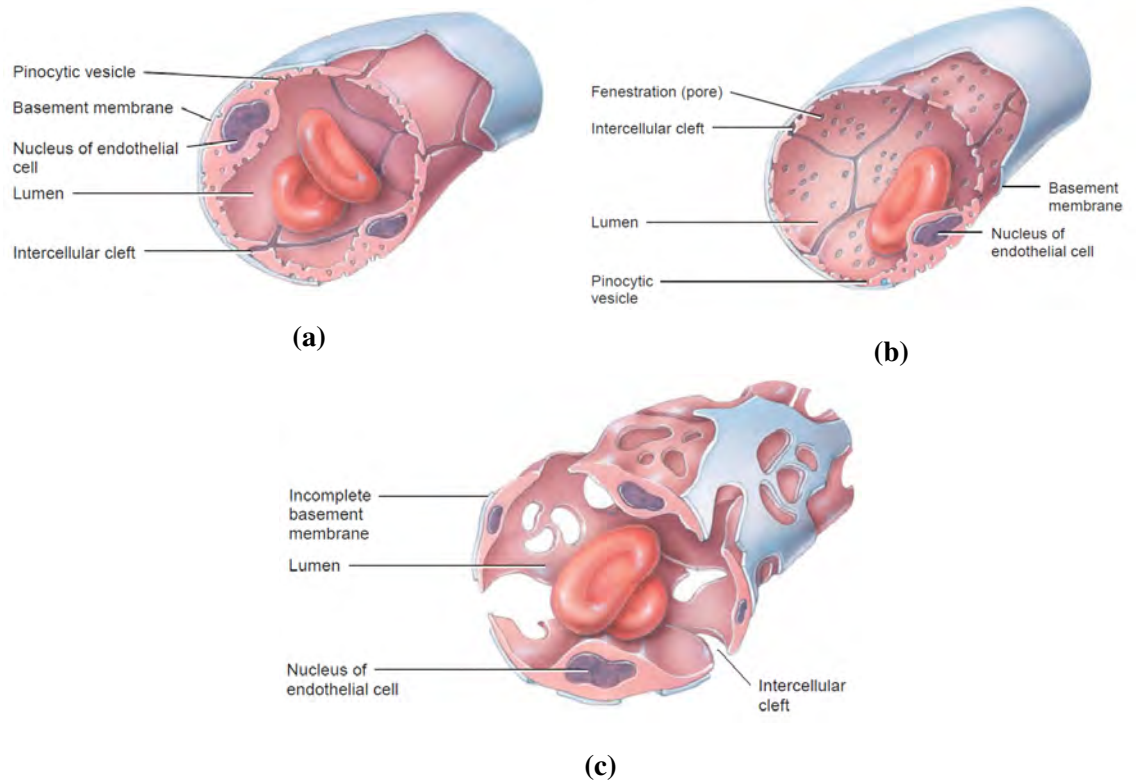

Figure 1.4: Capillary structure and types **(a)** Continuous **(b)** Fenestrated **(c)** Sinusoid. [5]

Capillaries are the smallest and most numerous blood vessels in the body. They consist of a single layer of endothelial cells, which are highly permeable to gases and nutrients. Capillaries have a very small diameter, typically between $8\mu m$ to $10\mu m$, which allow them to exchange substances with surrounding tissues through diffusion. Some capillaries also have pores or fenestrations in their endothelial layer, which allow larger molecules to pass through.The human body consists of three distinct types of capillaries: continuous capillaries, fenestrated capillaries, and sinusoids. The majority of capillaries present in the brain, lungs, skeletal and smooth muscle, and connective tissues are classified as continuous capillaries. Fenestrated capillaries can be observed within various anatomical structures, choroid

plexuses of the ventricles in the brain, including the kidneys, villi of the small intestine, ciliary processes of the eyes, and endocrine glands. The presence of sinusoids can be observed in the , anterior pituitary, spleen and parathyroid glands. A brief description of the structure of capillaries is discussed here

- Capillaries are composed of a single layer of **endothelial cells**, which line the inner surface of the vessel wall. These cells are flattened and elongated, creating a thin barrier between the blood and surrounding tissues. Endothelial cells are connected by tight junctions, which restrict the movement of larger molecules and cells between the blood and surrounding tissues.
- The endothelial cells are supported by a thin **basement membrane**, which is composed of a meshwork of collagen and glycoproteins. The basement membrane provides mechanical support and helps to maintain the integrity of the capillary wall.
- **Pericytes** are specialized cells that are located in close proximity to the endothelial cells. They wrap around the capillary wall and are thought to play a role in regulating blood flow and capillary permeability. Pericytes can also differentiate into other cell types, such as smooth muscle cells or fibroblasts.
- Small gaps, called **intercellular clefts**, are present between adjacent endothelial cells. These gaps allow for the exchange of small molecules, such as oxygen, carbon dioxide, and nutrients, between the blood and surrounding tissues.

The structure of capillaries is highly responsible to facilitate the exchange of substances between the blood and surrounding tissues. The thin layer of endothelial cells, supported by a basement membrane and pericytes, allows for a high degree of permeability, while tight junctions and intercellular clefts help to regulate the movement of larger molecules and cells.

1.1.2.3 Venules

Venules are small blood vessels that connect capillaries to larger veins. They have a similar structure to arterioles, with a muscular wall composed of smooth muscle cells and a layer of endothelial cells. Venules can also serve as sites for leukocyte migration, as they have a wider diameter than capillaries and a more porous endothelial layer.

Overall, the microvessels involved in microcirculation have distinct structural features that allow them to perform their specialized functions in exchanging substances between the blood and surrounding tissues. Arterioles can regulate blood flow to the capillaries, while

capillaries provide a highly permeable barrier for exchange, and venules serve as a site for leukocyte migration.

1.2 The Mechanical Aspects of Microcirculation

The long-neglected field of the mechanics of microcirculation has, in the last few years, begun to be subjected to more rigorous analysis through the application of the unifying principles of physics. To examine the mechanism of microcirculation, one must know the mechanical aspects affecting it. Some significant aspects are noted here.

(a) The micro structure of blood components affecting circulation and the adequate way to accommodate these interference in a mathematical frame work.

(b) The porous structure of permeable microvessel wall catering the transport and exchange process.

(c) The resistance or assistance provided through external factors such as radiation and magnetic field.

(d) The examination of solute dispersion process in microcirculation.

In order to examine the mechanism of microcirculation of blood, one must consider the blood as a fluid either Newtonian or non-Newtonian.

1.2.1 Newtonian Fluid

When the shear rates reach approximately 100/sec and the arteries are larger than 1 mm in diameter, blood demonstrates the characteristics of a Newtonian fluid, where the viscosity coefficient represents the constant proportionality between the strain rate and shear stress. Newtonian fluids are those that abide by Newton's law of viscosity, which can be mathematically expressed by stating that shear stress remains constantly proportional in relation to the strain rate.

$$\widetilde{\tau}_N = \widetilde{\mu}_N \frac{\partial \widetilde{w}_N}{\partial \widetilde{r}}, \tag{1.1}$$

where $\widetilde{\tau}_N$, $\widetilde{w}_N$, $\widetilde{\mu}_N$, $\frac{\partial \widetilde{w}_N}{\partial \widetilde{r}}$ denotes the shear stress, axial velocity, viscosity coefficient, and strain rate of unidirectional Newtonian fluid flow in a tube, respectively.

1.2.2 Non-Newtonian Fluid

Non-Newtonian behavior describes that fluid's viscosity and flow behavior is affected by elements other than the shear rate, for example blood's viscosity is affected by the blood's

composition, the presence of cells and proteins, and the features of the blood arteries through which the blood flows. Blood exhibits non-Newtonian behavior at the low shear rates typical of capillaries and other blood channels with diameters below 1 *mm*. This indicates that the shear stress and strain rate are not linearly related. The shear stress is the force per unit area that drives the fluid, and the strain rate is the rate at which the fluid deforms under stress. As the shear rate varies, so does the blood's viscosity.

Additionally, blood is thixotropic, which means its viscosity decreases with time under a constant stress or shear rate. This quality facilitates oxygen and nutrition delivery to tissues via the circulatory system by facilitating blood flow via capillaries and other tiny blood vessels. Blood can also show shear thinning behavior, where its viscosity reduces with an increasing shear rate. The presence of red blood cells, which may align and create structures that decrease flow resistance at high shear rates, is responsible for this behavior.

Research and clinical applications in biomedicine rely heavily on our knowledge of blood's non-Newtonian properties, including designing artificial organs, creating drug delivery devices, and investigating the mechanics of blood flow in conditions like hypertension and thrombosis. Let us take a look at two of the most well-known non-Newtonian fluid models in order to better understand the peculiar behaviour of blood.

1.2.2.1 Micropolar Fluid

In our circulatory system, blood is a composition of erythrocytes and plasma with nutrients and other fiber tissues, so the shape and size of the fluid molecules play a vital role in microcirculation through microvessels. The classical Navier-Stokes equations fails to examine the impact of fluid particles' substructure on circulation. Ariman [11] emphasized the inclusion of the deformable structure of blood in the form of microrotation and validated this micropolar model of blood by comparing it with the experimental work of Bugliarello and Hayden [12]. A detailed description of microcontinuum fluids with their applications for real and ideal fluid flow was also provided by him ([13], [14]). Eringen [15] introduced the fundamental theory of simple microfluids with molecules exhibiting micro-rotation, and he derived fluid motion equations governing a new class of viscous microfluids. He [16] extended his work for a class of micropolar fluid, which is a subclass of microfluids, and the molecules of these fluids have micro-motion and spin inertia. The micropolar fluid supports the couple stress and body couples only. Physically the micropolar fluid exhibits the independent rotation of molecules with its local vorticity. The constitutive equation for the motion of the micropolar fluid is derived by Eringen as follows.

$$\nabla \cdot v = 0, \tag{1.2a}$$

$$\rho \dot{v} = \rho F - \nabla p + (\mu_v + \kappa_v)\Delta v + \kappa_v \nabla \times \omega, \tag{1.2b}$$

$$\rho \hat{J} \cdot \dot{\omega} = \rho L + (\alpha + \beta)\nabla\nabla \cdot \omega + \gamma \Delta \omega + \kappa_v \nabla \times v - 2\kappa_v \omega, \tag{1.2c}$$

Burton [17] characterized the blood as a suspension of cells containing hydrocarbon and other molecules. Due to their flexible nature, RBCs can pass through relatively smaller capillaries. Fung [18] analyzed the viscous properties due to the flexible nature of RBCs. Devanathan [19] and Mekheimer [20] utilized the single fluid model of micropolar fluid through circular tubes with and without constrictions to analyze the effect of the microstructure of molecules through fluid flow. Srinivasacharya and Shiferaw [21] investigated the flow of micropolar fluid with hall and ionic effects flowing through a circular pipe under the influence of an external magnetic field of uniform strength. Khanukaeva *et al.* ([22]-[23]) analyzed the flow of micropolar fluid through a membrane with a porous layer using a cell model technique in which the flow is parallel and perpendicular to the axis of the cylindrical cell. Siddheshwar and Manjunath [24] discussed the impact of the shape and size of the fluid particles on the unsteady solute dispersion process in micropolar fluid flow through a tube with heterogeneous chemical reaction.

1.2.2.2 Herschel-Bulkley Fluid

Among the various relations used to characterize the behavior of viscous fluids, the Herschel-Bulkley model, also known as the yield power law model, is particularly useful for describing the behavior of fluids that display yield stress and for which the shear stress tends to behave like a power law at high shear rate. Since it generalizes the Bingham and power-law models, this one is frequently used to characterize the rheological behavior of non-Newtonian fluids [25]. The expression governing the Herschel-Bulkley fluid is given by [26]

$$\widetilde{\tau}_H = \widetilde{\tau}_y + \left[\widetilde{\mu}_H \left(-\frac{\partial \widetilde{w}_H}{\partial \widetilde{r}}\right)\right]^{\frac{1}{n}}, \quad \text{if} \quad \widetilde{\tau}_H > \widetilde{\tau}_y, \tag{1.3a}$$

$$\frac{\partial \widetilde{w}_H}{\partial \widetilde{r}} = 0, \quad \text{if} \quad \widetilde{\tau}_H \leq \widetilde{\tau}_y, \tag{1.3b}$$

where $\widetilde{\tau}_H$, $\widetilde{\tau}_y$, $\widetilde{w}_H$, $\widetilde{\mu}_H$, $\frac{\partial \widetilde{w}_H}{\partial \widetilde{r}}$, n are the shear stress, yield stress, axial velocity, viscosity coefficient, strain rate, and fluid behaviour parameter of Herschel-Bulkley fluid, respectively. Both shear-thinning and shear-thickening fluid behaviours are reflected in the flow by

fluid behaviour parameter n. The Herschel-Bulkley fluid has two parameters: the Herschel-Bulkley fluid behaviour parameter n and the yield-stress $\widetilde{\tau}_y$, and for particular values of these two parameters, the model reduces to the Newtonian and various non-Newtonian models, making it more realistic than other non-Newtonian models.

1.2.3 Two-Fluid Model

With experimental evidence and theoretical study, Bugliarello and Sevilla [27] established the multi-phase nature of blood in microcirculation through microvessels. Blood flow is partitioned into the core fluid exhibiting non-Newtonian behavior due to the suspension of cells (RBCs, WBCs, and platelets) encompassed by a thin layer of cell-free plasma near the microvessel wall. Thus for the realistic situation of the bloodstreams in microvessels, the two-fluid models are found significantly appropriate as it presumes the non-Newtonian behavior for all the erythrocytes occupying the core region of the blood vessels and the surrounding thin layer of plasma near the wall as Newtonian fluid [28].

Adopting blood as a two-fluid model, several studies ([29], [30], [31], [32], [33], [34], [35]) examined the diverse aspect of microcirculation through microvessels with or without constrictions and analyzed the impact of plasma layer thickness, plasma layer viscosity, constriction height, and non-Newtonian nature of blood in core region fluid on hemodynamical quantities such as flow rate and flow impedance. Following the presumptions of the two-fluid model, Debnath *et al.* [36] examined the solute dispersion for the periodic flow of blood through absorbing microvessels. Inspired by the two-fluid model, Rana and Murthy [37] considered blood flow as a flow of Casson fluid in the central region surrounded by a flow of Newtonian fluid in a peripheral region near the boundary and discussed the effect of plasma layer thickness, periodicity, pressure gradient amplitude, Schmidt number and wall reaction on the dispersion process in the circulation of blood through small blood vessels by taking the two-fluid model approach.

1.2.4 Viscosity of Blood

The term "blood viscosity" describes how thick and sticky blood is, which hinders its capacity to flow through blood arteries. The quantity and makeup of various blood components, such as RBCs, WBCs, plasma proteins, and platelets, primarily determine blood viscosity. Red blood cells, the most abundant cells in the blood, play a significant role in blood viscosity. They deliver oxygen to cells and eliminate waste products from the body. Their size and shape affect the fact that how easily red blood cells are carried through blood arteries. When people are healthy, their red blood cells adapt and alter their form to fit through small blood

arteries. However, if there are an excessively high number of red blood cells, as occurs in sickle cell disease, they might clump together and make the blood more viscous.

Blood viscosity is also affected by plasma proteins like fibrinogen and globulins. These proteins function in coagulation and immune system reactions. When present in high concentrations, these proteins can raise blood viscosity and impede the normal flow of blood through the body's blood vessels. Tiny blood cells called platelets are vital to the clotting process. Blood clots are formed when platelets clump together after an injury to a blood artery. Platelets are necessary for clotting, but excess can increase blood viscosity. Dehydration, excessive red blood cells, elevated plasma protein levels, and other diseases and medical situations all contribute to thicker blood. Polycythemia vera is one such condition; it is an uncommon blood ailment with too many red blood cells in the body. People at high risk for cardiovascular disease or stroke should have their blood viscosity monitored regularly. Aspirin and other blood-thinning drugs may be used in conjunction with a healthy diet and regular exercise to treat high blood pressure.

Blood viscosity being a key characteristic, is solely addressed as a function of shear rate in many studies. However, there are a number of additional physical variables impacting blood viscosity that must be taken into account due to the complexity of blood as a whole (consisting of cells, plasma, and other nutrients). Among these factors are hematocrit, body temperature, illness severity, and the RBCs' biological age [26].

1.2.4.1 Variable Nature of Blood Viscosity

Because viscosity is such a significant physical property of the blood, research into its varying nature is essential. According to Lih [38], the temperature, hematocrit, concentration, and vessel width all have a role in determining blood's viscosity. He also noticed that when blood passes through a tube with a smaller diameter and a low shear rate, the blood's viscosity may change. Several writers ([39], [40], [41], [42], [43], [44], [45], [46]) have taken this into account by examining the effect of altering viscosity. They discovered that the variable nature of viscosity is crucial to fluid flow in conduits of decreasing diameter.

Taking into account the blood in the core area as Newtonian or non-Newtonian fluids, numerous authors ([47], [48], [28]) have studied the effect of hematocrit-dependent viscosity on TFM of blood flow through the tube with or without constrictions. Tiwari and Chauhan ([28], [49], [50], [51]) explored the impact of position-dependent viscosity when discussing the TFM of blood flow in blood capillaries with a constriction or a porous patch near the tube wall. They demonstrated that flow variability and hematocrit are both affected by the presence of a glycocalyx layer and the non-constant character of viscosity.

1.2.5 Heat Transfer Aspect

In the modern era, cancer and other malignant tumors have become increasingly common as a result of environmental factors like increased pollution and the widespread use of toxic chemicals, so scientists have been working hard to find a way to eradicate them through a combination of experimental findings and mathematical modeling. In hyperthermia, where heat transport is involved, even a $2^{\circ}C$ or $3^{\circ}C$ temperature difference can profoundly affect the body's internal fluid dynamics. In addition, laser treatment, cryosurgery, and other methods aid in destroying active cancer cells. When body temperature rises, it causes harm to otherwise healthy tissue. Nevertheless, the therapeutic process, including the modest temperature shift, may be helpful in treating ailments like cancer or malignant tumors [44]. Radiation has been produced and directed toward the front lines of the contaminated region via the heat transfer aspect. The treatment's efficacy is evaluated by how well the absorbed energy warms the region around the infection without harming the surrounding healthy tissue. Heat (hyperthermia), radiation (laser therapy), and cold (cryosurgery) are all used to cure various diseases by destroying abnormal tissues and malignant cells without harming the healthy ones.

In addition to the discussed perspective, it has been shown that blood flow is closely related to the delivery of oxygen and nutrients to the organ. Increased circulation promotes body heat, which in turn increases the organ's delivery of oxygen and nutrients [52]. When a muscle receives enough oxygen, the repair process moves forward faster than when oxygen levels are low. Physiotherapy's ability to improve circulation to a sick body part is a significant benefit of the discipline. Ogulu and Abbey [53] considered the porous media within the artery to explore the impact of heat transmission during the treatment method for a malignant tumor or cancer. Using a heat transfer methodology and the Boussinesq approximation under the assumption of low electrical conductivity, Prakash and Ogulu [54] analyzed the oscillating flow of a power-law fluid through a constricted tube. They elucidated this method's application to deep heat muscle therapy. Chamkha [55] investigated the non-Darcian flow of an electrically conducting and heat-generating / absorbing fluid via a channel in a homogeneous porous media using hydromagnetic mixed convection. The free and mixed convection of a micropolar fluid moving in a vertical channel with asymmetric heating on the wall was studied by Chamkha *et al.* ([56],[57]), who provided both an analytical and numerical solution to this problem. Heat transfer was later shown to be crucial in medical therapy during surgery after several authors ([46],[58]) conducted studies on the flow of viscoelastic/non-viscoelastic fluids via constricted/porous conduits. Selimefendigi *et al.* [59] used numerical simulation to examine the effects of varying cylinder diameters on the mixed convection in a cavity containing nanofluid and porous layers.

1.2.6 Endothelial Glycocalyx Layer (EGL)

Glycocalyx refers to the thin gel-like coating that covers endothelial cells and protects the circulatory system from damage. Proteoglycans and glycosaminoglycans are found in the endothelial glycocalyx layer (EGL), a membrane-bound form of the EGL. By accumulating protein from the blood, the EGL becomes thicker, creating more friction for the blood to flow in microvessels. Due to its profound effect on circulatory parameters, the formation of atheromatous plaques in the artery wall as a result of the transport process taking place in arteries impelled researchers to analyze the phenomenon mathematically. It has been hypothesized that atherosclerotic plaques can be explained by the movement of a soluble substance through the blood vessel's porous layers. In order to fully understand how flow variables and transport phenomena in blood microcirculation are affected by an endothelial glycocalyx layer adjacent to vessel walls, it is essential to consider the influence of mechanical characteristics of it.

The increased arterial permeability caused by the thinning of EGL is the primary precipitating factor in the development of cardiovascular disease. In addition to decreasing porosity and slowing plasma flow in microvessels, the layer of macromolecules along the vessel walls may further increase flow resistance ([60]-[61]). Secomb *et al.* [3] conducted experiments to determine the existence of endothelial glycocalyx layer in the capillary, which plays a part in the increase in flow resistance and decrease in hematocrit. Based on the mechanical properties of endothelial glycocalyx layer, it can be depicted as a porous medium.

1.2.7 Flow through Porous Medium

Hill [62] concluded that the stability of a fluid's Poiseuille flow through a Darcy porous layer and a Brinkman layer is affected by the depth of the layer and the ratio of the porous layer's thickness to the fluid layer's thickness. To investigate the dynamical properties of the multi-phase flow in a cylindrical tube with porous boundaries, Sacheti *et al.* [63] used the Brinkman formulation for a porous medium to do a parametric analysis of bubble motion in the creeping flow of two immiscible fluids. The shear stress jump condition, first described by Ochoa-Tapia and Whitaker [1], involves a sudden change in shear stress at the fluid-porous interface. To better understand and analyse many physical and biological processes, several researchers have formalised the flow through porous media using the stress jump condition. Deo *et al.* [64] assumed the stress jump interfacial condition between the fluid and the endothelial glycocalyx layer (EGL) and used a cell model approach to calculate the hydrodynamic permeability of a population of porous cylinders surrounding an impermeable core.

The cyclic Newtonian fluid flow through a tube having a circular cross-section was studied by Tiwari and Deo [65] using the Brinkman equation and observed a phase lag between the flow characteristic and the pressure gradient. Blood flow with the two-fluid model through a porous multilayered blood artery has been studied by researchers ([66], [67], [68]). The vascular wall was thought to consist of a porous Darcy layer and a thinner Brinkman layer. For three-layer model of blood flow via a blood artery, Tiwari and Chauhan ([49],[50], [51]) presented the work for a thin porous region close to a wall. Researchers looked at how hematocrit, flow factors, and the Fåhræus effect were affected by blood's porous layer, its varying viscosity, its periodicity, and its non-Newtonian nature. Accurately estimating the flow quantities is more important in the medical sciences, and they discovered that a thin porous layer near a wall and fluctuating viscosity have influence on this.

1.2.8 Solute Dispersion

The objective of investigating the physical mechanism underlying solute dispersion in fluid flow is to gain a comprehensive understanding of the processes involved in the mixing and transportation of soluble substances within fluids. Due to wide range of applications in chemical engineering, physiological fluid dynamics, and the medical sciences, ([69], [70], [71], [72], [73]) the process has become one of the most intriguing subject for researchers. In recent development, many authors explored areas such as application of mass transport in environmental dispersion into a wetland [74], drug delivery for the effective cancer chemotherapy [75] and petroleum technology for the diffusion of surfactant into a matrix [76].

In circulatory systems, solute dispersion explains the mixing or transporting substances such as medications, nutrients, contaminants, plasma proteins, and metabolic materials into the blood circulation and respiratory flow. Life-threatening diseases like cancer have clinical management procedures in which medications (carrier particles) are administered into our physiological system via injection or capsule. In the case of capsule delivery, the carrier particles are directed to the site of infection, making solute dispersion research relevant. The indicator dilution method determines cardiac output in a living organism. Introducing the dye in the blood capillaries along the blood flow and then measuring its concentration at some downstream point is a benefit of this procedure. In addition to the uses mentioned above, we can witness the function of diffusion in artificial surgical devices and get insight into artificial aids like hemodialyzers and annular oxygenators [77]. As a result, the dispersion theory may be used to estimate the pace at which drugs will diffuse throughout living organisms.

Taylor [78] was the first to initiate the investigation of solute dispersion in a fluid that is in motion through a straight circular tube, and it was his observation that the solvent is spread by a process that involves molecular diffusion and velocity along the direction of flow occurring simultaneously, that laid the groundwork for further research. Concentration analysis offers a fresh perspective from which to calculate diffusion coefficients. Taylor's idea was expanded by Aris [79], who also abolished the limits placed on some parameters in the aforementioned theory. He proposed a novel method, the "*method of moments*" for studying the diffusion of a solvent in a uniformly cross-sectioned circular tube. The aforementioned method of dispersion analysis was only applicable over long periods of time, and hence it was of little use in studying the diffusion process during shorter periods of time. By conducting an analytical investigation of the unsteady diffusion equation, Gill and Sankarasubramanian [80] were able to circumvent this restriction. The authors presented a "*series expansion method*" for reliably obtaining an analytical solution to the convective diffusion process, valid for any time period.

1.3 Mathematical Expressions Governing the Microcirculation

The physical laws of mass conservation, momentum conservation, and energy conservation must be met by blood when it is in circulation. The governing mathematical expressions for such laws are illustrated here.

1.3.1 Law of Mass Conservation

The continuity equation, or law of mass conservation is a fundamental principle in fluid dynamics, states that the mass of a blood remains constant as it moves through a vessel. If there is no net gain or loss of fluid inside a system, then the mass of fluid remain constant at any point of time in the system. The mathematical expression for the law is given by

$$\frac{\partial \rho}{\partial t} = -\nabla.(\rho \widetilde{\mathbf{w}}), \tag{1.4}$$

where ρ, $\widetilde{\mathbf{w}}$ denotes the density and velocity of fluid, respectively. By solving the continuity equation, one can ensure that there are no sudden shifts in pressure or velocity that might cause harm to the system.

1.3.2 Law of Momentum Conservation

The law of momentum conservation in fluid flow is a fundamental principle that underlies much of our understanding of how fluids behave in motion and has wide-ranging applications in science and engineering. The law asserts that the mass and speed of fluid in a closed system remain unchanged until acted upon by some external force. In microcirculation such forces are blood viscosity, blood pressure and gravitational force. The principal can be mathematically stated as

$$\rho \frac{D\widetilde{\mathbf{w}}}{Dt} + \nabla p = \eta \nabla^2 \widetilde{\mathbf{w}} + \rho \widetilde{\mathbf{F}}, \tag{1.5}$$

where $\frac{D}{Dt}$, ∇^2 and $\widetilde{\mathbf{F}}$ denote the total/material derivative, the Laplacian operator and the external body force respectively. ρ, p, η and $\widetilde{\mathbf{w}}$ express the fluid density, pressure, the kinematic viscosity and velocity respectively.

When a solution is obtained for the law of momentum conservation in fluid flow, it signifies that the velocity, pressure, and other fluid properties have been determined at each point in the fluid domain under consideration. This solution provides valuable insights into the fluid flow behavior, such as the distribution of velocity and pressure in the fluid domain, the flow rate, the forces acting on the fluid, and so on. Furthermore, a solution to the law of momentum conservation can be used to predict how a fluid will behave under different conditions.

1.3.3 Law of Energy Conservation

When a fluid is moving in a closed system, its total energy does not change as long as no external work is done on it by things like the body and surface forces, thermal conduction, and heat sources like chemical reactions, according to the law of energy conservation, also known as Bernoulli's principle. Throughout the flow, there is no change in the fluid's total kinetic, potential, and pressure energies at any one location. This principle can be expressed mathematically as Bernoulli's equation.

$$\rho C_v \frac{D\widetilde{\mathbf{T}}}{Dt} - \widetilde{K} \nabla^2 \widetilde{\mathbf{T}} = \frac{\partial \widetilde{\mathbf{Q}}}{\partial t}, \tag{1.6}$$

where $\widetilde{\mathbf{T}}$, $\widetilde{K}$ symbolize the temperature and the thermal conductivity of the fluid respectively. At constant volume C_v denotes the specific.The external source or sink generates or absorbs heat, which is repesented here by $\widetilde{\mathbf{Q}}$.

As the fluid flows through the system, the solution may compute the changes in energy and utilise that data to infer the fluid's behaviour at various locations. In order to comprehend and foretell the actions of fluids in motion, its solution is crucial.

1.3.4 Law of Advection-Diffusion

When a scalar quantity such as the concentration of a chemical species or the temperature is being transported through a fluid, the advection-diffusion equation is used to characterise this process. The equation incorporates both advection and diffusion into the transport process. Transport of a scalar quantity can occur by either a fluid's bulk motion (advection) or random molecule motion (diffusion). The concentration equation is a partial differential equation that unifies these processes.

$$\frac{\partial \widetilde{\mathbf{C}}}{\partial t} + \nabla \cdot \left(\widetilde{\mathbf{w}} \ \widetilde{\mathbf{C}} \right) = \nabla \cdot \left(\widetilde{D}_m \nabla \widetilde{\mathbf{C}} \right), \tag{1.7}$$

where $\widetilde{\mathbf{w}}$ is the velocity of the fluid, $\widetilde{\mathbf{C}}$ is the local concentration of the solute, $\widetilde{D}_m$ is coefficient of molecular diffusion assumed to be constant, and ∇ is a gradient operator.

Change in concentration over time is represented by the first term on the left side of the equation (1.7). Advection of the scalar quantity due to fluid motion is represented by the second term. The first term on the right side of the equation (1.7) reflects the scalar amount diffusing as a result of random molecule motion.

1.3.5 Momentum Equation in Porous Medium

1.3.5.1 Brinkman Equation

Brinkman [81] modified Darcy's law and states that the flow rate of a fluid through a porous medium is proportional to the pressure gradient in the medium. Brinkman [81] expanded his research to include the permeability of the porous zone with micro-sized holes. Darcy's law does not account for the effects of fluid viscosity or boundary effects. The Brinkman equation incorporates these effects by adding an effective viscosity term and a gradient of velocity term to Darcy's law. The resulting equation is

$$\rho \frac{\partial \widetilde{\mathbf{w}}}{\partial t} = -\left(\frac{\partial p}{\partial z} + \frac{\mu}{k} \widetilde{\mathbf{w}} \right) + \mu_E \nabla^2 (\widetilde{\mathbf{w}}), \tag{1.8}$$

where ρ denotes the fluid density, p denotes the pressure, $\widetilde{\mathbf{w}}$ is the velocity, μ expresses blood viscosity, μ_E expresses effective blood viscosity and k represents the permeability

constant for the porous medium. When the medium is neither homogenous or isotropic, or when the fluid viscosity is large, this model outperforms Darcy's law.

1.3.5.2 The Brinkman-Forchheimer Equation

The Brinkman-Forchheimer equation is an extension of Darcy's law, which describes the flow of a fluid through a porous medium in the absence of any fluid inertia. The Brinkman-Forchheimer equation accounts for both viscous and inertial effects, making it more accurate for modeling flow in porous media under higher flow rates.
The Brinkman-Forchheimer equation can be written as follows

$$\rho\frac{\partial\widetilde{\mathbf{w}}}{\partial t}=-\left(\frac{\partial p}{\partial z}+\frac{\mu}{k}\widetilde{\mathbf{w}}\right)+\mu_E\nabla^2(\widetilde{\mathbf{w}})-\frac{C_F}{\sqrt{k}}\rho|\widetilde{\mathbf{w}}|\widetilde{\mathbf{w}}, \tag{1.9}$$

where ρ denotes the fluid density, p denotes the pressure, $\widetilde{\mathbf{w}}$ is the velocity, μ expresses blood viscosity, μ_E expresses effective blood viscosity, k represents the permeability constant for the porous medium and C_F denotes the inertial coefficient.

1.4 Boundary Conditions

Boundary conditions are of significant importance in the mathematical modelling of various processes. Using the assumptions established while modeling the physiological process they are used to solve the governing equations by analyzing the behavior of the solutions. The following boundary conditions may describe the more realistic and complex circumstances involved in blood microcirculation:

1. Velocity or shear stress and angular velocity are assumed to be finite at the microvessel axis [82].

2. Velocity profile, shear stress, temperature profile and concentration profile are assumed to be continuous at the interfaces[83].

3. The stress jump condition of tangential stress to take momentum transfer in an account is held at the fluid-porous interface [1].

4. There is no slip and no-couple stress assumed at the microvessel wall [82].

5. The microvessel wall is considered isothermal for temperature

6. Solute dispersion process is studied under the assumption of solute absorption at the vessel wall.

All the boundary and interface conditions described above are formulated mathematically in the respective chapters.

1.5 Mathematical Methods

To understand the microcirculation and predict the behavior of blood in microcirculation, the governing equations must be solved. The solution can aid to develop or improve clinical treatments and medical devices. It is not always easy to obtain exact analytical solution of the governing equations of fluid flow. Here discussed mathematical techniques are therefore utmost interest to us.

" The essence of mathematics is not to make simple things complicated, but to make complicated things simple."

— Stan Gudder

1.5.1 Perturbation Technique

The perturbation theory devised as an adequate technique for handling the complex calculations, in an attempt to understand the motion of celestial bodies. In academia, perturbation can be interpreted as a slight variation from an established state. A group of analytical methods embodied in perturbation theory can facilitate an approximate solution to a complex problem just utilising the well known analytical solution of a nearly related uncomplicated problem. The technique consist a crucial step which splits the problem into slowly varying solvable and rapidly varying perturbing components.

Perturbation techniques are based on a Taylor series expansion of the mechanical transformation involving a relatively small dimensionless parameter. To understand this thechnique, let's consider any real life phenomena which is mathematically governed by a boundary value problem in the form of

$$\begin{aligned} &\widetilde{F}[\widetilde{w}(\widetilde{r})] = 0, \\ &\widetilde{B}[\widetilde{w}(\widetilde{r})] = 0 \ \text{ on } \ \partial\widetilde{\delta}. \end{aligned} \tag{1.10}$$

When the above expression models the real life phenomenon quite nearly, it often becomes impossible or too dificult to obtain the exact analytical solution of (1.10). In these scenario, let's consider the non-dimensional form involving the relatively small parameter say "ε" of

(1.10).

$$\begin{aligned} &F[w(r);\varepsilon] = 0, \\ &B[w(r);\varepsilon] = 0 \text{ on } \partial\delta \qquad (0 < \varepsilon << 1). \end{aligned} \tag{1.11}$$

The technique begins with the decomposition of the problem $F[w(r);\varepsilon] = 0$ into two parts as

$$S[w(r)] + P[w(r);\varepsilon] = 0, \tag{1.12}$$

where $S[w(r)]$ denotes the nearly related uncomplicated problem whose exact analytical solution let's say "$w_0(r)$" can be easily obtained and $P[w(r);\varepsilon]$ is a perturbing component of the problem. In perturbation theory, the solution of (1.11) is expressed as a power series in a perterbed parameter ε as

$$w(r) = w_0(r) + \sum_{n=1}^{\infty} \varepsilon^n w_n(r). \tag{1.13}$$

The first term is the known exact analytical solution to the related simple problem $S[w(r)]$. One can obtain an approximate perturbation solution' of (1.11) by truncating (1.13) as successive terms in the series expansion with higher powers of ε usually become smaller.

$$w(r) \approx w_0(r) + \sum_{n=1}^{N} \varepsilon^n w_n(r) + \mathcal{O}(\varepsilon^{N+1}). \tag{1.14}$$

The series (1.14) is known as asymptotic series and such solution is known as asymptotic series solution. Customarily, only the first three terms, the solution to the known problem, the first and second order perturbation correction have been kept for practicality i.e.,

$$w(r) \approx w_0(r) + \varepsilon w_1(r) + \varepsilon^2 w_1(r) + \mathcal{O}(\varepsilon^3). \tag{1.15}$$

1.5.1.1 Regular Perturbation

A perturbation problem is regular when the perturbed component with nonzero small ε and the unperturbed component for vanishing ε share significant qualitative similarity. If the power series (1.14) in ε converges uniformly as ε approaches zero, the problem (1.11) is called a regular perturbation problem.
In this case, the approximate perturbed solution can be obtained by expanding the governing equations as a series in ε, collecting terms with equal powers of ε and solve them in turn as far as the solution is required.

As the perturbation parameter approaches the limit value, the approximate solution to a regular perturbed problem converge to the analytical solution of the unperturbed problem.

1.5.1.2 Singular Perturbation

Singular perturbation problem is qualitatively different from it's unperturbed problem. For a singular perturbation problem, the power series (1.14) in ε does not converge uniformly. Different time scales and length parameters affects the solutions of differential equations arising in singular perturbation problems. Broadly, singular perturbation problems can be classified into two types: Boundary layer problems and multiple-scale problems.
Boundary layer problems are of particular interest to us as it arises in Chapter 6 and can be handled adequately by matched asymptotic expansion method. The domain of singular perturbation problem can be segregated in two or more parts. There exist a large primary sub domain in which the problem could be treated as regular perturbation problem and the approximate solution can be achieved through an asymptotic series (1.14). In Other small subdomains known as boundary layers, an asymptotic series (1.14) could not approximate the solution. Boundary layers appears at narrow zones near the boundary of domain.
The approximate solution obtained through (1.14) for primary domain is only valid out side boundary layers and therefore known as outer solution and denoted by w^o.

Matched Asymptotic Expansions

In continuum mechanics, necessity of solution for classical problems gave rise to the conception of matched asymptotic expansions. As mentioned, boundary layers are narrow domains and hence required to be stretched or magnified to investigate it's behaviour which can help to draw the uniform solution for a singularly perturbed problem. The stretching parameter can be introduced as

$$\xi = \frac{(r-a)}{\varepsilon^k}, \tag{1.16}$$

where a is the point where boundary layer arising and k is the scale of magnification required. Utilising stretching parameter into the boundary value problem (1.11), it transforms into

$$\begin{aligned} F[w(\xi);\varepsilon] &= 0, \\ B[w(\xi);\varepsilon] &= 0 \text{ on } \partial\delta. \end{aligned} \tag{1.17}$$

Now the approximate solution for (1.17) can be obtained by a new asymptotic series expansion other than (1.14). This solution is considered an inner solution and denoted by $w^i(\xi)$ as it is only valid inside the boundary layer.
Here, the primary domain and boundary layers may not be separated exclusively and may

overlap. Therefore, the approximate solution of primary domain and boundary layers can not be combined directly. Instead, a suitable matching condition is enforced to generate a composite solution. Prandtl's boundary layer theory is very renowned in practice and therefore Prandtl's matching condition is usually employed to obtain the composite solution which is uniformly convergent for singularly perturbed problem.

Prandtl's matching condition

$$w_{overlap} = (w^i)^o = (w^o)^i. \tag{1.18}$$

Composite Solution

$$w(r) \approx w^i + w^o - w_{overlap}. \tag{1.19}$$

In (1.18), $(w^i)^o$ is the limiting value of the inner solution from outside of the boundary layer, $(w^o)^i$ is the limiting value of the outer solution from outside of the primary domain i.e., from inside the boundary layers and $w_{overlap}$ denotes the solution in the overlapping area between the primary domain and boundary layers.

The detailed procedure for acquiring the solution for singular perturbation problems with different matching conditions has been discussed substantially by Bush [84] and Nayfeh [85].

1.5.2 Technique of Eigenfunction Expansion

It could be really intriguing in complicated scenarios when solving the non-homogeneous boundary value problem with homogeneous boundary conditions is difficult, to obtain a solution with help of eigenfunctions of a related homogeneous problem. The non-homogeneous second-order partial differential equations with homogeneous boundary conditions is of particular interest and therefore a concise description about the technique of eigenfunction expansion employed for solving the same is demonstrated here.

Consider the BVP in the form,

$$\frac{d}{dr}\left(A(r)\frac{dw(r)}{dr}\right) + (B(r) - \Lambda C(r))w(r) = L[w(r)] - \Lambda C(r)w(r) = F(r), \tag{1.20}$$

together with the boundary conditions

$$a_1 w(r) = a_2 \frac{dw(r)}{dr} \quad \text{at} \quad r = 0, \quad \text{and} \quad b_1 w(r) = b_2 \frac{dw(r)}{dr} \quad \text{at} \quad r = 1. \tag{1.21}$$

where Λ denotes the provided constant and the function $F(r)$ is provided for $r \in [0,1]$.The functions $A(r)$, $B(r)$, $C(r)$ and $\frac{dA(r)}{dr}$ appearing in (1.20) are believed to be continuous for

$r \in [0,1]$ and $A(r) > 0,\ C(r) > 0$ and $L[w(r)] = \frac{d}{dr}\left(A(r)\frac{dw(r)}{dr}\right) + B(r)w(r)$.
The homogeneous problem corresponding to (1.20) is given by

$$L[w(r)] - \Lambda C(r)w(r) = 0, \tag{1.22}$$

Introducing the eigenvalues of (1.22) with the similar boundary conditions (1.21) as $\Lambda_1 < \Lambda_2 < \Lambda_3 < \cdots < \Lambda_m < \ldots$ and the corresponding orthogonal eigenfunctions be $\psi_1, \psi_2, \psi_3, \ldots, \psi_m, \ldots$. The series solution of the non-homogeneous differential equation (1.20) with corresponding homogeneous boundary conditions (1.21) can be denoted as $w = \psi(r)$ in the form

$$\psi(r) = \sum_{m=1}^{\infty} b_m \psi_m(r), \tag{1.23}$$

where

$$b_m = \frac{\int_0^1 C(r)\psi(r)\psi_m(r)dr}{\int_0^1 r\psi_m^2(r)dr}, \quad m = 1,2,3,... \tag{1.24}$$

However, (1.24) is not of any help to calculate b_m as $\psi(r)$ is not known. b_m must be obtained in a way such that (1.20) and (1.21) are satisfied. One must observe that each $\psi_m(r)$ satisfy boundary conditions (1.21) and hence $\psi_(r)$ given by (1.23) always satisfy boundary conditions (1.21). Therefore $\psi_(r)$ only requires to satisfy (1.21)

$$L[\psi(r)] = \Lambda C(r)\psi(r) + F(r), \tag{1.25}$$

To obtain b_m, substitute the series expansion given by (1.24) into (1.26). The left side of (1.26) becomes

$$\begin{aligned} L[\psi(r)] &= L[\sum_{m=1}^{\infty} b_n \psi_m(r)] = \sum_{m=1}^{\infty} b_m L[\psi_m(r)] \\ &= \sum_{m=1}^{\infty} b_m \Lambda_m C(r)\psi_m(r), \end{aligned} \tag{1.26}$$

One can rewrite the non-homogeneous term in (1.25) as $C(r)[F(r)/C(r)]$. If $F(r)/C(r)$ and it's derivative are piecewise continuous $0 \le r \le 1$ then in the open interval $0 < r < 1$ it can be expanded in a convergent series as

$$\frac{F(r)}{C(r)} = \sum_{m=1}^{\infty} c_m \psi_m(r), \tag{1.27}$$

where, using (1.25) with $\psi(r)$ replaced by $F(r)/C(r)$,

$$c_m = \frac{\int_0^1 C(r)\frac{F(r)}{C(r)}\psi_m(r)dr}{\int_0^1 r\psi_m^2(r)dr} = \frac{\int_0^1 F(r)\psi_m(r)dr}{\int_0^1 r\psi_m^2(r)dr}, \quad m = 1,2,3,... \tag{1.28}$$

Upon substituting for $\psi(r)$, $L[\psi(r)]$, and $F(r)$ in (1.25) from (1.23), (1.26), and (1.27), respectively, one obtains

$$\sum_{m=1}^{\infty} b_m m\Lambda_m C(r)\psi_m(r) = \Lambda C(r)\sum_{m=1}^{\infty} b_m\psi_m(r) + C(r)\sum_{m=1}^{\infty} c_m\psi_m(r). \tag{1.29}$$

After collecting terms and cancelling the common nonzero factor $C(r)$ we have

$$\sum_{m=1}^{\infty}\left[(\Lambda_m - \Lambda)b_m - c_m\right]\psi_m(r) = 0. \tag{1.30}$$

One can observe that the coefficient of $\psi_m(r)$ must be zero for each m if (1.30) is to hold for each r in the interval $0 \leq r \leq 1$. Therefore

$$(\Lambda_m - \Lambda)b_m - c_m = 0, \quad m = 1,2,3,.... \tag{1.31}$$

If Λ is not equal to any eigenvalue of the (1.23) then

$$b_m - = \frac{c_m}{(\Lambda_m - \Lambda)}, \quad m = 1,2,3,..., \tag{1.32}$$

and

$$\begin{aligned} w(r) = \psi(r) &= \sum_{m=1}^{\infty}\frac{c_m}{(\Lambda_m - \Lambda)}\psi_m(r) \\ &= \sum_{m=1}^{\infty}\frac{\int_0^1 F(r)\psi_m(r)dr}{(\Lambda_m - \Lambda)\int_0^1 r\psi_m^2(r)dr}\psi_m(r). \end{aligned} \tag{1.33}$$

The technique of the eigenfunction expansion elucidated here has been utilised in (1.5.3) to obtain the solution of the equations governing solute dispersion. Boyce *et al.* [86] have illustrated theory in great details by explaining it's application to solve different problems.

1.5.3 Solution Technique for Solute Dispersion Problem

Following the solution method given in Sankarasubramanian and Gill [2], the solution expression for the dimensionless form of the convective diffusion equation (1.7) in cylindrical coordinate system with help of appropriate boundary conditions is formulated as

$$C = \sum_{l=0}^{\infty} g_l(t,r)\frac{\partial^l C_M}{\partial z^l}, \tag{1.34a}$$

where g_l $(l = 0,1,2,...)$ are the function of time and radial distance. The cross-sectional average concentration C_M of the soluble matter is defined as

$$C_M = 2\int_0^1 Crdr. \tag{1.34b}$$

The equation (1.7) is multiplied by $2r$ throughout and integrating with respect to r from $(r=0)$ to $(r=1)$, the governing equation (1.7) can be rewritten by introducing the definition of cross-sectional average concentration

$$\frac{\partial C_M}{\partial t} + 2\frac{\partial}{\partial z}\left(\int_0^1 rw(r,t)C(t,z,r)dr\right) - 2\frac{\partial C}{\partial r}(t,z,1) - \frac{1}{Pe^2}\frac{\partial^2 C_M}{\partial z^2} = 0. \tag{1.35}$$

Introducing Eq. $(1.34a)$ into Eq. (1.35), the mean concentration is given as

$$\frac{\partial C_M}{\partial t} = \sum_{l=0}^{\infty} M_l(t)\frac{\partial^l C_M}{\partial z^l}, \tag{1.36a}$$

where

$$\begin{aligned} &g_{-1} = 0, \\ &M_l(t) - \frac{\delta_{l2}}{Pe^2} + 2\int_0^1 rg_{l-1}(t,r)w(r)dr - 2\frac{\partial g_l}{\partial r}(t,1) = 0, \quad l = 0,1,2,..., \end{aligned} \tag{1.36b}$$

and δ_{lm} denotes Kronecker delta

$$\delta_{lm} = \begin{cases} 0, & l \neq m, \\ 1, & l = m. \end{cases} \tag{1.36c}$$

As observed by Gill and Sankarsubramanian [80], the higher order coefficients possess very small magnitude for very large time in the solute dispersion process and the good approximation could be achieved without involving any terms above the second order term. Therefore, it has been decided to terminate the series expansion $(1.36a)$ at second order term.

Wall absorption attributes to the reduction of solute concentration in the system, which produces the negative sign and nonzero flux at wall for the exchange coefficient $M_0(t)$. $M_1(t)$ delineates the convection of solute caused by the velocity of the fluid flow and known as the convection coefficient. $M_2(t)$ denotes the dispersion coefficient and represents the dispersion process as the simultaneous outcome of the velocity driven convection and molecular diffusion process at a time. The resulting mean concentration is derived as

$$\frac{\partial C_M}{\partial t} = M_2(t)\frac{\partial^2 C_M}{\partial z^2} + M_1(t)\frac{\partial C_M}{\partial z} + M_0(t)C_M, \tag{1.37a}$$

where

$$M_l(t) - \frac{\delta_{l2}}{Pe^2} + 2\int_0^1 r g_{l-1}(t,r)w(r)dr - 2\frac{\partial g_l}{\partial r}(t,1) = 0, \;\; l = 0,1,2,.... \tag{1.37b}$$

To solve the above equations $(1.37a)$ and $(1.37b)$, we need to find out the diffusion coefficients $(M_l(t),\ l = 0,1,2)$ with help of the suitable initial and boundary conditions. For this, the corresponding unknown functions $g_l(t,r),\ l = 0,1,2$ must be determined in order to compute the expression for mean concentration from the equation $(1.37a)$. Introducing Eqs. $(1.34a)$ and $(1.37a)$ into the Eq. (1.7). On comparing the coefficient of $\frac{\partial^k C_M}{\partial z^k},\ (k = 0,1,2)$, the system of differential equations for the function g_k are outlined as

$$\frac{\partial g_k}{\partial t} = \frac{1}{r}\frac{\partial}{\partial r}\left(r\frac{\partial g_k}{\partial r}\right) - w(r)g_{k-1} + \frac{1}{Pe^2}g_{k-2} - \sum_{l=0}^{k} M_l g_{k-l}, \;\; k = 0,1,2, \tag{1.38}$$

where $g_{-1} = g_{-2} = 0$.

The initial and boundary conditions for g_k and C_M can be derived from the boundary conditions

$$C_M(0,z) = 2\chi(z)\int_0^1 X(r)rdr, \tag{1.39a}$$

which gives

$$g_k(0,r) = 0, \quad k = 1,2, \tag{1.39b}$$

$$g_0(0,r) = \frac{X(r)}{2\int_0^1 X(r)rdr}, \tag{1.39c}$$

$$g_k(t,0) = \text{finite}, \quad k = 0,1,2, \tag{1.39d}$$

$$\frac{\partial g_k}{\partial r}(t,1) = -\beta g_k(t,1), \quad k = 0,1,2, \tag{1.39e}$$

$$\int_0^1 g_k(t,r)rdr = \frac{1}{2}\delta_{k0}, \quad k = 0,1,2, \tag{1.39f}$$

and

$$C_M(t,z) = \frac{\partial C_M}{\partial z}(t,z) = 0, \ \text{ as } \ z \to \infty, \tag{1.39g}$$

where δ_{k0} is mentioned in Eq. $(1.36c)$. In the present study, we are interested to analyze the behavior of the diffusion coefficient as well as mean concentration of the solute at large time $(i.e.\ t \to \infty)$.

1.5.3.1 Estimation for the Function $\mathbf{g_0(t,r)}$ and Exchange Coefficient $\mathbf{M_0(t)}$

The equation for $g_0(t,r)$ in terms of exchange coefficient $M_0(t)$ from equation (1.38) may be written as

$$\frac{\partial g_0}{\partial t} = \frac{1}{r}\frac{\partial}{\partial r}\left(r\frac{\partial g_0}{\partial r}\right) - g_0 M_0. \tag{1.40a}$$

The suitable initial (IC) and boundary conditions (BCs) for the function $g_0(t,r)$ are evaluated from equations $(1.39c), (1.39d) - (1.39e)$ by substituting $k = 0$ and an additional condition can be obtained from $(1.39g)$

$$\int_0^1 g_0(t,r)rdr = \frac{1}{2}. \tag{1.40b}$$

The equation $(1.40a)$ for the function g_0 in terms of exchange coefficient M_0 is independent of the fluid velocity. Using the eigenfunction expansion method discussed earlier in $(1.5.2)$ [86], the solution of the non-homogeneous BVPs given in Eq. $(1.40a)$ for $g_0(t,r)$ satisfying the initial and boundary conditions $(1.39c), (1.39d) - (1.39e)$ and an additional condition

$(1.40b)$ is in form

$$g_0(t,r) = \frac{\sum_0^\infty A_k J_0(\alpha_k r) e^{-\alpha_k^2 t}}{2\sum_0^\infty \left(\frac{A_k}{\alpha_k}\right) J_1(\alpha_k) e^{-\alpha_k^2 t}}, \tag{1.41a}$$

where $\alpha_k' s$ are roots of the transcendental equation in terms of Bessel functions J_0, J_1 described below

$$\alpha_k J_1(\alpha_k) = \beta J_0(\alpha_k), \quad k = 0,1,2,... \tag{1.41b}$$

and the expansion coefficient $A_k' s$ are obtained from the initial condition as

$$A_k = \frac{\alpha_k^2 \int_0^1 rX(r) J_0(\alpha_k r) dr}{(\alpha_k^2 + \beta^2) J_0^2(\alpha_k) \int_0^1 rX(r) dr}, \quad k = 0,1,2,... \tag{1.41c}$$

The exchange coefficient $M_0(t)$ is obtained form the Eq. $(1.37b)$ using equation $(1.39e)$

$$M_0(t) = 2\frac{\partial g_0}{\partial r}(t,1) = -2\beta g_0(t,1) = -\frac{\sum_0^\infty A_k \alpha_k J_1(\alpha_k) e^{-\alpha_k^2 t}}{\sum_0^\infty \left(\frac{A_k}{\alpha_k}\right) J_1(\alpha_k) e^{-\alpha_k^2 t}}. \tag{1.42}$$

The solution expression for the exchange coefficient M_0 is precisely same as obtained in the previous studies ([2], [87], [88], [89]) as its computation does not include fluid velocity. So, the analysis of exchange coefficient is discarded in the present study as the expression of $M_0(t)$ remains invariant for fluid flow involving constant or variable viscosity model.

In the limiting case as $t \to \infty$, the aforementioned equations $(1.41a)$ and (1.42) give the limiting value in the form of asymptotic representation for the function g_0 and exchange coefficient M_0 as below,

$$\lim_{t\to\infty} M_0(t) = M_0(\infty) = -\alpha_0^2, \tag{1.43a}$$

$$\lim_{t\to\infty} g_0(t,r) = g_0(\infty,r) = \frac{\alpha_0}{2J_1(\alpha_0)} J_0(\alpha_0 r), \tag{1.43b}$$

where α_0 is the first root (least in magnitude) of the Eq. $(1.41b)$.

1.5.3.2 Asymptotic Representation of Diffusion Coefficients ($\mathbf{M_m(t)}$)

As per the above discussion, the function g_0 and the solution expression for the exchange coefficient $M_0(t)$ are independent of flow velocity, however the function $g_k(t,r)$ and the diffusion coefficients $(M_k(t),\ k = 1,2)$ depend on the flow velocity of the fluid. So, in this case, steady flow of two-fluid model using heat transfer approach is considered to obtain the diffusion coefficients. The asymptotic expression for the function $g_k' s$ are obtained from the

equation (1.38)

$$\frac{1}{r}\frac{d}{dr}\left(r\frac{dg_k}{dr}\right)+\alpha_0^2 g_k = w(r)g_{k-1}-\frac{1}{Pe^2}g_{k-2}+\sum_{l=1}^{k} M_l g_{l-l} \tag{1.44a}$$

where $k=1,2,\ g_{-1}=0$ and the diffusion coefficients $(M_k,\ k=1,2)$ are given by

$$M_k = \frac{\delta_{k2}}{Pe^2}+2\frac{dg_k}{dr}(1)-2\int_0^1 rw(r)g_{k-1}(r)dr. \tag{1.44b}$$

The boundary conditions (BCs) with an additional condition on $f_m(r)$ are described below from Eqs. (1.39)

$$\begin{gathered} g_k(0)=\text{finite}, \quad \frac{dg_k}{dr}(1)=-\beta g_k(1), \quad k=1,2, \\ \int_0^1 g_k r dr=0, \quad k=1,2. \end{gathered} \tag{1.45}$$

By following the solution strategy of the work of Sankarasubramanian and Gill [2], the diffusion coefficients $(M_k,\ k=1,2)$ are delineated in terms of the functions $(g_k,\ k=1,2)$

$$M_k = \frac{\int_0^1 rJ_0(\alpha_0 r)\left(\frac{g_{k-2}(r)}{Pe^2}-w(r)g_{k-1}(r)-\sum_{l=1}^{k-1} M_l g_{k-l}(r)\right)dr}{\int_0^1 rg_0(r)J_(\alpha_0 r)dr}, \quad k=1,2. \tag{1.46}$$

The convection coefficient (M_1) from Eq. (1.46) is obtained by using the limiting value of known function g_0 for large time and it is delineated by

$$M_1 = \frac{-\int_0^1 w(r)g_0(r)rJ_0(\alpha_0 r)dr}{\int_0^1 g_0(r)rJ_0(\alpha_0 r)dr} = \frac{-2\alpha_0^2}{(\alpha_0^2+\beta^2)J_0^2(\alpha_0)}\int_0^1 w(r)rJ_0^2(\alpha_0 r)dr. \tag{1.47}$$

The expression for the function g_1 can be obtained from $(1.44a)$ by putting $k=1$ and it is delineated by

$$\frac{1}{r}\frac{d}{dr}\left(r\frac{dg_1}{dr}\right)+\alpha_0^2 g_1 = w(r)g_0+M_1 g_0, \tag{1.48}$$

along with the following boundary conditions for g_1

$$\begin{gathered} g_1(0)=\text{finite}, \quad \frac{dg_1}{dr}(1)=-\beta g_1(1), \\ \int_0^1 g_1 r dr=0. \end{gathered} \tag{1.49}$$

Using Eqs. (1.47) in (1.48), the solution for g_1 satisfying the boundary conditions (1.49) is given by

$$g_1(r) = \sum_{k=0}^{\infty} B_k J_0(\alpha_k r), \tag{1.50a}$$

where the expansion coefficient B_0 is evaluated in terms of B_n $(n = 1, 2, ...)$.

$$B_0 = \frac{-\alpha_0}{J_1(\alpha_0)} \sum_{k=1}^{\infty} B_k \frac{J_1(\alpha_k)}{\alpha_k}, \tag{1.50b}$$

Introducing equations $(1.50b)$ into $(1.50a)$, the function g_1 can be rewritten as

$$g_1 = \sum_{k=1}^{\infty} B_k \left[J_0(\alpha_k r) - \frac{\alpha_0}{J_1(\alpha_0)} \frac{J_1(\alpha_k)}{\alpha_k} J_0(\alpha_0 r) \right], \tag{1.50c}$$

where $B_k's$ are given by

$$B_k = \frac{2\alpha_k^2}{(\alpha_0^2 - \alpha_k^2)(\alpha_k^2 + \beta^2) J_0^2(\alpha_k)} \int_0^1 (w(r) + M_1) g_0(r) r J_0(\alpha_k r) dr. \tag{1.50d}$$

The expression for dispersion coefficient (M_2) is obtained using the equations $(1.50c), (1.50d)$ and (1.46) and it is delineated by

$$M_2 = \frac{1}{Pe^2} - \frac{4\alpha_0 J_1(\alpha_0)}{(\alpha_0^2 + \beta^2) J_0^2(\alpha_0)} \int_0^1 (w(r) + M_1) g_1(r) r J_0(\alpha_0 r) dr. \tag{1.51}$$

1.5.3.3 Solution for Mean Concentration (C_M)

The solution expression of the Eq. $(1.37a)$ with help of the diffusion coefficients $(1.42), (1.47), (1.51)$ and boundary conditions $(1.39a), (1.39g)$ for solute mean concentration (C_M) is derived as

$$C_M(t, z) = \frac{1}{2Pe\sqrt{\pi T}} \mathrm{Exp}\left(\eta - \frac{z_1^2}{4T} \right), \tag{1.52}$$

where

$$\eta(t) = \int_0^t M_0(\xi) d\xi, \tag{1.53a}$$

$$z_1(t, z) = z + \int_0^t M_1(\xi) d\xi, \tag{1.53b}$$

$$T(t) = \int_0^t M_2(\xi) d\xi. \tag{1.53c}$$

The Eqs. $(1.53a)-(1.53c)$ can be approximated for large time $t(t \geq 0.5)$ as below [2]

$$T(t) \sim M_2 t, \tag{1.54a}$$

$$z_1(t,z) \sim z + M_1 t, \tag{1.54b}$$

$$\xi(t) \sim M_0 t. \tag{1.54c}$$

The exchange M_0, convective M_1 and dispersion coefficient M_2 are independent of radial non-uniformities with initial solute distribution (d).

> **" It is unworthy of excellent men to lose hours like slaves in the labour of calculation which could safely be relegated to anyone else if machines were used."**
>
> ***— Gottfried Leibniz***

MATHEMATICA 10.0.2 is employed where ever required for countering complex calculations arising throughout the proposed research work.

1.6 Gaps in Existing Research

To the best of our understanding and belief, following a literature review, it is evident that the following aspects of the microcirculation of blood through microvessels have yet to be extensively investigated.

- The two-fluid model investigating the impact of the microstructure of blood on the flow and drug deliverance process in microcirculation has yet to be thoroughly studied.
- The two-fluid model with or without varying viscosity model has not been investigated much for the flow through a porous layered straight or curved tube.
- The theoretical study on a two-fluid model with Hematocrit-dependent viscosity approaches has yet to be addressed for flow-through microvessels.
- The heat transfer aspect of a two-phase fluid model with temperature-dependent viscosity for blood has yet to be explored deeply in blood flow modeling through microvessels.
- Analysis of the non-Newtonian fluid flow approach through the conduit with a non-circular cross-section has received little consideration.

- Analysing solute dispersion in two-fluid flow of blood in micro circulation using the appropriate dispersion model has received less consideration.

1.7 Research Objectives

Based on literature survey and identified research gaps, objectives of the thesis work are,

- To conduct mathematical analysis regarding the impact of the microstructure of blood microcirculation by adopting an adequate mathematical model.
- To constitute a mathematical model accountable for temperature or Hematocrit dependent viscosity of blood and examine the impact of variable viscosity on microcirculation.
- To explore the heat transfer and solute dispersion aspect to gain theoretical understanding for the drug deliverance process and pave ways for devising new clinical procedures involving temperature variation.

1.8 Thesis Organisation

The thesis organizes the research effort into seven chapters. Chapter 1 highlights the need to study blood microcirculation in the human cardiovascular system and conduct a literature review to identify existing research gaps to establish objectives for the proposed work. The methodology to achieve research goals is devised, and fundamental concepts of Biomechanics, blood microcirculation, and mathematical approaches have been introduced.

The objective of Chapter 2 is to examine the influence of the microrotation of erythrocytes, external magnatic field and heat transfer on mechanical quantities of blood microcirculation through the microvessel with thin endothelial glycocalyx-layered microvessels. Graphical interpretations of the different parametric influences on blood microcirculation have been studied with both conditions at interface. Compared to the no-spin condition, the relatively strong influence of the no-couple stress condition on Fåhræus effect, flow characteristics, and hematocrit has been observed.

Chapter 3 considers blood microcirculation under the identical scenario of Chapter 2 with absorbing vessel walls and aims to extend the study to examine the mechanism of the solute dispersion phenomenon. To comprehend certain clinical features of blood microcirculation, the effect of erythrocyte spinning, coupling number, EGL thickness and permeability, thermal conductivity, radiation parameter, and Hartmann number on the solute dispersion coefficients and mean concentration interpreted graphically.

A theoretical attempt has been made in Chapter 4 to examine the impact of the heat transfer aspect on the flow characteristics of temperature-dependent viscous blood microcirculation through endothelial glycocalyx layered microvessels. The Brinkman-Forchheimer equation governs blood flow through the endothelium glycocalyx layer to encompass the permeability spectrum. The perturbation technique is employed to solve the Brinkman-Forchheimer governing equation analytically. Singular and regular perturbation problems are encountered for small Darcy numbers (SDN) and large Darcy numbers (LDN), respectively. The study concludes the impact of temperature on flow characteristics and comprehends the importance of studying temperature-dependent viscosity models for devising clinical procedures involving temperature variations.

Delivering drugs to the targeted location or transporting nutrients to needy organs involves the dispersion of solutes through blood microcirculation. The process is believed to be influenced by the varying characteristics of viscosity, heat transfer, and other related factors. Chapter 5 is motivated toward examining the dispersion of solutes in blood microcirculation through microvessels influenced by temperature-sensitive viscosity and heat transfer. The graphical analysis shed light on the solute dispersion process's sensitivity regarding heat transfer and temperature-sensitive viscosity. In addition, the dispersion process is accelerated with the dominance of thermal buoyancy forces.

The focus of Chapter 6 is to study the hydrodynamic characteristics of blood microcirculation through a microvessel having EGL adjacent to the absorbing wall with a sophisticated mathematical model. A comparison has been drawn between the generalized model and its reduced specific fluid models for the solute dispersion process. The graphical study interprets the sensitivity of the solute dispersion coefficients regarding EGL thickness, EGL porosity, plasma layer thickness, and wall absorbing capacity. EGL adjacent to the microvessel wall decreases both convective and axial dispersion in the case of a wall with high reactivity. One notable observation is that a decrease in the porosity of EGL adjacent to the microvessel wall leads to a decrease in the average solute concentration.

The thesis is summarised in Chapter 7, which highlights the noteworthy findings with physical significance and application. The advantages and limitations of the study are covered to make it more relevant for clinical application. In addition, the chapter recommends directions for future study and ways to strengthen the current work so that it may be used more effectively in clinical practice.

Chapter 2

Influence of Erythrocyte Microstructure and EGL on Microcirculation under Heat Transfer Aspect

The behavior of the physiological fluids and their physical mechanism are very crucial to understand the circulatory system in the human beings, which may help to classify the diseases, affecting the flow of fluids through vascular systems. With the help of mathematical modeling in fluid mechanics or medical sciences, several authors made efforts in the form of various interdisciplinary works to resolve or minimize the effect of diseases during the flow of fluid through vessels. Nowadays, cancer is one of the most dangerous diseases which is uncontrolled under the normal situations and its treatment involves the heat transfer approach. Besides this, another disease leading to circulatory disorder is the atherosclerosis, which may arise due to accumulation of fatty plaques of cholesterol, carbohydrates, fibrous tissues or macromolecules inside the arterial wall. The study of the blood flow through microvessels (arterioles, venules and capillaries) plays significantly different roles in comparison to the larger blood vessels. We hope that the present study may be helpful in understanding the several kinds of effect on the flow of blood through the blood vessels with a porous layer near the wall. The accumulation of fatty plaques inside the arterial wall at a specific place reduces the area of the flow through blood vessels in which enhanced flow impedance occurs due to the presence of fatty plaques of cholesterol known as stenosis. Many investigators ([90], [91]) studied the impact of constriction/catheterization on steady flow of Newtonian or non-Newtonian fluid through constricted/catheterized artery. A periodic nature of viscoelastic fluids flowing through constricted tube has been done by the several researchers in their studies ([92], [93]).

All the above studies performed the analysis of viscoelastic/non-Newtonian fluids flowing through conduit but the emphasis has not been given to the fluid particles and their structures.Recently, Khanukaeva *et al.* ([22], [23]) analyzed the flow of micropolar fluid through

[1]This work has published as **A. Tiwari, P.D. Shah, and S.S. Chauhan,"Analytical study of Micropolar fluid flow through porous layered microvessels with heat transfer approach", *Eur. Phys. J. Plus* 135 (2020) 209.**

a membrane with porous layer using cell model technique in which the flow is parallel and perpendicular to the axis of cylindrical cell. They formulated the governing equations for two different interface conditions namely, no-spin (NS) and no-couple stress (NCS) representing the zero and non-zero micro-rotational (angular) velocity at the interface.

All the above studies involve the impermeable nature of blood vessels but under different circumstances such as deposition of carbohydrates, fibrous tissues or micro-molecules inside the lumen obstruct the flow and further leads to the diseases like polycythemia and another microangiopathic disease. The development of atheromatous plaques in the arterial wall due to transport process occurring in arteries created the curiosity of researchers to mathematically analyze the same owing to its severe impact on circulation. The transportation of the fluid material through porous layered blood vessels has been used to understand the formation and development of atheromatous plaques. Although a large number of studies reveal an easier flow among vessel wall tissues for large blood vessels having an endothelial lining of macromolecules with low permeability but the same need not be true for small blood vessels. The study of blood flow through the porous medium has been a compelling topic for researchers and has wide practical situations in the areas of engineering and medical field. Darcy [94] gave an empirical method to formulate the mathematical equation of fluid flow through porous media in terms of permeability but this law was restricted for low permeability only. Brinkman [95] described the flow through porous mass by modifying the Darcy's equation and found a relation between the permeability of the porous media, particle size and density. Brinkman [96] extended his work to the permeability of the porous region with closely packed porous particles (micro-pores). Ochoa-Tapia and Whitaker ([1], [97]) introduced the discontinuity in shear stress at fluid-porous interface also known as the stress jump condition. The flow of Casson fluid through a porous tube was discussed by Dash *et al.* [98] under the constant as well as radially varying permeability assumptions.

The theoretical study of the hydrodynamic mixed convection of Newtonian fluid flow through vertical conduit with asymmetric and symmetric heating wall was done by Chamkha [99] under the presence or absence of heat absorption or generation impacts. He reported an analytical solution of velocity and temperature profiles for different three thermal boundary conditions on both the walls in the presence of uniform magnetic field in transverse direction of the fluid flow. The steady and transient laminar hydrodynamic flows and heat generation/absorption aspects through porous channels in the presence of a transverse magnetic field were discussed by Chamkha ([55], [100]) in which the induced magnetic field and Hall effect of hydromagnetic flow are assumed to be neglected due to very small magnetic Reynolds number. He [101] extended his work for double-diffusive convective flow through uniform porous medium channel with the assumption of temperature-dependent

heat source and sink within the enclosure of the boundaries of the channel. Srinivasacharya and Shiferaw [21] analyzed the impact of Hall and ionic effect on the flow of micropolar fluid through a circular tube and concluded that a rising Hall and ion-slip parameter contributes to enhancement in hemodynamical quantities such as linear and angular velocity, rate of fluid flow and flow impedance. The impact of heat transfer and the isothermal permeable nature of walls on unsteady oscillatory flow of two-immiscible fluids through horizontal channel was discussed by Umavathi *et al.* [102] and they found a decrement in velocity and temperature profile with increasing viscosity ratio however a growth in the above quantities is observed with rising frequency parameter. Ponalagusamy and Selvi [103] analyzed the combined effect of heat transfer and magnetic field on two-layer model of blood flow through a constricted tube by considering blood as Newtonian fluid in both the regions (core as well as plasma regions). Recently, Kumar *et al.* [104] discussed the two-fluid (micropolar-viscous) model of laminar flow through a vertical channel and analyzed the impact of micropolar fluid and heat transfer parameters on flow variables. The heat generation or absorption effects on the flow of two-immiscible fluids through porous or nonporous channel was discussed by Chamkha [105] due to presence of uniform magnetic field in the transverse direction of the flow pattern. The impact of porous medium and heat transfer parameters on the generalized plain Couette and unsteady oscillatory viscous fluid flow through composite porous medium channels with different temperatures at the walls were analyzed by Umavathi *et al.* ([106],[107]).

The two-phase flow representing the fluid-particle natural convection has wide applications in many physical and biological problems including the particle suspension model for blood flow. This motivated many researchers to work on application based problems using this approach. The steady and unsteady hydromagnetic fluid-particle flow through conduits with heat generation or absorption aspects were discussed analytically by several authors ([108]-[109]). Going through the aforementioned works and to the best of the author's knowledge, a lacunae in the existing research has been observed which may be useful in understanding the mechanical aspect of physiological systems. So far no attempt has been made in analyzing the effect of such a layer on flow variables using micropolar fluid model of blood flow. Besides this, the impact of zero and non-zero spins of the microlevel particles on the flow variables, hematocrit and Fåhræus effect under the dominance of thermal buoyancy forces has not yet been analyzed which may be important for therapeutic treatment of certain diseases involving radiation.

The present study aims to analyze the impact of glycocalyx layer near the wall and two different formulations (no-spin and no-couple stress conditions at the interface representing the zero and non-zero microrotational velocity at the interface) on three-layered model of

blood flow through porous layered tubes by taking micropolar fluid as a core region fluid. The motivation for taking micropolar fluid in this study is to analyze the impact of microlevel properties of the fluid like coupling, micro-scale parameters and an additional parameter ϕ_M on flow variables, hematocrit and Fåhræus effects. Besides the microlevel parameters, the effect of heat transfer and porous layer parameters on the above quantities is also analyzed graphically and compared with the previous works of single and two-fluid model without porous region near the tube walls.

2.1 Problem Formulation

The physical model concerns an axially symmetric, laminar, incompressible, steady and fully developed flow of blood through a heated circular blood vessel as shown in Figure2.1.

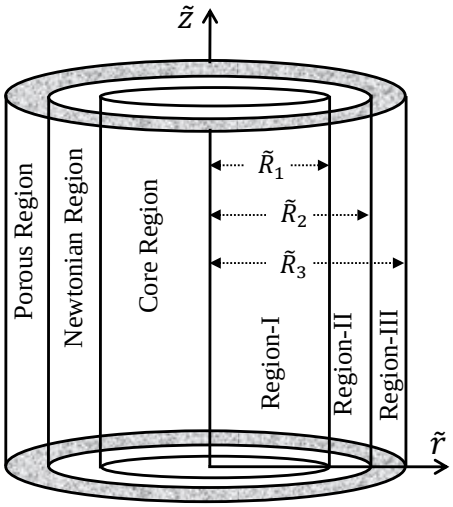

Figure 2.1: The schematic diagram of the microvessel model description for two-fluid model incorporating a thin endothelial glycocalyx layer adjacent to the microvessel wall

$\widetilde{R}_1, \widetilde{R}_2, \widetilde{R}_3$ are the radii of the central, intermediate and porous regions of blood vessel, respectively. The flow of blood is taken as two-fluid model. It is assumed that blood in the core region is micropolar fluid and in the plasma region, it is Newtonian fluid. An external magnetic field $\vec{B}$ of a uniform strength $|\vec{B}| = \widetilde{B}$ is applied in the transverse direction of the flow. The induced magnetic field and Hall effect of hydromagnetic flow are assumed to be neglected due to very small magnetic Reynolds number. The wall of blood vessel is composed by a thin Brinkman layer. We shall use the cylindrical polar coordinate system $(\widetilde{r}, \widetilde{\phi}, \widetilde{z})$, where $\widetilde{r}, \widetilde{z}$ are the radial and axial coordinates, respectively and the origin is situated on the vessel axis. The microrotational vector of the micropolar fluid in the core is given by $(0, \widetilde{\Omega}_M, 0)$. The flow in all the regions is assumed to be driven by the constant pressure gradient $(-\frac{\partial \widetilde{p}}{\partial \widetilde{z}} = p_s)$. The boundary condition for temperature on the wall is isothermal

condition.

The governing equations for the above problem will be:

Region- I, i.e. $0 < \widetilde{r} \leq \widetilde{R}_1$

$$\frac{\partial \widetilde{w}_M}{\partial \widetilde{z}} = 0, \tag{2.1a}$$

$$\frac{\partial \widetilde{p}_M}{\partial \widetilde{r}} = 0, \tag{2.1b}$$

$$-\frac{\partial \widetilde{p}_M}{\partial \widetilde{z}} + \frac{(\widetilde{\mu}_M + \widetilde{\kappa}_M)}{\widetilde{r}} \frac{\partial}{\partial \widetilde{r}} \left(\widetilde{r} \frac{\partial \widetilde{w}_M}{\partial \widetilde{r}} \right) + \frac{2\widetilde{\kappa}_M}{\widetilde{r}} \frac{\partial (\widetilde{r}\widetilde{\Omega}_M)}{\partial \widetilde{r}} - \widetilde{\sigma}_M \widetilde{B}^2 \widetilde{w}_M + \widetilde{g}\widetilde{\rho}_M \widetilde{\gamma}(\widetilde{T}_M - \widetilde{T}_\infty) = 0, \tag{2.1c}$$

$$(\widetilde{\lambda}_M + \widetilde{\zeta}_M) \left(\frac{\partial}{\partial \widetilde{r}} \left(\frac{1}{\widetilde{r}} \frac{\partial}{\partial \widetilde{r}} (\widetilde{r}\widetilde{\Omega}_M) \right) \right) - 2\widetilde{\kappa}_M \left(\frac{\partial \widetilde{w}_M}{\partial \widetilde{r}} + 2\widetilde{\Omega}_M \right) = 0, \tag{2.1d}$$

$$\widetilde{K}_M \left(\frac{\partial^2 \widetilde{T}_M}{\partial \widetilde{r}^2} + \frac{1}{\widetilde{r}} \frac{\partial \widetilde{T}_M}{\partial \widetilde{r}} \right) - \frac{\partial \widetilde{q}_M}{\partial \widetilde{r}} = 0, \tag{2.1e}$$

where $\widetilde{\rho}_M, \widetilde{p}_M, \widetilde{w}_M, \widetilde{\Omega}_M, \widetilde{K}_M, \widetilde{T}_M$ are the density, pressure, axial velocity, angular velocity, thermal conductivity and temperature of blood in core region, respectively; $\widetilde{\mu}_M, \widetilde{\lambda}_M, \widetilde{\zeta}_M$ and $\widetilde{\kappa}_M$ are the viscosities of the micropolar fluid, respectively; $\widetilde{\sigma}_M$ is an electrical conductivity; $\widetilde{B}$ is an uniform magnetic field; $\widetilde{T}_\infty$ is an ambient temperature and $\widetilde{g}$ is the gravitational force.

Region- II, i.e. $\widetilde{R_1} < \widetilde{r} \leq \widetilde{R_2}$

$$\frac{\partial \widetilde{p}_N}{\partial \widetilde{r}} = 0, \tag{2.2a}$$

$$-\frac{\partial \widetilde{p}_N}{\partial \widetilde{z}} + \frac{\widetilde{\mu}_N}{\widetilde{r}} \frac{\partial}{\partial \widetilde{r}} \left(\widetilde{r} \frac{\partial \widetilde{w}_N}{\partial \widetilde{r}} \right) - \widetilde{\sigma}_N \widetilde{B}^2 \widetilde{w}_N + \widetilde{g}\widetilde{\rho}_N \widetilde{\gamma}(\widetilde{T}_N - \widetilde{T}_\infty) = 0, \tag{2.2b}$$

$$\widetilde{K}_N \left(\frac{\partial^2 \widetilde{T}_N}{\partial \widetilde{r}^2} + \frac{1}{\widetilde{r}} \frac{\partial \widetilde{T}_N}{\partial \widetilde{r}} \right) - \frac{\partial \widetilde{q}_N}{\partial \widetilde{r}} = 0, \tag{2.2c}$$

where $\widetilde{\rho}_N, \widetilde{p}_N, \widetilde{w}_N, \widetilde{\mu}_N, \widetilde{K}_N, \widetilde{T}_N, \widetilde{\sigma}_N$ are the density, pressure, axial velocity, viscosity, thermal conductivity, temperature and electrical conductivity of blood in plasma region, respectively.

Region- III, i.e. $\widetilde{R}_2 < \widetilde{r} \leq \widetilde{R}_3$

$$\frac{\partial \widetilde{p}_B}{\partial \widetilde{r}} = 0, \tag{2.3a}$$

$$-\frac{\partial \widetilde{p}_B}{\partial \widetilde{z}} + \frac{\widetilde{\mu}_E}{\widetilde{r}} \frac{\partial}{\partial \widetilde{r}} \left(\widetilde{r} \frac{\partial \widetilde{w}_B}{\partial \widetilde{r}} \right) - \frac{\widetilde{\mu}_N \widetilde{w}_B}{\widetilde{k}} - \widetilde{\sigma}_N \widetilde{B}^2 \widetilde{w}_B + \widetilde{g}\widetilde{\rho}_N \widetilde{\gamma}(\widetilde{T}_B - \widetilde{T}_\infty) = 0, \tag{2.3b}$$

$$\widetilde{K}_N \left(\frac{\partial^2 \widetilde{T}_B}{\partial \widetilde{r}^2} + \frac{1}{\widetilde{r}} \frac{\partial \widetilde{T}_B}{\partial \widetilde{r}} \right) - \frac{\partial \widetilde{q}_B}{\partial \widetilde{r}} = 0, \tag{2.3c}$$

where $\widetilde{p}_B, \widetilde{w}_B, \widetilde{\mu}_E, \widetilde{T}_B$ are the pressure, velocity, effective viscosity of porous layer, temperature of blood in porous region, respectively and $\widetilde{k}$ is the permeability constant. Many of the earlier works used the Brinkman model assuming that the fluid viscosity and the Brinkman viscosity (i.e. effective viscosity $\widetilde{\mu}_E$) to be same however in the present model, the fluid viscosity and the Brinkman viscosity are different.

Here, the radiative heat fluxes in the core and plasma regions for micropolar and Newtonian fluids may respectively be expressed as ([53], [103])

$$\frac{\partial \widetilde{q}_M}{\partial \widetilde{r}} = 4\widetilde{\alpha}_M^2(\widetilde{T}_M - \widetilde{T}_\infty), \tag{2.4a}$$

$$\frac{\partial \widetilde{q}_N}{\partial \widetilde{r}} = 4\widetilde{\alpha}_N^2(\widetilde{T}_N - \widetilde{T}_\infty), \tag{2.4b}$$

$$\frac{\partial \widetilde{q}_B}{\partial \widetilde{r}} = 4\widetilde{\alpha}_N^2(\widetilde{T}_B - \widetilde{T}_\infty), \tag{2.4c}$$

where $\widetilde{\alpha}_M$ and $\widetilde{\alpha}_N$ the mean absorption coefficients for micropolar and Newtonian fluid, respectively which are much less than unity.

The pressure gradient is taken as constant for all the regions ([91], [28], [49])

$$\frac{\partial \widetilde{p}_M}{\partial \widetilde{z}} = \frac{\partial \widetilde{p}_N}{\partial \widetilde{z}} = \frac{\partial \widetilde{p}_B}{\partial \widetilde{z}} = -\widetilde{q}_0 p_s, \tag{2.5}$$

where $\widetilde{q}_0$ is the characteristic pressure gradient and p_s is the non-dimensional pressure gradient along the axis of the vessel.

To solve the above system of Eqs. $(2.1)-(2.5)$, the following non-dimensional variables are introduced:

$$\begin{aligned}
&p_M = \frac{\widetilde{p}_M \widetilde{R}_3}{W_0 \widetilde{\mu}_N},\ p_N = \frac{\widetilde{p}_N \widetilde{R}_3}{W_0 \widetilde{\mu}_N},\ p_B = \frac{\widetilde{p}_B \widetilde{R}_3}{W_0 \widetilde{\mu}_N},\ H^2 = \frac{\widetilde{\sigma}_N \widetilde{R}_3^2 \widetilde{B}^2}{\widetilde{\mu}_N},\ H_1^2 = \frac{\mu_R H^2}{\sigma_0},\\
&r = \frac{\widetilde{r}}{\widetilde{R}_3},\ z = \frac{\widetilde{D}_m \widetilde{z}}{\widetilde{R}_3^2 W_0},\ R_1 = \frac{\widetilde{R}_1}{\widetilde{R}_3},\ R_2 = \frac{\widetilde{R}_2}{\widetilde{R}_3},\ N_1^2 = \frac{4\widetilde{R}_3^2 \widetilde{\alpha}_N^2}{\widetilde{K}_N},\ \Omega_M = \frac{\widetilde{\Omega}_M \widetilde{R}_3}{W_0},\\
&\theta_B = \frac{\widetilde{T}_B - \widetilde{T}_\infty}{\widetilde{T}_w - \widetilde{T}_\infty},\ \theta_M = \frac{\widetilde{T}_M - \widetilde{T}_\infty}{\widetilde{T}_w - \widetilde{T}_\infty},\ \theta_N = \frac{\widetilde{T}_N - \widetilde{T}_\infty}{\widetilde{T}_w - \widetilde{T}_\infty},\ k = \frac{\widetilde{k}}{\widetilde{R}_3^2},\ \lambda_1^2 = \frac{\widetilde{\mu}_E}{\widetilde{\mu}_N},\\
&Gr = \frac{\widetilde{g}\widetilde{\rho}_N \widetilde{\gamma} \widetilde{R}_3^2 (\widetilde{T}_w - \widetilde{T}_\infty)}{W_0 \widetilde{\mu}_N},\ w_M = \frac{\widetilde{w}_M}{W_0},\ w_N = \frac{\widetilde{w}_N}{W_0},\ w_B = \frac{\widetilde{w}_B}{W_0},\ W_0 = \frac{\widetilde{q}_0 \widetilde{R}_3^2}{4\widetilde{\mu}_N},\\
&\rho_0 = \frac{\widetilde{\rho}_N}{\widetilde{\rho}_M},\ K_0 = \frac{\widetilde{K}_N}{\widetilde{K}_M},\ \sigma_0 = \frac{\widetilde{\sigma}_N}{\widetilde{\sigma}_M},\ \alpha_0 = \frac{\alpha_N}{\alpha_M},\ \mu_R = \frac{\widetilde{\mu}_N}{\widetilde{\mu}_M},\ H_2^2 = \frac{1}{\lambda_1^2}\left(\frac{1}{k} + H^2\right),
\end{aligned} \tag{2.6}$$

where $\rho_0, \sigma_0, K_0, \alpha_0, \mu_R$ are the density ratio, electrical conductivity ratio, thermal conductivity ratio, mean heat absorption ratio, viscosity ratio, respectively; W_0 is the average velocity; Gr is the Grashof number; λ_1 is the viscosity ratio parameter and $\widetilde{T}_w$ is the temperature

at wall.

Using the above non-dimensional variables (2.6), the governing Eqs. $(2.1)-(2.5)$ in non-dimensional form will become:

Region- I, i.e. $0 < r \leq R_1$

$$\frac{\partial w_M}{\partial z} = 0, \tag{2.7a}$$

$$\frac{\partial p_M}{\partial r} = 0, \tag{2.7b}$$

$$4p_s(1-N)\mu_R + \frac{1}{r}\frac{\partial}{\partial r}\left(r\frac{\partial w_M}{\partial r}\right) + \frac{2N}{r}\frac{\partial}{\partial r}\left(r\frac{\partial \Phi_M}{\partial r}\right) - (1-N)H_1^2 w_M + \frac{\mu_R Gr(1-N)}{\rho_0}\theta_M = 0, \tag{2.7c}$$

$$\frac{\partial}{\partial r}\left(\frac{1}{r}\frac{\partial}{\partial r}\left(r\frac{\partial \Phi_M}{\partial r}\right) - \frac{N}{2n^2(1-N)}\left(w_M + 2\Phi_M\right)\right) = 0 \tag{2.7d}$$

$$\frac{\partial^2 \theta_M}{\partial r^2} + \frac{1}{r}\frac{\partial \theta_M}{\partial r} + \frac{N_1^2 K_0}{\alpha_0^2}\theta_M = 0, \tag{2.7e}$$

where $N = \frac{\widetilde{\kappa}_M}{\widetilde{\kappa}_M + \widetilde{\mu}_M}$ is known as coupling parameter which demonstrates the rotational effects of micropolar particles; $n^2 = \frac{\widetilde{\lambda}_M + \widetilde{\zeta}_M}{4\widetilde{\mu}_M \widetilde{R}_3^2}$ is a micro-scale parameter (particle size); $H_1^2 = \frac{\mu_R H^2}{\sigma_0}$ is a magnetic number; $N_1^2 = \frac{4\widetilde{R}_3^2 \widetilde{\alpha}_N^2}{\widetilde{\kappa}_N}$ is the radiation parameter and the angular velocity is taken as $\Omega_M = \frac{d\Phi_M}{dr}$.

Region- II, i.e. $R_1 < r \leq R_2$

$$\frac{\partial p_N}{\partial r} = 0, \tag{2.8a}$$

$$4p_s + \frac{1}{r}\frac{\partial}{\partial r}\left(r\frac{\partial w_N}{\partial r}\right) - H^2 w_N + Gr\theta_N = 0, \tag{2.8b}$$

$$\frac{\partial^2 \theta_N}{\partial r^2} + \frac{1}{r}\frac{\partial \theta_N}{\partial r} + N_1^2 \theta_N = 0. \tag{2.8c}$$

Region- III, i.e. $R_2 < r \leq 1$

$$\frac{\partial p_B}{\partial r} = 0, \tag{2.9a}$$

$$4p_s + \frac{\lambda_1^2}{r}\frac{\partial}{\partial r}\left(r\frac{\partial w_B}{\partial r}\right) - \left(\frac{1}{k} + H^2\right)w_B + Gr\theta_B = 0, \tag{2.9b}$$

$$\frac{\partial^2 \theta_B}{\partial r^2} + \frac{1}{r}\frac{\partial \theta_B}{\partial r} + N_1^2 \theta_B = 0. \tag{2.9c}$$

The dimensionless boundary conditions are given as follows:

1. The conditions for velocity, angular velocity and temperature on the axis have been considered as

$$\frac{\partial w_M}{\partial r} = 0, \;\; \Omega_M = 0 \;\text{ and }\; \frac{\partial \theta_M}{\partial r} = 0 \quad \text{at} \quad r = 0. \tag{2.10a}$$

2. Continuity of velocity at micropolar-Newtonian fluid interface and Newtonian fluid-porous interface i.e.

$$w_M = w_N \quad \text{at} \quad r = R_1, \tag{2.10b}$$

$$w_N = w_B \quad \text{at} \quad r = R_2. \tag{2.10c}$$

3. Continuity of shear stresses at micropolar and Newtonian fluid interface, i.e.

$$\frac{1}{(1-N)}\frac{\partial w_M}{\partial r} + \frac{N}{(1-N)}\Omega_M(r) = \mu_R \frac{\partial w_N}{\partial r} \quad \text{at} \quad r = R_1. \tag{2.10d}$$

4. No spin condition at the micropolar-Newtonian fluid interface, i.e.

$$\Omega_M(r) = 0, \;\; \text{at} \;\; r = R_1. \tag{2.10e}$$

The physical interpretation of the above condition represents the zero angular velocity at the micropolar-Newtonian interface i.e. the movement of the molecules without micro-rotation.

5. No couple stress condition at micropolar-Newtonian fluid interface, i.e

$$\frac{\partial \Omega_M(r)}{\partial r} - \frac{\phi_M}{r}\Omega_M(r) = 0, \;\; \text{at} \;\; r = R_1, \tag{2.10f}$$

where $\phi_M = \frac{(\widetilde{\lambda}_M - \widetilde{\zeta}_M)}{(\widetilde{\lambda}_M + \widetilde{\zeta}_M)}$ is an additional parameter that demonstrates the constraints on viscosity coefficient can vary in the interval $[-1, 1]$ ([22]). The parameter ϕ_M is introduced as the non-symmetric couple stress tensor do not reduce the dimensional form of the boundary conditions $(2.10d)$ and $(2.10f)$ in terms of microlevel parameters N and n. The situation $\widetilde{\lambda}_M = \widetilde{\zeta}_M$ is of great significance as it makes the boundary condition $(2.10f)$ and hence the solution of the problem independent of the flexibility parameter $\widetilde{\lambda}_M$ and $\widetilde{\zeta}_M$. The physical interpretation of the above condition represents the non-zero angular velocity at the micropolar-Newtonian interface i.e. the movement of the molecules with non-zero micro-rotation.

6. Continuity of temperature at micropolar-Newtonian fluid interface and Newtonian fluid-porous interface i.e.

$$\theta_M = \theta_N, \quad \frac{\partial \theta_M}{\partial r} = K_0 \frac{\partial \theta_N}{\partial r} \quad \text{at} \quad r = R_1, \tag{2.10g}$$

$$\theta_N = \theta_B, \quad \frac{\partial \theta_N}{\partial r} = \frac{\partial \theta_B}{\partial r} \quad \text{at} \quad r = R_2. \tag{2.10h}$$

7. The stress jump condition of tangential stress at Newtonian fluid and porous interface ([1], [97]), i.e.

$$\frac{1}{\alpha_p}\frac{\partial w_B}{\partial r} - \frac{\partial w_N}{\partial r} = \frac{\beta_S}{\sqrt{k}} w_B \quad \text{at} \quad r = R_2, \tag{2.10i}$$

where α_p is the porosity parameter and β_S is stress jump parameter.

8. Isothermal condition for temperature and no-slip condition for velocity at the wall, i.e.

$$w_B = 0, \quad \theta_B = 1 \quad \text{at} \quad r = 1. \tag{2.10j}$$

The rate of fluid flow Q_s in non-dimensional form is given by ([91], [28], [49])

$$\begin{aligned} Q_s &= 8\int_0^1 r w(r) dr, \\ &= 8\left(\int_0^{R_1} r w_M dr + \int_{R_1}^{R_2} r w_N dr + \int_{R_2}^1 r w_B dr\right). \end{aligned} \tag{2.11}$$

The frictional resistance λ_s per unit length of the tube is given by ([91], [28], [49])

$$\lambda_s = \frac{p_s}{Q_s}. \tag{2.12}$$

The fraction of volume occupied by red blood cells (RBCs) and total volume of the blood is defined as hematocrit (Ht) i.e. volume concentration of RBCs in whole blood ([47], [49], [51])

$$Ht = \frac{\int_0^{R_1} C_v(r) w_M(r) dr}{\int_0^{R_3} r w(r) dr}, \tag{2.13}$$

where $C_v(r)$ is the concentration profile of the RBCs

$$C_v(r) = \frac{c_v}{R_1^2}(R_1^2 - r^2) H(R_1 - r) H(r), \tag{2.14}$$

where $H(r)$ is Heaviside unit function and c_v is constant in concentration relation.

The ratio of tube hematocrit H_T to discharge hematocrit H_D is defined as Fåhræus effect Fe which is expressed as below ([3], [49])

$$Fe = \frac{H_T}{H_D} = \frac{\bar{W}}{W_{rbc}}, \tag{2.15}$$

where $\bar{W}$ is the average velocity flowing through the tube and W_{rbc} is the velocity of the red blood cells (RBCs).

2.2 Solution of the Problem

The momentum and energy equations $(2.7)-(2.9)$ are solved subject to the boundary and interface conditions Eq. (2.10) for the velocity and temperature distributions. The transformed governing equations under the assumptions mentioned in problem formulation section are coupled system of linear ordinary differential equations. Solving the Eqs. $(2.7)-(2.9)$, we get the following:
The temperature and velocity profiles for micropolar fluid are obtained as below

$$\theta_M = C_1 J_0(N_2 r) + C_2 Y_0(N_2 r), \tag{2.16a}$$

$$w_M = C_3 I_0(\alpha_1 r) + C_4 K_0(\alpha_1 r) + C_5 I_0(\alpha_2 r) + C_6 K_0(\alpha_2 r) + \frac{4 p_s \mu_R}{H_1^2} + \left(\frac{\mu_R Gr C_1}{\rho_0}\right)\left(\frac{N_2^2(1-N)n^2+N}{n^2}\right)\left(\frac{J_0(N_2 r)}{\left(\alpha_1^2+N_2^2\right)\left(\alpha_2^2+N_2^2\right)}\right), \tag{2.16b}$$

and angular velocity Ω_M is obtained using the expressions $(2.16a)-(2.16b)$ of axial velocity and temperature profile

$$\Omega_M = \frac{n^2(1-N)}{2N^2}\left((1-N)H_1^2\frac{dw_M}{dr} - \frac{d(D^2 w_M)}{dr}\right) - \frac{1}{2}\frac{dw_M}{dr} + \left(\frac{n^2(1-N)}{2N^2}\right)\left(\frac{\mu_R Gr(1-N)C_1 N_2}{\rho_0}\right) J_1(N_2 r),$$

$$\Omega_M = \frac{1}{2N^2}\left(\frac{1}{n^2\rho_0\left(\alpha_1^2+N_2^2\right)\left(\alpha_2^2+N_2^2\right)}\right.$$
$$\left(C_1 Gr\mu_R N_2 J_1(N_2 r)\left(H_1^2 n^2(N-1)^2\left(n^2N_2^2(N-1)-N\right)\right.\right.$$
$$\left.+n^4(N-1)^2\left(\alpha_2^2\left(\alpha_1^2+N_2^2\right)+\alpha_1^2N_2^2\right)\right) - n^2N_2^2(N-1)^2N + N^3\Big)$$
$$+\alpha_1\left(H_1^2n^2(N-1)^2 + \alpha_1^2n^2(N-1) - N^2\right)\left(C_3 I_1(r\alpha_1) - C_4 K_1(r\alpha_1)\right)$$

$$+\alpha_2\left(H_1^2n^2(N-1)^2+\alpha_2^2n^2(N-1)-N^2\right)\left(C_5I_1(r\alpha_2)-C_6K_1(r\alpha_2)\right)\Big), \tag{2.16c}$$

where $D^2=\frac{1}{r}\frac{d}{dr}\left(r\frac{d}{dr}\right)$ is a differential operator and $N_2=\frac{N_1^2K_0}{\alpha_0^2}$. The parameters α_1 and α_2 are defined in this form

$$\begin{aligned}\alpha_1^2+\alpha_2^2&=(1-N)H_1^2+\frac{N}{n^2},\\ \alpha_1^2\alpha_2^2&=\frac{NH_1^2}{n^2}.\end{aligned} \tag{2.17}$$

The temperature and velocity profiles for Newtonian fluid are obtained as below

$$\theta_N=C_7J_0(N_1r)+C_8Y_0(N_1r), \tag{2.18a}$$

$$w_N=C_9I_0(Hr)+C_{10}K_0(Hr)+\frac{Gr}{H^2+N_1^2}(C_7J_0(N_1r)+C_8Y_0(N_1r))+\frac{4p_s}{H^2}. \tag{2.18b}$$

The temperature and velocity profiles for Brinkman region are obtained as below

$$\theta_B=C_{11}J_0(N_1r)+C_{12}Y_0(N_1r), \tag{2.19a}$$

$$\begin{aligned}w_B=&C_{13}I_0(H_2r)+C_{14}K_0(H_2r)+\frac{4p_s}{H_2^2\lambda_1^2}\\&+\frac{Gr}{\lambda_1^2\left(H_2^2+N_1^2\right)}(C_{11}J_0(N_1r)+C_{12}Y_0(N_1r)),\end{aligned} \tag{2.19b}$$

where $H_2^2=\frac{1}{\lambda_1^2}\left(\frac{1}{k}+H^2\right)$. Using the boundary conditions $(2.10a)-(2.10j)$, the constants C_1-C_{14} are evaluated through MATHEMATICA 10.0.2 but the due to large expressions, these are not mentioned here.

2.3 Results and Discussion

The present study is the first attempt to perform a comparative analysis between no-couple stress and no-spin formulation of three-layered fluid flow through a tube with a glycocalyx (porous) layer near wall by taking micropolar fluid in the core region. The selection of micropolar fluid play an important role to understand circulation process of fluid in microvessels with the microrotation property of the fluid molecules. The present model reduces to two-fluid model (Newtonian fluid in core as well as the plasma regions) for $N\to 0$. The effect of various parameters like radiation parameter, coupling number, Hartmann number, thermal conductivity, Grashof number, viscosity ratio and microrotation parameter of the fluid particles on flow variables, hematocrit and Fåhræus effect are depicted pictorially

and compared with previous studies. We have fixed the values of following parameters $\sigma_0 = \alpha_0 = \rho_0 = c_v = 1, \beta_S = 0.5, k = 5, h = 0.05$ throughout the analysis.

The range of values of various parameters is taken from the previous studies to perform the graphical analysis is given in Table 2.1.

Parametric values		
Parameters	Values	Resources
Absorption ratio α_0	1.00	[103]
Coupling parameter N	$0 \leq N < 1$	[22], [68], [21]
Density ratio ρ_0	0.92-1.00	[34], [103]
Grashof number Gr	0.5-17	[41], [45], [103]
Hartmann number H	0.1-4.0	[68], [21], [103]
Micro-scale parameter n	$[0, \infty)$	[22], [23]
Parameter ϕ_M	$-1 \leq \phi_M \leq 1$	[22], [23]
Plasma layer thickness h	0.015-0.05	[110], [28], [49]
Radiation parameter N_1	2-15	[53], [103]
Steady pressure gradient p_s	1-10	[91], [28], [49]
Stress jump parameter β_S	$-1 \leq \beta_S \leq 1$	[49], [51], [68]
Thermal conductivity ratio K_0	0.4-1.0	[103], [104]
Viscosity ratio μ_R	0.5-1.0	[68], [103]
Viscosity ratio parameter λ_1	1.0-1.6	[49], [51]

Table 2.1: The range of parameters appropriate for flow through narrow tubes with their resources

2.3.1 Velocity Profile

The velocity profile w with radial distance r for different thermal conductivity ratio K_0 is depicted in Figure 2.2:(a) representing a slight dominance of no-couple stress (NCS) formulation over no-spin condition (NS). This can be explained from the fact that a reduced angular velocity at the interface for no-spin formulation leads to reduction in linear (axial)

velocity. This observation is in agreement with the previous work of Khanukaeva *et al.* [22] although in that case the basic model was different. Rising velocity due to growth in conductivity ratio K_0 is validating the finding of Ponalagusamy and Selvi [103] for Newtonian fluid as coupling parameter N is taken very small.

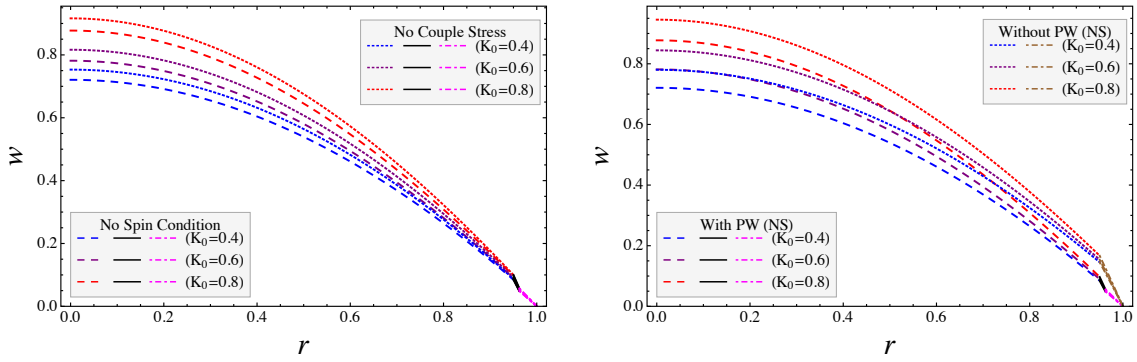

(a) **(b)**

Figure 2.2: Impact of conductivity ratio K_0 on velocity profile w varying with radial distance r under **(a)** the different interface conditions $(\phi_M = 0.5)$ and **(b)** TFM with and without porous walls. $(H = \mu_R = 0.5, n = 0.2, N = 0.1, p_s = 1, N_1 = 2, Gr = \lambda_1 = 1.5)$

A noteworthy observation is that rising conductivity ratio K_0 leads to slightly higher difference between the two formulations (no-spin and no-couple stress conditions) which may be acredited to the dependence of microrotation vector on thermal conductivity. A comparative analysis of velocity profile between tubes with and without porous layer near the wall for no-spin condition is depicted in Figure 2.2:(b). The difference in fluid velocities in tubes with and without porous region near the wall slightly widen with the increase in thermal conductivity ratio K_0.

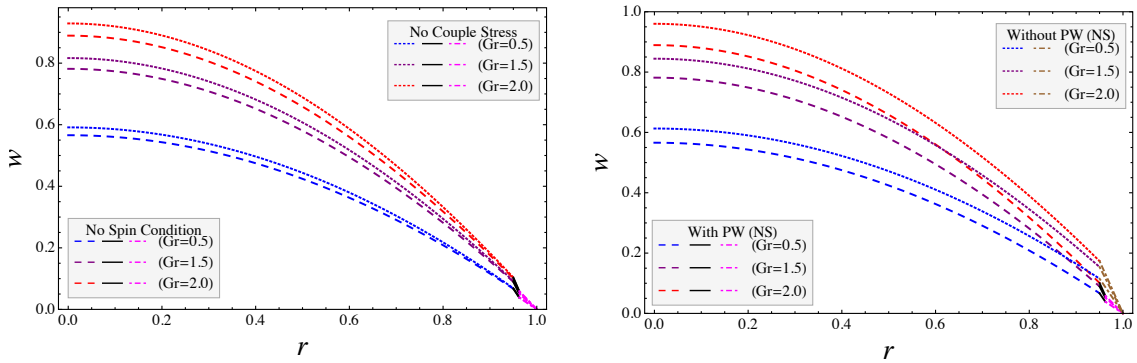

(a) **(b)**

Figure 2.3: Impact of Grashof number Gr on velocity profile w varying with radial distance r under **(a)** the different interface conditions $(\phi_M = 0.5)$ and **(b)** TFM with and without porous walls. $(H = \mu_R = 0.5, n = 0.2, N = 0.1, p_s = 1, N_1 = 2, K_0 = 0.6, \lambda_1 = 1.5)$

The effect of thermal buoyancy and viscous forces on the velocity profile for two different interface boundary conditions (no-spin and no-couple stress) has been done in Figure 2.3:(a). The graphical analysis reveals that the difference in the fluid velocity for the two formulations slightly increases with the dominance of the thermal buoyancy forces showing that heat transfer aspect also affects the microlevel effects. A similar observation has been made in Figure 2.3:(b) depicting widening of difference in velocity profile for fluid flow in tubes with and without PW under the dominance of the thermal buoyancy forces (with increase in Grashof number Gr) over viscous forces.

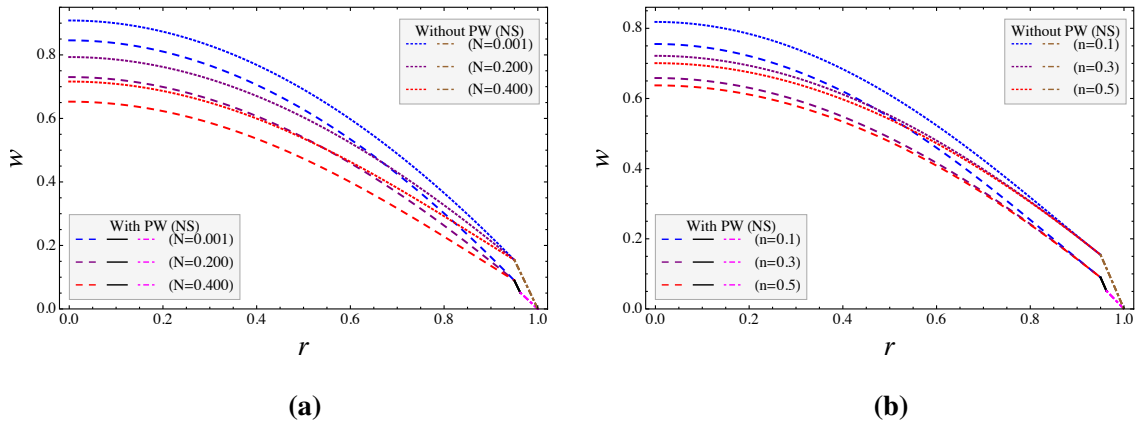

Figure 2.4: Velocity profile w varying with radial distance r influenced by **(a)** coupling number N $(n = 0.2)$ and **(b)** micro-scale parameter n $(N = 0.3)$. $(H = \mu_R = 0.5, p_s = 1, N_1 = 2, K_0 = 0.6, \lambda_1 = Gr = 1.5)$

A rising coupling number N leads to significant decay in axial (linear) velocity w depicted in Figure 2.4:(a) which signifies that a dominance of microlevel parameters leads to significant reduction in axial velocity w. The effect of micro-scale parameter n on the axial velocity w for flow in tubes with and without PW under no-spin condition reveals a significant decay in the fluid velocity with growing micro-scale parameter n (Figure 2.4:(b)). Besides this, it also reveals the diminishing difference in fluid velocity for flow through tubes with and without PW. The conclusion suggests a relatively larger fluid velocity in tubes without glycocalyx layer and for relatively lesser micro-scale parameter n (smaller particle size).

Figure 2.5:(a) represents the profile of angular velocity Ω_M for both the formulations under different thermal conductivity ratio K_0. Vanishing of the angular velocity Ω_M at the interface (micropolar-Newtonian fluid interface) leads to a relatively smaller value of angular velocity for no-spin condition in comparison to the values of no-couple stress condition. It is perceived that the larger values of K_0 affect the angular velocity more significantly for no-couple stress formulation in comparison to the no-spin condition. Another observation is

that for no-spin condition, the effects of K_0 are at its peak in the middle while for no-couple stress condition, this effect continuously increased till the interface.

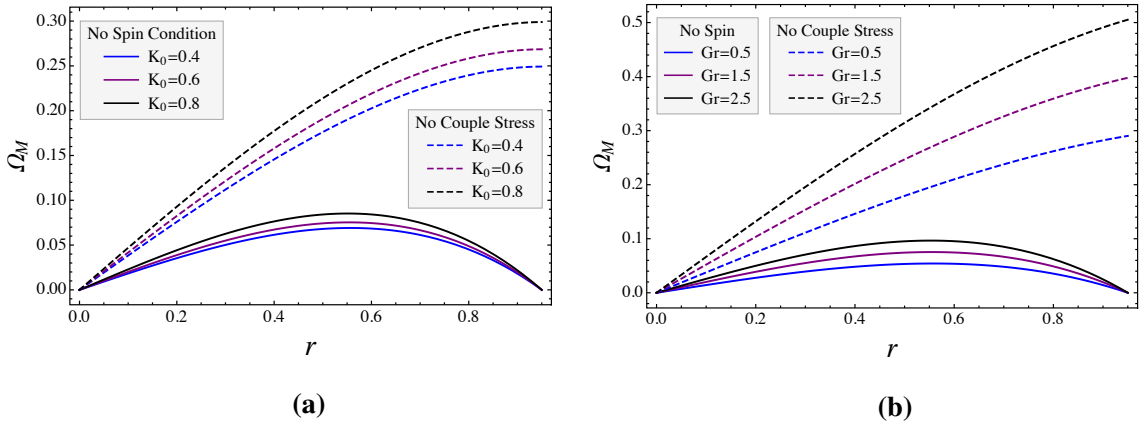

(a) **(b)**

Figure 2.5: Angular velocity Ω_M varying with radial distance r influenced by **(a)** conductivity ratio K_0 $(\phi_M = 0.01, Gr = 1.5)$ and **(b)** Grashof number Gr $(\phi_M = 0.5, K_0 = 0.6)$. $(H = \mu_R = 0.5, n = 0.2, p_s = 1, N_1 = 2, N = 0.1, \lambda_1 = 1.5)$

Figure 2.5:(b) reveals that the dominance of thermal buoyancy forces over the viscous forces leads to slight increase in angular velocity for no-spin condition. However, the same leads to significant growth in angular velocity for no-couple stress condition. Therefore Figures 2.5:(a) and 2.5:(b) reveal that the heat transfer aspect significantly affects the angular velocity for no-couple stress formulation in comparison to no-spin condition. In comparison to axial velocity profiles, we observe a relatively significant difference in the angular velocity between two formulations owing to the involvement of angular velocity Ω_M in formulating the condition at the interface. For a different model an almost similar observation was concluded by Khanukaeva *et al.* [22].

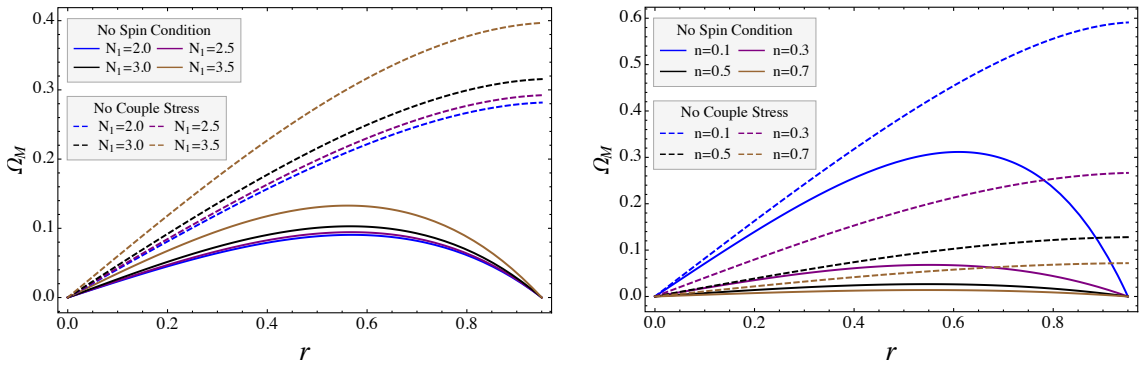

(a) **(b)**

Figure 2.6: Angular velocity Ω_M varying with radial distance r influenced by **(a)** radiation parameter N_1 $(n = 0.2, K_0 = 0.3, Gr = 0.5)$ and **(b)** micro-scale parameter n $(N_1 = 2.0, K_0 = 0.6, Gr = 1.5)$. $(H = \mu_R = 0.5, N = 0.2, p_s = 1, \lambda_1 = 1.5, \phi_M = 0.1)$

Rise in radiation parameter N_1 leads to growth in angular velocity Ω_M for both the formulations as depicted in Figure 2.6:(a). A noteworthy observation is that beyond a specific value $(N_1 = 3.0)$, the radiation parameter N_1 significantly increases the angular velocity. This reveals that the larger the rate at which the heat conduction is transferred to the thermal radiation, the more change will take place in angular velocity and the same leads to changes in micro-scale properties of the fluid motion. The effect of micro-scale parameter n on angular velocity Ω_M is shown in Figure 2.6:(b) which clearly indicates that smaller the particle size (micro-scale parameter $n = 0.1$), the larger will be angular velocity for both the formulations. This effect gradually reduces upon increase in the particle size.

2.3.2 Flow Rate

Figure 2.7:(a) depicts a decreasing flow rate Q_s with Hartmann number H for both the formulations under different thermal conductivity ratio K_0. This observation is in agreement with the results of Jaiswal and Yadav [68]. A new observation is that this decay rate is slightly higher for no-couple stress formulation owing to higher linear velocity for no-couple stress condition. The difference in the flow rate Q_s for both the formulations is significantly reduced for large Hartmann number (i.e. higher magnetic field). A comparative analysis of flow rate Q_s variation with Hartmann number H for flow through tubes with and without PW reveals a significantly higher flow rate for the latter case. Besides this, the decay rate is also slightly higher for the flow through tube without PW as evident from the Figure 2.7:(b).

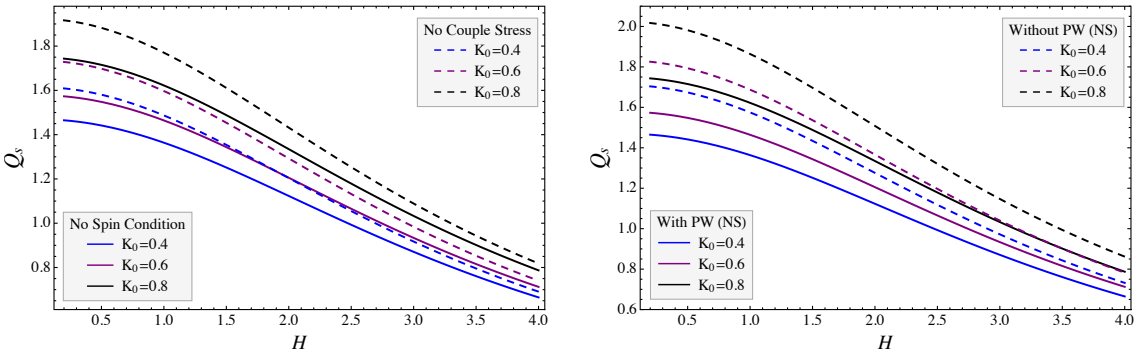

(a) **(b)**

Figure 2.7: Impact of conductivity ratio K_0 on flow rate Q_s varying with Hartmann number H under **(a)** different interface conditions $(\phi_M = 1.0)$ and **(b)** TFM with and without PW. $(\mu_R = 0.5, n = 5, p_s = 1, N_1 = 2, N = 0.1, \lambda_1 = Gr = 1.5)$

A comparison between two-fluid model with and without porous region near the tube wall and single-fluid model without PW is being pictorially depicted in Figure 2.8:(a). The flow rate Q_s increases with the Grashof number Gr for flow through tubes with and without PW as evident from the Figure 2.8:(a). It is perceived that the growth rate of Q_s is higher for

flow through tube without PW; however, this value as well as the growth rate significantly decays with rise in the coupling parameter N. This decay can be justified from the fact that a rising coupling parameter N leads to higher coefficient of microrotational viscosities and hence microlevel effects which further slows down the fluid flow.

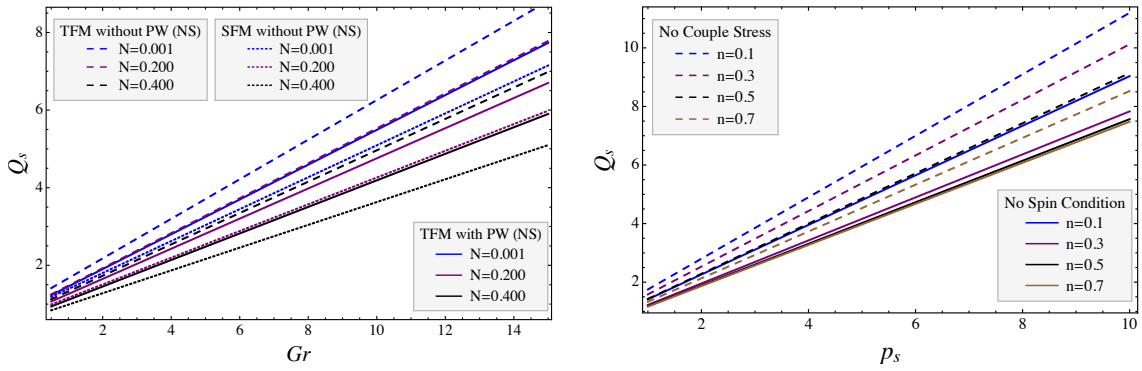

(a) **(b)**

Figure 2.8: Flow rate Q_s influenced by **(a)** Grashof number Gr for different values of coupling parameter N $(n = 0.2, p_s = 1)$ and **(b)** pressure gradient p_s for different values of micro-scale parameter n $(N = 0.4, Gr = 1.5)$. $(H = \mu_R = \phi_M = 0.5, K_0 = 0.6, N_1 = 2, \lambda_1 = 1.5)$

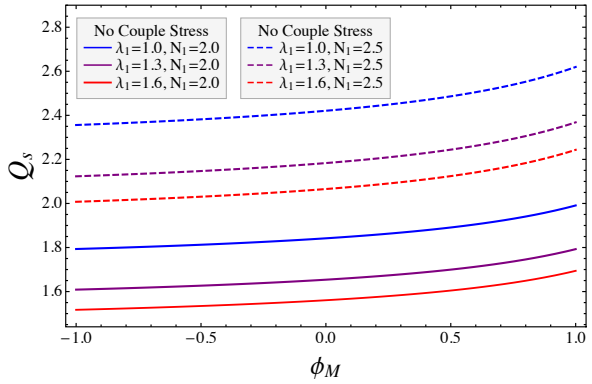

Figure 2.9: Flow rate Q_s varying with parameter ϕ_M influenced by radiation parameter N_1 and viscosity ratio parameter λ_1. $(\mu_R = H = 0.5, p_s = 1, K_0 = 0.6, Gr = 1.5, N = n = 0.2)$

This observation clearly shows that the microlevel effects significantly affect the effect of thermal buoyancy forces on the flow rate. The present study is reduced to SFM without PW for plasma layer thickness $(h = 0)$. This specific case is used to validate our study with previous works ([56]-[57]). Variation of the flow rate Q_s with the pressure gradient p_s for both the formulations under varying micro-scale parameter n is depicted in Figure 2.8:(b). It is perceived that the flow rate linearly increases with the pressure gradient p_s but the growth rate consistently decays with increase in the micro-scale parameter owing to an increased particle size which results in lowering the flow rate. A novel observation is that the difference in no-couple stress and no-spin formulations significantly widens at higher

pressure gradient and lower particle size $(n = 0.1)$. Besides this, the growth rate for Q_s is significantly higher for no-couple stress condition in comparison to no-spin condition.

Figure 2.9 reveals that flow rate uniformly increases with parameter ϕ_M for different viscosity ratio parameter λ_1 and radiation parameter N_1 which is in agreement with a different model of Khanukaeva *et al.* [22].

2.3.3 Flow Resistance

The decay of flow resistance λ_s with decreasing Hartmann number H and increasing thermal conductivity ratio K_0 is in agreement with previously established results ([68], [21]) as evident from the Figure 2.10:(a).

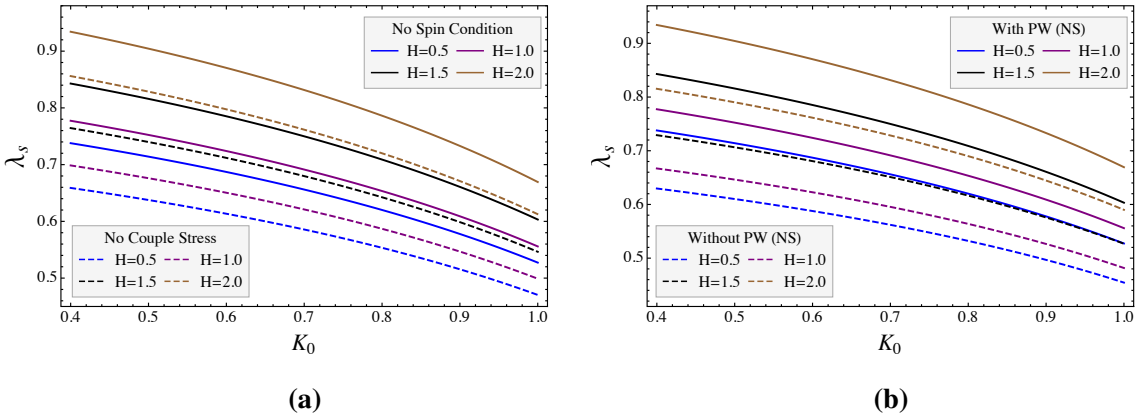

(a) **(b)**

Figure 2.10: Impact of Hartmann number H on flow resistance λ_s varying with conductivity ratio K_0 under **(a)** two different interface conditions and **(b)** TFM with and without PW. $(\mu_R = \phi_M = 0.5, p_s = 1, n = N = 0.2, Gr = \lambda_1 = 1.5, N_1 = 2)$

A novel observation is that the decay rate of flow resistance λ_s with K_0 is slightly higher for no-spin condition in comparison to no-couple stress condition. From Figure 2.10:(b), a similar observation is reported in comparative analysis of variation of λ_s with K_0 between flow through tubes with and without porous region near the tube walls under no-spin condition. It is evident that for flow through tube with PW, the flow resistance λ_s as well as its decay rate with K_0 is higher.

A comparison between two-fluid model with and without porous region near the tube wall and single-fluid model without PW is being graphically demonstrated in Figure 2.11:(a). A rising coupling parameter (i.e. microlevel effects) leads to significant increase in flow resistance λ_s as evident from the Figure 2.11:(a) however, this growth rate significantly reduces with the dominance of thermal buoyancy forces over viscous forces. The above observation concludes that a rising coupling parameter N leads to rise in coefficient of microrotation viscosity which further enhances the obstruction against the flow but it is seen that this effect is significantly reduced in case of enhancement in temperature.

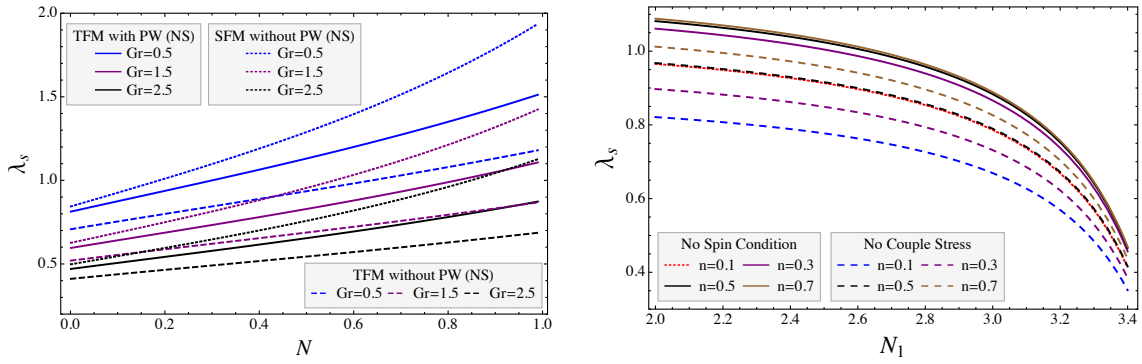

(a) **(b)**

Figure 2.11: Flow resistance λ_s influenced by **(a)** coupling parameter $(0.001 \leq N \leq 0.99)$ for different values of Grashof number Gr $(n = 0.2, K_0 = 0.6, N_1 = 2)$ and **(b)** radiation parameter N_1 for different values of micro-scale parameter n $(N = 0.3, Gr = 0.5, K_0 = 0.4)$. $(\mu_R = H = \phi_M = 0.5, p_s = 1, \lambda_1 = 1.5)$

The present study is reduced to SFM without PW for plasma layer thickness $(h = 0)$. This specific case is used to validate our study with previous works ([56]-[57]). From Figure 2.11:(b), a comparative analysis of λ_s with radiation parameter N_1 for both the formulations reveals a significant decay in flow resistance with increasing radiation parameter N_1. While a slight change in λ_s is reported for no-spin condition under the increasing micro-scale parameters, this change is significant for no-couple stress condition. It is evident that the micro-scale parameter is more effective in no-couple stress formulation due to presence of flexibility parameter in the solution.

2.3.4 Hematocrit (Ht)

Effect of Hartmann number H, conductivity ratio K_0 for both the formulations (no-spin and no-couple stress conditions) and for flow through tubes with and without PW have been depicted in Figure 2.12. A rising Hartmann number H leads to decay in the hematocrit Ht with a slightly higher decay rate for no-couple stress condition and this decay rate further reduces for higher K_0. For all possible values of K_0, the hematocrit Ht is slightly higher for no-couple stress formulation (Figure 2.12:(a)). It is also reported by analysing Figure 2.12:(b) that flow through tube with PW has significantly higher hematocrit Ht in comparison to flow through tube without PW which may be accredited to a reduced flow resistance λ_s and hence smooth flow through tubes. A reduced decay rate for Ht is reported for higher K_0 in both cases.

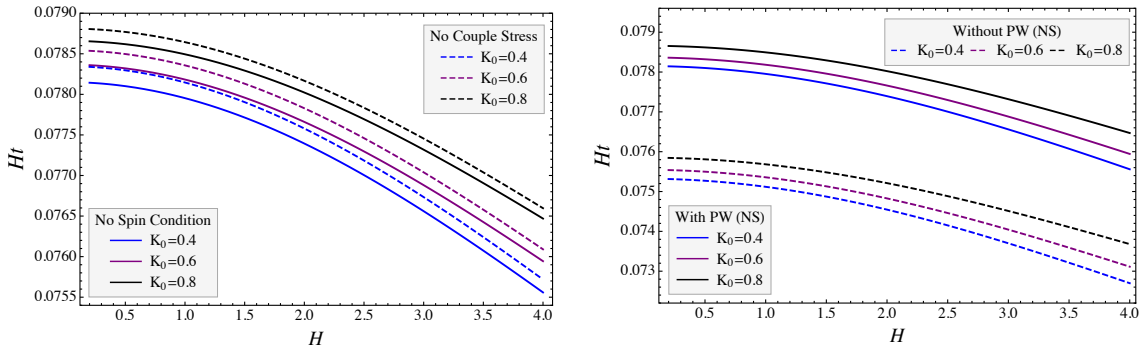

(a) **(b)**

Figure 2.12: Impact of conductivity ratio K_0 on hematocrit Ht varying with Hartmann number H under **(a)** different interface conditions ($\phi_M = 1.0$) and **(b)** TFM with and without PW. ($\mu_R = 0.5, n = 5, p_s = c_v = 1, N_1 = 2, N = 0.1, \lambda_1 = Gr = 1.5$)

A slight growth followed by an almost steady plot for Ht is reported in Figure 2.13:(a) with increasing Grashof number Gr showing that the Ht is almost independent of the thermal buoyancy forces when it significantly dominates the viscous forces (higher Grashof number Gr). This observation is same for flow through tubes with and without PW. It is also observed that a rising coupling parameter N affects the Ht more significantly in flow through tube without PW in comparison to flow through tube with PW. A similar observation is reported for hematocrit variation with thermal buoyancy forces under different micro-scale parameter. As evident from the Figure 2.13:(b), the hematocrit assumes higher values for flow through tube with porous region near the tube wall in comparison to the flow through the tube without porous region near the tube wall. A rising micro-scale parameter leads to decay in hematocrit for larger particle size.

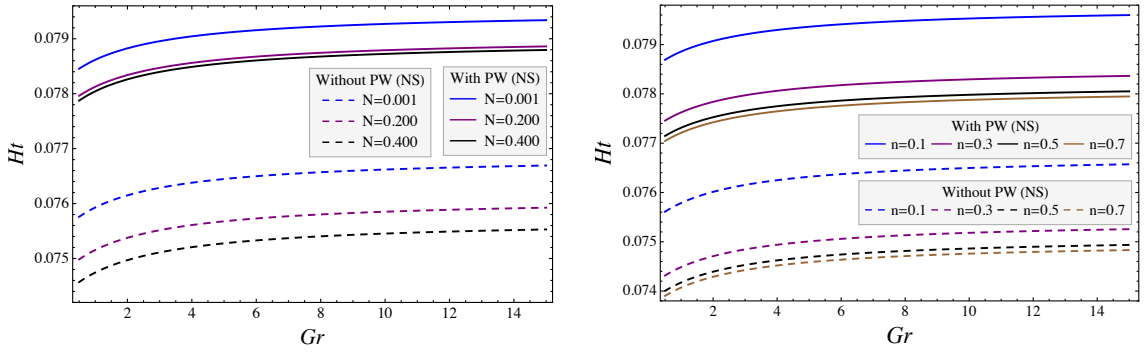

(a) **(b)**

Figure 2.13: Hematocrit Ht varying with Grashof number Gr influenced by **(a)** coupling parameter N ($n = 0.2$) and **(b)** micro-scale parameter n ($N = 0.3$). ($H = \mu_R = 0.5, c_v = p_s = 1, N_1 = 2, K_0 = 0.6, \lambda_1 = 1.5$)

A rising viscosity ratio parameter λ_1 leads to rise in hematocrit Ht which is in good agreement with our previous work [49] for viscoelastic fluid (Figure 2.14:(a)).An increase

in the viscosity ratio μ_R $(=\widetilde{\mu}_N/\widetilde{\mu}_M)$ leads to a significant rise in Ht which is more significant for high porosity glycocalyx layer. This can be justified due to a relative increase in Newtonian viscosity causing reduced plasma flow and hence a higher RBCs concentration. Besides this, a rising radiation parameter N_1 leads to rise in hematocrit Ht. This can be justified as the rising radiation parameter N_1 leads to higher transfer rate from heat energy to radiation leading to reduced temperature profile which further reduces the effect of thermal buoyancy forces leading to a decay in flow rate and hence growth in concentration. This rising concentration of RBCs leads to growth in hematocrit Ht. From the Figure 2.14:(b), an almost similar observation is reported for variation of Ht with radiation parameter N_1 for both the formulations.

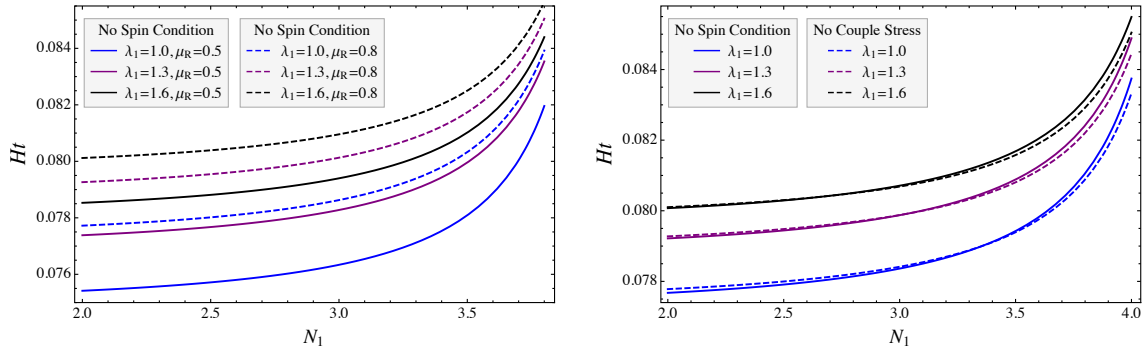

(a) **(b)**

Figure 2.14: Hematocrit Ht varying with radiation parameter N_1 influenced by **(a)** viscosity ratio parameter λ_1 and viscosity ratio μ_R and **(b)** between two interface conditions $(\mu_R = 0.8)$. $(H = 0.5, c_v = p_s = \phi_M = 1, K_0 = 0.35, Gr = 1.5, N = 0.1, n = 0.2)$

2.3.5 Fåhræus Effect (Fe)

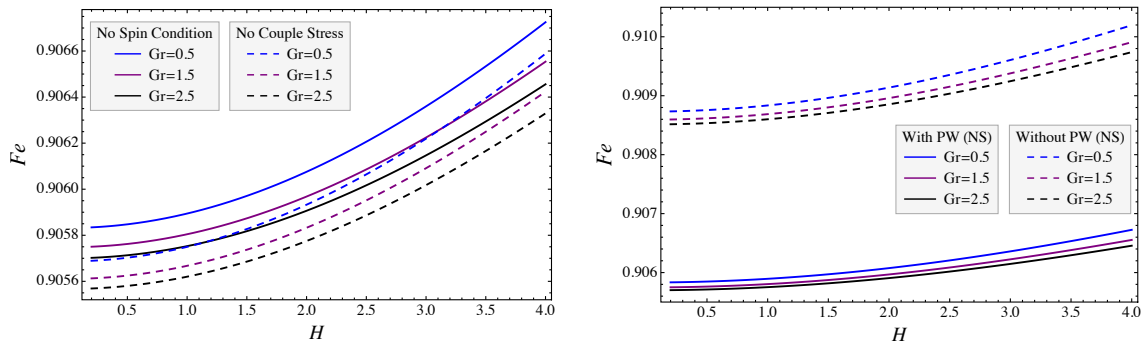

(a) **(b)**

Figure 2.15: Impact of Grashof number Gr on Fåhræus effect Fe varying with Hartmann number H between **(a)**two interface conditions and **(b)** TFM with and without PW. $(\mu_R = 0.5, n = 5, p_s = \phi_M = 1, K_0 = 0.6, \lambda_1 = 1.5, N = 0.1, N_1 = 2)$

A significant growth in Fåhræus effect Fe is reported in Figure 2.15:(a) for rising Hartmann number H owing to decay in the hematocrit and hence RBCs concentration in the core region. A noteworthy observation is that a rising Grashof number Gr leads to decay in Fe in both the formulations. A similar observation is reported in Figure 2.15:(b) for comparative analysis of Fåhræus effect between flow through tubes with and without porous region near the tube walls. An existence of a porous layer near the wall causes obstruction in flow of plasma leading towards enhanced RBCs concentration and hence the hematocrit which further reduces the Fåhræus effect Fe.

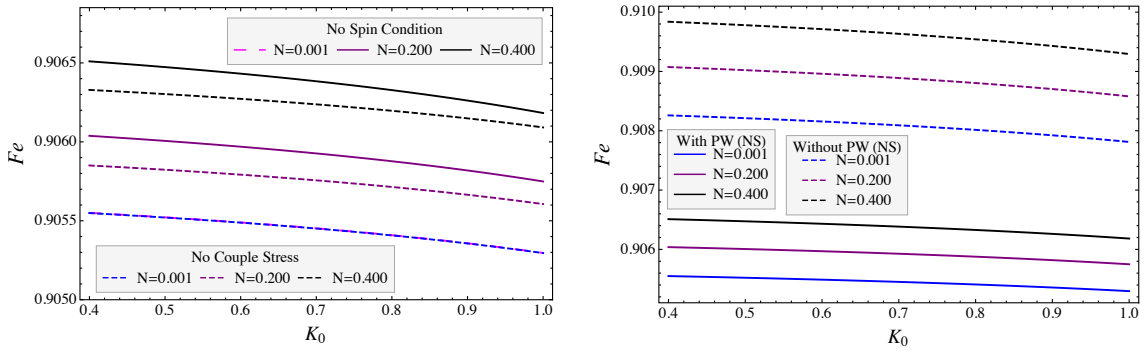

(a) **(b)**

Figure 2.16: Impact of coupling parameter N on Fåhræus effect Fe varying with conductivity ratio K_0 between **(a)** two interface conditions and **(b)** TFM with and without PW. $(H = \mu_R = 0.5, n = 0.2, p_s = \phi_M = 1, \lambda_1 = Gr = 1.5, N_1 = 2)$

A rising conductivity ratio K_0 leads to decay in the Fåhræus effect Fe for both the formulations as evident from the Figure 2.16:(a).

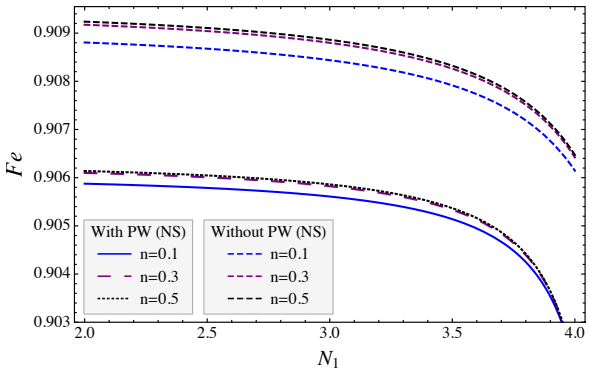

Figure 2.17: Fåhræus effect Fe varying with radiation parameter N_1 for different values of micro-scale parameter n between TFM with and without PW. $(\mu_R = H = 0.5, p_s = 1, K_0 = 0.4, Gr = \lambda_1 = 1.5, N = 0.2)$

The difference in both the formulations widen as the coupling parameter N increases leading to dominance of microlevel effects for small K_0. A similar observation is reported in Figure 2.16:(b) revealing a relatively strong effect of microlevel parameters on the Fåhræus

effect for the flow through tube without PW in comparison to the flow through tube with PW.

Decay in the Fåhræus effect with the radiation parameter N_1 is shown in the Figure 2.17 for the flow through tubes with and without porous region near the tube wall. It is evident that the transformation of heat energy into the radiation at a larger rate leads to decay in Fe. Besides this, a rise in micro-scale parameter (particle size) leads to growth in Fe however further increasing particle size has an insignificant impact on the Fåhræus effect Fe.

2.4 Conclusions

The present study is a novel approach to examine a comparative analysis between two different formulations (no-spin and no-couple stress conditions) on the flow of micropolar fluid through a glycocalyx layered microvessel under the heat transfer approach. No-spin and no-couple stress conditions represent the zero and non-zero angular velocities at the interface (micropolar-Newtonian fluid interface i.e. R_1). The dependencies of the hemodynamical quantities, hematocrit and Fåhræus effect on the microlevel properties of the micopolar fluid, porous layer, heat transfer parameters are analyzed and compared with flow through tubes with and without porous walls for two different formulations (no-spin and no-couple stress conditions). Throughout the whole discussions, the following main outcomes as conclusions have been made:

1. A slight dominance of no-couple stress formulation over the no-spin condition on the hemodynamical quantities such as axial and angular velocity, flow rate and hematocrit is observed; however, no-spin formulation dominates the no-couple stress condition on the flow resistance and Fåhræus effect for the fixed values of the other parameters.

2. Most of the important flow variables are significantly affected by the microlevel parameters, which includes a significant reduction in velocity, flow rate and hematocrit while the same leads to growth in flow resistance and Fåhræus effect.

3. A novel observation is that the heat transfer parameters such as Grashof number, thermal conductivity ratio and radiation parameter significantly affect the hematocrit and Fåhræus effect.

4. A reduction in volume concentration of RBCs in whole blood (hematocrit) is observed with rising magnetic field for both the formulations and also found that the hematocrit is slightly lower for no-spin condition; however, a significant growth in Fåhræus effect is reported with increase in magnetic field.

5. A relatively thick plasma (increasing viscosity ratio μ_R) leads to higher hematocrit Ht and slightly lesser effect of radiation parameter N_1 on hematocrit Ht.

The present study is a theoretical attempt to conclude a significant impact of heat transfer parameters, porous layer parameters and two different formulations on flow quantities, hematocrit and Fåhræus effect, which need to be experimentally verified. The outcomes can be used for the treatment of the various diseases like cancer or malignant tumor in the medical sciences, which involve temperature variation or applying magnetic field.

Chapter 3

Solute Dispersion into Microcirculation Influenced by EGL, Erythrocyte Structure and Heat Transfer Aspect

3.1 Introduction

The wall of the blood vessel plays a major barrier in the transportation of materials between blood and tissues in the circulation through microvessels (arterioles, venules, and capillaries). The study of the mass transport in the microcirculation is the primary concern with a physiological mechanism involving the transportation of metabolites and catabolites across the wall of the capillary tube. The physical behavior of mass transportation involves smooth exchange of metabolism, respiratory gases, nutrients, and catabolites through vessel walls during the diffusion process. Large numbers of practical situations of heat and mass transfer involve interphase mass transport such as open tube chromatography, thermal pollution in natural streams, etc. Sankarasubramanian and Gill [2] studied the theory of the exchangeable interphase mass transportation due to the first-order reactive wall to analyze the solute dispersion process in a tube by using the "*generalized dispersion model*". The inclusion of the first-order boundary reaction leads to the rise of a new term "*exchange coefficient*" reflecting the inter-phase mass transportation.

All the above investigations concerned the effect of various hemodynamical parameters on Newtonian fluid flow through larger diameter tube, but due to different circumstances like shape and size of the blood vessels, blood behaves like non-Newtonian fluids. Adopting the presumption of wall reactions (reversible or irreversible boundary reactions), several authors ([87], [88], [89]) analyzed the impact of first-order wall reaction on solute dispersion in a non-Newtonian fluid flow through circular vessels. Recently, Rana and Murthy

[2]This work has been published as **P.D. Shah, A. Tiwari and S.S. Chauhan,"Solute dispersion in Micropolar-Newtonian fluid flowing through porous layered tubes with absorbing walls",** ***International Communications in Heat and Mass Transfer*** **119 (2020) 104724.**

([111], [112]) studied the longitudinal dispersion of a solute in non-Newtonian (Casson and Herschel-Bulkley) fluids flowing through small blood vessels with absorbing wall and the flow was driven by the periodic pressure gradient. They observed the effect of various parameters like the Womersley parameter, wall absorption parameter, Herschel-Bulkley fluid (HB) parameter, and amplitude of the periodic pressure gradient on the whole dispersion process. Roy *et al.* [113] employed the homogenization method to study the average of mass transport phenomenon by considering nonlinear chemical decay within the bulk flow for reversible/irreversible reactions at the annular tube wall.

While dispersion can be applied to understand the transportation of drugs to tissues, various clinical treatments involve a slight rise in temperature or use of radiation and it is an interesting problem to mathematically analyze its impact on circulation or transport of nutrients to our tissues. In recent times, due to rising pollution and significantly increasing toxic materials in our surroundings, the human being is severely suffering from cancer or malignant tumor and the researchers made an effort to treat such kind of diseases through mathematical modeling with experimental experience. The heat transfer aspect has been used to generate the radiation into the forefront of the infected area. The absorbed energy leads to a rise in the temperature around the infected area without damaging any healthy tissues. Chamkha *et al.* ([56], [57]) presented numerical and analytical solutions of the fully developed laminar free and mixed convection of a micropolar fluid in a vertical channel with asymmetrical distribution of temperature at the wall. Many authors ([114], [41], [45]) covered the heat transfer aspect in their studies on the flow of fluid through conduits with constriction. Misra *et al.* [115] calculated the flow of blood through blood vessels during electromagnetic hyperthermia and therapeutic procedure for cancer or malignant tumor. Mekheimer and Abd Elmaboud [42] analyzed the combined effect of heat transfer and magnetic field on the circulation of Newtonian fluid flowing through the vertical annulus and the governing equations were solved under the assumptions of long wavelength approximations and zero Reynolds number. The steady and unsteady laminar MHD flows and heat generation/absorption aspects through homogeneous porous channels were discussed by Chamkha ([55], [100]) in which the induced magnetic field and Hall effect of hydromagnetic flow are assumed to be neglected due to very small magnetic Reynolds number.

Many authors also covered the other aspects of Soret and Dufour effects, natural or mixed convection on heat and mass transfer in flow through tubes or channels. In the presence or absence of heat generation or absorption and first-order chemical reaction effects, an analytical study of steady and oscillatory flow was carried out by Modather *et al.* [116] and Magyari and Chamkha [117], for the combined aspects of heat and mass transfer by natural convection of micropolar, viscous fluid flow near a continuously moving vertical

permeable infinitely long surface. To motivate future experimental work, a numerical investigation was undertaken by Chamkha and Rashad [118], which examined the transfer of heat and mass by mixed convection flow of MHD under the influence of first-order chemical reaction, magnetic field, Soret, and Dufour effects over a rotating vertical cone. In the presence of heat generation or absorption and natural convection effects, Chamkha [105] obtained an analytical solution of the steady, hydromagnetic, fully developed flow of two viscous immiscible fluids through a vertical impermeable channel filled with or without the homogeneous porous medium. Ponalagusamy and Selvi [103] analyzed the combined effect of heat transfer and magnetic field on a two-layer model of blood flow through a constricted tube by considering blood as Newtonian fluid in both the regions (core as well as plasma regions). Ghalambaz *et al.* [119] pioneered the study investigating the suspension and heat transfer behavior of NEPCM nanoparticles and concluded that they circulate with free convection in the cavity. Shashikumar *et al.* [120] explored the influence of nanoparticles shape on the flow of viscous fluid through microchannel under the impact of magnetism and radiation while considering convection and partial slipping at the boundary. Ayoubloo *et al.* [121] analyzed the unsteady flow of free convection behavior of non-Newtonian power-law fluid through a co-axial cylindrical pipe with a thin layer of homogeneous porous medium adjacent to the inner cylindrical tube.

The transportation of the solvent material of drugs or toxins in a two-fluid model of blood flowing through porous layered small blood vessels has been studied in the present work. Two-fluid model for blood flow through small blood vessels has been taken in which the central region is occupied by the micropolar fluid and a plasma layer surrounded over the central region occupied is by Newtonian fluid. A thin porous layer near the wall of the blood vessel is considered, which is governed by the Brinkman equation and the transportation of lipoprotein through the intimal of vessel wall tissue has been analyzed. The heat transfer approach has also been considered due to more realistic phenomena for the complex physiological system of the human body. Analytical expressions for axial velocities and microrotational velocity for micropolar fluid and temperature profiles have been obtained in terms of Bessel functions and the concentration equation for the solute is solved by the series expansion method of Sankarasubramanian and Gill [2]. The effect of numerous parameters on diffusion coefficients and mean concentration are depicted graphically and compared with the previous works.

3.2 Problem Formulation

Steady, incompressible blood flowing through the blood vessel is assumed to be axially symmetric, laminar, and fully developed as shown in Figure 3.1. As the study suggests ([27], [28]), for a more realistic representation of the blood flow in a microvessel, the two-fluid approach is employed. In the present study, microscopic effects due to local behavior and micro-motion of the suspended blood particles like RBCs, WBCs, and platelets are taken into account by assuming blood as a micropolar fluid in the core region and the nature of cell-free blood plasma is exhibited as Newtonian fluid in the peripheral region. The peripheral layer of plasma is divided into two regions (intermediate and porous regions) and both regions are occupied by Newtonian fluid. A thin Brinkman layer mathematically replicates the mechanical aspects of an endothelial glycocalyx layer near the wall. Considering magnetic Reynolds numbers to be very small, there exists a negligible Hall Effect of MHD flow and weak induced magnetic field, hence both should be neglected ([55], [100]). The cylindrical polar coordinate system with origin on the vessel axis has been adopted. Vector representation for the micro-rotation of the blood particles thorough the core is denoted by $(0,\widetilde{\Omega}_M,0)$. The pressure gradient advancing the flow through both regions is assumed to be constant [49]. The exchange of heat at the boundary has not been taken into consideration (isothermal condition). The existence of clinical procedures under the external magnetic field compels to apply the uniform magnetic field $|\vec{B}| = \widetilde{B}$ on the flow by an external source in the transverse direction in the present work [122]. Following the above hypothesis, the governing equations for the above problem are described below:

Region- I, i.e., $0 < \widetilde{r} \leq \widetilde{R}_1$

$$\frac{\partial \widetilde{w}_M}{\partial \widetilde{z}} = 0, \tag{3.1a}$$

$$\frac{\partial \widetilde{p}_M}{\partial \widetilde{r}} = 0, \tag{3.1b}$$

$$-\frac{\partial \widetilde{p}_M}{\partial \widetilde{z}} + \frac{(\widetilde{\mu}_M + \widetilde{\kappa}_M)}{\widetilde{r}} \frac{\partial}{\partial \widetilde{r}} \left(\widetilde{r} \frac{\partial \widetilde{w}_M}{\partial \widetilde{r}} \right) + \frac{2\widetilde{\kappa}_M}{\widetilde{r}} \frac{\partial (\widetilde{r}\widetilde{\Omega}_M)}{\partial \widetilde{r}} - \widetilde{\sigma}_M \widetilde{B}^2 \widetilde{w}_M + \widetilde{g}\widetilde{\rho}_M \widetilde{\gamma}(\widetilde{T}_M - \widetilde{T}_\infty) = 0, \tag{3.1c}$$

$$(\widetilde{\lambda}_M + \widetilde{\zeta}_M) \left(\frac{\partial}{\partial \widetilde{r}} \left(\frac{1}{\widetilde{r}} \frac{\partial}{\partial \widetilde{r}} (\widetilde{r}\widetilde{\Omega}_M) \right) \right) - 2\widetilde{\kappa}_M \left(\frac{\partial \widetilde{w}_M}{\partial \widetilde{r}} + 2\widetilde{\Omega}_M \right) = 0, \tag{3.1d}$$

$$\widetilde{K}_M \left(\frac{\partial^2 \widetilde{T}_M}{\partial \widetilde{r}^2} + \frac{1}{\widetilde{r}} \frac{\partial \widetilde{T}_M}{\partial \widetilde{r}} \right) - \frac{\partial \widetilde{q}_M}{\partial \widetilde{r}} = 0, \tag{3.1e}$$

where $\widetilde{\rho}_M, \widetilde{p}_M, \widetilde{w}_M, \widetilde{\Omega}_M, \widetilde{K}_M, \widetilde{T}_M, \widetilde{\sigma}_M$ are the density, pressure, axial velocity, angular velocity, thermal conductivity, temperature and electrical conductivity of blood in the core region,

respectively; $\widetilde{\mu}_M, \widetilde{\lambda}_M, \widetilde{\zeta}_M$ and $\widetilde{\kappa}_M$ are the viscosities of the micropolar fluid, respectively; $\widetilde{T}_\infty$ is an ambient temperature, $\widetilde{g}$ is the gravitational force and $\widetilde{B}$ is a uniform magnetic field.

Region- II, i.e., $\widetilde{R}_1 < \widetilde{r} \leq \widetilde{R}_2$

$$\frac{\partial \widetilde{w}_N}{\partial \widetilde{z}} = 0, \tag{3.2a}$$

$$\frac{\partial \widetilde{p}_N}{\partial \widetilde{r}} = 0, \tag{3.2b}$$

$$-\frac{\partial \widetilde{p}_N}{\partial \widetilde{z}} + \frac{\widetilde{\mu}_N}{\widetilde{r}} \frac{\partial}{\partial \widetilde{r}} \left(\widetilde{r} \frac{\partial \widetilde{w}_N}{\partial \widetilde{r}} \right) - \widetilde{\sigma}_N \widetilde{B}^2 \widetilde{w}_N + \widetilde{g} \widetilde{\rho}_N \widetilde{\gamma} (\widetilde{T}_N - \widetilde{T}_\infty) = 0, \tag{3.2c}$$

$$\widetilde{K}_N \left(\frac{\partial^2 \widetilde{T}_N}{\partial \widetilde{r}^2} + \frac{1}{\widetilde{r}} \frac{\partial \widetilde{T}_N}{\partial \widetilde{r}} \right) - \frac{\partial \widetilde{q}_N}{\partial \widetilde{r}} = 0, \tag{3.2d}$$

where $\widetilde{\rho}_N, \widetilde{p}_N, \widetilde{w}_N, \widetilde{\mu}_N, \widetilde{K}_N, \widetilde{T}_N, \widetilde{\sigma}_N$ are the density, pressure, axial velocity, viscosity, thermal conductivity, temperature and electrical conductivity of blood in the plasma region, respectively.

Brinkman [95] formulation has been used to model the flow through porous media. Region- III, i.e., $\widetilde{R}_2 < \widetilde{r} \leq \widetilde{R}_3$

$$\frac{\partial \widetilde{w}_B}{\partial \widetilde{z}} = 0, \tag{3.3a}$$

$$\frac{\partial \widetilde{p}_B}{\partial \widetilde{r}} = 0, \tag{3.3b}$$

$$-\frac{\partial \widetilde{p}_B}{\partial \widetilde{z}} + \frac{\widetilde{\mu}_E}{\widetilde{r}} \frac{\partial}{\partial \widetilde{r}} \left(\widetilde{r} \frac{\partial \widetilde{w}_B}{\partial \widetilde{r}} \right) - \frac{\widetilde{\mu}_N \widetilde{w}_B}{\widetilde{k}} - \widetilde{\sigma}_N \widetilde{B}^2 \widetilde{w}_B + \widetilde{g} \widetilde{\rho}_N \widetilde{\gamma} (\widetilde{T}_B - \widetilde{T}_\infty) = 0, \tag{3.3c}$$

$$\widetilde{K}_N \left(\frac{\partial^2 \widetilde{T}_B}{\partial \widetilde{r}^2} + \frac{1}{\widetilde{r}} \frac{\partial \widetilde{T}_B}{\partial \widetilde{r}} \right) - \frac{\partial \widetilde{q}_B}{\partial \widetilde{r}} = 0, \tag{3.3d}$$

where $\widetilde{p}_B, \widetilde{w}_B, \widetilde{\mu}_E, \widetilde{T}_B$ are the pressure, velocity, effective viscosity of porous layer, temperature of blood in porous region, respectively and $\widetilde{k}$ is the permeability constant.

The radiative heat fluxes in the core and plasma regions for micropolar and Newtonian fluids may respectively be expressed as ([114], [103])

$$\frac{\partial \widetilde{q}_M}{\partial \widetilde{r}} = 4 \widetilde{\alpha}_M^2 (\widetilde{T}_M - \widetilde{T}_\infty), \tag{3.4a}$$

$$\frac{\partial \widetilde{q}_N}{\partial \widetilde{r}} = 4 \widetilde{\alpha}_N^2 (\widetilde{T}_N - \widetilde{T}_\infty), \tag{3.4b}$$

$$\frac{\partial \widetilde{q}_B}{\partial \widetilde{r}} = 4 \widetilde{\alpha}_N^2 (\widetilde{T}_B - \widetilde{T}_\infty), \tag{3.4c}$$

where $\widetilde{\alpha}_M$ and $\widetilde{\alpha}_N$ are the mean radiation absorption coefficients for micropolar and New-

tonian fluids, respectively which are much less than unity.

The pressure gradient is taken as constant for all the regions ([28], [122])

$$\frac{\partial \widetilde{p}_M}{\partial \widetilde{z}} = \frac{\partial \widetilde{p}_N}{\partial \widetilde{z}} = \frac{\partial \widetilde{p}_B}{\partial \widetilde{z}} = -\widetilde{q}_0 p_s, \tag{3.5}$$

where $\widetilde{q}_0$ is the characteristic pressure gradient and p_s is the pressure gradient for steady flow.

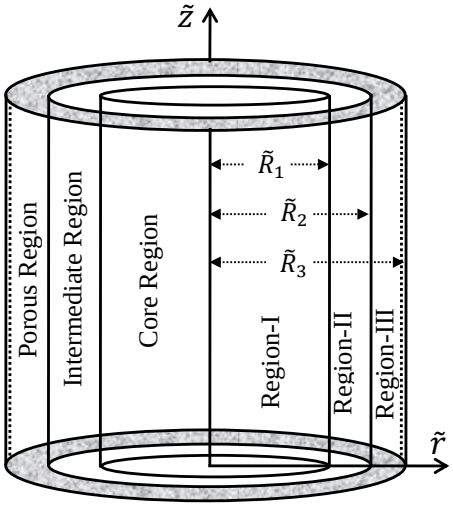

Figure 3.1: The schematic diagram of the three-layered liquid model for having a thin endothelial glycocalyx layer adjacent to the absorbing microvessel wall

The physical sketch of the three-layered liquid model with absorbing walls is presented in Figure 3.1, where $\widetilde{R}_1, \widetilde{R}_2, \widetilde{R}_3$ are the radii of the central, intermediate and porous regions of blood vessel, respectively. As depicted in Figure 3.1, micropolar fluid exhibiting micro-rotational behavior of the cell, a dense fragment of blood that flows through the central passage of the vessel denoted by Region-I. The endothelial glycocalyx layer at the vessel wall is replicated as the porous layer at the boundary of the cylindrical tube and identified as Region-III. The cell-free fragment of blood functions as Newtonian fluid and known as plasma that flows through both Region-II and Region-III.

To solve the above system of Eqs. $(3.1) - (3.5)$, the following non-dimensional variables are introduced:

$$
\begin{aligned}
p_M &= \frac{\widetilde{p}_M \widetilde{R}_3}{W_0 \widetilde{\mu}_N},\ p_N = \frac{\widetilde{p}_N \widetilde{R}_3}{W_0 \widetilde{\mu}_N},\ p_B = \frac{\widetilde{p}_B \widetilde{R}_3}{W_0 \widetilde{\mu}_N},\ H^2 = \frac{\widetilde{\sigma}_N \widetilde{R}_3^2 \widetilde{B}^2}{\widetilde{\mu}_N},\ H_1^2 = \frac{\mu_R H^2}{\sigma_0}, \\
r &= \frac{\widetilde{r}}{\widetilde{R}_3},\ z = \frac{\widetilde{D}_m \widetilde{z}}{\widetilde{R}_3^2 W_0},\ R_1 = \frac{\widetilde{R}_1}{\widetilde{R}_3},\ R_2 = \frac{\widetilde{R}_2}{\widetilde{R}_3},\ N_1^2 = \frac{4\widetilde{R}_3^2 \widetilde{\alpha}_N^2}{\widetilde{K}_N},\ \Omega_M = \frac{\widetilde{\Omega}_M \widetilde{R}_3}{W_0}, \\
\theta_B &= \frac{\widetilde{T}_B - \widetilde{T}_\infty}{\widetilde{T}_w - \widetilde{T}_\infty},\ \theta_M = \frac{\widetilde{T}_M - \widetilde{T}_\infty}{\widetilde{T}_w - \widetilde{T}_\infty},\ \theta_N = \frac{\widetilde{T}_N - \widetilde{T}_\infty}{\widetilde{T}_w - \widetilde{T}_\infty},\ k = \frac{\widetilde{k}}{\widetilde{R}_3^2},\ \lambda_1^2 = \frac{\widetilde{\mu}_E}{\widetilde{\mu}_N}, \\
Gr &= \frac{\widetilde{g}\widetilde{\rho}_N \widetilde{\gamma} \widetilde{R}_3^2 (\widetilde{T}_w - \widetilde{T}_\infty)}{W_0 \widetilde{\mu}_N},\ w_M = \frac{\widetilde{w}_M}{W_0},\ w_N = \frac{\widetilde{w}_N}{W_0},\ w_B = \frac{\widetilde{w}_B}{W_0},\ W_0 = \frac{\widetilde{q}_0 \widetilde{R}_3^2}{4\widetilde{\mu}_N}, \\
\rho_0 &= \frac{\widetilde{\rho}_N}{\widetilde{\rho}_M},\ K_0 = \frac{\widetilde{K}_N}{\widetilde{K}_M},\ \sigma_0 = \frac{\widetilde{\sigma}_N}{\widetilde{\sigma}_M},\ \alpha_0 = \frac{\alpha_N}{\alpha_M},\ \mu_R = \frac{\widetilde{\mu}_N}{\widetilde{\mu}_M},\ H_2^2 = \frac{1}{\lambda_1^2}\left(\frac{1}{k} + H^2\right),
\end{aligned}
\tag{3.6}
$$

where $\rho_0, \sigma_0, K_0, \alpha_0, \mu_R$ are the density ratio, electrical conductivity ratio, thermal conductivity ratio, mean heat absorption ratio, viscosity ratio respectively; W_0 is the characteristic velocity, Gr is the Grashof number, λ_1 is the viscosity ratio parameter and $\widetilde{T}_w$ is the temperature at wall.

Using the above non-dimensional variables (3.6), the governing equations in the non-dimensional form will become for different regions

Region- I, i.e., $0 < r \leq R_1$

$$\frac{\partial w_M}{\partial z} = 0, \tag{3.7a}$$

$$\frac{\partial p_M}{\partial r} = 0, \tag{3.7b}$$

$$4p_s(1-N)\mu_R + D^2 w_M + 2ND^2\Phi_M - (1-N)H_1^2 w_M + \frac{\mu_R Gr(1-N)}{\rho_0}\theta_M = 0, \tag{3.7c}$$

$$\frac{\partial}{\partial r}\left(D^2\Phi_M - \frac{N}{2n^2(1-N)}\left(w_M + 2\Phi_M\right)\right) = 0 \tag{3.7d}$$

$$D^2\theta_M + \frac{N_1^2 K_0}{\alpha_0^2}\theta_M = 0, \tag{3.7e}$$

where $D^2 = \frac{1}{r}\frac{\partial}{\partial r}\left(r\frac{\partial}{\partial r}\right)$ is a differential operator, $N = \frac{\widetilde{\kappa}_M}{\widetilde{\kappa}_M + \widetilde{\mu}_M}$ is known as coupling parameter which demonstrates the rotation effects of micropolar particles, $n^2 = \frac{\widetilde{\lambda}_M + \widetilde{\zeta}_M}{4\widetilde{\mu}_M \widetilde{R}_3^2}$ is a micropolar (micro-scale) parameter, $H_1^2 = \frac{\mu_R H^2}{\sigma_0}$ is a magnetic number, $N_1^2 = \frac{4\widetilde{R}_3^2 \widetilde{\alpha}_N^2}{\widetilde{\kappa}_N}$ is the radiation parameter and the angular velocity is taken as $\Omega_M = \frac{\partial \Phi_M}{\partial r}$.

Region- II, i.e., $R_1 < r \leq R_2$

$$\frac{\partial w_N}{\partial z} = 0, \tag{3.8a}$$

$$\frac{\partial p_N}{\partial r} = 0, \tag{3.8b}$$

$$4p_s + D^2 w_N - H^2 w_N + Gr\theta_N = 0, \tag{3.8c}$$

$$D^2\theta_N + N_1^2\theta_N = 0, \tag{3.8d}$$

Region- III, i.e., $R_2 < r \leq 1$

$$\frac{\partial w_B}{\partial z} = 0, \tag{3.9a}$$

$$\frac{\partial p_B}{\partial r} = 0, \tag{3.9b}$$

$$4p_s + \lambda_1^2 D^2 w_B - \left(\frac{1}{k} + H^2\right) w_B + Gr\theta_B = 0, \tag{3.9c}$$

$$D^2\theta_B + N_1^2\theta_B = 0. \tag{3.9d}$$

The dimensionless boundary conditions are given as follows:

1. The conditions for velocity, angular velocity, and temperature on the axis have been considered as

$$\frac{\partial w_M}{\partial r} = 0, \;\; \Omega_M = 0 \;\text{ and }\; \frac{\partial \theta_M}{\partial r} = 0 \quad \text{at} \quad r = 0. \tag{3.10a}$$

2. Continuity of velocities and temperatures at the micropolar-Newtonian fluid interface and Newtonian fluid-porous interface, i.e.,

$$w_M = w_N \quad \text{at} \quad r = R_1, \tag{3.10b}$$

$$\theta_M = \theta_N, \;\; \frac{\partial \theta_M}{\partial r} = K_0 \frac{\partial \theta_N}{\partial r} \quad \text{at} \quad r = R_1, \tag{3.10c}$$

$$w_N = w_B \quad \text{at} \quad r = R_2, \tag{3.10d}$$

$$\theta_N = \theta_B, \;\; \frac{\partial \theta_N}{\partial r} = \frac{\partial \theta_B}{\partial r} \quad \text{at} \quad r = R_2. \tag{3.10e}$$

3. Continuity of shear stresses at the micropolar and Newtonian fluid interface, i.e.,

$$\frac{1}{(1-N)} \frac{\partial w_M}{\partial r} + \frac{N}{(1-N)} \Omega_M(r) = \mu_R \frac{\partial w_N}{\partial r} \quad \text{at} \quad r = R_1. \tag{3.10f}$$

4. No-spin condition at the micropolar-Newtonian fluid interface, i.e.,

$$\Omega_M(r) = 0, \quad \text{at} \quad r = R_1. \tag{3.10g}$$

5. No-couple stress condition on the micropolar-Newtonian fluid interface, i.e.,

$$\frac{\partial \Omega_M(r)}{\partial r} - \frac{\phi_M}{r}\Omega_M(r) = 0, \quad \text{at} \quad r = R_1, \tag{3.10h}$$

where $\phi_M = \frac{(\widetilde{\lambda}_M - \widetilde{\zeta}_M)}{(\widetilde{\lambda}_M + \widetilde{\zeta}_M)}$ is an additional parameter which reflects the constrains on viscosity coefficient and it can vary in the interval $[-1; 1]$ ([22], [122]).

6. The momentum transfer condition at Newtonian fluid and porous interface which is known as stress-jump condition of tangential stress [1], i.e.,

$$\frac{1}{\alpha_p}\frac{\partial w_B}{\partial r} - \frac{\partial w_N}{\partial r} = \frac{\beta_S}{\sqrt{k}} w_B \quad \text{at} \quad r = R_2, \tag{3.10i}$$

where α_p is the porosity parameter and β_S is the stress-jump parameter.

7. Isothermal and no-slip condition at the tube wall, i.e.,

$$w_B = 0, \quad \theta_B = 1 \quad \text{at} \quad r = 1. \tag{3.10j}$$

3.3 Solution of the Problem

Analytical expressions for velocity, micro-rotational velocity, and temperature profiles are obtained by solving the Eqs. $(3.7) - (3.9)$, we get the followings:
Region- I, i.e., $0 < r \leq R_1$

$$\theta_M = E_1 J_0(N_2 r) + E_2 Y_0(N_2 r), \tag{3.11a}$$

$$\begin{aligned} w_M = {} & E_3 I_0(a_1 r) + E_4 K_0(a_1 r) + E_5 I_0(a_2 r) + E_6 K_0(a_2 r) + \frac{4 p_s \mu_R}{H_1^2} \\ & + \left(\frac{\mu_R Gr E_1}{\rho_0}\right)\left(\frac{N_2^2(1-N)n^2 + N}{n^2}\right)\left(\frac{J_0(N_2 r)}{\left(a_1^2 + N_2^2\right)\left(a_2^2 + N_2^2\right)}\right), \end{aligned} \tag{3.11b}$$

$$\begin{aligned} \Omega_M = {} & \frac{1}{2N^2}\Big(\frac{1}{n^2\rho_0\left(a_1^2 + N_2^2\right)\left(a_2^2 + N_2^2\right)}\left(\mu_R E_1 Gr N_2 J_1(N_2 r)\left(H_1^2 n^2 (N-1)^2\left(n^2 N_2^2 (N-1) - N\right)\right.\right. \\ & \left. + n^4 (N-1)^2\left(a_2^2\left(a_1^2 + N_2^2\right) + a_1^2 N_2^2\right)\right) - n^2 N_2^2 (N-1)^2 N + N^3\Big) \\ & + a_1\left(H_1^2 n^2 (N-1)^2 + a_1^2 n^2 (N-1) - N^2\right)\left(E_3 I_1(a_1 r) - E_4 K_1(a_1 r)\right) \end{aligned}$$

$$+a_2\left(H_1^2n^2(N-1)^2+a_2^2n^2(N-1)-N^2\right)\left(E_5I_1(a_2r)-E_6K_1(a_2r)\right)\Big), \tag{3.11c}$$

where $N_2=\frac{N_1^2K_0}{\alpha_0^2}$ and a_1 and a_2 are defined in this form

$$\begin{aligned} a_1^2+a_2^2&=(1-N)H_1^2+\frac{N}{n^2},\\ a_1^2a_2^2&=\frac{NH_1^2}{n^2}. \end{aligned} \tag{3.12}$$

Region- II, i.e., $R_1\leq r\leq R_2$

$$\theta_N=E_7J_0(N_1r)+E_8Y_0(N_1r), \tag{3.13a}$$

$$w_N=E_9I_0(Hr)+E_{10}K_0(Hr)+\frac{Gr}{H^2+N_1^2}(E_7J_0(N_1r)+E_8Y_0(N_1r))+\frac{4p_s}{H^2}, \tag{3.13b}$$

Region- III, i.e., $R_2\leq r\leq 1$

$$\theta_B=E_{11}J_0(N_1r)+E_{12}Y_0(N_1r), \tag{3.14a}$$

$$\begin{aligned} w_B=&E_{13}I_0(H_2r)+E_{14}K_0(H_2r)+\frac{4p_s}{H_2^2\lambda_1^2}\\ &+\frac{Gr}{\lambda_1^2\left(H_2^2+N_1^2\right)}(E_{11}J_0(N_1r)+E_{12}Y_0(N_1r)), \end{aligned} \tag{3.14b}$$

where $H_2^2=\frac{1}{\lambda_1^2}\left(\frac{1}{k}+H^2\right)$. The constants E_1-E_{14} appeared in the solutions $(3.11)-(3.14)$ of the given equations are evaluated analytically through MATHEMATICA 10.0 software using the given boundary conditions (3.10). The complete expressions for velocities for different regions are not mentioned in the manuscript due to very large expressions.

3.4 Concentration Solution

3.4.1 Governing Equations

Let us consider the inoculation of the unsteady solute dispersion into the flowing stream of blood flow depicted here as a two-fluid (micropolar-Newtonian) model through a vessel of radius $\widetilde{R}_3$ with a thin porous layer near the absorbing walls. The solvent material in a blood vessel with reactive walls is delineated in Figure 3.1. The occurrence of the first-order irreversible catalytic reaction let the solvent material to be absorbed continuously with the rate of absorption proportional to the concentration of solute at the outer wall.

The dimensional form of the unsteady convective diffusion equation is written below describes the concentration $\widetilde{C}$ of the solvent material in the unidirectional steady, incompressible blood flow which assumed to be axially symmetric, laminar and fully developed through the narrow blood vessel.

$$\frac{\partial \widetilde{C}}{\partial \widetilde{t}} + \widetilde{w}(\widetilde{r})\frac{\partial \widetilde{C}}{\partial \widetilde{z}} = \widetilde{D}_m \left(\frac{1}{\widetilde{r}} \frac{\partial}{\partial \widetilde{r}} \left(\widetilde{r} \frac{\partial \widetilde{C}}{\partial \widetilde{r}} \right) + \frac{\partial^2 \widetilde{C}}{\partial \widetilde{z}^2} \right), \tag{3.15}$$

$\widetilde{\mathbf{w}}$ is the axial velocity of the fluid in blood vessel and, $\widetilde{\mathbf{C}}$ is the local concentration of the solute, and $\widetilde{D}_m$ is coefficient of molecular diffusion assumed to be constant.

3.4.2 Initial and Boundary Conditions

3.4.2.1 Initial Condition (IC)

A uniform distribution of the solute is assumed at the beginning (i.e., $t = 0$) and the distribution of the concentration at the beginning of the diffusion process is reported as below.

$$C(0,z,r) = \psi(z)X(r), \tag{3.16a}$$

with

$$\psi(z) = \frac{\delta(z)}{d^2 Pe}, \tag{3.16b}$$

and

$$X(r) = \begin{cases} 1, & 0 < r \leq d, \\ 0, & d < r \leq 1, \end{cases} \tag{3.16c}$$

where $\delta(z)$ is Dirac delta function.

3.4.2.2 Boundary Conditions (BCs)

The boundary conditions (BCs) signifying a first-order heterogeneous irreversible reaction at the tube wall and a finite concentration in the system at any instant of time are given by

$$\frac{\partial C}{\partial r}(t,z,1) = -\beta C(t,z,1), \tag{3.17a}$$

$$C(t,\infty,r) = \frac{\partial C}{\partial z}(t,\infty,r) = 0, \tag{3.17b}$$

$$C(t,z,0) = \text{finite}, \tag{3.17c}$$

where β is the non-dimensional wall reactive (absorption) parameter or first-order reaction rate representing the rate of loss on the tube wall. It is obvious that as the wall absorption parameter $\beta \to 0$, the results should approach for the case of no reactant flux at the tube wall [2].

3.4.3 Diffusion Coefficients and Mean Concentration

The solution of the equation (3.15) with the help of the initial and boundary conditions $(3.16)-(3.17)$ has been obtained using Sankarasubramanian and Gill [2] approach to finally obtain the diffusion coefficients and mean concentration. The solution expression for the exchange coefficient $M_0(t)$ is obtained as

$$M_0(t) = -\frac{\sum_0^\infty A_k \alpha_k J_1(\alpha_k) e^{-\alpha_k^2 t}}{\sum_0^\infty \left(\frac{A_k}{\alpha_k}\right) J_1(\alpha_k) e^{-\alpha_k^2 t}}, \tag{3.18a}$$

which is exactly the same as derived in the previous works ([2], [87], [88], [89]) as its computation does not include fluid velocity.
The expression for convection coefficient (M_1) is obtained as

$$M_1 = \frac{-2\alpha_0^2}{(\alpha_0^2+\beta^2)J_0^2(\alpha_0)} \int_0^1 w(r) r J_0^2(\alpha_0 r) dr. \tag{3.18b}$$

The expression for the dispersion coefficient (M_2) is given by

$$M_2 = \frac{1}{Pe^2} - \frac{4\alpha_0 J_1(\alpha_0)}{(\alpha_0^2+\beta^2)J_0^2(\alpha_0)} \int_0^1 (w(r)+M_1) g_1(r) r J_0(\alpha_0 r) dr. \tag{3.18c}$$

The expression for the mean concentration (C_M) of the solute is obtained as

$$C_M(t,z) = \frac{1}{2Pe\sqrt{\pi T}} \text{Exp}\left(\eta - \frac{z_1^2}{4T}\right). \tag{3.18d}$$

The detailed description of the solution method and derivation of the diffusion coefficients as well as mean concentration has been provided in Chapter 1 (1.5.3). All the integrations involved in the expressions of convective coefficient $(-M_1)$, dispersion coefficient (M_2) and

mean concentration (C_M) are evaluated in MATHEMATICA 10.0.2 software using numerical integration.

3.5 Results and Discussion

An analytical treatment of solute dispersion in a micropolar-Newtonian fluid flowing through porous layered microvessels with absorbing walls has been performed in the present study by considering the heat transfer aspect of the flow. The selection of micropolar fluid

Values of parameters		
Parameters	Values	Resources
Absorption ratio α_0	1.00	[103], [122]
Coupling parameter N	$0 \leq N < 1$	[68], [22], [21]
Densities ratio ρ_0	0.92-1.00	[36], [103], [37]
Grashof number Gr	0.5-17	[103], [41], [45]
Hartmann number H	0.1-4.0	[103], [68], [21]
Micropolar parameter n	$[0, \infty)$	[22], [122]
Parameter ϕ_M	$-1 \leq \phi_M \leq 1$	[22], [122]
Plasma layer thickness h	0.015-0.05	[28], [49]
Permeability k	$(0, \infty)$	[65], [49], [51]
Radiation parameter N_1	2-15	[114], [103]
Steady pressure gradient p_s	1-10	[28], [49]
Stess-jump parameter β_S	$-1 < \beta_S < 1$	[49], [51], [68]
Thermal conductivity ratio K_0	0.4-1.0	[103], [122]
Viscosity ratio μ_R	0.5-1.0	[36], [103]
Viscosity ratio parameter λ_1	1.0-1.6	[49], [51]
Wall absorption parameter β	0.01-100	[87], [111], [112]

Table 3.1: The range of parameters appropriate for flow through narrow tubes with their resources

plays an important role to understand the impact of micro-level effects on the solute dispersion process in fluid flowing through microvessels. The core region of the blood vessel is occupied by micropolar fluid and the intermediate and porous regions of the blood

vessel are occupied by Newtonian fluid. The plasma region consists of the intermediate and porous regions. The range of the core, intermediate and porous regions radii are $0 < r \leq R_1$, $R_1 < r \leq R_2$ and $R_2 < r \leq 1$, respectively. The thickness of core and plasma regions are taken as h_1 and h, respectively and $h_1 + h = 1$. The thickness of the intermediate region $(R_1 < r \leq R_2)$ is taken as 25% of the whole plasma layer width ([3], [62], [49]). Therefore, the typical estimates for core, intermediate and porous regions radii are $R_1 = 1 - h$, $R_2 = 1 - \frac{3h}{4}$ and 1, respectively. The effect of various parameters like radiation parameter, coupling number, Hartmann number, thermal conductivity, Grashof number and micro-rotation of the fluid particles on the diffusion coefficients and mean concentration are depicted pictorially and compared with the previous studies. The values have been fixed for the parameters $\sigma_0 = \alpha_0 = \rho_0 = 1$ and the Peclet number $Pe = 10^3$.

The range of values of various parameters are taken from the previous studies to perform the graphical analysis which is given in Table 3.1.

3.5.1 Convective Coefficient (M_1)

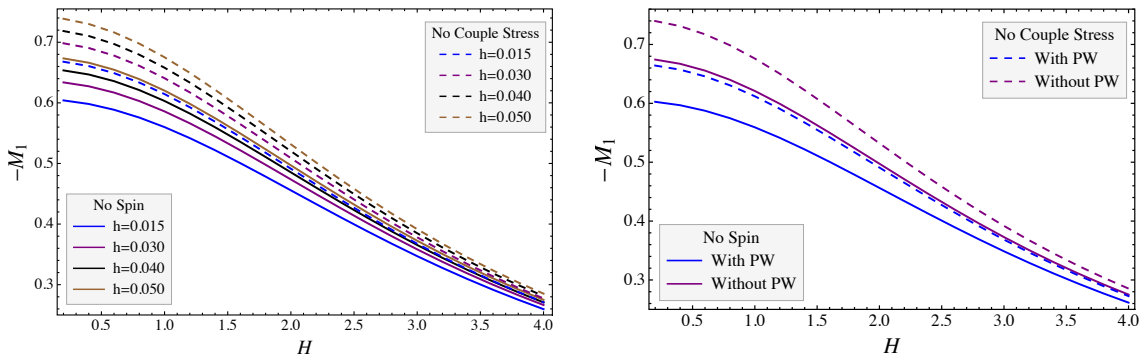

(a) **(b)**

Figure 3.2: Convective coefficient $(-M_1)$ with Hartmann number H **(a)** for different values of plasma layer thickness h $(\lambda_1 = 1.0)$ and **(b)** between flow through tubes with and without porous walls $(\lambda_1 = 1.6, h = 0.05)$. $(\beta_S = \mu_R = 0.5, k = n = 5, K_0 = 0.6, N = 0.1, p_s = \phi_M = 1, N_1 = 2, Gr = 1.5, \beta = 100)$

A comparative analysis of variation of convective coefficient with Hartmann number H for varying peripheral layer thickness h is depicted in Figure 3.2:(a) for no-spin (NS) and no-couple stress (NCS) formulations at the fluid-fluid interface. A decay in convective coefficient $(-M_1)$ is observed for rising Hartmann number owing to reduced velocity profile which is in agreement with the previous results [122]. An increase in peripheral layer thickness leads to a rise in convective coefficient which can be accredited to a relatively smoother flow in the tube [37]. A relatively higher convective coefficient is reported for NCS formulation in comparison to no-spin condition at the fluid-fluid interface. This can

be explained from work [122] of a relatively higher velocity profile for NCS formulation. Figure 3.2:(b) reveals a significantly higher difference in convective coefficient between no-spin and no-couple stress formulations as well as between two-fluid model (TFM) of blood flowing through tubes with and without porous region near the tube walls for low Hartmann number. This difference reduces with increasing Hartmann number.

The dominance of thermal buoyancy forces over the viscous forces leads to a rise in the convective coefficient for both the formulations (NS and NCS) as depicted in Figure 3.3:(a). However, a decay in porosity near the tube wall leads to decay in the convective coefficient. The above variation can be accredited to the change taking place in velocity profile due to rising Grashof number Gr and viscosity ratio parameter λ_1 ([123], [124]). A similar analysis of variation of convective coefficient with Grashof number for flow through tubes with and without porous region near the tube walls is depicted in Figure 3.3:(b).

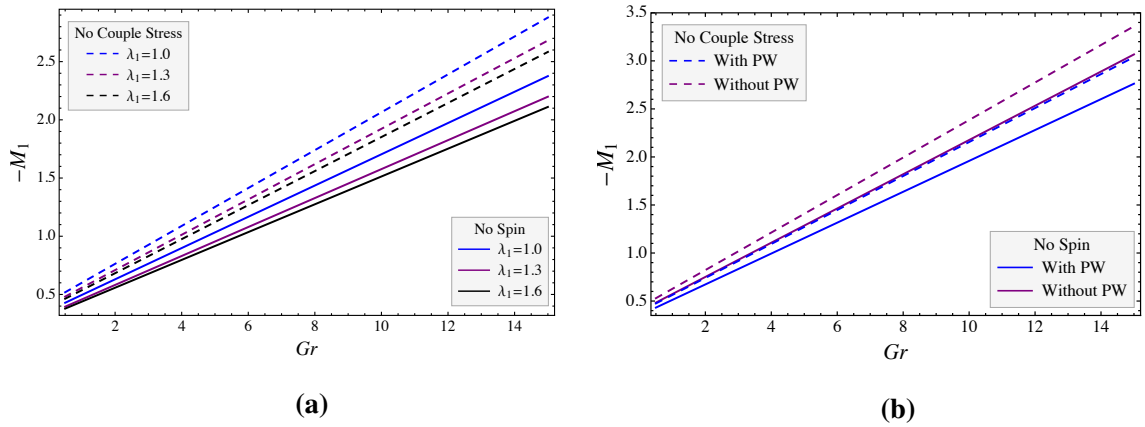

Figure 3.3: Convective coefficient $(-M_1)$ varying with Grashof number Gr **(a)** influenced by viscosity ratio parameter λ_1 $(N = 0.2, K_0 = 0.4)$ and **(b)** between flow through tubes with and without porous walls $(\lambda_1 = 1.6, N = 0.1, K_0 = 0.6)$. $(\beta_S = H = \mu_R = 0.5, p_s = \phi_M = 1, N_1 = 2, k = n = 5, h = 0.05, \beta = 100)$

Here also convective coefficient is higher for flow-through tubes without a porous region near the vessel wall (PW) and for NCS formulation. The growth rate of variation of convective coefficient with Grashof number is higher for higher porosity near the tube wall (for infinitely large permeability, the porous region reduces to the fluid region and hence observed a relatively larger M_1 for this case).

Figure 3.4:(a) reveals a nonlinear growth in convective coefficient with a rising thermal conductivity ratio K_0. The growth rate is slightly higher for NCS formulation relative to NS condition and further increases for higher wall absorption ($\beta = 100$). A consistent increase in convective coefficient with increasing β is in agreement with previous studies ([87], [37]). From Figure 3.4:(b), a decay in convective coefficient with rising coupling number N shows that a stronger micro-rotational effect significantly affects the solute dispersion

in flow through tubes. It is further observed that a higher viscosity ratio (μ_R) (relatively more obstruction in flow through the peripheral region) leads to growth in convective coefficient and this difference slightly reduces with the dominance of micro-rotational effects.

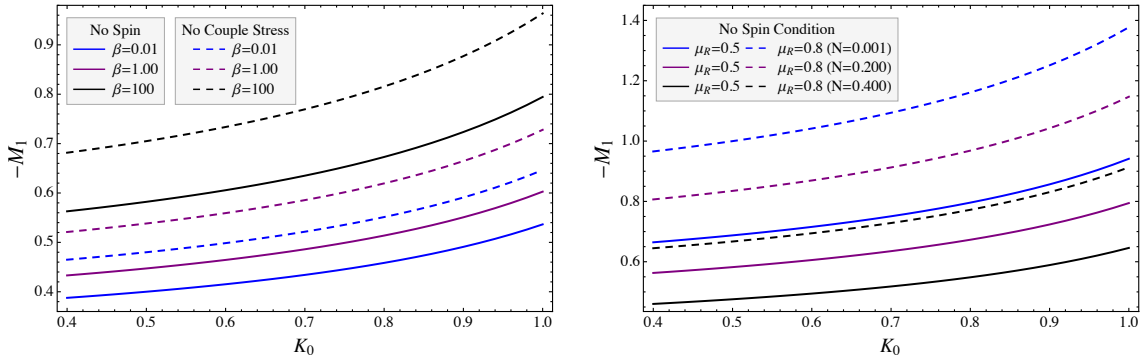

(a) **(b)**

Figure 3.4: Convective coefficient $(-M_1)$ varying with conductivity ratio K_0 influenced by **(a)** wall absorption parameter β $(N = 0.2, \mu_R = 0.5)$ and **(b)** coupling number N and viscosity ratio μ_R $(\beta = 100)$. $(\beta_S = H = 0.5, Gr = 1.5, p_s = \lambda_1 = \phi_M = 1, N_1 = 2, k = n = 5, h = 0.05)$

Linear growth in $-M_1$ with pressure gradient p_s is observed owing to an increase in velocity as depicted in Figure 3.5:(a) which is in agreement with the previous works ([49], [122]). A rising radiation parameter N_1 leads to growth in $-M_1$ for both the formulations (NS and NCS) which may be accredited to a slightly enhanced flow rate [122]. This further signifies that solute dispersion in flow through tubes is significantly affected with the rate at which the heat energy is transformed into the radiation and this growth is significant for radiation parameter $(N_1 > 2.5)$.

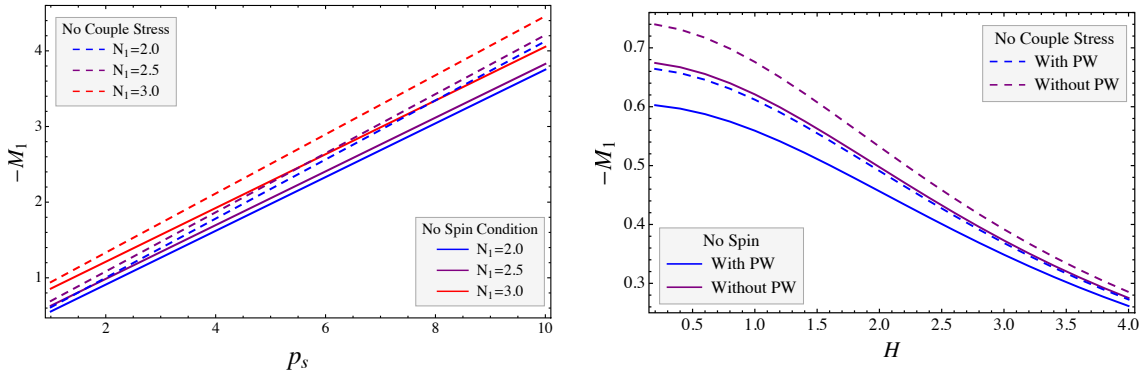

(a) **(b)**

Figure 3.5: Impact of radiation parameter N_1 on convective coefficient $(-M_1)$ varying with pressure gradient p_s under **(a)** different conditions (NS and NCS) and **(b)** between flow through tubes with and without porous walls. $(\beta_S = H = \mu_R = 0.5, \lambda_1 = Gr = 1.5, K_0 = 0.4, \phi_M = 1, N = 0.1, k = n = 5, h = 0.05, \beta = 100)$

Figure 3.5:(b) reveals a greater impact of radiation parameter N_1 on the convective coefficient in case of flow through tubes without PW in comparison to flow through tubes with PW. The gap between growth rate of $-M_1$ between NS and NCS in (Figure 3.5:(a)) and flow through tubes without PW compared to with PW (Figure 3.5:(b)) widens with increment in pressure gradient p_s.

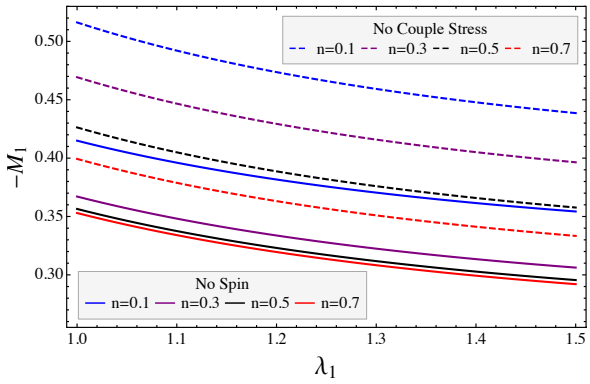

Figure 3.6: Impact of micro-scale parameter n on convective coefficient $(-M_1)$ varying with viscosity ratio parameter λ_1. $(\beta_S = H = \phi_M = \mu_R = 0.5, h = 0.05, N = 0.4, K_0 = 0.6, p_s = 1, N_1 = 2, Gr = 1.5, k = 5, \beta = 0.01)$

The effect of micro-scale parameter (particle size n) on the convective coefficient is shown in Figure 3.6. It is observed that an increase in micro-scale parameter leads to decay in the convective coefficient although its variation pattern with viscosity ratio parameter λ_1 remains unchanged. It is also perceived that for no-couple stress condition, the decay in $-M_1$ with particle size n is significantly reduced for large particle size; however, this variation shows slight reduction for no-spin formulation.

A rising permeability leads to smoother flow and hence a slight increase in convective coefficient is witnessed from Table 3.2:(a). Further, an increase in parameter ϕ_M leads to a slight increase in convective coefficient owing to enhancement in flow rate [122]. An increasing value of the stress-jump parameter β_S contributes to a slight decay in the convective coefficient as shown in Table 3.2:(b) for both the formulations (NS and NCS). The justification of this observation is that an increase in the stress-jump parameter β_S leads to a relatively higher shear stress of porous region in comparison to clear fluid (non-porous) region leading to reduced flow rate [49] and hence reduced convection.

k	No Spin	$\phi_M = -1.0$	$\phi_M = -0.5$	$\phi_M = 0.0$	$\phi_M = 0.5$	$\phi_M = 1.0$
0.5	0.8945	0.8946	0.8946	0.8946	0.8947	0.9853
1.0	0.8947	0.8948	0.8948	0.8948	0.8949	0.9854
3.0	0.8949	0.8949	0.8949	0.8950	0.8951	0.9856
5.0	0.8949	0.8950	0.8950	0.8950	0.8951	0.9857
7.0	0.8950	0.8950	0.8950	0.8951	0.8951	0.9857
9.0	0.8950	0.8950	0.8951	0.8951	0.8952	0.9857

(a)

β_S	No Spin	$\phi_M = -1.0$	$\phi_M = -0.5$	$\phi_M = 0.0$	$\phi_M = 0.5$	$\phi_M = 1.0$
-0.9	0.8955	0.8955	0.8955	0.8955	0.8956	0.9862
-0.6	0.8953	0.8954	0.8954	0.8954	0.8955	0.9861
-0.3	0.8952	0.8953	0.8953	0.8953	0.8954	0.9860
0.0	0.8951	0.8952	0.8952	0.8952	0.8953	0.9859
0.3	0.8950	0.8951	0.8951	0.8951	0.8952	0.9858
0.6	0.8949	0.8950	0.8950	0.8950	0.8951	0.9856
0.9	0.8948	0.8948	0.8949	0.8949	0.8950	0.9855

(b)

Table 3.2: Convective coefficient $(-M_1)$ varying with **(a)** permeability k $(\beta_S = 0.5)$ and **(b)** stress-jump parameter β_S $(k = 5)$ for different values of no-couple stress parameter ϕ_M. $(H = 0.5, n = 5, h = 0.05, \lambda_1 = Gr = 1.5, \mu_R = 0.8, K_0 = 0.6, p_s = 1, N = 0.1, N_1 = 2, \beta = 100)$

3.5.2 Dispersion Coefficient (M_2)

The impact of Hartmann number H and varying peripheral layer thickness h on the variation of dispersion coefficient M_2 is depicted in Figure 3.7:(a) for no-spin (NS) and no-couple stress (NCS) formulations at the fluid-fluid interface.

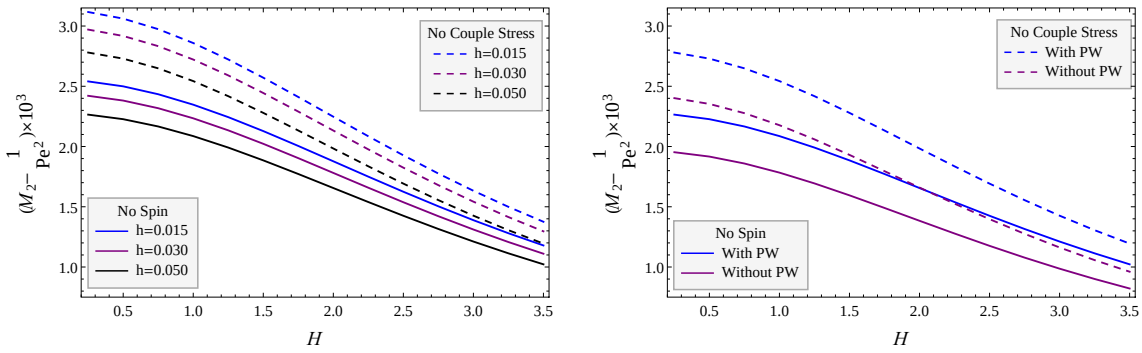

(a) **(b)**

Figure 3.7: Axial dispersion coefficient $(M_2 - 1/Pe^2)$ varying with Hartmann number H **(a)** for different values of plasma layer thickness h and **(b)** between flow through tubes with and without porous walls $(h = 0.05)$. $(\beta_S = \mu_R = 0.5, k = n = 5, K_0 = 0.6, N = 0.1, \beta = p_s = \phi_M = 1, N_1 = 2, Gr = \lambda_1 = 1.5)$

A rising Hartmann number H leads to decay in axial dispersion M_2 with a slightly lesser decay rate for the no-spin condition in comparison to no-couple stress formulation. A slight increase in peripheral layer thickness leads to decay in dispersion coefficient M_2 which is in agreement with the previous study [37]. Figure 3.7:(b) reveals a significantly higher difference in dispersion coefficient between no-spin and no-couple stress formulations as well as between TFM of blood flow through tubes with and without porous region near the tube walls for low Hartmann number. This difference reduces with increasing Hartmann number ([125], [126], [127], [128] [129]).

The dominance of thermal buoyancy forces over the viscous forces contributes to enhancement in dispersion coefficient for both the formulations (NS and NCS) as shown in Figure 3.8:(a). An increasing nature of the dispersion coefficient with Grashof number is almost negligibly affected by the variation in the porosity of the porous layer near the tube wall. This observation is the same for both the formulations. A similar analysis of variation of dispersion coefficient with Grashof number for flow through tubes with and without porous region near the tube walls is depicted in Figure 3.8:(b). Here also, dispersion coefficient is higher for flow through tubes with PW and for NCS formulation. The growth rate of variation of dispersion coefficient with Grashof number is higher for lower porosity near the tube wall (for infinitely large permeability, the porous region reduces to the fluid region

and hence observed a relatively larger M_2 for this case). The gap between growth rate of the dispersion coefficient between NS and NCS widens with increment in Grashof number.

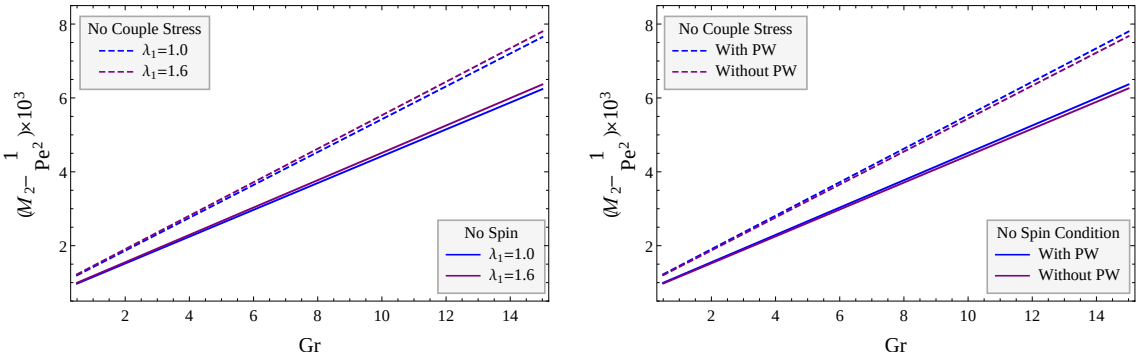

(a) **(b)**

Figure 3.8: Axial dispersion coefficient $(M_2 - 1/Pe^2)$ varying with Grashof number Gr **(a)** for different values of viscosity ratio parameter λ_1 and **(b)** between flow through tubes with and without porous walls $(\lambda_1 = 1.6)$. $(\beta_S = H = \mu_R = 0.5, K_0 = 0.6, N = 0.1, p_s = \phi_M = 1, N_1 = 2, k = n = 5, h = 0.05, \beta = 0.01)$

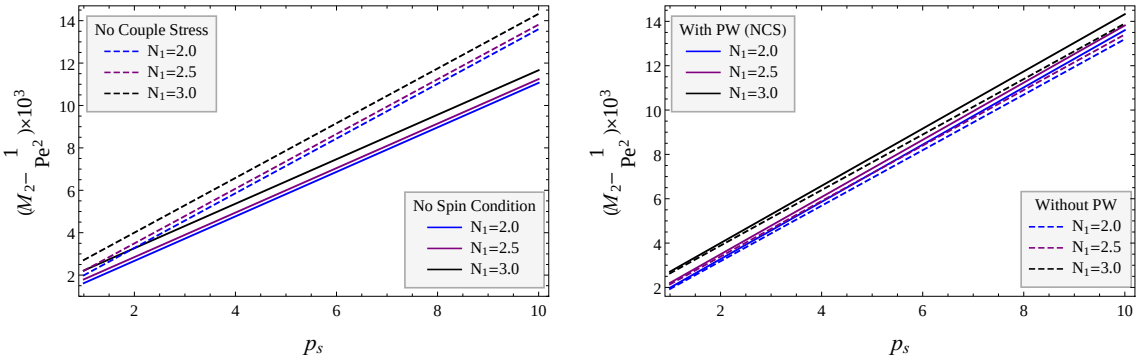

(a) **(b)**

Figure 3.9: Axial dispersion coefficient $(M_2 - 1/Pe^2)$ varying with pressure gradient p_s **(a)** for different values of radiation parameter N_1 and **(b)** between flow through tubes with and without porous walls. $(\beta_S = H = \mu_R = 0.5, K_0 = 0.4, N = 0.1, Gr = \lambda_1 = 1.5, \beta = \phi_M = 1, k = n = 5, h = 0.05)$

Linear growth in dispersion coefficient M_2 with pressure gradient p_s is observed owing to an increase in velocity which is in agreement with the previous works ([49], [122]) as depicted in Figure 3.9:(a). A rising radiation parameter N_1 contributes to growth in M_2 for both the formulations (NS and NCS) which may be accredited to a slightly enhanced flow rate [122]. This further signifies that the solute dispersion in flow through tubes is significantly affected with the rate at which the heat energy is transformed into the radiation and this growth is significant for radiation parameter $(N_1 > 2.5)$. The gap between growth rate of the dispersion coefficient between NS and NCS widens with increment in pressure gradient p_s. Figure 3.9:(b) suggests a slightly reduced dispersion coefficient for flow through

tubes without PW. It is also observed that the growth rate of M_2 with a pressure gradient is slightly higher for flow through tubes with PW.

3.5.3 Mean Concentration (C_M)

A comparative analysis of mean concentration C_M for both the formulations (NS and NCS) under varying wall absorption parameter β is discussed in Figure 3.10. For both the formulations, the mean concentration significantly reduces with an increase in β which is in agreement with the previous studies ([87], [89]). Also for low wall absorption ($\beta = 0.01$), the mean concentration is slightly higher for no-spin condition owing to relatively low velocity profile. However the behavior changes for moderate and higher values of β $(1, 100)$ i.e. for moderately and highly absorbing walls despite the larger velocity profile, the mean concentration for NCS formulation is slightly higher. Figure 3.10:(b) reveals that the diffusion process is more dominant for no-spin condition near the point of injection. However, as we move away from the point of injection, the same is dominated by NCS formulation.

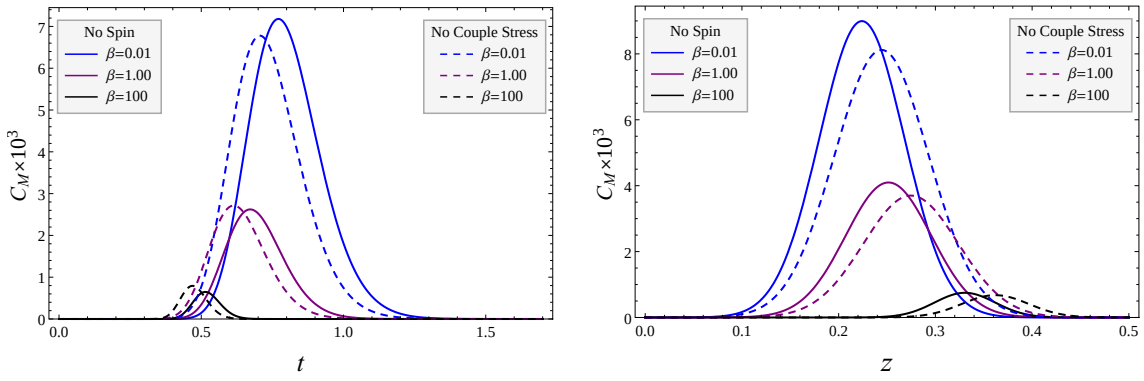

Figure 3.10: Effect of wall absorption parameter β on mean concentration C_M varying with **(a)** time t $(z = 0.35)$ and **(b)** axial distance z $(t = 0.5)$. $(\beta_S = H = \mu_R = 0.5, K_0 = 0.6, Gr = 1.5, \lambda_1 = p_s = \phi_M = 1, N_1 = 2, k = n = 5, h = 0.05, N = 0.1)$

An increase in Hartmann number H leads to decay in mean concentration C_M for both the formulations (NS and NCS) as evident from Figure 3.11:(a). However, an increase in peripheral layer thickness h leads to significant growth in the peak of the mean concentration C_M. It is also observed that for both the formulations, the mean concentration C_M curve widen with the increase in Hartmann number H and decrease in plasma layer thickness h indicating that these two parameters lead to a slight increase in the time elapsed in the diffusion process. Besides this, the comparative analysis shows that for no-couple stress formulation, the diffusion process begins and ends relatively earlier in comparison to the no-spin formulation at the interface. From Figure 3.11:(b), the variation of C_M along the

axial distance for both the formulations shows that near the point of injection, a rise in Hartmann number H leads to growth in C_M.

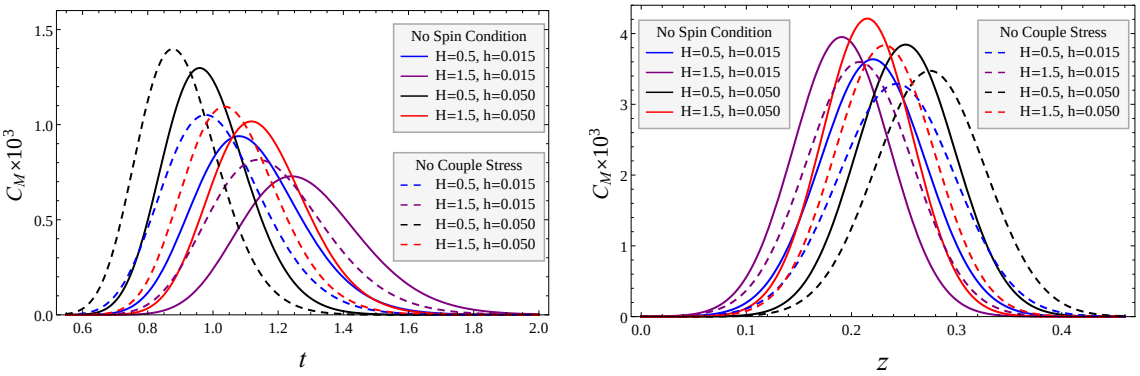

(a) **(b)**

Figure 3.11: Impact of Hartmann number H and plasma layer thickness h on mean concentration C_M varying with **(a)** time t $(z = 0.5)$ and **(b)** axial distance z $(t = 0.5)$. $(\beta_S = \mu_R = 0.5, K_0 = 0.6, Gr = 1.5, \lambda_1 = \beta = p_s = \phi_M = 1, N_1 = 2, k = n = 5, N = 0.1)$

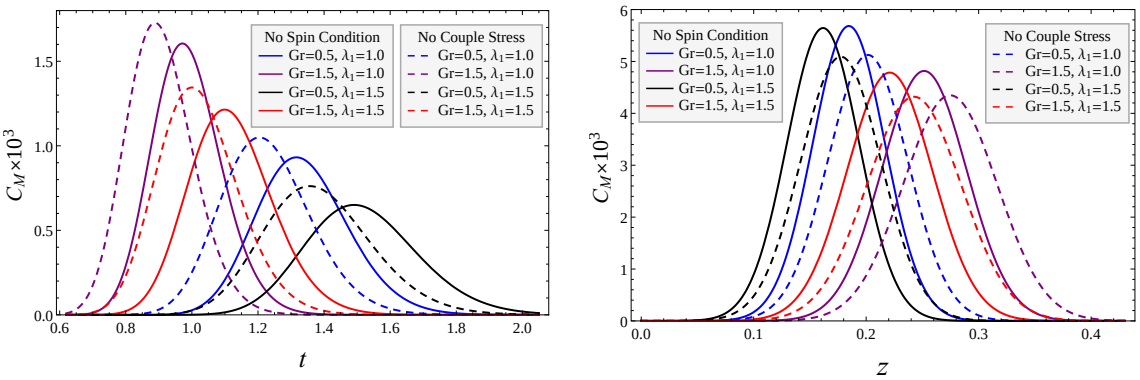

(a) **(b)**

Figure 3.12: Impact of Grashof number Gr and viscosity ratio parameter λ_1 on mean concentration C_M varying with **(a)** time t $(z = 0.5)$ and **(b)** axial distance z $(t = 0.5)$. $(\beta_S = \mu_R = H = 0.5, K_0 = 0.6, h = 0.05, \beta = p_s = \phi_M = 1, N_1 = 2, k = n = 5, N = 0.1)$

However, an increase in peripheral layer thickness h leads to growth in the peak of C_M but as we move away from the point of injection (larger axial distance z) the variation in C_M for varying H and h changes which are in agreement with the Figure 3.11:(a). From Figure 3.12:(a), a comparative analysis of time variation of mean concentration for both the formulations under varying Grashof number Gr and viscosity ratio parameter λ_1 suggests a significant delay in dispersion process and lower peak in C_M for no-spin formulation in comparison to no-couple stress formulation. However, the variation of C_M along the axial distance shows an almost negligible difference in C_M for both the formulations (NS and NCS).

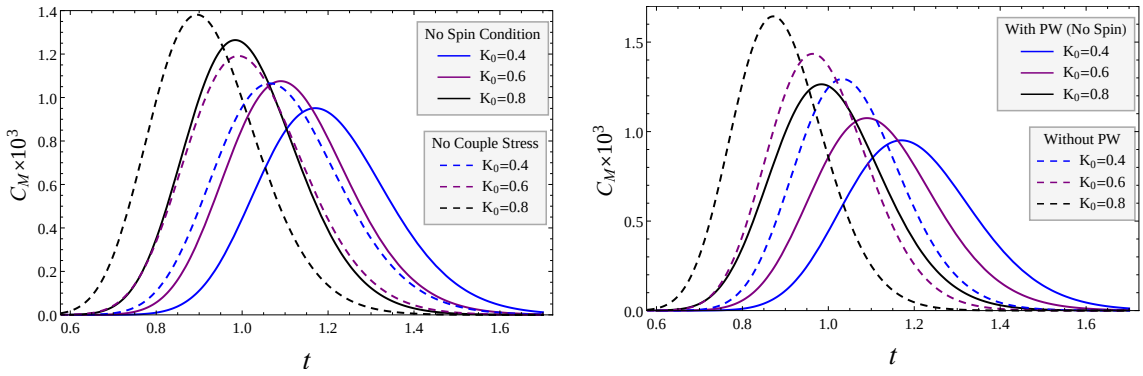

(a) **(b)**

Figure 3.13: Mean concentration C_M varying with time t for **(a)** different conditions (No-spin and no-couple stress) and **(b)** different models (TFM of blood flow through tubes with and without PW). ($\beta_S = H = \mu_R = z = 0.5, h = 0.05, \lambda_1 = Gr = 1.5, \phi_M = \beta = p_s = 1, N_1 = 2, N = 0.1, k = n = 5$)

A rising thermal conductivity ratio K_0 leads to growth in the mean concentration for both the formulations (NS and NCS) although the same leads to a slightly early appearance in the peak of the C_M as evident from Figure 3.13:(a). A comparative analysis of the time profile of C_M for dispersion in tubes with and without porous region near the tube wall for no-spin formulation suggests a slightly reduced time for dispersion process for the later case. This observation can be accredited to a relatively smoother flow in tubes without PW. Besides this, the peak of C_M assumes relatively higher values for dispersion in flow through tubes without porous region near the tube wall.

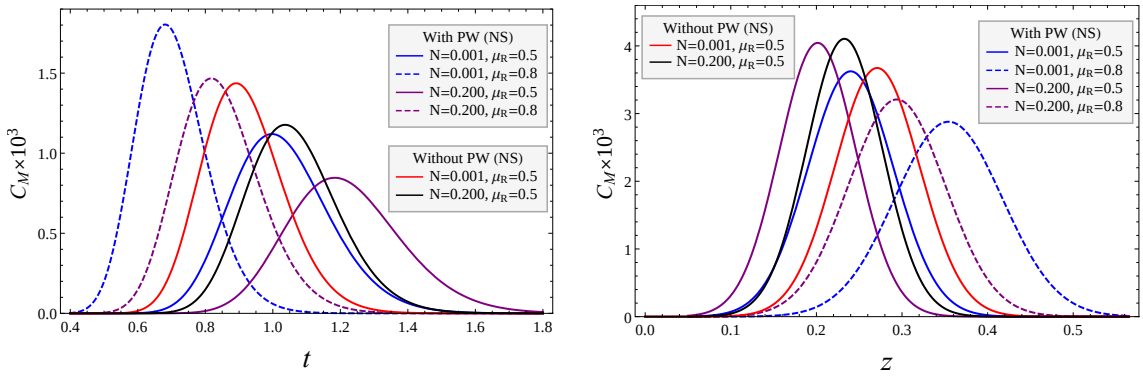

(a) **(b)**

Figure 3.14: Impact of coupling number N and viscosity ratio μ_R on mean concentration C_M varying with **(a)** time t ($z = 0.5$) and **(b)** axial distance z ($t = 0.5$). ($\beta_S = H = 0.5, K_0 = 0.6, h = 0.05, \lambda_1 = Gr = 1.5, \beta = p_s = 1, N_1 = 2, k = n = 5$)

The time profile of the mean concentration under varying coupling number N shows a decay in the peak of the value of C_M as well as a significant delay in the completion of the solute dispersion process which is evident from the widening of the profile curve (Figure

3.14:(a)). These observations are the same for dispersion in tubes with and without PW. An increase in viscosity ratio μ_R (i.e. relatively higher viscosity of Newtonian fluid or fluid in the peripheral region) results in a significant reduction in time to complete the diffusion process. From Figure 3.14:(b), the effect of coupling number N on the variation of mean concentration along axial distance for dispersion in tubes with and without porous region near the tube wall reveals a slight increase in C_M for higher coupling number near the point of injection but this behavior changes as we move away from the point of injection (higher axial distance z). An increase in viscosity ratio μ_R results in slight widening of the mean concentration curve.

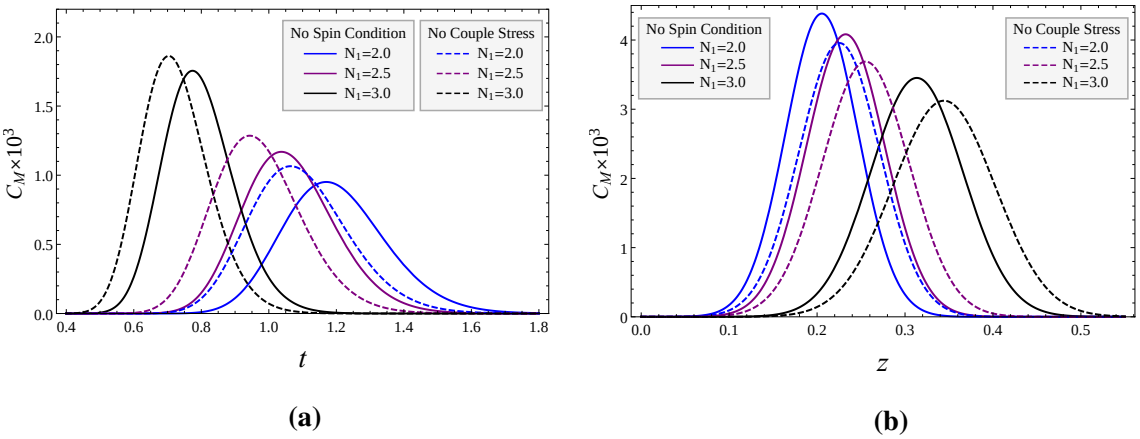

Figure 3.15: Effect of radiation parameter N_1 on mean concentration C_M with **(a)** time t $(z = 0.5)$ and **(b)** axial distance z $(t = 0.5)$. $(\beta_S = \mu_R = H = 0.5, K_0 = 0.4, \lambda_1 = Gr = 1.5, h = 0.05, \beta = p_s = \phi_M = 1, N = 0.1, k = n = 5)$

An increase in radiation parameter N_1 leads to significantly reduced time for completion of the diffusion process (Figure 3.15:(a)). This can be justified from the fact that a larger rate of transformation of heat energy to the thermal radiation leads to an increase in flow rate [122] and hence results in reduced time for the completion of the diffusion process. Variation of the mean concentration along the axial distance for different radiation parameter N_1 reveals that near the point of injection, an increasing N_1 leads to a slow dispersion process with reduced peak of the mean concentration and a slightly widen mean concentration curve as evident from the Figure 3.15:(b).

Effect of particle size (n) on the time profile of the mean concentration is depicted in Figure 3.16. Figure 3.16:(a) reveals that an increase in particle size leads to a slightly higher peak of the mean concentration and a slightly delayed diffusion process as evident from the widening of the curve. A similar observation can be made for no-couple stress formulation except for the fact that the peak of the mean concentration is not changing. From Figure 3.16:(b), a comparative analysis of the time profile of the mean concentration for the dispersion in tubes with and without porous region near the tube wall reveals a negligible change

in peak of the mean concentration with increasing particle size for the dispersion in tubes without porous region near the tube wall.

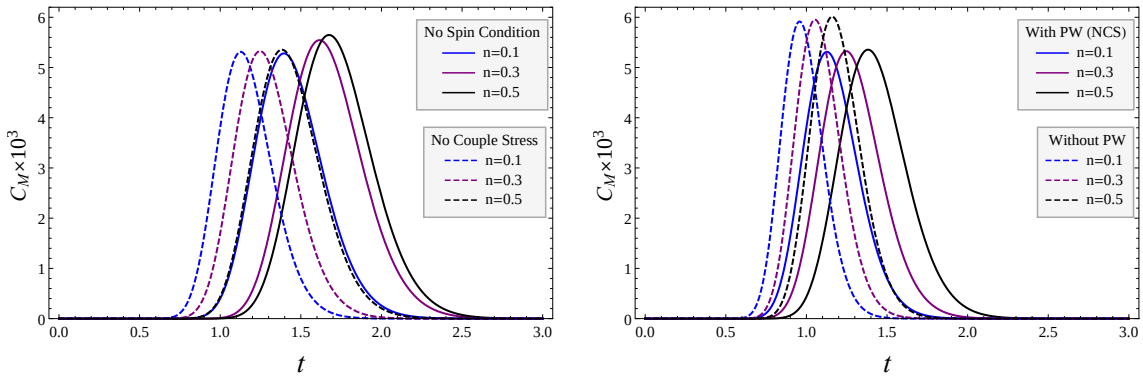

(a) **(b)**

Figure 3.16: Impact of micro-scale parameter n on mean concentration C_M varying with time t under **(a)** different conditions (NS and NCS) and **(b)** TFM of blood flow through tubes with and without PW (for no-couple stress condition). ($\beta_S = \mu_R = H = z = \phi_M = 0.5, K_0 = 0.6, \lambda_1 = Gr = 1.5, h = 0.05, p_s = 1, N = 0.4, N_1 = 2, k = 5, \beta = 0.01$)

3.6 Conclusions

A novel approach of heat and mass transfer on solute dispersion in a two-fluid model of blood flow through narrow blood vessels with absorbing walls has been done in the present study which is physically realistic in the cardiovascular system to perform the mixing or transporting drug in bloodstreams through vascular systems. It is observed that the heat transfer and microlevel parameters of the fluid particles have a significant impact on the diffusion process. The important determinations of the present study are pointed out as below:

1. Relatively higher diffusion coefficients (convective and dispersion coefficients) are reported for no-couple stress formulation in comparison to no-spin condition at the fluid-fluid interface.

2. A rising Hartmann number H leads to decay in diffusion coefficients as well as time profile of mean concentration showing a clear impact of the magnetic field on the diffusion process.

3. Microlevel parameters (N and n) have a significant impact on the diffusion coefficients and mean concentration in both the formulations (NS and NCS). Specifically, a higher coupling parameter N leads to a delay in the diffusion process.

4. The variation in porosity significantly affects the convection process but has an almost negligible effect on the axial dispersion.

5. For no-couple stress formulation, the peak in the time profile of mean concentration appears relatively earlier in comparison to the no-spin formulation.

The present work shows a significant impact of microlevel parameters on the diffusion process in flow through a tube. The model is physiologically realistic in the sense that micropolar fluid resembles the blood as suggested by Ariman [11] and the existence of the porous layer near the wall resembles the endothelial glycocalyx layer. So, the outcome of the present work may have a significant impact on the transportation of nutrients into the physiological system.

Chapter 4

Influence of Varying Viscosity Nature and EGL on Microcirculation under Heat Transfer Aspect

4.1 Introduction

The alarming situation of sudden elevation in the cases of cardiovascular diseases due to rising pollution and the unhealthy lifestyle of an individual has posed a stiff challenge for researchers to reanalyze the functioning of the circulatory system from the mechanical and modeling perspective to enable duly required rapid transformation of medical treatments. A mathematical study of heat transfer effects on the blood flowing through permeable medium could give an imperative insight into the mechanism of hemodynamics, which is accountable for the progression of such diseases and could help in developing effective cure care. Numerous mathematical studies have been conducted to replicate blood's Newtonian and non-Newtonian fluid behavior in separate regions of the lumen of a blood vessel. Several works ([90]-[130]) have been done on the flow of Newtonian/non-Newtonian fluid flow through constricted tubes. The Herschel-Bulkley fluid is considered as the core region fluid owing to its validity for low, moderate as well as high shear rates [91].

All the above discussions did not consider the permeable nature of the tube wall, which is an important aspect of the physiological fluid flow through tubes. It is believed that due to unusual lifestyle and food habits, the reporting of cardiovascular diseases has significantly increased causing a severe concern for the society owing to the presence of lipids (macromolecules) in the blood. Darcy [94] was first to examine the flow of fluids through porous media which was only valid for a porous medium with low permeability. Brinkman [95] removed Darcy's restriction and gave the Brinkman equation, which is valid for low as well as high permeability. The Brinkman model replicates the resistance offered against the flow of

[3]The work has been published as **S.S. Chauhan, P.D. Shah and A. Tiwari, "Analytical Study of the Effect of Variable Viscosity and Heat Transfer on Two Fluid Flowing through Porous Layered Tubes", *Transport in Porous Media* 142 (2022) 641.**

fluid through the porous medium. It was used to analyze the circulation of non-Newtonian Casson fluid in a tube using constant and varying Darcy numbers of the porous medium (Dash *et al.* [98]).

A theoretical investigation of heat transfer in the flow of Newtonian fluid through the porous saturated conduits was done by Hooman and Gurgenci ([131]-[132]) and the flow through the porous medium was perceived by the Brinkman-Forchheimer model which is valid for governing the flow through all kind of porous medium. The regular perturbation technique was utilized to solve the equations for large Darcy number however, a matched asymptotic method was applied to solve for small Darcy number. By applying the magnetic field in the normal direction of the liquid flow, many authors studied the single or multi-phase flow of liquids through conduits. Misra *et al.* [115] developed a mathematical model to analyze the flow of second-grade viscoelastic liquid through homogeneous porous conduits. Kumar *et al.* [104] presented an analytical solution of the fully-developed laminar free-convection flow of a micropolar and viscous fluid in a vertical channel. For an unsteady laminar flow of an electrically conducting fluid, Chamkha **[Chamkh99]** employed finite difference method to investigate the heat transfer arises due to particulate suspension in fluid flowing through channels and circular pipes. He [99]studied the hydromagnetic mixed convection flow in a vertical channel with symmetric and asymmetric wall heating conditions analytically and also numerically examined the viscous dissipation effect as well as Joule heating effect. Several other researchers [133]-[134] also explored the heat transfer of nanofluid in different situations with the presense of thermal radiation and Joule heating. Toghraie *et al.* [135] examined a two-phase flow in a micro concentric annulus under non-uniform heat flux boundary conditions. Ponalagusamy and Selvi [103] developed a mathematical model that investigated the simultaneous procedure of heat transfer and constriction size on the flow of two-immiscible Newtonian fluids through a constricted vessel. Recently, Tiwari *et al.* [122] analyzed the impact of heat transfer on microlevel properties of fluid by using micropolar fluid model in the core region.

Viscosity of blood is a crucial parameter and in all the above cited works, it is discussed only as a function of shear rate. However, blood being a complex quantity constituting the cells, plasma, and other nutrients, one must take several other physical factors into consideration affecting the blood viscosity. These parameters include hematocrit, temperature, disease state and natural age of RBCs with exercise level [26]. The theoretical and experimental work of Lih [38] concluded that the viscosity of the blood is variable at the low shear rate region. Adopting the assumption of Lih, many authors ([41]-[136]) considered the temperature-dependent viscosity of the blood and investigated the impact of variable viscosity on hemodynamical quantities. Sharma *et al.* [137] developed the blood flow as a

two fluid model having viscoelastic Jeffrey fluid in the central region to derive the analytic expressions for velocity in a stenotic artery. The study was extended by Sharma and Yadav [138] to understand the biomagnetic fluid aspect of blood flow. Further, Yadav *et al.* [139] modelled the flow as an oscillatory flow to take the pulsatile nature of blood flow in an account. Recently, Tiwari and Chauhan ([49]-[51]) considered the TFM of blood flow through tubes comprising an endothelial glycocalyx layer porous region adjacent with the tube wall by assuming the flow pattern of blood to be steady as well as pulsatile and analyzed the impact of hematocrit-dependent viscosity on flow variables, hematocrit, and Fahraeus effect. The significance of heat transfer and mass transport in the blood flowing through a narrow vessel having porous layer near the absorbing wall was attempted to be understood by Shah *et al.* [140]. Tiwari *et al.* [141] studied the impact of viscosity varying with respect to the temperature and heat transfer on the process of drug delivery in two-fluid model of blood. Saini *et al.* [142] utilized Brinkman-Forchheimer equation to investigate the influence of temperature-dependent viscosity on the creeping flow of non-Newtonian fluid. The above literature survey suggests that so far the Brinkman-Forchheimer model for the formulation of the flow through endothelial glycocalyx layer in microvessels with temperature-dependent viscosity has not been done. This may give us some useful results emphasizing how flows through microvessels will be affected due to the treatment of disease like malignant tumor.

In the proposed study, the physical aspect of an endothelial glycocalyx layer adjacent with the vessel wall is attempted to be understood by considering the Brinkman-Forchheimer equation governing the flow through an EGL. The heat transfer and viscosity describing the temperature-dependent nature on the two-fluid model of the blood flow through an endothelial glycocalyx layered tube has been investigated. Mathematical expressions for flow velocities in different regions are obtained analytically. The impact of endothelial glycocalyx layer, temperature and viscosity describing the variable nature, on flow variables have been analyzed. To validate the proposed work, the influence of an endothelial glycocalyx layer (and hence porous layer parameters), varying viscosity and temperature parameters have been examined graphically and the comparison have been drawn with the previous studies.

4.2 Formulation of Problem

4.2.1 Problem Statement and Description of Model

In the proposed study, the cylindrical frame of reference $(\widetilde{r}, \phi, \widetilde{z})$ having origin fixed at the vessel axis is employed to replicate the flow of blood in a heated porous blood vessel. The flow of blood is depicted here as a fully developed, steady, laminar flow of an incompressible three-layered fluid comprising of HB and Newtonian fluids to incorporate varying viscous

behavior of blood at the core region and to exhibit Newtonian behavior of plasma in the peripheral region, respectively. Brinkman-Forchheimer equation governs the circulation of blood through a thin endothelial glycocaly layer adjacent with the wall of the microvessel.

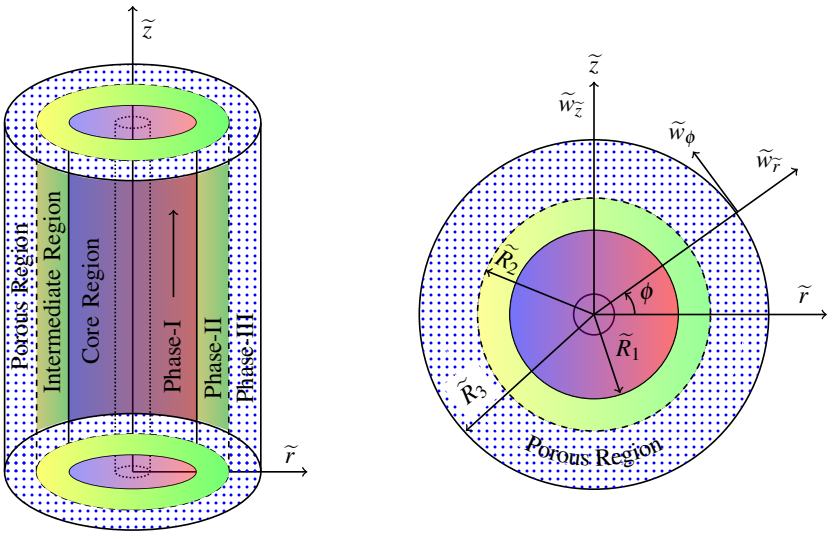

Figure 4.1: The schematic diagram of model description for two-fluid model with an endothelial glycocalyx layer adjacent to the microvessel wall

Figure 4.1 delineates the physical model of the problem and the circulation of blood through microvessel is divided into three phases, where $\widetilde{R}_1, \widetilde{R}_2, \widetilde{R}_3$ are the radii of the Phase- I, Phase-II and III of the microvessel, respectively and $\widetilde{R}_p$ represents the radius of plug flow region. The core microvessel region filled with Herschel-Bulkley fluid exhibiting non-Newtonian behaviour is denoted by Phase-I. Newtonian fluid flow through both Phase-II and III together representing the plasma region. The intermediate region delineated by Phase-II is governed by Newtonian fluid and Phase-III replicates an EGL adjacent with the microvessel's wall depicting the porous region of the microvessel.

4.2.2 Governing Equations

To delineate the mass conservation and the momentum of blood flow through vessel, continuity equation and Navier–Stokes equations have been modeled to govern the fluid flow in different regions as follow:
Phase- I, i.e., $0 < \widetilde{r} \leq \widetilde{R}_1$

$$\frac{\partial \widetilde{w}_H}{\partial \widetilde{z}} = 0, \tag{4.1a}$$

$$\frac{\partial \widetilde{p}_H}{\partial \widetilde{r}} = 0, \tag{4.1b}$$

$$-\frac{\partial \widetilde{p}_H}{\partial \widetilde{z}} - \frac{1}{\widetilde{r}}\frac{\partial}{\partial \widetilde{r}}(\widetilde{r}\widetilde{\tau}_H) + \widetilde{g}\widetilde{\rho}_H\widetilde{\gamma}(\widetilde{T}_H - \widetilde{T}_\infty) = 0, \tag{4.1c}$$

$$\widetilde{K}_H\left(\frac{\partial^2 \widetilde{T}_H}{\partial \widetilde{r}^2} + \frac{1}{\widetilde{r}}\frac{\partial \widetilde{T}_H}{\partial \widetilde{r}}\right) + \widetilde{Q}_H = 0, \tag{4.1d}$$

The mathematical expression for the Herschel-Bulkley fluid is given as

$$\widetilde{\tau}_H = \widetilde{\tau}_y + \left[\widetilde{\mu}(\widetilde{T}_H)\left(-\frac{\partial \widetilde{w}_H}{\partial \widetilde{r}}\right)\right]^{\frac{1}{n}}, \quad \text{if} \quad \widetilde{\tau}_H \geq \widetilde{\tau}_y, \tag{4.1e}$$

$$\frac{\partial \widetilde{w}_H}{\partial \widetilde{r}} = 0, \quad \text{if} \quad \widetilde{\tau}_H \leq \widetilde{\tau}_y, \tag{4.1f}$$

where $\widetilde{w}_H, \widetilde{\rho}_H, \widetilde{p}_H$ are the flow parameters of Herschel-Bulkley fluid describing the axial velocity, density, and pressure, respectively. The parameters associated with heat transfer are $\widetilde{\mu}(\widetilde{T}_H), \widetilde{K}_H, \widetilde{T}_H, \widetilde{Q}_H$, describing the temperature dependent variable viscosity, thermal conductivity, temperature, and constant heat absorption of blood in core region, respectively; the acceleration resulting from gravity is denoted by $\widetilde{g}$, $\widetilde{\tau}_H, \widetilde{\tau}_y$ corresponds to the shear and yield stress of Herschel-Bulkley fluid, respectively; coefficient of the temperature stimulated volume expansion is denoted by $\widetilde{\gamma}$, and $\widetilde{T}_\infty$ is the ambient temperature of the blood.
Phase- II, i.e., $\widetilde{R}_1 < \widetilde{r} \leq \widetilde{R}_2$

$$\frac{\partial \widetilde{w}_N}{\partial \widetilde{z}} = 0, \tag{4.2a}$$

$$\frac{\partial \widetilde{p}_N}{\partial \widetilde{r}} = 0, \tag{4.2b}$$

$$-\frac{\partial \widetilde{p}_N}{\partial \widetilde{z}} + \frac{\widetilde{\mu}_N}{\widetilde{r}}\frac{\partial}{\partial \widetilde{r}}\left(\widetilde{r}\frac{\partial \widetilde{w}_N}{\partial \widetilde{r}}\right) + \widetilde{g}\widetilde{\rho}_N\widetilde{\gamma}(\widetilde{T}_N - \widetilde{T}_\infty) = 0, \tag{4.2c}$$

$$\widetilde{K}_N\left(\frac{\partial^2 \widetilde{T}_N}{\partial \widetilde{r}^2} + \frac{1}{\widetilde{r}}\frac{\partial \widetilde{T}_N}{\partial \widetilde{r}}\right) + \widetilde{Q}_N = 0, \tag{4.2d}$$

where $\widetilde{\rho}_N, \widetilde{p}_N, \widetilde{w}_N, \widetilde{\mu}_N$, are the flow parameters of the Newtonian fluid describing the density, pressure, velocity along the axial direction, and viscosity, respectively; $\widetilde{K}_N, \widetilde{T}_N, \widetilde{Q}_N$ are the heat transfer parameters of Newtonian fluid describing the thermal conductivity, temperature, constant heat absorption of blood in plasma region, respectively.
Phase- III, i.e., $\widetilde{R}_2 < \widetilde{r} \leq \widetilde{R}_3$

$$\frac{\partial \widetilde{w}_B}{\partial \widetilde{z}} = 0, \tag{4.3a}$$

$$\frac{\partial \widetilde{p}_B}{\partial \widetilde{r}} = 0, \tag{4.3b}$$

$$-\frac{\partial \widetilde{p}_B}{\partial \widetilde{z}}+\frac{\widetilde{\mu}_E}{\widetilde{r}}\frac{\partial}{\partial \widetilde{r}}\left(\widetilde{r}\frac{\partial \widetilde{w}_B}{\partial \widetilde{r}}\right)-\frac{\widetilde{\mu}_N}{\widetilde{k}}\widetilde{w}_B-\frac{C_F\widetilde{\rho}_N\widetilde{w}_B^2}{\sqrt{\widetilde{k}}}+\widetilde{g}\widetilde{\rho}_N\widetilde{\gamma}(\widetilde{T}_B-\widetilde{T}_\infty)=0, \tag{4.3c}$$

$$\widetilde{K}_N\left(\frac{\partial^2\widetilde{T}_B}{\partial \widetilde{r}^2}+\frac{1}{\widetilde{r}}\frac{\partial \widetilde{T}_B}{\partial \widetilde{r}}\right)+\widetilde{Q}_N=0, \tag{4.3d}$$

where $\widetilde{p}_B, \widetilde{w}_B, \widetilde{\mu}_E, \widetilde{T}_B$ are the flow parameters of an endothelial glycocalyx layer describing the pressure, velocity along the axial direction, effective viscosity of Brinkman-Forchheimer layer, temperature, respectively; C_F is the inertial coefficient and $\widetilde{k}$ is the permeability (Darcy number) constant in the porous medium.

For solving the differential Eqs. $(4.1)-(4.3)$, firstly, we non-dimensionalise these Eqs $(4.1)-(4.3)$ using the following variables:

$$\begin{aligned}
&\tau_H=\frac{\widetilde{\tau}_H\widetilde{R}_3}{\widetilde{\mu}_N W_0},\ p_H=\frac{\widetilde{p}_H\widetilde{R}_3}{W_0\widetilde{\mu}_N},\ p_N=\frac{\widetilde{p}_N\widetilde{R}_3}{W_0\widetilde{\mu}_N},\ p_B=\frac{\widetilde{p}_B\widetilde{R}_3}{W_0\widetilde{\mu}_N},\ \Theta=\frac{\widetilde{\tau}_y\widetilde{R}_3}{\widetilde{\mu}_N W_0},\ R_p=\frac{\widetilde{R}_p}{\widetilde{R}_3},\\
&r=\frac{\widetilde{r}}{\widetilde{R}_3},\ R_1=\frac{\widetilde{R}_1}{\widetilde{R}_3},\ R_2=\frac{\widetilde{R}_2}{\widetilde{R}_3},\ \gamma_1=\frac{\widetilde{Q}_H\widetilde{R}_3^2}{\widetilde{K}_N(\widetilde{T}_w-\widetilde{T}_\infty)},\ F=\frac{C_F\widetilde{\rho}_N\widetilde{q}_0\widetilde{R}_3^3}{\widetilde{\mu}_E\widetilde{\mu}_N},\\
&\theta_B=\frac{\widetilde{T}_B-\widetilde{T}_\infty}{\widetilde{T}_w-\widetilde{T}_\infty},\ \theta_H=\frac{\widetilde{T}_H-\widetilde{T}_\infty}{\widetilde{T}_w-\widetilde{T}_\infty},\ \theta_N=\frac{\widetilde{T}_N-\widetilde{T}_\infty}{\widetilde{T}_w-\widetilde{T}_\infty},\ \gamma_2=\frac{\widetilde{Q}_N\widetilde{R}_3^2}{\widetilde{K}_N(\widetilde{T}_w-\widetilde{T}_\infty)},\\
&Gr=\frac{\widetilde{g}\widetilde{\rho}_N\widetilde{\gamma}\widetilde{R}_3^2(\widetilde{T}_w-\widetilde{T}_\infty)}{W_0\widetilde{\mu}_N},\ w_H=\frac{\widetilde{w}_H}{W_0},\ w_N=\frac{\widetilde{w}_N}{W_0},\ w_B=\frac{\widetilde{w}_B}{W_0},\ k=\frac{\widetilde{k}}{\widetilde{R}_3^2},\\
&z=\frac{\widetilde{z}}{\widetilde{R}_3},\ \rho_0=\frac{\widetilde{\rho}_N}{\widetilde{\rho}_H},\ K_0=\frac{\widetilde{K}_N}{\widetilde{K}_H},\ \lambda_1^2=\frac{\widetilde{\mu}_E}{\widetilde{\mu}_N},\ S^2=\frac{1}{k\lambda_1^2},\ W_0=\frac{\widetilde{q}_0\widetilde{R}_3^2}{\widetilde{\mu}_N},
\end{aligned} \tag{4.4}$$

where $W_0, \rho_0, K_0, \lambda_1$ are the average (characteristic) velocity, density ratio, thermal conductivity ratio, viscosity ratio parameter, respectively; F is the Forchheimer number, S is the shape parameter in porous media, k is the permeability (Darcy number) of the porous medium and Gr is the free convection parameter or Grashof number.

Using (4.4), the governing equations $(4.1)-(4.3)$ are reduced to the following dimensionless form:

Phase- I, i.e., $0<r\le R_1$

$$\frac{\partial w_H}{\partial z}=0, \tag{4.5a}$$

$$\frac{\partial p_H}{\partial r}=0, \tag{4.5b}$$

$$-\frac{\partial p_H}{\partial z}-\frac{1}{r}\frac{\partial}{\partial r}(r\tau_H)+\frac{Gr\theta_H}{\rho_0}=0, \tag{4.5c}$$

$$\frac{\partial^2\theta_H}{\partial r^2}+\frac{1}{r}\frac{\partial\theta_H}{\partial r}+\gamma_1 K_0=0, \tag{4.5d}$$

where the mathematical expression for Herschel-Bulkley fluid is given as

$$\tau_H = \Theta + \left[e^{-\alpha\theta_H} \left(-\frac{\partial w_H}{\partial r} \right) \right]^{\frac{1}{n}}, \quad \text{if} \quad \tau_H \geq \Theta, \tag{4.5e}$$

$$\frac{\partial w_H}{\partial r} = 0, \quad \text{if} \quad \tau_H \leq \Theta, \tag{4.5f}$$

where $\Theta = \frac{\widetilde{\tau}_y \widetilde{R}_3}{\widetilde{\mu}_N W_0}$ is dimensionless yield stress and $\widetilde{\mu}_H = \widetilde{\mu}_N \left(\frac{\widetilde{R}_3}{W_0 \widetilde{\mu}_N} \right)^{1-n}$ is the constant viscosity coefficient of Herschel-Bulkley fluid.

Phase- II, i.e., $R_1 < r \leq R_2$

$$\frac{\partial w_N}{\partial z} = 0, \tag{4.6a}$$

$$\frac{\partial p_N}{\partial r} = 0, \tag{4.6b}$$

$$-\frac{\partial p_N}{\partial z} + \frac{1}{r}\frac{\partial}{\partial r}\left(r\frac{\partial w_N}{\partial r} \right) + Gr\theta_N = 0, \tag{4.6c}$$

$$\frac{\partial^2 \theta_N}{\partial r^2} + \frac{1}{r}\frac{\partial \theta_N}{\partial r} + \gamma_2 = 0. \tag{4.6d}$$

Phase- III, i.e., $R_2 < r \leq 1$

$$\frac{\partial w_B}{\partial z} = 0, \tag{4.7a}$$

$$\frac{\partial p_B}{\partial r} = 0, \tag{4.7b}$$

$$-\frac{1}{\lambda_1^2}\left(\frac{\partial p_B}{\partial z} \right) + \frac{1}{r}\frac{\partial}{\partial r}\left(r\frac{\partial w_B}{\partial r} \right) - S^2 w_B - FS\lambda_1 w_B^2 + \frac{Gr\theta_B}{\lambda_1^2} = 0, \tag{4.7c}$$

$$\frac{\partial^2 \theta_B}{\partial r^2} + \frac{1}{r}\frac{\partial \theta_B}{\partial r} + \gamma_2 = 0. \tag{4.7d}$$

The dimensionless boundary conditions which are taken into consideration for the present work as follows:

1. The finite temperature and shear stress have been considered on the axis, i.e.,

$$\frac{\partial \theta_H}{\partial r} = 0, \ \text{and} \ \tau_H \ \text{is finite} \quad \text{at} \quad r = 0. \tag{4.8a}$$

2. The flow velocities are considered continuous at both the core-intermediate and intermediate-porous interfaces, i.e.,

$$w_H = w_N \quad \text{at} \quad r = R_1, \tag{4.8b}$$

$$w_N = w_B \quad \text{at} \quad r = R_2. \tag{4.8c}$$

3. At the interface of the Herschel-Bulkley and Newtonian fluid, the continuity of shear stresses have been considered, i.e.,

$$\tau_H = -\frac{\partial w_N}{\partial r} \quad \text{at} \quad r = R_1. \tag{4.8d}$$

4. At the interface of the HB-NF and Newtonian fluid-porous, we considered the continuity of the temperatures, i.e.,

$$\theta_H = \theta_N, \quad \frac{\partial \theta_H}{\partial r} = K_0 \frac{\partial \theta_N}{\partial r} \quad \text{at} \quad r = R_1, \tag{4.8e}$$

$$\theta_N = \theta_B, \quad \frac{\partial \theta_N}{\partial r} = \frac{\partial \theta_B}{\partial r} \quad \text{at} \quad r = R_2. \tag{4.8f}$$

5. Ochoa-Tapia and Whitaker [1] introduced the stress jump condition that delineates the discontinuity in the shear stress of liquid in porous and non-porous regions at the interface. The stress jump interfacial condition is assumed at the fluid-endothelial glycocalyx layer interface [1], i.e.,

$$\frac{1}{\alpha_p}\frac{\partial w_B}{\partial r} - \frac{\partial w_N}{\partial r} = \frac{\beta_S}{\sqrt{k}} w_B \quad \text{at} \quad r = R_2, \tag{4.8g}$$

where α_p denotes the parameter measuring the porosity of medium and β_S denotes the parameter associated with stress jump.

6. The temperature is finite and there is no slip at the microvessels wall, i.e.,

$$\theta_B = 1, \quad w_B = 0 \quad \text{at} \quad r = 1. \tag{4.8h}$$

The non-dimensional volumetric flow rate is denoted by Q_s and given by ([91], [49])

$$\begin{aligned} Q_s &= 8\int_0^1 r w(r) dr, \\ &= 8\left(\int_0^{R_1} r w_H dr + \int_{R_1}^{R_2} r w_N dr + \int_{R_2}^1 r w_B dr\right). \end{aligned} \tag{4.9}$$

The frictional resistance λ_s per unit length of the tube is given by

$$\lambda_s = \frac{p_s}{Q_s}. \tag{4.10}$$

4.3 Solution of the Problem

The pressure gradient in core, intermediate and porous regions are considered as to be non varying, i.e.,

$$\frac{\partial p_H}{\partial z} = \frac{\partial p_N}{\partial z} = \frac{\partial p_B}{\partial z} = -p_s. \tag{4.11}$$

The Reynolds model has been utilize to model the dimensionless viscosity ([41], [45])

$$\mu(\theta_H) = e^{-\alpha\theta_H}, \quad \mu(\theta_H) = 1-\alpha\theta_H \quad \text{for} \quad \alpha \ll 1, \tag{4.12}$$

where α denote the Reynolds model viscosity parameter (index).
Solving the Eqs. (4.5) – (4.6) by using Eqs. (4.11) and (4.12), we get the followings:
Phase- I, i.e., $0 < r \leq R_1$

$$\theta_H = C_1 \ln r + C_2 - \left(\frac{\gamma_1 K_0}{4}\right) r^2, \tag{4.13a}$$

$$\tau_H = \frac{1}{r}\left(\frac{p_s r^2}{2} - \frac{C_1 Gr^2}{4\rho} + \frac{C_1 r^2 Gr \log(r)}{2\rho} + \frac{C_2 r^2 Gr}{2\rho} - \frac{\gamma_1 Gr K_0 r^4}{16\rho}\right) + \frac{C_3}{r}, \tag{4.13b}$$

$$\begin{aligned} w_H = {} & C_4 - \frac{2^{-4n-3}}{(n+1)(n+3)(\alpha C_2 - 1)(C_2 Gr + p_s\rho)} \left(\frac{r\left(8C_2 Gr + \gamma_1(-Gr)K_0 r^2 + 8p_s\rho\right)}{\rho}\right)^n \\ & \left(1 - \frac{\gamma_1 Gr K_0 r^2}{8C_2 G + 8p_s\rho}\right)^{-n} \left(16\Theta\left(n^2+4n+3\right)\rho F_1\left(\frac{n}{2}; 1-n, 1; \frac{n+2}{2}; \frac{Gr K_0 r^2 \gamma_1}{8C_2 Gr + 8p_s\rho}, \frac{K_0 r^2 \alpha \gamma_1}{4C_2\alpha - 4}\right)\right. \\ & + r\left(\gamma_1 Gr K_0 (n+1) r^2 F_1\left(\frac{n+3}{2}; 1-n, 1; \frac{n+5}{2}; \frac{Gr K_0 r^2 \gamma_1}{8C_2 Gr + 8p_s\rho}, \frac{K_0 r^2 \alpha \gamma_1}{4C_2\alpha - 4}\right)\right. \\ & \left.\left. -8(n+3)(C_2 Gr + p_s\rho) F_1\left(\frac{n+1}{2}; 1-n, 1; \frac{n+3}{2}; \frac{Gr K_0 r^2 \gamma_1}{8C_2 Gr + 8p_s\rho}, \frac{K_0 r^2 \alpha \gamma_1}{4C_2\alpha - 4}\right)\right)\right). \end{aligned} \tag{4.13c}$$

Phase- II, i.e., $R_1 \leq r \leq R_2$

$$\theta_N = C_5 \log(r) + C_6 - \left(\frac{\gamma_2}{4}\right) r^2, \tag{4.14a}$$

$$w_N = \left(C_7 - \frac{C_5 r^2 Gr}{4}\right) \log(r) + C_8 + \frac{Gr(C_5 - C_6) r^2}{4} + \frac{\gamma_2 r^4 Gr}{64} - \frac{p_s r^2}{4} \tag{4.14b}$$

4.3.1 Solution for Large Darcy Number

Phase- III, i.e., $R_2 < r \leq 1$

An asymptotic expansion for the velocity distribution in terms of the small parameter S can be written as [85]

$$w_B = w_{B0} + S w_{B1} + S^2 w_{B2} + ..., \tag{4.15}$$

with the assumption that the parameter $S = \frac{1}{\lambda_1 \sqrt{k}}$ is much less than unity, where k is the Darcy number in the porous medium. Mathematically for large Darcy number k, the parameter $S \ll 1$.

Putting the expression of velocity w_B from the above in Eq. (4.15) in the Eq. (4.7b), we have obtained the expressions up to second order for the velocity profile w_B of Forchheimer region as

$$\theta_B = C_9 \log(r) + C_{10} - \left(\frac{\gamma_2}{4}\right) r^2, \tag{4.16a}$$

$$w_{B0} = \frac{1}{64\lambda_1^2}\left(-16\left(GrC_9 r^2 - 4C_{11}\lambda_1^2\right)\log(r) + 64C_{12}\lambda_1^2 + 16Gr(C_9 - C_{10})r^2 + Gr\gamma_2 r^4 - 16p_s r^2\right), \tag{4.16b}$$

$$\frac{\partial^2 w_{B1}}{\partial r^2} + \frac{1}{r}\frac{\partial w_{B1}}{\partial r} = F\lambda_1 w_{B0}^2, \tag{4.16c}$$

$$\frac{\partial^2 w_{B2}}{\partial r^2} + \frac{1}{r}\frac{\partial w_{B2}}{\partial r} = w_{B0} + 2F\lambda_1 w_{B0} w_{B1}. \tag{4.16d}$$

The first and second-order expressions of velocity in the Forchheimer region are cumbersome, so they are not mentioned here.

4.3.2 Solution for Small Darcy Number

Phase- III, i.e., $R_2 < r \leq 1$

For SDN k, the parameter S is very large. Dividing Eq. (4.7b) by S^2, we have

$$-\frac{1}{S^2\lambda_1^2}\left(\frac{\partial p_B}{\partial z}\right) + \frac{S^{-2}}{r}\frac{\partial}{\partial r}\left(r\frac{\partial w_B}{\partial r}\right) - w_B - FS^{-1}\lambda_1 w_B^2 + \frac{Gr\theta_B}{S^2\lambda_1^2} = 0, \tag{4.17}$$

The above equation (4.17) represents singular perturbation problem in respect of a very small parameter S^{-1} because the limiting case $S^{-1} \to 0$ reduces the order of the Eq. (4.17). The work of Bush [84] discusses the detailed description about singular perturbation problem with matched asymptotic technique. Imitating the same approach, first the outer solution

of velocity w_B^o can be written as below by skipping some intermediate terms

$$\begin{aligned} w_B^o(r) &= \frac{w_{B2}}{S^2} + \frac{w_{B4}}{S^4} + \frac{w_{B5}}{S^5} \\ &= \frac{1}{\lambda_1^3 S^5}\left(\lambda_1 S^3\left(Gr\left(C_{10} + C_9\log(r) - \frac{\gamma_2 r^2}{4}\right) + p_s\right) - \gamma_2 Gr\lambda_1 S\right. \\ &\left. -F\left(Gr\left(C_{10} + C_9\log(r) - \frac{\gamma_2 r^2}{4}\right) + p_s\right)^2\right), \end{aligned} \tag{4.18}$$

where the zeroth w_{B0}, first w_{B1} and third w_{B3} order approximation of velocity profile w_B vanishes and the expressions for the second, forth and fifth order velocity profile are given below

$$\begin{aligned} w_{B2} &= \frac{p_s + Gr\theta_B}{\lambda_1^2}, \\ w_{B4} &= \frac{\partial^2 w_{B2}}{\partial r^2} + \frac{1}{r}\frac{\partial w_{B2}}{\partial r}, \\ w_{B5} &= -F\lambda_1 w_{B2}^2. \end{aligned} \tag{4.19}$$

The limit of outer solution can be obtained in terms of inner limit as follow

$$(w_B^o)^{in} = \lim_{S\to\infty} w_B^o = 0. \tag{4.20}$$

Now to obtain the expression representing inner solution, one should adopt the stretched variable as

$$\eta = S(1-r), \tag{4.21}$$

and then to obtain a solution as a single-term, the smaller term $(S^{-1} \to 0)$ should be neglected. The momentum equation reduces to the form

$$\frac{\partial^2 w_B^{in}}{\partial \eta^2} - w_B^{in} = 0. \tag{4.22}$$

The solution ot the above equation is obtained as

$$w_B^{in}(r) = C_{13}e^{-\eta} = C_{13}e^{-S(1-r)}. \tag{4.23}$$

The limit of inner solution can be obtained in terms of outer limit as follow

$$(w_B^{in})^o = \lim_{\eta\to\infty} w_B^{in} = 0 \tag{4.24}$$

To obtain the matching solution from Eq. (4.20) and Eq. (4.24), Prandtl's matching condition has been utilized

$$w_B^m(r) = 0. \tag{4.25}$$

We use the Prandtl's matching condition as described in Bush [84] to find the composite solution of the problem

$$\begin{aligned} w_B &= w_B^o(r) + w_B^{in}(r) - w_B^m(r), \qquad (4.26)\\ &= \frac{1}{\lambda_1^3 S^5}\left(\lambda_1 S^3\left(Gr\left(C_{10} + C_9\log(r) - \frac{\gamma_2 r^2}{4}\right) + p_s\right) - \gamma_2 Gr\lambda_1 S\right.\\ &\left. -F\left(Gr\left(C_{10} + C_9\log(r) - \frac{\gamma_2 r^2}{4}\right) + p_s\right)^2\right) + C_{13}e^{-S(1-r)}. \qquad (4.27)\end{aligned}$$

Where $C_1 - C_{13}$ are arbitrary constants and the values of these constants are obtained using given boundary conditions. Being too complicated, the expressions of constants are not manageable to be mentioned here. The expressions of flow rate Q_s and flow resistance λ_s involves integrals and are numerically calculated through Mathematica 10.0.2 software.

4.4 Results and Discussion

The proposed work intends to research the simultaneous effects of the heat transfer and a permeable glycocalyx layer near the vessel wall on the blood flow modeled here as the flow of a three-layered fluid having a viscosity as a function of temperature through microvessels. Brinkman-Forchheimer equation leads the blood flow through a thin permeable glycocalyx layer at the wall. The investigation of the flow quantities under the influence of numerous parameters such as variable viscosity, porous layer, and heat transfer parameters have been carried out.

4.4.1 Selection of Parametric Values and Validation of the Model

The results have been compared with two-fluid models having constant viscosity and in the absence of the permeable glycocalyx layer near the wall independently. The parameter Gr is actually the Richardson number defined as $Ri = Gr/Re^2$. It is a parameter telling us if the flow is dominated by free convection $Ri > 10$, forced convection $Ri < 1$ or mixed if $1 < Ri < 10$ ([143]-[144]). Keeping the low Reynolds number Re validity in our problem $(0.005 \leq Re \leq 0.5)$, and based on the other literature, the values of Richardson number Ri for forced and free convection are taken as 0.9 and 10^3, respectively. The Brinkman model for

the porous medium is a specific case of our model in the absence of Forchheimer number F. We have fixed the values of some of the parameters $\gamma_0 = \rho_0 = \lambda_1 = 1$ and $\beta_S = 0.5$ throughout the whole study. The work of Tiwari and Chauhan ([28], [49]) provided the various parametric values and the range of additional parameters with their resources are given in Table 4.1.

Values of parameters		
Parameters	Values	Resources
Absorption ratio α_0	$\alpha_0 = 1.00$	[103]
Density ratio ρ_0	$0.92 \leq \rho_0 \leq 1.00$	[34], [103]
Forchheimer number F	$0 \leq F \leq 2$	[131], [132]
Grashof number Gr	$0.5 \leq Gr \leq 10$	[103], [41], [45]
HB fluid parameter n	$0.90 \leq n \leq 1.10$	[91], [28]
Plasma layer thickness h	$0.015 \leq h \leq 0.10$	[103], [28]
Permeability k	$0 < k < \infty$	[131], [132], [49]
Reynolds number Re	$0.005 \leq Re \leq 0.5$	[145], [146]
Richardson number Ri	$0.01 \leq Ri \leq 1000$	[143], [144]
Steady pressure gradient p_s	$1 \leq p_s \leq 10$	[91], [28], [49]
Stress jump parameter β_S	$-1 \leq \beta_S \leq 1$	[68], [49], [51]
Thermal conductivity ratio K_0	$0.4 \leq K_0 \leq 1.0$	[103], [104]

Table 4.1: The range of parameters appropriate for flow through narrow tubes with their resources

4.4.2 Velocity Profile (w)

Figure 4.2:(a) depicts the impact of viscosity index on the variation of flow profile w with radial distance under small and large Darcy number. A decay in flow profile with distance r is observed for constant and variable viscosity under both the cases (SDN and LDN) which is in excellent understanding with the previous work of Tiwari and Chauhan [49]. A novel result is that an increasing viscosity index α contributes to decay in viscosity of the core region fluid owing to smother the fluid velocity (i.e. growth in velocity). A slight difference in velocity profile between large and small Darcy numbers can be accredited to the reduced permeability of the porous medium for the latter case. In Figure 4.2:(b), the difference in velocity profile for the TFM with and without an EGL adjacent to the wall (PW) for small Darcy number and with an EGL adjacent to the wall for large Darcy number are depicted.

As evident in the case of a tube without porous layer at the wall, the fluid velocity is slightly higher owing to reduced resistance. However, for large Darcy numbers, the porous layer reduces to hyperporous cases (i.e. significantly reduced resistance) resulting in the velocity profile almost coinciding with the case of TFM without an endothelial glycocalyx layer adjacent to the wall. For LDN $(k \to \infty)$, the permeability of the porous region will be very high resulting in an almost negligible Brinkman resistance. This situation is depicted in Figure 4.2:(c) where the velocity profile for TFM with the PW for LDN and TFM without PW are almost coincident.

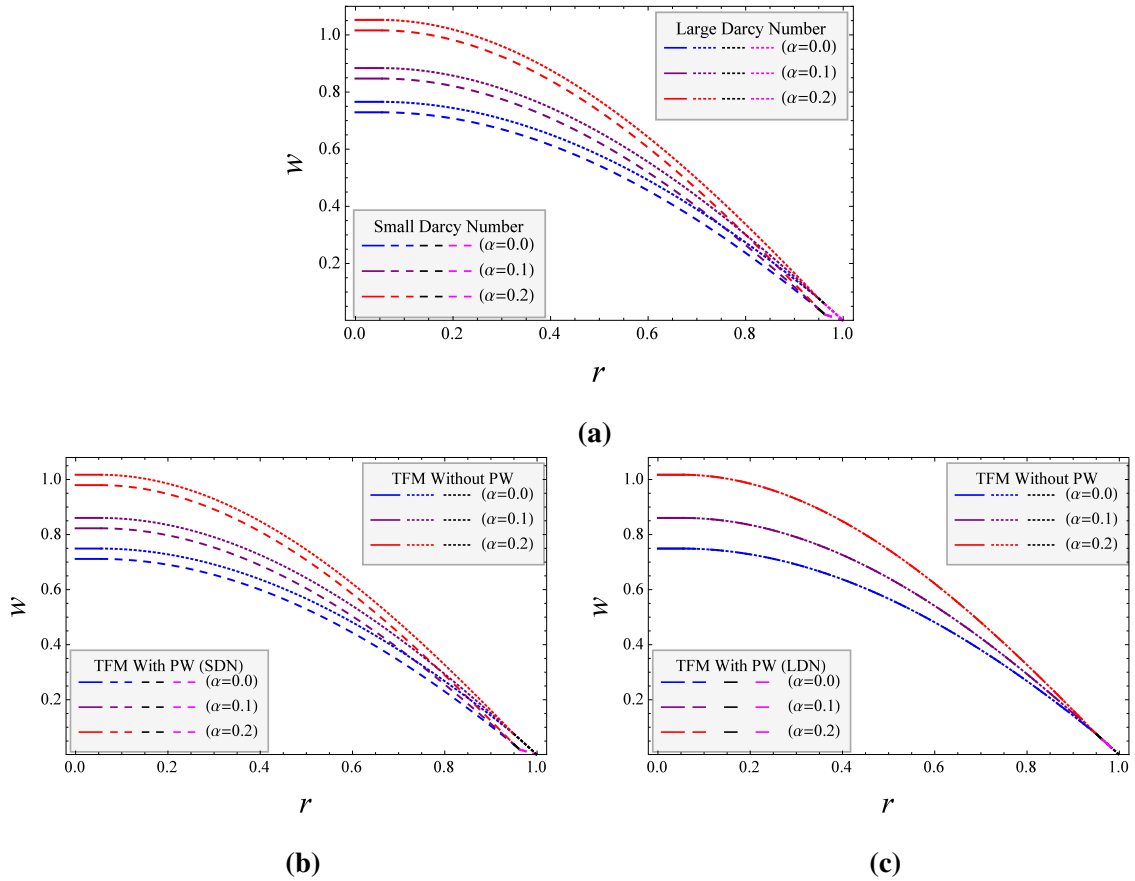

Figure 4.2: Impact of viscosity index α on velocity profile w varying with radial distance r between **(a)** small $(k = 0.05)$ and large Darcy number $(k = 100)$ and **(b)**-**(c)** TFM with and without PW. $(p_s = 1, h = 0.05, K_0 = 0.6, Gr = 1.5)$

Figure 4.3 depicts the effect of the Forchheimer number on velocity profile w_B in the porous region. An increasing Forchheimer number leads to a slight decay in the fluid velocity for the porous region owing to growth in nonlinear resistance term. For Forchheimer number $(F = 0)$, the specific case of Brinkman formulation of the porous region is verified [49].

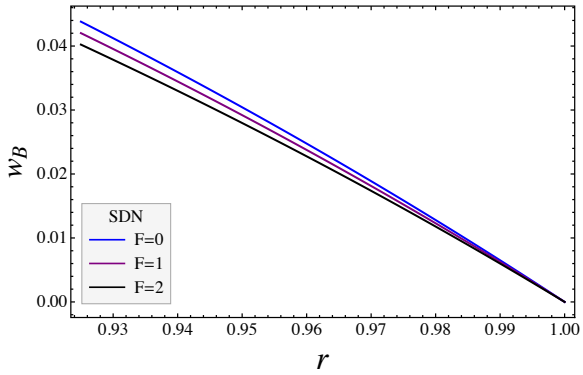

Figure 4.3: Impact of Forchheimer number F on velocity w_B in porous region varying with radial distance r. $(p_s = 1, h = 0.10, k = 0.05, K_0 = 0.6)$

A dominance of free convection over forced convection in the variation of plug flow velocity w_p with pressure gradient is observed in Figure 4.4 for both the formulations (SDN and LDN) under low Reynolds number $(Re = 0.05)$ assumption. The difference in small and large Darcy numbers is wider for free convection in comparison to the forced convection. It is also evident that the growth rate of plug flow velocity is relatively higher for LDN owing to the smoother flow through the porous medium.

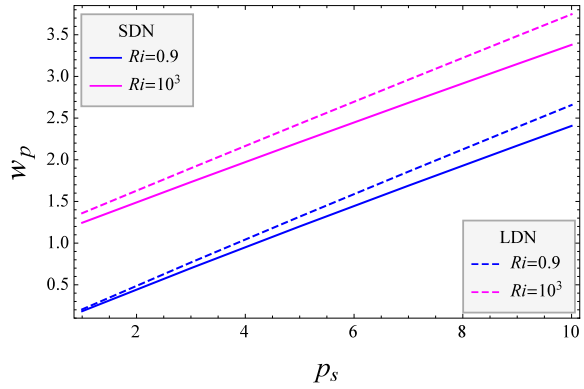

Figure 4.4: Effect of Richardson number Ri on plug core velocity w_p varying with pressure gradient p_s. $(\alpha = h = \Theta = 0.10, k = (0.05, 100), Re = 0.05, K_0 = 0.6, F = 2, n = 0.95)$

The rising thermal buoyancy forces lead to linear enhancement in plug flow velocity w_p as depicted in Figure 4.5:(a) for SDN and LDN. A noteworthy observation is that a rising viscosity parameter leads to an increase in the plug flow velocity for both the cases, which can be accredited to the reduction in viscosity of the core region fluid. A slight difference in plug core velocity with Grashof number is observed in Figure 4.5:(b) for TFM with and without an endothelial glycocalyx layer adjacent with the wall. It is also observed that plug flow velocity is higher for LDN (hyperporous case) in comparison to SDN.

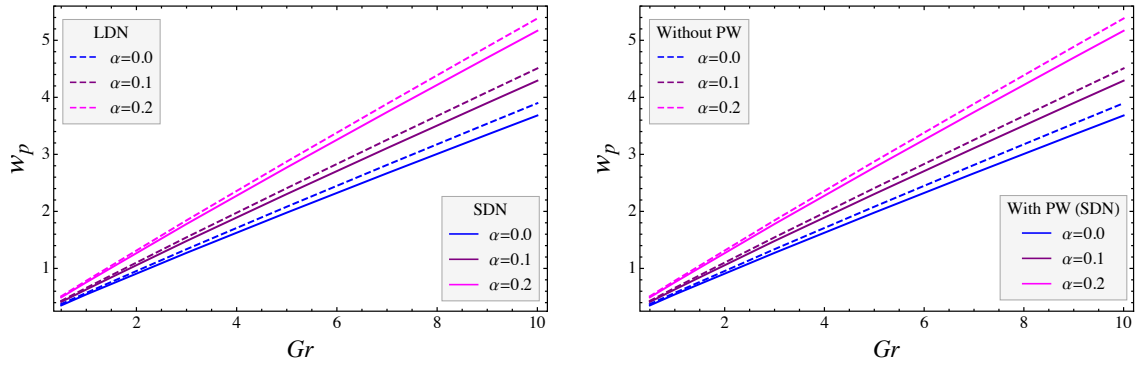

(a) **(b)**

Figure 4.5: Impact of viscosity index α on plug core velocity w_p varying with Grashof number Gr between **(a)** SDN and LDN and **(b)** TFM with and without PW. ($p_s = 1, h = 0.05, K_0 = 0.6, F = 2, \Theta = 0.10, k = (0.05, 100)$)

The plug core velocity increases with rising conductivity ratio as evident from Figure 4.6:(a). This growth rate further increases for higher viscosity parameter and this observation is for both SDN and LDN. Although for LDN, the plug core velocity is slightly higher owing to a relatively smooth flow through porous region. A comparison between flow through microvessels with and without an endothelial glycocalyx layer adjacent with the wall shows a similar observation along with a relatively higher plug core velocity for flow through microvessels without an endothelial glycocalyx layer adjacent with the walls (Figure 4.6:(b)).

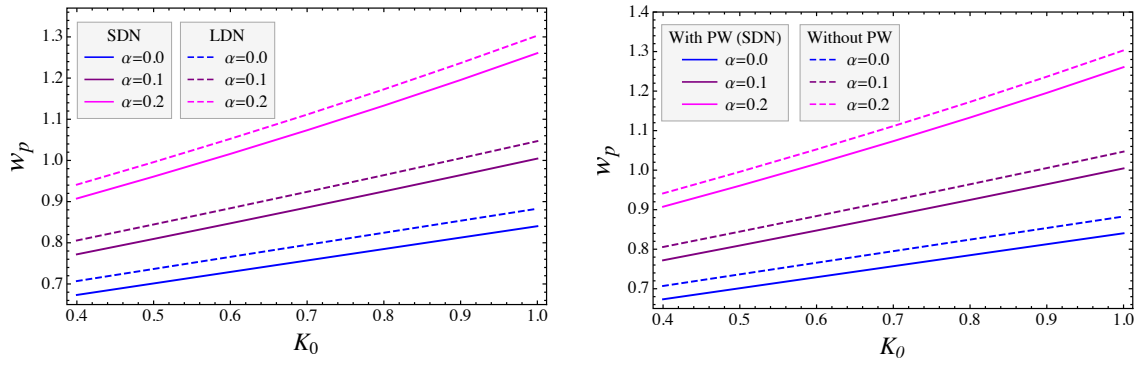

(a) **(b)**

Figure 4.6: Impact of viscosity index α on plug core velocity w_p varying with conductivity ratio K_0 between **(a)** SDN and LDN and **(b)** TFM with and without PW. ($p_s = 1, h = 0.05, Gr = 1.5, F = 2, \Theta = 0.10, k = (0.05, 100)$)

4.4.3 Wall Shear Stress (τ_w)

Like the previous studies, the dominance of thermal buoyancy forces leads to significant growth in wall shear stress τ_w as depicted in Figure 4.7:(a) which is significantly higher

for LDN (hyperporous layer). A noteworthy observation is that increasing Forchheimer number F leads to decay in τ_w for SDN and makes this variation nonlinear, which may be accredited to a significant presence of the non-linear resistance term due to Forchheimer number. however no variation is observed in τ_w with increasing Forchheimer number F for LDN due to negligible presence of the non-linear resistance term into formulation.

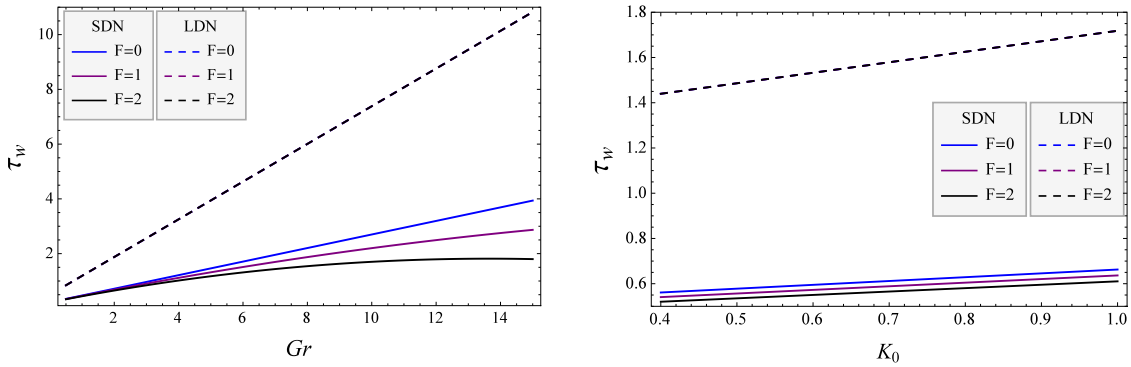

Figure 4.7: Impact of Forchheimer number F on wall shear stress τ_w varying with **(a)** Grashof number Gr $(K_0 = 0.6)$ and **(b)** thermal conductivity ratio K_0 $(Gr = 1.5)$. $(p_s = 1, h = 0.05, \beta_S = 0.1, k = (0.05, 100))$

Figure 4.7:(b) depicts the slight growth in wall shear stress with a conductivity ratio K_0 for SDN and LDN. The growth rate is higher for LDN in comparison to SDN. A remarkable observation is that wall shear stress is slightly higher in case of Brinkman formulation $(F = 0)$ in comparison to Brinkman-Forchheimer formulation $(F \neq 0)$, which may be accredited to a significant presence of the non-linear resistance term due to Forchheimer number.

4.4.4 Flow Rate (Q_s)

Figure 4.8:(a) reveals an increasing flow rate with rising thermal buoyancy forces for small and large Darcy numbers under varying viscosity assumptions. A reduction in core region viscosity (i.e. enhancement in the values of viscosity parameter) contributes to growth in the rate of fluid flow for SDN and LDN cases. Like the above observation in velocity profiles, the value of flow rate is slightly higher for LDN in comparison to SDN under the assumptions of both constant and variable viscosity. A slight difference in the fluid flow rate Q_s with Grashof number is observed in Figure 4.8:(b) for TFM with and without an EGL adjacent with the wall. It is also observed that the flow rate Q_s is higher for flow through tube without porous layer in comparison to with porous layer having small Darcy numbers.

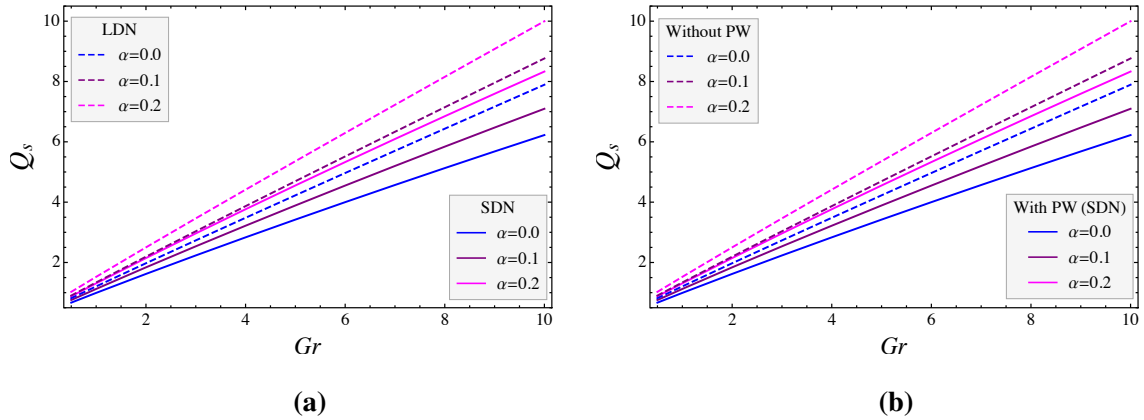

Figure 4.8: Impact of viscosity index α on flow rate Q_s varying with Grashof number between **(a)** SDN and LDN and **(b)** TFM with and without PW. ($p_s = 1, \Theta = h = 0.10, K_0 = 0.6, n = 0.95, F = 2, k = (0.05, 100)$)

The rising thermal conductivity ratio leads to a linear growth in flow rate for SDN and LDN as presented in Figure 4.9. The effect of Forchheimer number F is slightly visible for SDN. For LDN, the effect of Forchheimer number on the variation of flow rate with K_0 is negligible. The Forchheimer number's moderate influence on flow rate can be attributed to very thin porous layer near the wall. This effect may be more significant for a thick porous layer.

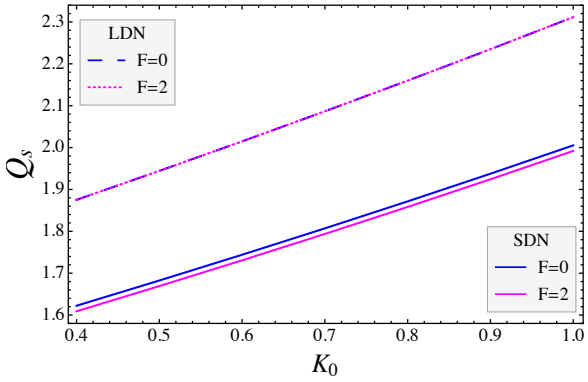

Figure 4.9: Impact of Forchheimer number F on flow rate Q_s varying with conductivity ratio K_0 between SDN and LDN. ($p_s = 1, \Theta = h = 0.10, n = 0.95, \alpha = 0.2, Gr = 1.5, k = (0.05, 100)$)

An increasing flow rate with pressure gradient for all four fluids (Power-law fluid-PL, NF, HB fluid and Bingham-plastic fluid-BP) is observed in Figure 4.10 for natural as well as forced convection. This analysis is being done for SDN. It is further noticed that the difference of growth rate in flow rate Q_s between shear thickening fluids (PL, HB) and non shear thickening fluids (NF, BP) widens with increasing pressure gradient.

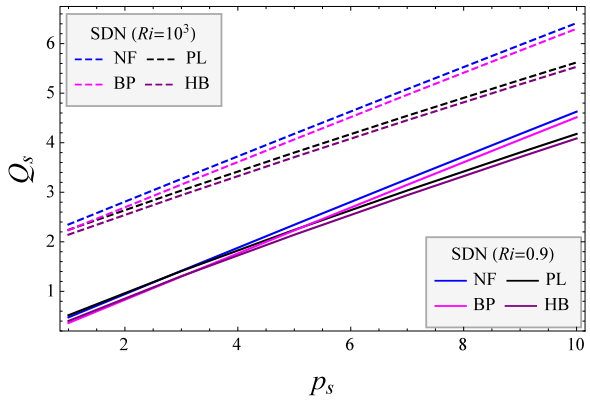

Figure 4.10: Impact of Richardson number Ri on plug core velocity Q_s varying with pressure gradient p_s. ($\alpha = h = \Theta = 0.10, k = Re = 0.05, K_0 = 0.6, F = 2, n = 0.90$)

4.4.5 Flow Resistance (λ_s)

An increasing thermal conductivity ratio contributes to a linear decay in flow resistance for SDN and LDN as demonstrated in Figure 4.11. The effect of Forchheimer number F is slightly visible for SDN. For LDN, the effect of Forchheimer number on the variation of flow resistance with K_0 is negligible. Forchheimer number's moderate influence on flow resistance can be attributed to very thin porous layer near the wall. For a thick porous layer, this effect may be more significant.

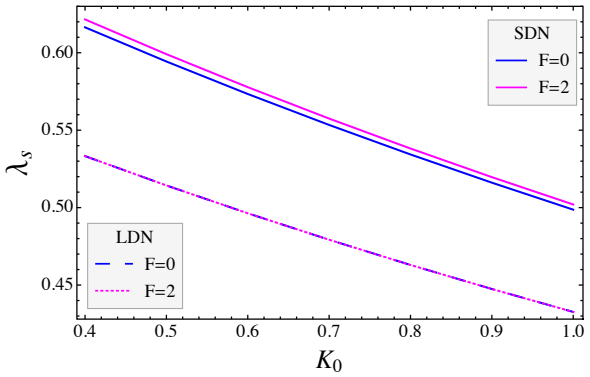

Figure 4.11: Impact of Forchheimer number F on flow resistance λ_s varying with conductivity ratio K_0 between SDN and LDN. ($p_s = 1, \Theta = h = 0.10, n = 0.95, \alpha = 0.2, Gr = 1.5, k = (0.05, 100)$)

A flow resistance λ_s decays with increasing Grashof number Gr as demonstrated in Figure 4.12:(a) which is in good understanding with authors work on micropolar fluid [122]. However, the decay rate slightly reduces with increasing viscosity parameter α. Flow resistance for LDN is relatively lesser in comparison to SDN. A comparison between flow

through microvessels with and without an EGL adjacent to the wall shows a similar observation along with a relatively higher flow resistance for flow through microvessels with an EGL adjacent to the wall (Figure 4.12:(b)).

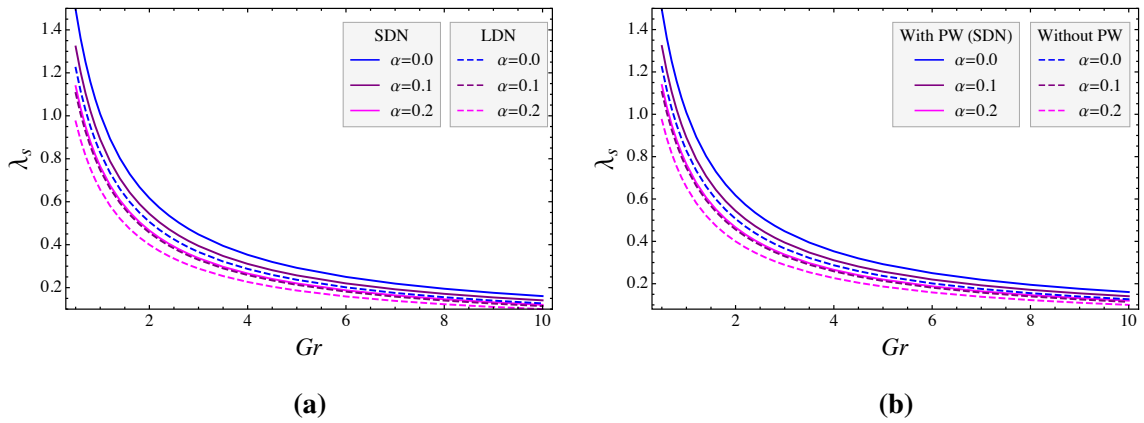

(a) **(b)**

Figure 4.12: Impact of viscosity index α on flow resistance λ_s varying with Grashof number Gr **(a)** under SDN and LDN and **(b)** between TFM with and without PW. ($p_s = 1, K_0 = 0.6, n = 0.95, F = 2, h = \Theta = 0.10, k = (0.05, 100)$)

4.5 Conclusions

The present work investigates the flow characteristic of a three-layer liquid model of blood flow through an endothelial glycocalyx layered microvessels using temperature-dependent viscosity. The Brinkman-Forchheimer model is used for the flow through porous medium, which occurs due to the presence of a glycocalyx layer near the wall which is an extension of the Brinkman model. Throughout the whole discussions, the following interferences can be made:

1. A relatively higher velocity, plug flow velocity and flow rate is observed for lager Darcy number in comparison to small Darcy number however, a reverse observation is made for flow resistance.

2. The viscosity index rises for less viscous core fluid and results into the growth of velocity profile, the higher velocity in plug core region and higher flow rate of fluid. But the flow impedance is observed to be reduced in less viscous core fluid.

3. The significance of high Grashof number and conductivity ratio is observed due to the relative increment in the fluid velocity through plug core region and higher flow rate of fluid.

4. The impact of Forchheimer number on flow quantities is slightly visible for small Darcy number however, it is negligible in case of large Darcy number. This effect is more significant for a thick endothelial glycocalyx layer adjacent with the wall.

5. All the flow variables except the flow resistance assume relatively higher values for flow through microvessels without an EGL adjacent with the wall in comparison to the flow through microvessels with an EGL adjacent with the wall owing to absence of the Brinkman and nonlinear Forchheimer resistance of the porous medium.

Proposed analysis examines the influence of heat transfer over various quantities related to hemodynamic and also establish that the flow quantities are significantly affected by the temperature-dependent viscosity. In the peripheral region, the plasma flow is dominated by the Forchheimer parameter and it may govern the hematocrit by affecting the RBCs concentration.

These effects will be more significant if the endothelial glycocalyx layer thickness become larger. The findings of the present work can be important in such cases as the correct information of the flow variables will be helpful in accurate computation of blood pressure and hematocrit, which may be crucial for medical treatment due to various pathological situations. However, the work defining need to be experimentally verified.

Chapter 5

Solute Dispersion into Microcirculation: A Temperature Dependent Viscosity Approach

5.1 Introduction

Flow through a tube was always a topic of interest among the mathematicians due to its direct application in blood flow through narrow vessels (arterioles, venules and capillaries) ([147], [148]). The mathematical modeling of our physiological systems reveals the influence of various factors on the flow through blood vessels as well as the diffusion of solute due to injecting drugs or nutrients into the tissues through our physiological systems. Due to a complex network of arteries and veins in our body and almost each one having certain distinct properties, it is really difficult to develop a model perfect for all arteries and veins. Now days, due to unusual life style and food habits, the reporting of the cardiovascular diseases have significantly increased causing a big concern for the society. The clinical treatment of various diseases such as cancer involved the transportation of drug through injection or capsule (carrier particles) into our physiological system. The drug is transported to the tissues through diffusion process via circulatory system. In case of treatment through capsule, the carrier particles are targeted at the location of the infected area, which makes the study of solute dispersion pertinent to clinical treatment of diseases like cancer. Besides the above applications, we can also see the role of diffusion process in artificial devices during surgery and the dispersion theory is applied to understand the fabricated accessories like hemodialyzers and annular oxygenators [77].

The wall of the blood vessels are the major barrier in the transportation of the solvent materials among tissues and blood. The mechanism of the mass transportation across their boundaries in circulation are elementary concern in which metabolites and catabolites are exchanged across the narrow tube. This observation makes it more appropriate to look into

[4]This work has been published as **A. Tiwari, P.D. Shah and S.S. Chauhan, "Unsteady solute dispersion in two-fluid flowing through narrow tubes: A temperature-dependent viscosity approach",** ***International Journal of Thermal Sciences*** **161 (2021) 106651.**

the mass transport across the boundaries (vessel walls) which was missing in earlier works. In order to address this issue, Sankarasubramanian and Gill [2] developed a new approach of mass transport across their boundaries in which they applied the series expansion method to solve the convective dispersion equation with inter-phase mass transfer. A novel observation was that a new term “exchange coefficient" arise by including the absorption effect at wall reflecting the interphase mass transport of the solute. The impact of irreversible boundary reactions on solute dispersion in viscoelastic/non-viscoelastic fluids (Casson and HB fluid) through a conduit or annular tube has been discussed by many investigators ([149], [87], [150], [151], [152], [88]) and they observed that the diffusion coefficients and mean concentration are influenced by non-Newtonian behavior of fluid, mass transport across the boundary, catheter size and reaction at wall ([153], [154]). Recently, Rana and Murthy ([111], [112]) discussed the impact of irreversible wall reactions on solute dispersion in yield-stress fluids (Casson and Herschel-Bulkley fluids) flowing through a tube by assuming a periodic pressure driven flow and they analyzed the effect of Womersley number, yield stress and boundary retention on diffusion process. They [89] also studied the solute dispersion in different non-Newtonian fluids (Carreau and Carreau-Yasuda fluids) flowing through a tube with boundary absorption.

In the recent times, the most dangerous disease is well known as cancer or malignant tumor causing concern for society. The researchers made their contributions via mathematical modeling to develop the treatment for the cure of diseases. In this process, the infected cancerous cells are targeted through the radiation obtained from the transformation of the absorbed energy without damaging the healthy tissues. The combined effect of heat transfer with temperature parameters and magnetic field in transverse direction on the circulation of Newtonian fluid (NF) flowing through the vertical annulus was analyzed by Mekheimer and Abd Elmaboud [20] in which the governing equations are solved under the presumptions of long wavelength approximations and zero Reynolds number. Misra *et al.* [115] computed the flow rate of blood flow in blood vessels during electromagnetic hyperthermia which is applicable in therapeutic procedure for cancer or malignant tumor treatment. The periodic nature of NF flowing through a catheterized tube with mild constriction under heat transfer was done by Abd Elmaboud and Mekheimer [155] and they pointed out that the flow quantities are influenced by the heat transfer, catheter size and constriction height. The aforementioned studies pertains the flow of SFM of blood through conduit but according to the experimental work of Bugliarello and Sevilla [27], the blood exhibit the two-fluid nature whenever it flows through narrow tube. Ponalagusamy and Selvi [103] theoretically investigated the oscillatory flow of TFM in a constricted tube by assuming blood as Newtonian fluid in both the regions using heat transfer and magnetic field approach and they observed

that the dominance of thermal buoyancy forces and rise in the peripheral layer thickness lead to decay in frictional resistance. Recently, Tiwari *et al.* [122] discussed the impact of micro-level properties of the fluid on three-layered model of the micropolar-Newtonian fluid flow through microvessels with porous region near the wall using heat transfer approach.

Recently, Tiwari *et al.* [156] analyzed the influence of porous layer and position-dependent viscosity parameters on solute dispersion in the circulation of two-fluid model of blood flowing through microvessels consisting a porous region near the absorbing walls and observed that the inclusion of porous layer near the absorbing vessel wall and position-dependent viscosity reduces the convective coefficient.

Going through the above literature and to the best of author's knowledge, the composition of variable nature of viscosity (temperature-dependent viscosity) for Herschel-Bulkley fluid and heat transfer aspect on solute dispersion process in two-fluid model of blood flow through smaller diameter blood vessels with reactive walls did not receive enough attention, despite a physiologically realistic situation in transportation or mixing of drugs or injecting the solute in vascular systems of the human body and resolve the medical problems.

An analytical treatment of solute dispersion in a TFM of blood flowing through a smaller diameter tube with reactive walls under the temperature-dependent viscosity and heat transfer aspect has been done in the present study by taking blood as viscoelastic (Herschel-Bulkley) fluid occupied in a central region and Newtonian fluid occupied in a plasma region near the wall. Mathematical expressions of diffusion coefficients have also been found by using the generalized dispersion model [2] by assuming the viscosity parameter of Reynolds model to be less than unity. Influence of viscosity and temperature parameters on diffusion coefficients like convective, dispersion coefficients and mean concentration are analyzed and the results are compared with previous studies on constant viscosity model.

The present work is divided into 5 sections. The mathematical formulation of the hydrodynamic flow is demonstrated in Sec. 2 comprising the statement of the problem, model description, governing equations for flow profile, non-dimentionalization and their respective analytical solutions of the governing equations for core as well as plasma regions. The mathematical statement and governing equation for unsteady convective diffusion equation is presented in Sec. 3 which includes the initial and boundary conditions, the solution expressions for the diffusion coefficients and mean concentration. Results and graphical analysis is presented in Sec. 4 for diffusion coefficients and mean concentration of the solution. The summary and conclusions are presented at the end of the work.

5.2 Mathematical Formulation

5.2.1 Statement of the Problem and Model Description

Blood flowing through the narrow vessels can be segregated into plasma fluid and cells infused core fluid and therefore modeling the flow of blood as the flow of two fluids is quintessential for microvessels. Plasma being a cell free fluid and exhibiting a Newtonian behavior is assumed to be the Newtonian fluid with constant viscosity in Region-II. In the core, suspension of blood cells triggers non-Newtonian behavior and therefore represented as Herschel-Bulkley fluid with temperature-dependent viscosity in Region-I. Based on the above assumptions, the physical model concerns the steady flow of a two-fluid model of blood flow through microvessels under the presumptions of interphase mass transport through the vessel walls. The flow is assumed to be laminar, unidirectional (along the axial direction only $(0,0,\widetilde{w}_{\widetilde{z}})$), axially symmetric and fully developed. Due to a cylindrical tube representation of blood vessel, the cylindrical coordinates systems $(\widetilde{r},\phi,\widetilde{z})$ has been used for mathematical formulations, where $\widetilde{r}$, $\widetilde{z}$ are the transverse and axial coordinates and whose origin is situated on the vessel axis. To replicate the transportation of nutrients through the vessel wall, the absorbing nature of vessel walls have been considered.

The physical sketch of the present work for two-fluid model is demonstrated in Figure 5.1, where $\widetilde{R}_1$ and $\widetilde{R}_2$ are the radii of the central and plasma regions of the blood vessel, respectively and $\widetilde{R}_p$ is the plug core radius.

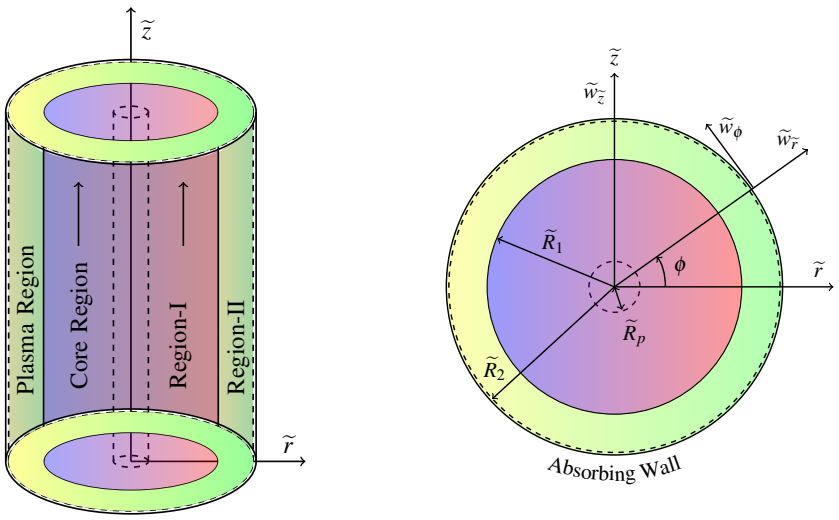

Figure 5.1: The schematic diagram of model description for two-fluid model through microvessel with absorbing walls

5.2.2 Governing Equations of Hydrodynamical Flow

Following the above presumptions, the equations which drive the flow are as follows:

Region- I, i.e., $0 < \widetilde{r} \leq \widetilde{R}_1$

$$\frac{\partial \widetilde{w}_H}{\partial \widetilde{z}} = 0, \tag{5.1a}$$

$$\frac{\partial \widetilde{p}_H}{\partial \widetilde{r}} = 0, \tag{5.1b}$$

$$-\frac{\partial \widetilde{p}_H}{\partial \widetilde{z}} - \frac{1}{\widetilde{r}}\frac{\partial}{\partial \widetilde{r}}(\widetilde{r}\widetilde{\tau}_H) + \widetilde{g}\widetilde{\rho}_H\widetilde{\gamma}(\widetilde{T}_H - \widetilde{T}_\infty) = 0, \tag{5.1c}$$

$$\widetilde{K}_H\left(\frac{\partial^2 \widetilde{T}_H}{\partial \widetilde{r}^2} + \frac{1}{\widetilde{r}}\frac{\partial \widetilde{T}_H}{\partial \widetilde{r}}\right) + \widetilde{Q}_H = 0, \tag{5.1d}$$

where shear stress $\widetilde{\tau} = |\widetilde{\tau}_{\widetilde{r}\widetilde{z}}| = -\widetilde{\tau}_{\widetilde{r}\widetilde{z}}$ (since $\widetilde{\tau} = \widetilde{\tau}_H$ or $\widetilde{\tau} = \widetilde{\tau}_N$).

The mathematical expression for the Herschel-Bulkley fluid is given as

$$\widetilde{\tau}_H = \widetilde{\tau}_y + \left[\widetilde{\mu}(\widetilde{T}_H)\left(-\frac{\partial \widetilde{w}_H}{\partial \widetilde{r}}\right)\right]^{\frac{1}{n}}, \quad \text{if} \quad \widetilde{\tau}_H > \widetilde{\tau}_y, \tag{5.1e}$$

$$\frac{\partial \widetilde{w}_H}{\partial \widetilde{r}} = 0, \quad \text{if} \quad \widetilde{\tau}_H \leq \widetilde{\tau}_y, \tag{5.1f}$$

where $\widetilde{\rho}_H, \widetilde{p}_H, \widetilde{w}_H, \widetilde{\mu}(\widetilde{T}_H), \widetilde{K}_H, \widetilde{T}_H, \widetilde{Q}_H$ are the density, pressure, axial velocity, temperature dependent viscosity, thermal conductivity, temperature, constant heat absorption of blood in core region, respectively and $\widetilde{g}$ the acceleration due to gravity; $\widetilde{\tau}_H$ the shear stress of HB fluid; $\widetilde{\tau}_y$ the yield stress; $\widetilde{\gamma}$ the coefficient of the volume expansion due to the temperature and $\widetilde{T}_\infty$ is the uniform temperature of the fluid at the center of the constriction.

Region- II, i.e., $\widetilde{R}_1 < \widetilde{r} \leq \widetilde{R}_2$

$$\frac{\partial \widetilde{w}_N}{\partial \widetilde{z}} = 0, \tag{5.2a}$$

$$\frac{\partial \widetilde{p}_N}{\partial \widetilde{r}} = 0, \tag{5.2b}$$

$$-\frac{\partial \widetilde{p}_N}{\partial \widetilde{z}} + \frac{\widetilde{\mu}_N}{\widetilde{r}}\frac{\partial}{\partial \widetilde{r}}\left(\widetilde{r}\frac{\partial \widetilde{w}_N}{\partial \widetilde{r}}\right) + \widetilde{g}\widetilde{\rho}_N\widetilde{\gamma}(\widetilde{T}_N - \widetilde{T}_\infty) = 0, \tag{5.2c}$$

$$\widetilde{K}_N\left(\frac{\partial^2 \widetilde{T}_N}{\partial \widetilde{r}^2} + \frac{1}{\widetilde{r}}\frac{\partial \widetilde{T}_N}{\partial \widetilde{r}}\right) + \widetilde{Q}_N = 0, \tag{5.2d}$$

where $\widetilde{\rho}_N, \widetilde{p}_N, \widetilde{w}_N, \widetilde{\mu}_N, \widetilde{K}_N, \widetilde{T}_N, \widetilde{Q}_N$ are the density, pressure, axial velocity, viscosity, thermal conductivity, temperature, constant heat absorption of blood in plasma region, respectively. The expression of the temperature-dependent viscosity of Reynolds model is assumed as

([47], [41], [28])

$$\widetilde{\mu}(\widetilde{T}_H) = \widetilde{\mu}_H e^{-\alpha\left(\frac{\widetilde{T}_H - \widetilde{T}_\infty}{\widetilde{T}_w - \widetilde{T}_\infty}\right)}, \tag{5.3}$$

where α ($\ll 1$) is the viscosity parameter (index); $\widetilde{\mu}_H$ is the constant viscosity coefficient of HB fluid and $\widetilde{T}_w$ is the temperature of the vessel wall.
The boundary conditions (BCs) are given as

$$\begin{gathered}
\widetilde{\tau}_H \text{ is finite and } \frac{\partial \widetilde{T}_H}{\partial \widetilde{r}} = 0, \text{ at } \widetilde{r} = 0, \\
\widetilde{\tau}_H = -\widetilde{\mu}_N \frac{\partial \widetilde{w}_N}{\partial \widetilde{r}},\ \widetilde{w}_H = \widetilde{w}_N,\ \widetilde{T}_H = \widetilde{T}_N,\ \widetilde{K}_H \frac{\partial \widetilde{T}_H}{\partial \widetilde{r}} = \widetilde{K}_N \frac{\partial \widetilde{T}_N}{\partial \widetilde{r}}, \text{ at } \widetilde{r} = \widetilde{R}_1, \\
\widetilde{w}_N = 0,\ \widetilde{T}_N = \widetilde{T}_w, \text{ at } \widetilde{r} = \widetilde{R}_2.
\end{gathered} \tag{5.4}$$

Let the pressure gradient for different regions to be constant ([28], [49], [91]) i.e.

$$\frac{\partial \widetilde{p}_H}{\partial \widetilde{z}} = \frac{\partial \widetilde{p}_N}{\partial \widetilde{z}} = -\widetilde{q}_0 p_s, \tag{5.5}$$

where $\widetilde{q}_0$ is the negative pressure gradient and p_s is the non-dimensional steady state pressure gradient.

5.2.3 Non-Dimensional Parameters and Governing Equations

To solve the above system of Eqs. $(5.1-5.3)$ with boundary conditions (5.4), the following dimensionless variables are introduced:

$$\begin{gathered}
\tau_H = \frac{\widetilde{\tau}_H \widetilde{R}_2}{\widetilde{\mu}_N W_0},\ p_H = \frac{\widetilde{p}_H \widetilde{R}_2}{W_0 \widetilde{\mu}_N},\ p_N = \frac{\widetilde{p}_N \widetilde{R}_2}{W_0 \widetilde{\mu}_N},\ \Theta = \frac{\widetilde{\tau}_y \widetilde{R}_2}{\widetilde{\mu}_N W_0},\ \gamma_1 = \frac{\widetilde{Q}_H \widetilde{R}_2^2}{\widetilde{K}_N (\widetilde{T}_w - \widetilde{T}_\infty)}, \\
r = \frac{\widetilde{r}}{\widetilde{R}_2},\ z = \frac{\widetilde{D}_m \widetilde{z}}{\widetilde{R}_2^2 W_0},\ w_H = \frac{\widetilde{w}_H}{W_0},\ w_N = \frac{\widetilde{w}_N}{W_0},\ R_1 = \frac{\widetilde{R}_1}{\widetilde{R}_2},\ \gamma_2 = \frac{\widetilde{Q}_N \widetilde{R}_2^2}{\widetilde{K}_N (\widetilde{T}_w - \widetilde{T}_\infty)}, \\
\theta_H = \frac{\widetilde{T}_H - \widetilde{T}_\infty}{\widetilde{T}_w - \widetilde{T}_\infty},\ \theta_N = \frac{\widetilde{T}_N - \widetilde{T}_\infty}{\widetilde{T}_w - \widetilde{T}_\infty},\ Gr = \frac{\widetilde{g} \widetilde{\rho}_N \widetilde{\gamma} \widetilde{R}_2^2 (\widetilde{T}_w - \widetilde{T}_\infty)}{W_0 \widetilde{\mu}_N},\ Pe = \frac{W_0 \widetilde{R}_2}{\widetilde{D}_m}, \\
\rho_0 = \frac{\widetilde{\rho}_N}{\widetilde{\rho}_H},\ \gamma_0 = \frac{\gamma_2}{\gamma_1},\ K_0 = \frac{\widetilde{K}_N}{\widetilde{K}_H},\ t = \frac{\widetilde{D}_m \widetilde{t}}{\widetilde{R}_2^2},\ C = \frac{\widetilde{C}}{C_0},\ W_0 = \frac{\widetilde{q}_0 \widetilde{R}_2^2}{\widetilde{\mu}_N},\ \beta = \frac{\widetilde{k} \widehat{R}_2}{\widetilde{D}_m},
\end{gathered} \tag{5.6}$$

where γ_0 is the fraction of absorption coefficient in cell free region to absorption coefficient in core region; W_0 is the average velocity; Pe is the Peclet number and ρ_0 is the density ratio. Using Eq. (5.6), the governing Eqs. $(5.1)-(5.3)$ with boundary conditions (5.4) in dimensionless form will become:

Region- I, i.e., $0 < r \leq R_1$

$$\frac{\partial p_H}{\partial r} = 0, \tag{5.7a}$$

$$-\frac{\partial p_H}{\partial z} - \frac{1}{r}\frac{\partial}{\partial r}(r\tau_H) + \frac{Gr\theta_H}{\rho_0} = 0, \tag{5.7b}$$

$$\frac{\partial^2 \theta_H}{\partial r^2} + \frac{1}{r}\frac{\partial \theta_H}{\partial r} + \gamma_1 K_0 = 0, \tag{5.7c}$$

where the mathematical expression for Herschel-Bulkley fluid is given as

$$\tau_H = \Theta + \left[e^{-\alpha\theta_H}\left(-\frac{\partial w_H}{\partial r}\right)\right]^{\frac{1}{n}}, \quad \text{if} \quad \tau_H > \Theta, \tag{5.7d}$$

$$\frac{\partial w_H}{\partial r} = 0, \quad \text{if} \quad \tau_H \leq \Theta, \tag{5.7e}$$

where $\Theta = \frac{\widetilde{\tau}_y \widetilde{R}_2}{\widetilde{\mu}_N W_0}$ is dimensionless yield stress and $\widetilde{\mu}_H = \widetilde{\mu}_N \left(\frac{\widetilde{R}_2}{W_0 \widetilde{\mu}_N}\right)^{1-n}$.
Region- II, i.e., $R_1 < r \leq 1$

$$\frac{\partial w_N}{\partial z} = 0, \tag{5.8a}$$

$$\frac{\partial p_N}{\partial r} = 0, \tag{5.8b}$$

$$-\frac{\partial p_N}{\partial z} + \frac{1}{r}\frac{\partial}{\partial r}\left(r\frac{\partial w_N}{\partial r}\right) + Gr\theta_N = 0, \tag{5.8c}$$

$$\frac{\partial^2 \theta_N}{\partial r^2} + \frac{1}{r}\frac{\partial \theta_N}{\partial r} + \gamma_2 = 0, \tag{5.8d}$$

where K_0 is the fraction of thermal conductivity in cell free plasma layer to thermal conductivity in core region and Gr is the free convection parameter or Grashof number.
The boundary conditions (BCs) in dimensionless form are given as

$$\begin{gathered} \tau_H \text{ is finite and } \frac{\partial \theta_H}{\partial r} = 0 \quad \text{at} \quad r = 0, \\ \tau_H = -\frac{\partial w_N}{\partial r},\ w_H = w_N,\ \theta_H = \theta_N,\ \frac{\partial \theta_H}{\partial r} = K_0 \frac{\partial \theta_N}{\partial r}, \quad \text{at} \quad r = R_1, \\ w_N = 0,\ \theta_N = 1 \quad \text{at} \quad r = 1. \end{gathered} \tag{5.9}$$

The Reynolds model of viscosity for Herschel-Bulkley fluid can be approximated as ([41], [45])

$$\mu(\theta_H) = e^{-\alpha\theta_H}, \quad \mu(\theta_H) = 1 - \alpha\theta_H \quad \text{for} \quad \alpha \ll 1, \tag{5.10}$$

where α denote the Reynolds model viscosity parameter (index).
Let the pressure gradients to be constant for steady flow state ([28], [49], [91])

$$\frac{\partial p_H}{\partial z} = \frac{\partial p_N}{\partial z} = -p_s. \tag{5.11}$$

5.2.4 Analytical Solution of the Governing Equations

Solving Eqs. (5.7) and (5.8) by using Eqs. (5.10) and (5.11), we get the followings:

The temperature profile, shear stress and axial velocity of core region fluid are obtained as below

$$\theta_H = C_1 \log(r) + C_2 - \frac{\gamma_1 K_0}{4} r^2, \tag{5.12a}$$

$$\tau_H = \frac{r^2\left(-4C_1 Gr + 8C_2 Gr - \gamma_1 Gr K_0 r^2 + 8p_s\rho_0\right) + 8GrC_1 r^2 \log(r)}{16\rho_0 r} + \frac{C_3}{r}, \tag{5.12b}$$

$$\begin{aligned} w_H = {} & C_4 - \frac{2^{-4n-3}}{(n+1)(n+3)(\alpha C_2 - 1)(C_2 Gr + p_s\rho_0)} \\ & \times \left(\frac{r\left(8C_2 Gr - \gamma_1 Gr K_0 r^2 + 8p_s\rho_0\right)}{\rho_0}\right)^n \left(1 - \frac{\gamma_1 Gr K_0 r^2}{8C_2 Gr + 8p_s\rho_0}\right)^{-n} \\ & \times \left(8(n+3)\left(2\Theta(n+1)\rho_0 F_1\left(\frac{n}{2}; 1-n, 1; \frac{n+2}{2}; \frac{Gr K_0 r^2 \gamma_1}{8C_2 Gr + 8p_s\rho_0}, \frac{K_0 r^2 \alpha \gamma_1}{4C_2\alpha - 4}\right)\right.\right. \\ & -r(C_2 Gr + p_s\rho_0) F_1\left(\frac{n+1}{2}; 1-n, 1; \frac{n+3}{2}; \frac{Gr K_0 r^2 \gamma_1}{8C_2 Gr + 8p_s\rho_0}, \frac{K_0 r^2 \alpha \gamma_1}{4C_2\alpha - 4}\right)\Big) \\ & \left.+\gamma_1 Gr K_0 (n+1) r^3 F_1\left(\frac{n+3}{2}; 1-n, 1; \frac{n+5}{2}; \frac{Gr K_0 r^2 \gamma_1}{8C_2 Gr + 8p_s\rho_0}, \frac{K_0 r^2 \alpha \gamma_1}{4C_2\alpha - 4}\right)\right). \end{aligned} \tag{5.12c}$$

and temperature profile and axial velocity of plasma region fluid are obtained as

$$\theta_N = C_5 \log(r) + C_6 - \frac{\gamma_2 r^2}{4}, \tag{5.13a}$$

$$w_N = \log(r)\left(C_7 - \frac{1}{4} Gr C_5 r^2\right) + C_8 + \frac{1}{4} Gr C_5 r^2 - \frac{1}{4} Gr C_6 r^2 + \frac{1}{64} Gr\gamma_2 r^4 - \frac{p_s r^2}{4}, \tag{5.13b}$$

where $C_1 - C_8$ are arbitrary constants. Due complexity of the expressions, constants are evaluated by using MATHEMATICA 10.0.2 with help of the boundary conditions (5.9) which are not mentioned here due to very large expressions and hence the complete mathematical expressions for the axial velocities have not been presented in the manuscript.

5.3 Concentration Solution

5.3.1 Governing Equations

Taylor's dispersion of a solute injected into the two-fluid model portraying the flow of blood flowing through the vessel with absorbing wall and having radius $\widetilde{R}_2$ is delineated in Figure 5.2. The convection which arises due to fluid velocity represents the movement of the cross-section consisting a swarm of particles. Scattering of solute particles along the radial direction in axially symmetric manner leads to the introduction of molecular diffusion term which is represented through red dashed arrows in the Figure 5.2. Further, the concentration profile owing to the combined effect of the convection and dispersion is depicted near the exit end of the tube. The concentration C of the solvent into the unidirectional fully de-

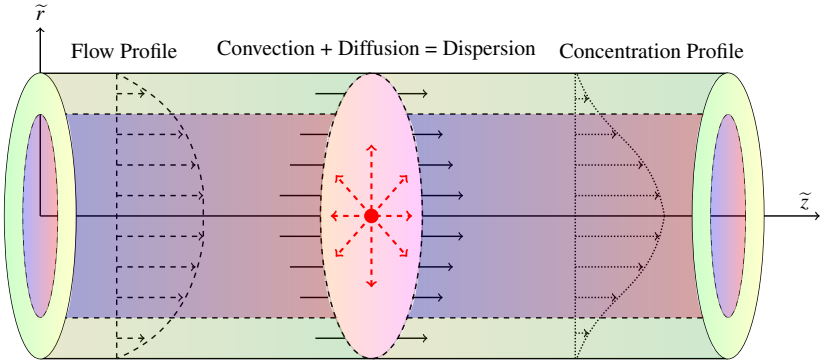

Figure 5.2: The physical sketch of the solute dispersion process for two-fluid model

veloped, axisymmetric, laminar, steady flow of incompressible fluid through narrow blood vessel is governed by the non-dimensional diffusion equation as scripted bellow.

$$\frac{\partial C}{\partial t} + w(r)\frac{\partial C}{\partial z} = \frac{1}{r}\frac{\partial}{\partial r}\left(r\frac{\partial C}{\partial r}\right) + \frac{1}{Pe^2}\frac{\partial^2 C}{\partial z^2}, \tag{5.14}$$

where $w(r)$ is the axial velocity of the fluid in artery and $\widetilde{D}_m$ is coefficient of molecular diffusion (molecular diffusivity), which is assumed to be constant, C_0 is the reference concentration, Pe is the Peclet number and $\frac{d\widetilde{p}}{d\widetilde{z}}$ is the applied pressure gradient along the axis of the artery.

5.3.2 Initial and Boundary Conditions

5.3.2.1 Initial Condition (IC)

Initially the solute is believed to be uniformly distributed and as the diffusion process initiates, the concentration distribution in the system is noted as below

$$C(0,z,r) = \psi(z)X(r), \tag{5.15a}$$

with

$$\psi(z) = \frac{\delta(z)}{d^2 Pe}, \tag{5.15b}$$

and

$$X(r) = \begin{cases} 1, & 0 < r \leq d, \\ 0, & d < r \leq 1, \end{cases} \tag{5.15c}$$

where $\delta(z)$ is Dirac delta function.

5.3.2.2 Boundary Conditions (BCs)

At any instant of time, the first ordered irreversible reaction at tube wall is heterogeneous and the system having a finite concentration can be drafted as the boundary conditions given by

$$\frac{\partial C}{\partial r}(t,z,r) = -\beta C(t,z,r), \text{ at } r = 1, \tag{5.16a}$$

$$C(t,z,r) = \frac{\partial C}{\partial z}(t,z,r) = 0, \text{ as } z \to \infty, \tag{5.16b}$$

$$C(t,z,r) = \text{finite}, \text{ at } r = 0, \tag{5.16c}$$

here $\beta = \frac{\widetilde{k}\widetilde{R}_2}{\widetilde{D}_m}$ denotes the parameter of wall absorption in non-dimensional form and $\widetilde{k}$ is the constant reaction rate.

5.3.3 Diffusion Coefficients and Mean Concentration

The solution of the equation (5.14) with the help of the initial and boundary conditions $(5.15)-(5.16)$ has been obtained using Sankarasubramanian and Gill [2] approach to finally obtain the diffusion coefficients and mean concentration. The solution expression for the

exchange coefficient $M_0(t)$ is obtained as

$$M_0(t) = -\frac{\sum_0^\infty A_k \alpha_k J_1(\alpha_k) e^{-\alpha_k^2 t}}{\sum_0^\infty \left(\frac{A_k}{\alpha_k}\right) J_1(\alpha_k) e^{-\alpha_k^2 t}}, \tag{5.17a}$$

which is exactly the same as derived in the previous works ([2], [87], [88], [89]) as its computation does not include fluid velocity.
The expression for convection coefficient (M_1) is obtained as

$$M_1 = \frac{-2\alpha_0^2}{(\alpha_0^2+\beta^2)J_0^2(\alpha_0)} \int_0^1 w(r) r J_0^2(\alpha_0 r) dr. \tag{5.17b}$$

The expression for the dispersion coefficient (M_2) is given by

$$M_2 = \frac{1}{Pe^2} - \frac{4\alpha_0 J_1(\alpha_0)}{(\alpha_0^2+\beta^2)J_0^2(\alpha_0)} \int_0^1 (w(r)+M_1) g_1(r) r J_0(\alpha_0 r) dr. \tag{5.17c}$$

The expression for the mean concentration (C_M) of the solute is obtained as

$$C_M(t,z) = \frac{1}{2Pe\sqrt{\pi T}} \mathrm{Exp}\left(\eta - \frac{z_1^2}{4T}\right). \tag{5.17d}$$

The detailed description of the solution method and derivation of the diffusion coefficients as well as mean concentration has been provided in 1.5.3.

5.4 Results and Discussion

The simultaneous impact of temperature-dependent viscosity and heat transfer on solute dispersion in a two-fluid model of blood flowing through narrow blood vessels with reactive walls has been done in the present work by assuming the generalized dispersion model [2]. Blood is taken as two-fluid model consisting with a central region occupied by viscoelastic (Herschel-Bulkley) fluid and a cell free region near wall occupied by Newtonian fluid. Heat transfer approach and temperature-dependent viscosity has been taken into account, which helps us in better way in the medical treatments. The impact of various parameters such as thermal buoyancy forces Gr, thermal conductivity ratio K_0, wall reactive parameter β, viscosity parameter α and pressure gradient p_s on diffusion coefficients $(M_1,\ M_2)$ and mean concentration C_M have been analyzed. A comparative study between viscoelastic (BP, HB) and non-viscoelastic (NF, PL) fluids has been presented in graphical form. Another analysis

of the shear thinning $(n > 1)$ and shear thickening $(n < 1)$ behavior of fluids affecting the solute dispersion process has also been done.

5.4.1 Parameter Selection and Model Validation

Following range of values of various parameters are taken from the previous studies to perform the graphical analysis which is given in Table 5.1.

Values of parameters		
Parameters	Values	Resources
Absorption ratio γ_0	1.00	[103]
Densities ratio ρ_0	0.92-1.00	[34], [36], [103]
Grashof number Gr	0.5-17	[103], [41], [45]
Plasma layer thickness h	0.015-0.05	[31], [28], [49]
Power-law index n	0.90-1.10	[28], [49], [91]
Steady pressure gradient p_s	1-10	[28], [49], [91]
Thermal conductivity ratio K_0	0.2-1.0	[103]
Viscosity parameter α	0.0-0.5	[41], [45]
Wall absorption parameter β	0-100	[87], [111], [112]
Yield stress Θ	0.00-0.25	[87], [91]

Table 5.1: The range of parameters appropriate for flow through narrow tubes with their resources

The present study is validated through comparison of results with limiting case of Ramana and Sarojamma [88] in Figure 5.3:(a) and another limiting case of Sankarasubramanian and Gill [2] in Figure 5.3:(b). It is perceived that in the limiting case of $Gr \to 0, \alpha \to 0, R_1 = 1$, the present model reduces to the case of single fluid model (Herschel-Bulkley fluid with constant viscosity) without heat transfer approach (Ramana and Sarojamma [88]) and in this case, our results representing the valiation of convective coefficient $(-M_1)$ with yield stress Θ graphically matches with the result of Ramana and Sarojamma [88]. Further the values $n = 1, \Theta = 0.0$ reduces the present model into the single-fluid model (Newtonian fluid with constant viscosity) studied by Sankarasubramanian and Gill [2]. Here also, we observed

that the variation of convective coefficient with steady state pressure gradient shows a good agreement between the limiting case of present study and the study of Sankarasubramanian and Gill [2]. For this validation the formulation of Sankarasubramanian and Gill [2] was used with a general parametric term of pressure gradient. Under the limiting cases $(Gr \to 0, \alpha = 0)$, the present work reduces to specific case of Tiwari *et al.* [156] representing the dispersion in two-fluid flow through tubes with constant viscosity and without heat transfer.

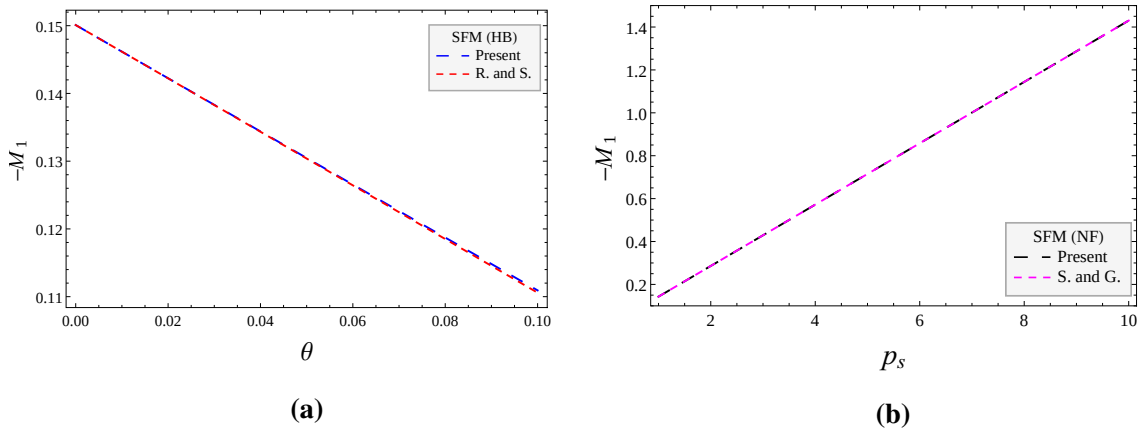

(a) **(b)**

Figure 5.3: Convection coefficient $(-M_1)$ varying with **(a)** yield stress Θ between the limiting case $(Gr \to 0, \alpha \to 0, R_1 = p_s = 1)$ of the present study and the work of Ramana and Sarojamma [88] for single Herschel-Bulkley fluid model with constant viscosity and **(b)** pressure gradient p_s between the limiting case $(Gr \to 0, \alpha \to 0, R_1 = n = 1, \Theta = 0.0)$ of the present study and the work of Sankarasubramanian and Gill [2] for single Newtonian fluid model with constant viscosity. $(\beta = 1)$

Our results for variation of convective coefficient with plug core radius R_p exactly matches with the work of Tiwari *et al.* [156] in this limiting case (Figure 5.4).

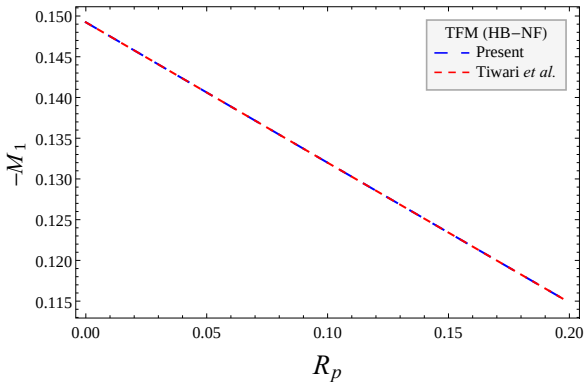

Figure 5.4: Convection coefficient $(-M_1)$ varying with plug flow radius R_p between the limiting case $(Gr \to 0, \alpha \to 0)$ of the present study and the limiting case $(K = 0, \lambda_1 = 1, k \to \infty)$ of the work of Tiwari *et al.* [156] for two-fluid model with constant viscosity. $(p_s = 1, R_1 = n = 0.95, h = 0.05)$

$\widetilde{\tau}_y$ (N/m^2)	$\alpha=0.0$, $\widetilde{k}=6\times10^{-8}$	$\alpha=0.2$, $\widetilde{k}=6\times10^{-8}$	$\alpha=0.0$, $\widetilde{k}=6\times10^{-6}$	$\alpha=0.2$, $\widetilde{k}=6\times10^{-6}$	$\alpha=0.0$, $\widetilde{k}=6\times10^{-4}$	$\alpha=0.2$, $\widetilde{k}=6\times10^{-4}$
0.0×10^{-3}	0.537789	0.718444	0.617463	0.833854	0.850650	1.17720
4.0×10^{-3}	0.537256	0.717682	0.616823	0.832934	0.849675	1.175770
8.0×10^{-3}	0.536723	0.716921	0.616184	0.832014	0.848701	1.17435
12.0×10^{-3}	0.536190	0.716159	0.615544	0.831094	0.847726	1.17292
16.0×10^{-3}	0.535657	0.715397	0.614904	0.830173	0.846757	1.17150
20.0×10^{-3}	0.535125	0.714635	0.614265	0.829253	0.845776	1.17007

Table 5.2: Impact of dimensional yield-stress $\widetilde{\tau}_y$, viscosity parameter α and constant reaction rate $\widetilde{k}$ (m/s) on convection coefficient $(-M_1)$. $(n=0.95,\ p_s=1$ ([91]), $\widetilde{Q}_H=\widetilde{Q}_N=1.0\times10^8 W/m^3$, $\widetilde{\gamma}=7.964/^\circ C$ ([41]), $\widetilde{T}_w-\widetilde{T}_\infty=0.5^\circ C$, $\widetilde{R}_1=95\mu m$, $\widetilde{R}_2=100\mu m$, $\widetilde{\mu}_N=1.2\times10^{-3}N.s/m^2$, $\widetilde{D}_m=6\times10^{-10}m^2/s$ ([37]), $\widetilde{K}_H=0.5W/m^\circ C$, $\widetilde{K}_N=0.4W/m^\circ C$ ([157]))

For the variation of the dimensional form of the yield-stress $\widetilde{\tau}_y$ from $0-20\times10^{-3}N/m^2$, the values of convective coefficient (non-dimensional value) are presented in Table 5.2. Further for the same case, the values of other dimensional form of the parameters are presented to give an insight of correspondence between the range of the non-dimensional parameters considered in the analysis and the corresponding range of dimensional parameters involved.

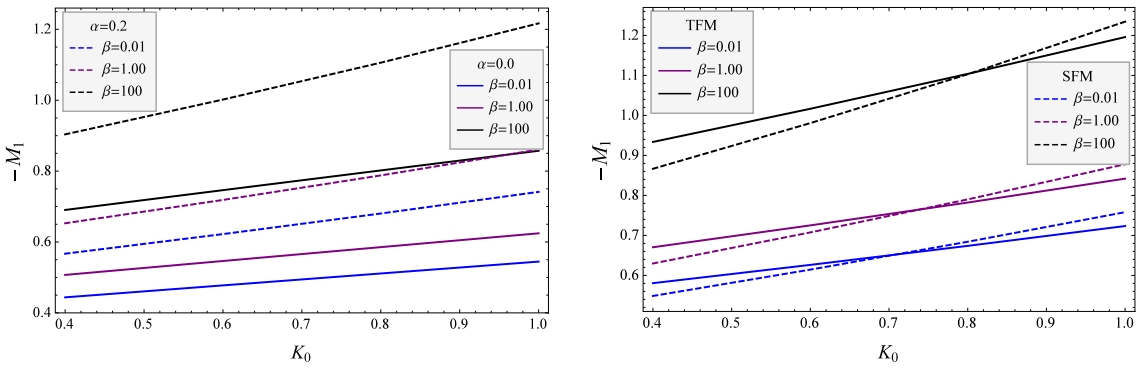

(a) **(b)**

Figure 5.5: Impact of wall absorption parameter β on convection coefficient $(-M_1)$ varying with respect to conductivity ratio K_0 with **(a)** viscosity parameter α $(R_1=0.95)$ (Solid lines for constant viscosity model $(\alpha=0.0)$ and dashed lines for variable viscosity model $(\alpha=0.2)$) and **(b)** plasma layer thickness h $(\alpha=0.2, R_1=0.90)$ (Solid lines for two-fluid model and dashed lines for single-fluid model). $(Gr=2, \Theta=0.10, p_s=1, n=0.95)$

As evident from the Table 5.2, a rising yield-stress $\widetilde{\tau}_y$ leads to decay in convective coefficient and for increasing constant reaction rate $\widetilde{k}$ (reactive walls), growth in convective coefficient is observed, which is same as the observations made using non-dimensional parameters in Figure 5.3:(a) and Figure 5.5:(a).

5.4.2 Convective Coefficient $(-M_1)$

Figure 5.5:(a) demonstrates the effect of reactive (absorbing) walls and varying viscosity on variation of convective dispersion $(-M_1)$ with thermal conductivity ratio K_0. The convective dispersion $(-M_1)$ slightly increases with increase in thermal conductivity ratio K_0. However this growth is relatively higher for varying viscosity model $(\alpha = 0.2)$. This can be justified as the varying nature of viscosity lead to reduced viscosity owing to smoother flow in the region. A noteworthy finding is that the effect of thermal conductivity ratio K_0 on convective dispersion for varying viscosity model is significant (high) when the tube walls are highly reactive $(\beta = 100)$. Another observation is that the growth rate of convective coefficient is relatively higher for varying viscosity model which further increases very significantly for highly reactive walls $(\beta = 100)$. Figure 5.5:(b) depicts a comparative study of variation of convective coefficient with thermal conductivity ratio K_0 between two-fluid model (TFM) and single-fluid model (SFM) under varying viscosity assumption. The convective coefficient is higher for two-fluid model when thermal conductivity is low but at higher thermal conductivity, this behavior reverses. This behavior is independent of the wall reactivity.

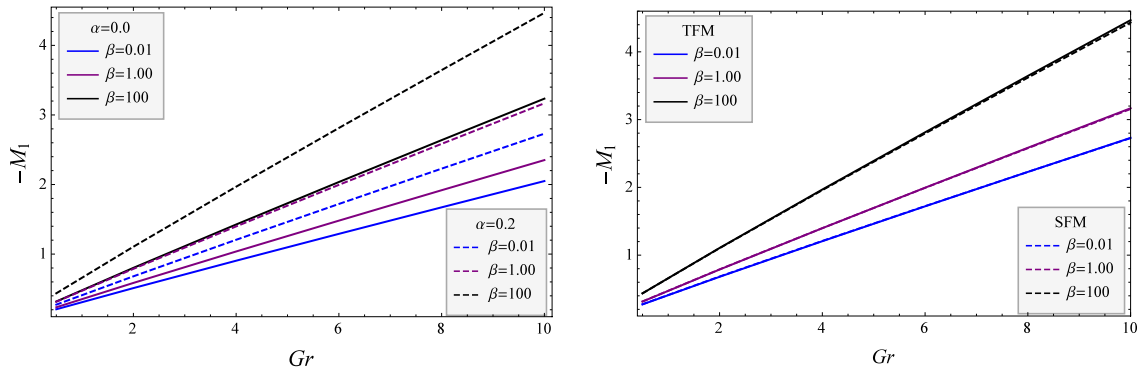

(a) **(b)**

Figure 5.6: Impact of wall absorption parameter β on convection coefficient $(-M_1)$ varying with Grashof number Gr with **(a)** viscosity parameter α $(R_1 = 0.95)$ (Solid lines for constant viscosity model $(\alpha = 0.0)$ and dashed lines for variable viscosity model $(\alpha = 0.2)$) and **(b)** plasma layer thickness h $(\alpha = 0.2, R_1 = 0.90)$ (Solid lines for two-fluid model and dashed lines for single-fluid model). $(K_0 = 0.8, \Theta = 0.10, p_s = 1, n = 0.95)$

The effect of Grashof number Gr on convective coefficient $(-M_1)$ is pictorially described in Figure 5.6:(a). It is clear that dominance of thermal buoyancy forces (larger

Grashof number $Gr > 1$) lead to rise in convective coefficient and the growth rate of convective coefficient increases for varying viscosity model ($\alpha = 0.2$) and it further increases with highly reactive walls ($\beta = 100$). This observation further asserts that the dispersion phenomena is significantly affected by the heat transfer. Figure 5.6:(b) demonstrates the comparative study between single and two-fluid model on variation of convective coefficient with Grashof number Gr under varying viscosity assumption. It is evident from the figure that the convective coefficient is slightly higher for two fluid model when the Grashof number is high (approximately $Gr > 4$) but at low value of Grashof number (approximately $Gr < 4$) this effect is negligibly small.

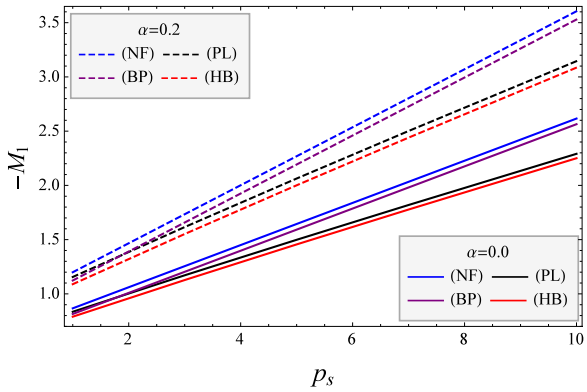

Figure 5.7: Impact of viscosity parameter α on convection coefficient $(-M_1)$ varying with pressure gradient p_s. ($Gr = 2, K_0 = 0.8, \Theta = 0.1, R_1 = 0.95, n = 0.9, \beta = 100$) (Solid lines for constant viscosity model ($\alpha = 0.0$) and dashed lines for variable viscosity model ($\alpha = 0.2$))

Figure 5.7 reveals an increase in convective coefficient with rising steady state pressure gradient p_s owing to increased fluid flow through the tube. Like the previous study of Ramana and Sarojamma [88] for the case of single-fluid model, the convective coefficient is highest for Newtonian fluid and lowest for Herschel-Bulkley fluid model. It is evident that the varying viscosity assumption leads to a higher growth rate in convective coefficient.

5.4.3 Dispersion Coefficient ($M_2 - 1/Pe^2$)

Figure 5.8 illustrates the effect of thermal conductivity K_0 on axial dispersion for varying viscosity under different walls reactivity. It is evident that the influence of thermal conductivity K_0 on axial dispersion is very strong for least absorbing walls ($\beta = 0.01$) and in all cases, a rising conductivity ratio K_0 leads to growth in axial dispersion M_2. Like the previous studies ([87], [88], [111]), axial dispersion M_2 decays with increasing wall reactivity β. A rise in varying viscosity parameter leads to growth in axial dispersion owing to reduced viscosity and smoother flow velocity. It is also evident that the growth rate of

axial dispersion with conductivity ratio K_0 is higher for varying viscosity $(\alpha = 0.1)$ and least reactive walls $(\beta = 0.01)$. So, we conclude that the effect of conductivity ratio K_0 will have almost negligible impact on axial dispersion when a significant interphase mass transport occurs through vessel walls (highly reactive walls $\beta = 100$). A comparative study reveals that the difference in axial dispersion M_2 between SFM and TFM is relatively more for varying viscosity approach in comparison to constant viscosity model. It is also evident that the difference in axial dispersion between two models rises with K_0 with slightly wider different for varying viscosity. This shows that heat transfer aspect significantly affect the axial dispersion in flows through tubes with moderate or less reactive walls.

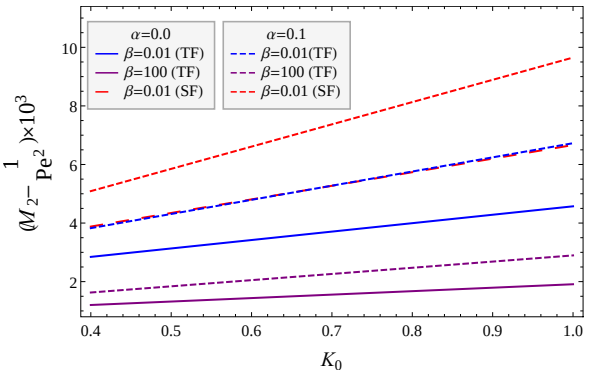

Figure 5.8: Impact of viscosity parameter α and absorption parameter β on dispersion coefficient $(M_2 - 1/Pe^2)$ varying with conductivity ratio K_0. $(Gr = 2, \Theta = 0.1, p_s = 1, n = 0.95)$ (Solid lines for constant viscosity model $(\alpha = 0.0)$ and dashed lines for variable viscosity model $(\alpha = 0.1)$)

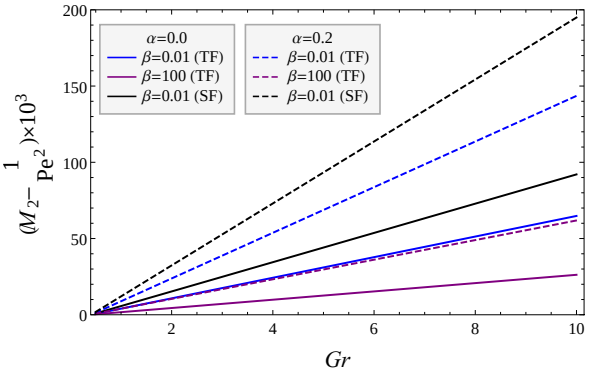

Figure 5.9: Impact of viscosity parameter α and absorption parameter β on dispersion coefficient $(M_2 - 1/Pe^2)$ varying with Grashof number Gr. $(K_0 = 0.8, \Theta = 0.1, p_s = 1, n = R_1 = 0.95)$ (Solid lines for constant viscosity model $(\alpha = 0.0)$ and dashed lines for variable viscosity model $(\alpha = 0.2)$)

The effect of Grashof number Gr (and hence the dominance of thermal buoyancy forces) on axial dispersion M_2 is depicted in Figure 5.9 for high $(\beta = 100)$ and least $(\beta = 0.01)$ reactive walls. It is clear from the observation that rise in Grashof number Gr leads to growth

in axial dispersion M_2 revealing the effect of heat transfer on axial dispersion M_2. However the effect of Grashof number Gr on axial dispersion M_2 is more dominant for varying viscosity model in comparison to the constant viscosity model as evident from their higher growth rate. Like the thermal conductivity ratio K_0, the thermal buoyancy forces also have more dominating effect on axial dispersion for lesser reactive walls i.e. lesser interphase mass transport through the vessel wall leads to more rapid increase in axial dispersion with Grashof number Gr. This figure also reveals a significant difference in axial dispersion M_2 for SFM and TFM and this difference is relatively higher for varying viscosity model.

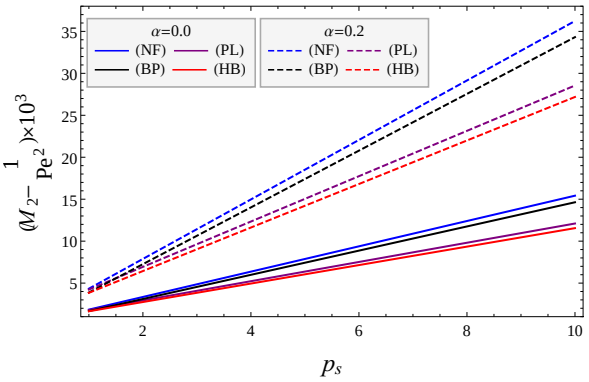

Figure 5.10: Impact of viscosity parameter α on dispersion coefficient $(M_2 - 1/Pe^2)$ varying with pressure gradient p_s. $(Gr = 2, K_0 = 0.8, \Theta = 0.1, R_1 = 0.95, n = 0.9, \beta = 100)$ (Solid lines for constant viscosity model $(\alpha = 0.0)$ and dashed lines for variable viscosity model $(\alpha = 0.2)$)

Like the previous study of Ramana and Sarojamma [88] for the single-fluid model, a rise in pressure gradient p_s leads to growth in axial dispersion M_2 owing to the increased fluid flow in tubes and the axial dispersion is relatively higher for varying viscosity model (Figure 5.10). It is perceived that the axial dispersion is highest for NF and least for HB fluid model for both the formulations $(\alpha = 0.0$ and $\alpha \neq 0.0)$. A remarkable observation is that the varying viscosity assumption leads to a larger growth rate in axial dispersion.

5.4.4 Mean Concentration (C_M)

The time profile of mean concentration C_M for varying viscosity assumption is depicted in Figure 5.11 for low $(Gr = 0.5)$ and high $(Gr = 2.0)$ thermal buoyancy forces under highly reactive walls. It is perceived from the Figure 5.11:(a) that with rise in viscosity parameter α, the mean concentration C_M significantly increases and the difference between TFM and SFM is significantly reduced for higher viscosity parameter $(\alpha = 0.2)$. A rise in viscosity parameter α leads to relatively quicker beginning of the diffusion process. For large thermal

buoyancy forces (i.e. higher Grashof number Gr) the diffusion process starts relatively earlier as evident form the Figure 5.11:(b).

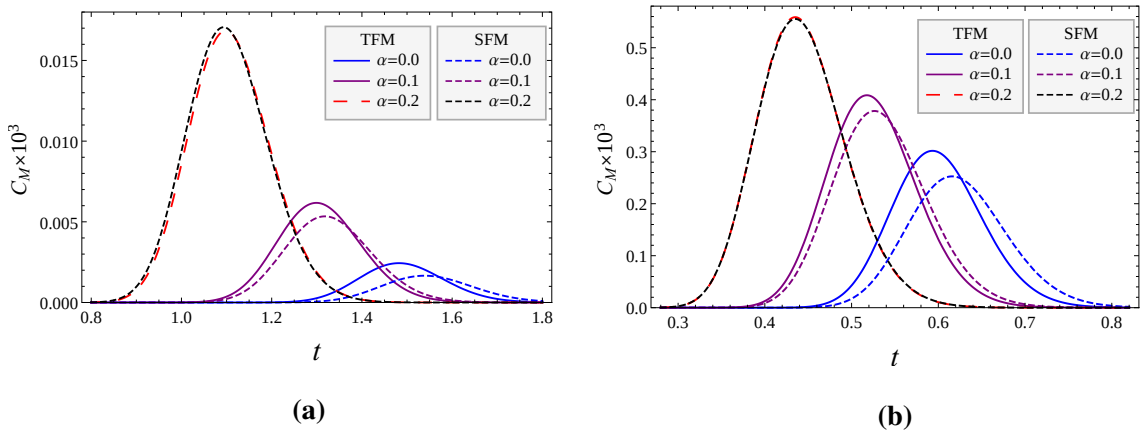

Figure 5.11: Impact of viscosity parameter α on mean concentration C_M varying with time t for different Grashof numbers **(a)** $Gr = 0.5$ and **(b)** $Gr = 2$ ($K_0 = 0.8, \Theta = 0.1, n = 0.9, p_s = 1, \beta = 100, z = 0.5$). (Solid lines for two-fluid model (TFM) and dashed lines for single-fluid model (SFM))

A noteworthy finding is that there is a significant rise in value of mean concentration C_M in comparison to the value for low buoyancy forces showing a significant impact of heat transfer on diffusion process. A relatively larger difference in the peak of mean concentration C_M is reported between TFM and SFM in comparison to low buoyancy forces. This shift of peak in mean concentration C_M is reduced for varying viscosity model.

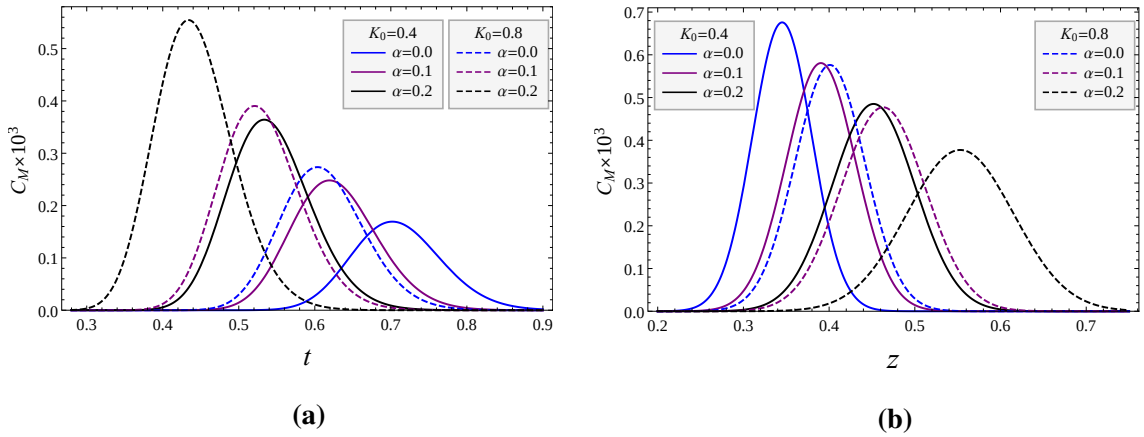

Figure 5.12: Impact of viscosity parameter α and conductivity ratio K_0 on mean concentration C_M varying with respect to **(a)** time t ($z = 0.5$) and **(b)** axial distance z ($t = 0.5$). ($Gr = 2, \Theta = 0.1, R_1 = n = 0.95, p_s = 1, \beta = 100$) (Solid lines for low conductivity ratio ($K_0 = 0.4$) and dashed lines for high conductivity ratio ($K_0 = 0.8$))

Variation of mean concentration C_M with time t and axial distance z for different thermal conductivity ratio K_0 under varying α and higher wall absorption parameter ($\beta = 100$) are depicted in Figure 5.12:(a) and Figure 5.12:(b). A rise in conductivity ratio K_0 leads to

enhanced mean concentration C_M as well as quicker beginning of diffusion process. Apart form that, a significant shift in peak of mean concentration C_M is also reported. However, a reverse effect of conductivity ratio K_0 on mean concentration C_M is observed in variation along axial distance z (Figure 5.12:(b)). A noteworthy finding is that for rising conductivity ratio K_0 the positions of peak of the mean concentration C_M are relatively farther for varying viscosity model in comparison to constant viscosity model.

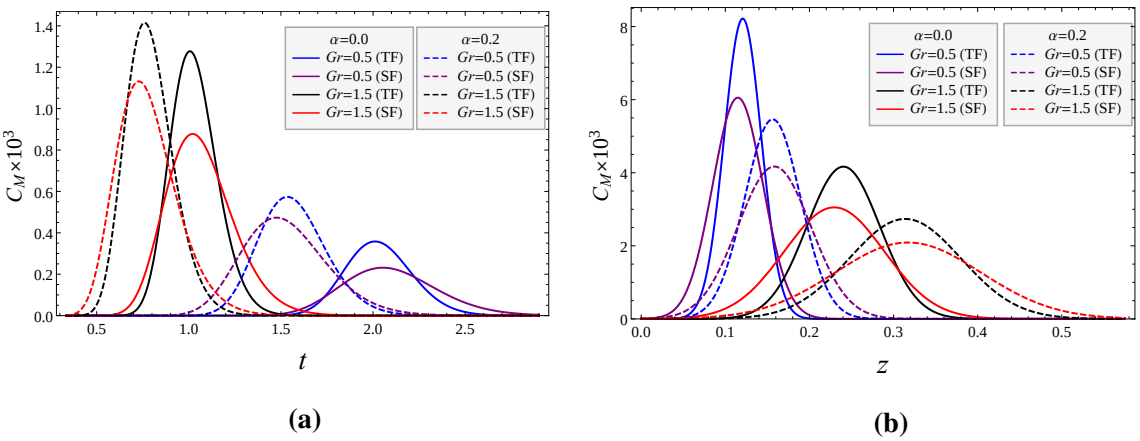

Figure 5.13: Impact of viscosity parameter α and Grashof number Gr on average concentration C_M varying with respect to C_M with **(a)** time t $(z = 0.5)$ and **(b)** axial distance z $(t = 0.5)$. $(K_0 = 0.8, \Theta = 0.10, R_1 = 0.9, = n = 0.95, p_s = \beta = 1)$ (Solid lines for constant viscosity model $(\alpha = 0.0)$ and dashed lines for variable viscosity model $(\alpha = 0.2)$)

The time profile of mean concentration C_M for different Grashof number Gr and viscosity parameter α suggests that the shifting in peak of C_M for varying viscosity is reduced in case of more dominant thermal buoyancy forces (in case of moderate reactive walls). It is also perceived that for low thermal buoyancy forces the time for diffusion process is increased in comparison to high Gr. The difference in peak of mean concentration C_M between TFM and SFM is higher for higher Grashof number Gr. A noteworthy finding is that the difference in time to complete the diffusion process for TFM and SFM is significantly reduced in case of varying viscosity approach. The axial variation of mean concentration C_M for different viscosity parameter α and Grashof number Gr are presented in Figure 5.13:(b). For low thermal buoyancy forces, a slight increase and shift in peak of mean concentration is reported for TFM in comparison to SFM. However, in case of dominating thermal buoyancy forces not only the shift in peak of C_M is very significant but also the axial span covered for diffusion process in SFM is relatively higher than TFM. All these observations are same for varying viscosity model with an exception that the shifting in peak is relatively lesser.

Figure 5.14 reveals that the time and axial distance profile of mean concentration C_M agrees with the previous results for low, moderate and highly reactive walls ([87], [89], [112]). The mean concentration C_M profile suggests a shift in peak for varying viscosity

model with a reduced peak for mean concentration C_M in case of insignificant wall reactivity and higher peak for moderate and higher wall reactivity. The axial distance profile of mean concentration is depicted in Figure 5.14:(b) reveals that for varying viscosity, a significant decay in peak of mean concentration is observed for low and moderate reactive walls but this decay is insignificant for highly reactive walls. The shifting in peak of mean concentration is also observed which is most for highly reactive walls.

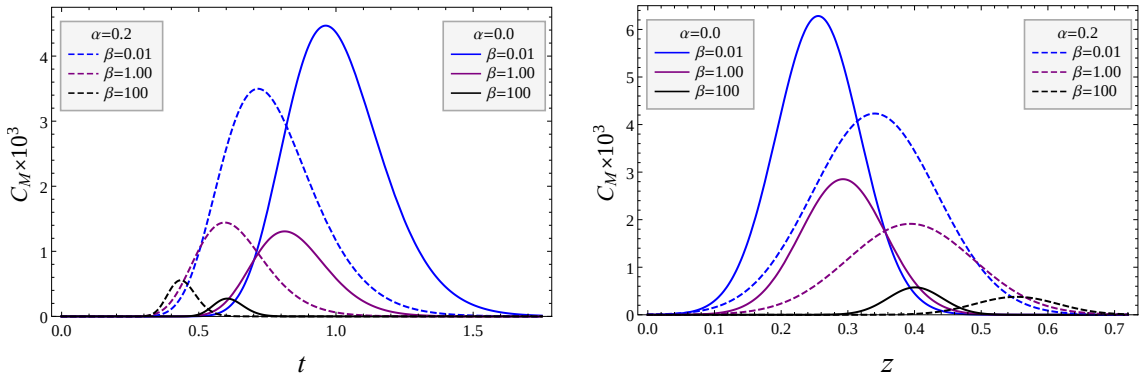

(a) **(b)**

Figure 5.14: Impact of viscosity parameter α and absorption parameter β on mean concentration C_M varying with respect to **(a)** time t $(z=0.5)$ and **(b)** axial distance z $(t=0.5)$. $(K_0=0.8, R_1=n=0.95, Gr=2, \Theta=0.1, p_s=1)$ (Solid lines for constant viscosity model $(\alpha=0.0)$ and dashed lines for variable viscosity model $(\alpha=0.2)$)

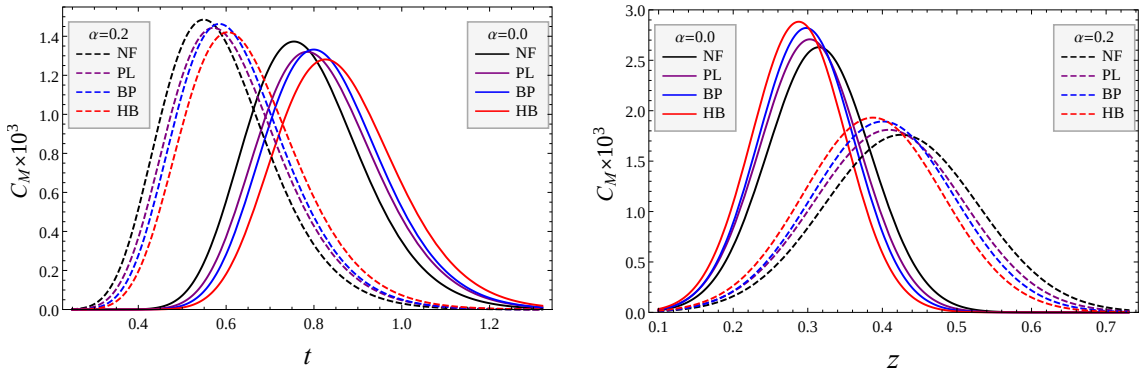

(a) **(b)**

Figure 5.15: Impact of viscosity parameter α on mean concentration C_M varying with respect to **(a)** time t $(z=0.5)$ and **(b)** axial distance z $(t=0.5)$. $(n=0.9, K_0=0.8, R_1=0.95, Gr=2, \Theta=0.1, p_s=\beta=1)$ (Solid lines for constant viscosity model $(\alpha=0.0)$ and dashed lines for variable viscosity model $(\alpha=0.2)$)

A comparative study of time profile of mean concentration for all four fluid models is depicted in Figure 5.15:(a). It is perceived that the peak of mean concentration for viscoelastic fluids are slightly lesser than the peak of non-viscoelastic fluids and for all four fluids the varying viscosity leads to increase in peak of C_M. A similar analysis for all four fluids shows

that the peak of C_M is attained nearer to the point of injection for constant viscosity model in comparison to varying viscosity model (Figure 5.15:(b)).

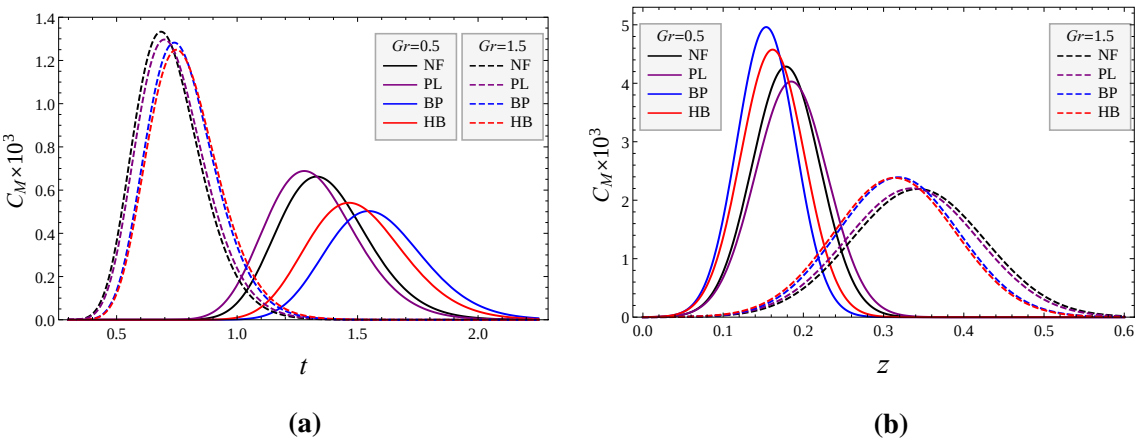

Figure 5.16: Impact of Grashof number Gr on mean concentration C_M varying with respect to **(a)** time t $(z = 0.5)$ and **(b)** axial distance z $(t = 0.5)$. $(\alpha = 0.2, n = 0.9, K_0 = 0.8, R_1 = 0.95, \Theta = 0.1, p_s = \beta = 1)$ (Solid lines for low Grashof number $(Gr = 0.5)$ and dashed lines for high Grashof number $(Gr = 1.5)$)

A comparative analysis of variation of mean concentration C_M with time and axial distance are depicted in Figure 5.16:(a) and Figure 5.16:(b). For low Grashof number $(Gr = 0.5)$ as demonstrated in Figure 5.16:(a), a significant shifting in peak of C_M for yield-stress fluids (Bingham-Plastic and Herschel-Bulkley fluids) and fluids with no yield-stress (Newtonian and Power-Law fluids) is observed but the same reduces in case of high Grashof number $(Gr = 1.5)$.

Another observation is that for low Grashof number $(Gr = 0.5)$, the peak of C_M is highest for Power-law fluid and least for Bingham-plastic fluid but on increasing the value of thermal buoyancy forces $(Gr = 1.5)$, the peak of Newtonian fluid become largest and the peak of Herschel-Bulkley fluid become smallest. This indicates that the dominance of thermal buoyancy forces have significant impact on the mean concentration C_M for all four fluid models. From Figure 5.16:(b), the axial variation of C_M for all four fluid models shows a significant shifting in peak of C_M from the point of injection for high thermal buoyancy forces $(Gr = 1.5)$ in comparison to low Grashof number $(Gr = 0.5)$.

As demonstrated in Figure 5.17:(b), the profile for mean concentration along the axis shows a reduced difference in peak of C_M between constant and varying viscosity model with increase in time for highly reactive wall. However for highly reactive walls $(\beta = 100)$, the span covered along axis for diffusion process is significantly reduced for constant as well as varying viscosity model. For constant viscosity model, the above observations agrees with previous studies ([87], [88], [89]). For walls with low reactivity, the corresponding

mean concentration curve is wider indicating a larger reaction is covered for completion of diffusion process (Figure 5.17:(a)).

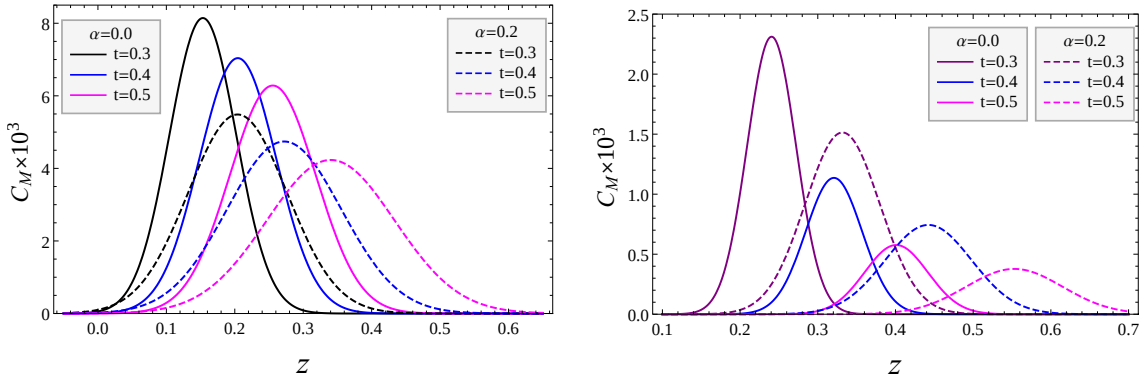

Figure 5.17: Impact of viscosity parameter α on mean concentration C_M varying with z for different values of time t under different wall absorption parameter **(a)** $\beta = 0.01$ and **(b)** $\beta = 100$ ($K_0 = 0.8, R_1 = n = 0.95, Gr = 2, \Theta = 0.1, p_s = 1$). (Solid lines for constant viscosity model ($\alpha = 0.0$) and dashed lines for variable viscosity model ($\alpha = 0.2$))

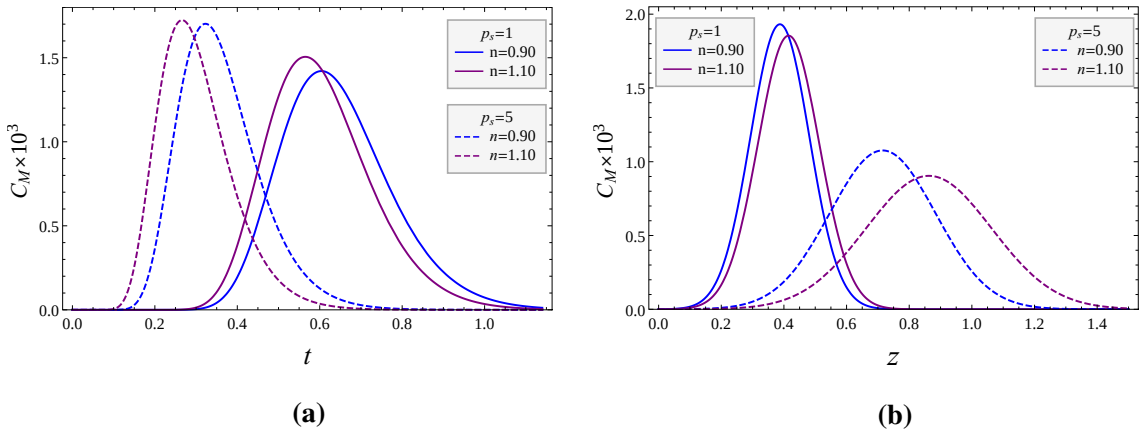

Figure 5.18: Impact of pressure gradient p_s and Herschel-Bulkley fluid parameter n on mean concentration C_M varying with respect to **(a)** time t ($z = 0.5$) and **(b)** axial distance z ($t = 0.5$). ($\alpha = 0.2, K_0 = 0.8, R_1 = 0.95, Gr = 2.0, \Theta = 0.10, \beta = 1$) (Solid lines for lower pressure gradient ($p_s = 1$) and dashed lines for higher pressure gradient ($p_s = 5$))

The effect of shear thinning/thickening behavior of fluids on C_M is depicted in Figure 5.18:(a) for different pressure gradient. The time profile of C_M suggests a slightly larger peak for C_M in case of shear thinning fluid and this difference further increases for higher pressure gradient. It is also observed that the peak of C_M is attained relatively earlier for shear thinning fluids. A reverse observation is noted in Figure 5.18:(b) for variation of C_M along the axis showing a reduced peak and a farther peak position from the point of injection for shear thinning fluids. This difference widens for higher pressure gradient p_s.

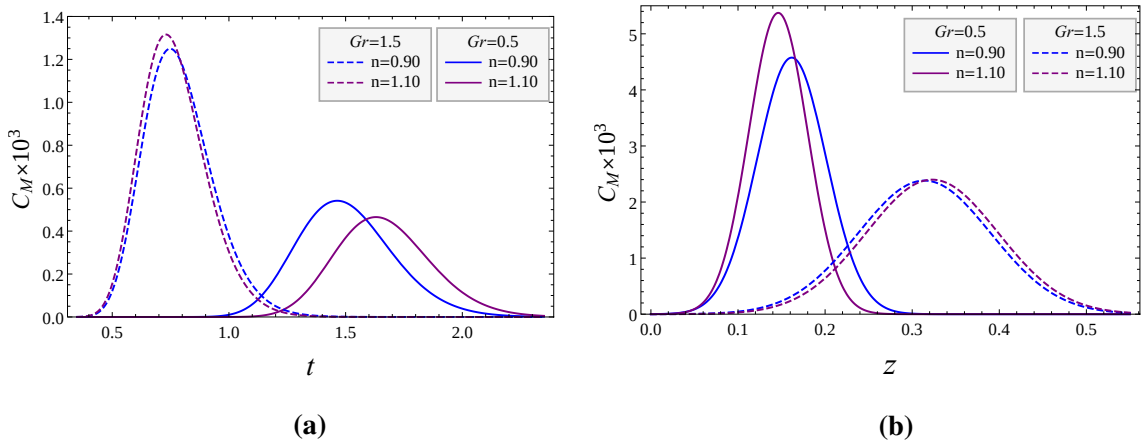

Figure 5.19: Impact of Grashof number Gr and Herschel-Bulkley fluid parameter n on mean concentration C_M with respect to **(a)** time t $(z = 0.5)$ and **(b)** axial distance z $(t = 0.5)$. $(\alpha = 0.2, K_0 = 0.8, R_1 = 0.95, \Theta = 0.10, p_s = \beta = 1)$. (Solid lines for low Grashof number $(Gr = 0.5)$ and dashed lines for high Grashof number $(Gr = 1.5)$)

The effect of shear thinning/thickening behavior of fluids on mean concentration C_M for different thermal buoyancy forces Gr are depicted in Figure 5.19:(a) and Figure 5.19:(b). The time profile suggests a reduced peak of C_M for shear thinning fluids in comparison to shear thickening fluids. However this difference is reduced for large buoyancy forces $(Gr = 1.5)$ although in this case the peak of C_M for shear thinning fluids is higher in comparison to shear thickening fluids. From Figure 5.19:(b), the axial variation of C_M for different values of HB fluid parameter n and Grashof number Gr shows that on increasing the shear thickening behavior of fluid, the peak of C_M is attained slightly farther from the point of injection. However this shifting of peak on increasing the shear thinning behavior of fluid is significantly reduced for high Grashof number $(Gr = 1.5)$.

5.5 Summary and Conclusions

A novel approach of heat transfer and temperature-dependent viscosity on solute dispersion in a two-fluid model of blood flow through narrow blood vessels has been employed in the present study which is physically realistic in cardiovascular system to perform the mixing or drug transportation to tissues through blood vessels or other vascular systems. The combined impact of temperature parameters and viscosity parameter on diffusion coefficients and mean concentration has also been discussed in detail and it is found that all these parameters have definite impact on these quantities.

The following important (novel) determinations of the present study are pointed out:

1. All the diffusion coefficients and mean concentration are significantly affected by the thermal buoyancy forces Gr, thermal conductivity ratio K_0 and varying viscosity parameter α.

2. The time to complete diffusion process is significantly lesser under the dominance of thermal buoyancy forces (i.e. higher Grashof number Gr).

3. For all types of vessel wall (low, moderate and highly reactive), the difference in convective coefficient for two-fluid model (TFM) and single-fluid model (SFM) reduces with increasing conductivity ratio K_0 which further starts increasing after a certain value. However, the above difference for axial dispersion consistently increases with thermal conductivity ratio K_0.

4. The temperature-dependent viscosity reduces the difference in mean concentration C_M for two-fluid model (TFM) and single-fluid model (SFM).

5. The dominance of thermal buoyancy forces reduces shifting of peak of mean concentration C_M between yield-stress fluids and with no yield-stress fluids.

Above outcomes suggest that transportation of nutrients to physiological system or drug delivery to tissues under medical treatment involving slightly high temperature are severely affected. The heat transfer aspects included in this study suggests that the above process may be delayed under slightly higher temperature arising due to certain medical treatments. It will be interesting to experimentally validates these observations for further applications to various medical treatments of diseases related to the physiological systems.

Chapter 6

Solute Dispersion into Microcirculation Influenced by EGL and Varying Viscosity Nature

6.1 Introduction

The complex physiological system of the human body has various situations where interface mass transport plays a significant role such as the transport of lipoprotein through the intimal of vessel wall tissue. Sankarasubramanian and Gill [2] analyzed the interface transportation of mass on solute dispersion in a fluid flowing through vessels in which the exchange coefficient arise with interface mass transfer. This coefficient strongly depends on the rate of interfacial mass transport and also affects the dispersion phenomena. Following the presumption of wall reaction (reversible or irreversible boundary reaction), many authors ([149], [87], [150], [151], [152], [88]) analyzed the effect of wall reaction on solute dispersion in a Newtonian/non-Newtonian fluid flow through vessels having circular cross-section with or without catheters.

Recently, Rana and Murthy ([111], [112]) studied the longitudinal dispersion of a solute in yield-stress fluids (Casson and Herschel-Bulkley fluids) flowing through small blood vessels with absorbing wall and the flow was driven by the periodic nature of pressure gradient. They observed the effect of various parameters like the Womersley parameter, wall absorption parameter, Herschel-Bulkley fluid (HB) parameter and amplitude of the periodic pressure gradient on the whole dispersion process. A comparative study of diffusion process among the non-Newtonian fluids flowing through smaller diameter tubes with absorbing walls has been done by Rana and Murthy [89].

A multi-phase flow of fluids consists of two-immiscible fluids (a liquid bubble embedded in another fluid) through a vertical tube with a porous boundary was discussed by Sacheti *et*

[5]The work has appeared in **A. Tiwari, P.D. Shah and S.S. Chauhan, "Solute dispersion in two-fluid flowing through tubes with a porous layer near the absorbing wall: Model for dispersion phenomenon in microvessels", *International Journal of Multiphase Flow* 131 (2020) 103380.**

al. [63]. Tiwari and Deo [158] studied the impact of Womersley number and permeability in the porous medium on the periodic flow of Newtonian fluid flowing through a tube of circular cross-section and the Brinkman equation was used to formulate the motion of the fluid through the porous media. They analyzed the effect of porosity near the wall on the phase lag in flow rate and pressure gradient. Shaw *et al.* [159] used a two-fluid model with Casson fluid nature of blood in the core region to predict the magnet targeting of carrier particles. A theoretical study of a two-layer fluid model of blood flowing through capillaries has been examined by Boodoo *et al.* [66] where blood was assumed as micropolar fluid in the central region and Newtonian fluid in the peripheral region. The model assumed a thin Brinkman layer overlying a porous Darcy layer composing the wall of the capillary. Sharma and Yadav [83] covered the combined aspect of porous layer near the wall and constriction on the two-fluid model of blood flow through narrow constricted tubes and analyzed the impact of permeability and different constriction size on the flow variables such as wall shear stress, velocity, and rate of flow. They used the fluid-porous interface boundary condition of Ochoa-Tapia and Whitaker ([1], [1]) and Brinkman-Darcy interface boundary condition (BC) of Beavers and Joseph [160]. Jaiswal and Yadav [68] presented the impact of a uniform magnetic field and porous layer near the wall on micropolar-Newtonian fluid flow through narrow tubes with different permeabilities of the porous medium. They found that the micro-rotation of the particles and permeabilities of Brinkman and Darcy's regions significantly affected the flow quantities. Recently, Tiwari *et al.* [122] applied the two-fluid model of blood flowing through tubes with a porous layer near the wall by taking micro-structures into account. Recently, Tiwari and Chauhan ([49], [50], [51]) analyzed the simultaneous impact of the porous layer and variable viscosity on the two-fluid model of blood flow through arteries with a porous layer near the tube wall. Following the above presumptions, not much work has been done on the solute dispersion process in a two-fluid model of blood flowing through tubes with a porous layer near the tube wall.

In the present analysis, an attempt has been made to understand the physical significance of the solute dispersion through porous media flow and the impact of the porous layer on the diffusion process like convective and dispersion coefficients. In the present model, we are going to analyze the combined effect of the porous layer and variable nature of viscosity on solute dispersion in a two-fluid model of blood flowing through tubes with a thin porous layer near the tube wall. Mathematical expressions for flow velocity are obtained for different regions and following the generalized dispersion model of Sankarasubramanian and Gill [2], the analytical expressions for exchange, convective, dispersion coefficients and mean concentration have been obtained. The impact of porous layer (and hence porous layer parameters), varying viscosity and wall absorption has been analyzed pictorially and compared

with the previous studies.

6.2 Problem Formulation

The solute dispersion in the two-fluid model of blood flow through a tube with a porous layer near the wall as depicted in Figure 6.1 has been analyzed. Blood is assumed to be Herschel-Bulkley fluid (HB) with variable viscosity in the core region and Newtonian fluid with constant viscosity representing plasma in the outer region. The peripheral layer of plasma is divided in to two regions (intermediate and porous regions) and both regions are occupied by Newtonian fluid. The one-dimensional steady flow through a tube is assumed to be laminar, incompressible, fully developed with flow symmetry about the axis of the tube. A thin deposition of the Brinkman layer near the wall is assumed which accounts for a porous layer as suggested by Secomb *et al.* [3]. The flow in the porous medium is governed by Brinkman equation with the effective viscosity different from that of the Newtonian fluid viscosity. The blood vessel is assumed to be a cylinder with rigid wall due to which the standard cylindrical polar coordinates system $(\widetilde{r},\phi,\widetilde{z})$ has been employed where $(\widetilde{r},\widetilde{z})$ represents the coordinates in radial and axial directions respectively with origin lying on the axis of the vessel. Since the flow pattern of the blood is assumed to be unidirectional, so the radial component of velocity vanishes for all the regions (central, intermediate and porous regions).

Adopting the above hypotheses, the equations governing the fluid flow through tubes of circular cross-section with a porous layer near the boundaries of the tube are described below ([49]).

For non-Newtonian region, i.e., $0<\widetilde{r}\leq\widetilde{R}_1$

$$\frac{\partial\widetilde{w}_H}{\partial\widetilde{z}}=0, \tag{6.1a}$$

$$\frac{\partial\widetilde{p}_H}{\partial\widetilde{r}}=0, \tag{6.1b}$$

$$\frac{\partial\widetilde{p}_H}{\partial\widetilde{z}}+\frac{1}{\widetilde{r}}\frac{\partial}{\partial\widetilde{r}}(\widetilde{r}\widetilde{\tau}_H)=0. \tag{6.1c}$$

For constitutive equation of non-Newtonian (Herschel-Bulkley) fluid $\widetilde{\tau}_H$ is given as

$$\widetilde{\tau}_H=\widetilde{\tau}_y+\left[\widetilde{\mu}_1(\widetilde{r})\left(-\frac{\partial\widetilde{w}_H}{\partial\widetilde{r}}\right)\right]^{\frac{1}{n}},\quad \text{if}\quad \widetilde{\tau}_H>\widetilde{\tau}_y, \tag{6.1d}$$

$$\frac{\partial\widetilde{w}_H}{\partial\widetilde{r}}=0,\quad \text{if}\quad \widetilde{\tau}_H\leq\widetilde{\tau}_y, \tag{6.1e}$$

where $\widetilde{p}_H, \widetilde{w}_H, \widetilde{\mu}_1(\widetilde{r}) = \widetilde{\mu}_H(1+K-K(\widetilde{r}/\widetilde{R}_3)^m)$ are the pressure, velocity, radially varying viscosity of blood in core region, respectively; $\widetilde{\mu}_H, \widetilde{\tau}_H$ constant viscosity coefficient and shear stress of Herschel-Bulkley fluid, respectively; $\widetilde{\tau}_y$ is the yield stress, n is the Herschel-Bulkley fluid parameter, K is the constant in viscosity relation and m is varying viscosity index of the core region fluid.

For intermediate region, i.e., $\widetilde{R}_1 < \widetilde{r} \leq \widetilde{R}_2$

$$\frac{\partial \widetilde{w}_N}{\partial \widetilde{z}} = 0, \tag{6.2a}$$

$$\frac{\partial \widetilde{p}_N}{\partial \widetilde{r}} = 0, \tag{6.2b}$$

$$-\frac{\partial \widetilde{p}_N}{\partial \widetilde{z}} + \frac{\widetilde{\mu}_N}{\widetilde{r}} \frac{\partial}{\partial \widetilde{r}} \left(\widetilde{r} \frac{\partial \widetilde{w}_N}{\partial \widetilde{r}} \right) = 0, \tag{6.2c}$$

where $\widetilde{p}_N, \widetilde{w}_N, \widetilde{\mu}_N$ are the pressure, velocity, constant viscosity coefficient of blood in plasma in the peripheral region, respectively.

Flow through porous medium involves the modeling of flow through pores which also offer some resistance against the flow. Darcy (1856) employed the term “permeability" to conduct a mathematical study describing the flow of fluid through the porous media having low permeability. Brinkman [95] extended Darcy’s mathematical study by considering particle size and particle density with the permeability of the porous media to elucidate the flow of fluid through porous mass and carried out the study for the flow of fluid through microporous medium [96]. In lieu of the above discussion, the Brinkman equation has been used to model flow through porous layer near the wall.

For porous region, i.e., $\widetilde{R}_2 < \widetilde{r} \leq \widetilde{R}_3$

$$\frac{\partial \widetilde{w}_B}{\partial \widetilde{z}} = 0, \tag{6.3a}$$

$$\frac{\partial \widetilde{p}_B}{\partial \widetilde{r}} = 0, \tag{6.3b}$$

$$-\frac{\partial \widetilde{p}_B}{\partial \widetilde{z}} + \frac{\widetilde{\mu}_E}{\widetilde{r}} \frac{\partial}{\partial \widetilde{r}} \left(\widetilde{r} \frac{\partial \widetilde{w}_B}{\partial \widetilde{r}} \right) - \frac{\widetilde{\mu}_N}{\widetilde{k}} \widetilde{w}_B = 0, \tag{6.3c}$$

where $\widetilde{p}_B, \widetilde{w}_B, \widetilde{\mu}_E$ are the pressure, velocity, effective viscosity of porous region, respectively and $\widetilde{k}$ is permeability in the porous region.

Ochoa-Tapia and Whitaker ([1], [97]) gave a detail description of the solutions of the equation of motion of homogeneous fluid past a porous medium and suggested the stress-jump condition at the boundary between a homogeneous fluid and a porous medium which was further used in the various applications by the researchers. Bhattacharyya and Raja Sekhar [161] employed stress-jump boundary condition at the fluid-porous interface to study flow

past a porous spherical shell. Srivastava and Srivastava [124] observed a reduced drag on the porous sphere with the rise in permeability using Stokes flow formulation. The momentum transfer condition known as stress-jump condition was employed at the fluid-porous interface to examine the hydrodynamic permeability of swarm of porous cylindrical particles (Deo *et al.* [64]).

The boundary conditions are given as

$$\begin{gathered}
\widetilde{\tau}_H \text{ is finite, at } \widetilde{r}=0, \\
\widetilde{\tau}_H=-\widetilde{\mu}_N\frac{\partial \widetilde{w}_N}{\partial r},\ \widetilde{w}_H=\widetilde{w}_N, \text{ at } \widetilde{r}=\widetilde{R}_1, \\
\widetilde{w}_N=\widetilde{w}_B,\ \frac{1}{\alpha_p}\frac{\partial \widetilde{w}_B}{\partial \widetilde{r}}-\frac{\partial \widetilde{w}_N}{\partial \widetilde{r}}=\frac{\beta_S}{\sqrt{\widetilde{k}}}\widetilde{w}_B, \text{ at } \widetilde{r}=\widetilde{R}_2, \\
\widetilde{w}_B=0, \text{ at } \widetilde{r}=\widetilde{R}_3.
\end{gathered} \tag{6.4}$$

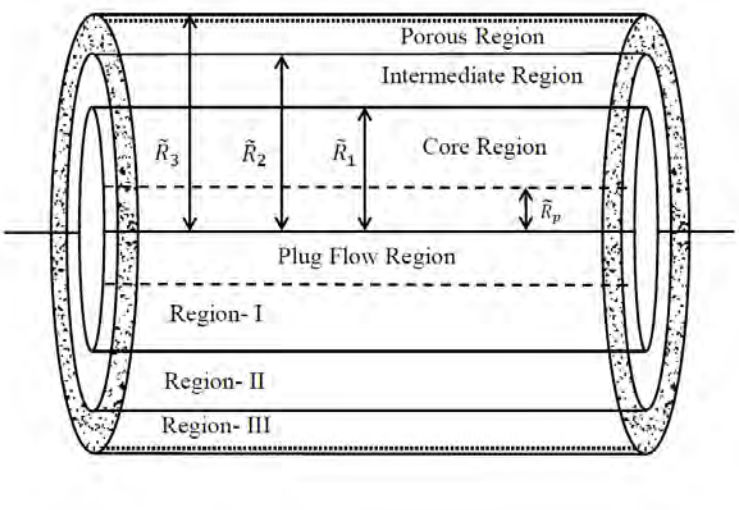

Figure 6.1: The schematic diagram of model description for two-fluid model with an endothelial glycocalyx layer adjacent to the microvessel wall

The physical sketch for the present model is demonstrated in Figure 6.1, where $\widetilde{R}_1, \widetilde{R}_2, \widetilde{R}_3$ are the central, intermediate and porous regions radii of the tube, respectively and $\widetilde{R}_p$ is the plug flow radius. Region-I replicates the core (central) region of the blood vessel which is occupied by non-Newtonian (Herschel-Bulkley) fluid, Region-II presents the intermediate region that is governed by Newtonian fluid and Region-III replicates the porous region of the blood vessel which is occupied by Newtonian fluid. Region-II and III constitutes the

plasma region. The following dimensionless variables are introduced: ([89], [36], [49])

$$\begin{gathered}\tau_H=\frac{\widetilde{\tau}_H\widetilde{R}_3}{\widetilde{\mu}_N W_0},\Theta=\frac{\widetilde{\tau}_y\widetilde{R}_3}{\widetilde{\mu}_N W_0},p_H=\frac{\widetilde{p}_H\widetilde{R}_3}{W_0\widetilde{\mu}_N},p_N=\frac{\widetilde{p}_N\widetilde{R}_3}{W_0\widetilde{\mu}_N},p_B=\frac{\widetilde{p}_B\widetilde{R}_3}{W_0\widetilde{\mu}_N},r=\frac{\widetilde{r}}{\widetilde{R}_3},\\ w_H=\frac{\widetilde{w}_H}{W_0},\ w_N=\frac{\widetilde{w}_N}{W_0},\ w_B=\frac{\widetilde{w}_B}{W_0},\ R_1=\frac{\widetilde{R}_1}{\widetilde{R}_3},\ R_2=\frac{\widetilde{R}_2}{\widetilde{R}_3},\ Pe=\frac{W_0\widetilde{R}_3}{\widetilde{D}_m},\\ t=\frac{\widetilde{D}_m\widetilde{t}}{\widetilde{R}_3^2},\ C=\frac{\widetilde{C}}{C_0},\ W_0=\frac{\widetilde{q}_0\widetilde{R}_3^2}{4\widetilde{\mu}_N},\ \lambda_1^2=\frac{\widetilde{\mu}_E}{\widetilde{\mu}_N},\ k=\frac{\widetilde{k}}{\widetilde{R}_0^2},\ z=\frac{\widetilde{D}_m\widetilde{z}}{W_0\widetilde{R}_3^2},\end{gathered}\tag{6.5}$$

where W_0 is the average velocity, Θ is the non-dimensional yield-stress, $\widetilde{q}_0$ is the characteristic pressure gradient, D_m is constant molecular diffusivity, C_0 is the reference concentration and λ_1^2 is the viscosity ratio ([124], [156]).

Using the non-dimensional variables (6.5), Eqs. $(6.1)-(6.4)$ transformed into non-dimensional form as given below

Region- I, i.e., $0<r\leq R_1$

$$\frac{\partial w_H}{\partial z}=0,\tag{6.6a}$$

$$\frac{\partial p_H}{\partial r}=0,\tag{6.6b}$$

$$4\left(\frac{\partial p_H}{\partial z}\right)+\frac{1}{r}\frac{\partial}{\partial r}(r\tau_H)=0,\tag{6.6c}$$

where the equation for Herschel-Bulkley (HB) fluid is given as

$$\tau_H=\Theta+\left[(1+K-Kr^m)\left(-\frac{\partial w_H}{\partial r}\right)\right]^{\frac{1}{n}},\quad \text{if}\quad \tau_H>\Theta,\tag{6.6d}$$

$$\frac{\partial w_H}{\partial r}=0,\quad \text{if}\quad \tau_H\leq\Theta,\tag{6.6e}$$

where $\widetilde{\mu}_H=\widetilde{\mu}_N\left(\frac{\widetilde{R}_3}{W_0\widetilde{\mu}_N}\right)^{1-n}$ is the constant viscosity coefficient of Herschel-Bulkley fluid.

Region- II, i.e., $R_1<r\leq R_2$

$$\frac{\partial w_N}{\partial z}=0,\tag{6.7a}$$

$$\frac{\partial p_N}{\partial r}=0,\tag{6.7b}$$

$$-4\left(\frac{\partial p_N}{\partial z}\right)+\frac{1}{r}\frac{\partial}{\partial r}\left(r\frac{\partial w_N}{\partial r}\right)=0.\tag{6.7c}$$

Region- III, i.e., $R_2 < r \leq 1$

$$\frac{\partial w_B}{\partial z} = 0, \tag{6.8a}$$

$$\frac{\partial p_B}{\partial r} = 0, \tag{6.8b}$$

$$-4\left(\frac{\partial p_B}{\partial z}\right) + \frac{\lambda_1^2}{r}\frac{\partial}{\partial r}\left(r\frac{\partial w_B}{\partial r}\right) - \frac{w_B}{k} = 0, \tag{6.8c}$$

where λ_1 is the viscosity ratio parameter and k is the permeability of the porous layer.

The boundary conditions in dimensionless form are given as

$$\begin{gathered}
\tau_H \text{ is finite, at } r = 0, \\
\tau_H = -\frac{\partial w_N}{\partial r},\ w_H = w_N, \text{ at } r = R_1, \\
w_N = w_B,\ \frac{1}{\alpha_p}\frac{\partial w_B}{\partial r} - \frac{\partial w_N}{\partial r} = \frac{\beta_S}{\sqrt{k}} w_B, \text{ at } r = R_2, \\
w_B = 0, \text{ at } r = 1.
\end{gathered} \tag{6.9}$$

6.2.1 Analytical Solution

Consider the pressure gradients to be constant in central, intermediate and porous regions ([91], [49])

$$\frac{\partial p_H}{\partial z} = \frac{\partial p_N}{\partial z} = \frac{\partial p_B}{\partial z} = -p_s, \tag{6.10}$$

where p_s is the steady pressure gradient along the axis of the tube.
Solving dimensionless governing Eqs. (6.6), (6.7) and (6.8) for different regions by using Eq. (6.10), we have obtained the following expressions:
Region- I, i.e., $0 < r \leq R_1$

$$\tau_H = 2p_s r + \frac{C_1}{r}, \tag{6.11a}$$

$$\begin{aligned}
w_H = C_2 - \frac{2^{n-1}(p_s r)^n}{(K+1)p_s}\left(\frac{2p_s r}{n+1} - \Theta + \frac{K^3 r^{3m}}{(K+1)^3}\left(\frac{2p_s r}{3m+n+1} - \frac{\Theta n}{3m+n}\right)\right. \\
\left. + \frac{K^2 r^{2m}}{(K+1)^2}\left(\frac{2p_s r}{2m+n+1} - \frac{\Theta n}{2m+n}\right) + \frac{K r^m}{K+1}\left(\frac{2p_s r}{m+n+1} - \frac{\Theta n}{m+n}\right)\right).
\end{aligned} \tag{6.11b}$$

Region- II, i.e., $R_1 < r \leq R_2$

$$w_N = C_3 \ln r + C_4 - p_s r^2. \tag{6.11c}$$

Region- III, i.e., $R_2 < r \leq 1$

$$w_B = C_5 I_0\left(\frac{\gamma r}{\lambda_1}\right) + C_6 K_0\left(\frac{\gamma r}{\lambda_1}\right) + \frac{4p_s}{\gamma^2}, \tag{6.11d}$$

where $\frac{1}{k} = \gamma^2$; $C_1 - C_6$ are arbitrary constants which can be evaluated by using given boundary conditions (6.9) and I_0, K_0 are modified Bessel functions. The complete expressions for velocities $(w_H(r),\ w_N(r),\ w_B(r))$ has been evaluated in MATHEMATICA 10.0.2 and due to very large expressions, these have not been presented in the Manuscript.

6.3 Concentration Solution

6.3.1 Governing Equations

The solute dispersion in the two-fluid model of blood flow through a tube of radius $\widetilde{R}_3$ with porous layer near the boundary is depicted in Figure 6.1.

The unidirectional steady flow through the tube is assumed to be laminar, incompressible, fully developed with flow symmetry about the axis of the tube, the diffusion equation that demonstrates the concentration C of the soluble material can be scripted as in the dimensionless form

$$\frac{\partial C}{\partial t} + w(r)\frac{\partial C}{\partial z} = \frac{1}{r}\frac{\partial}{\partial r}\left(r\frac{\partial C}{\partial r}\right) + \frac{1}{Pe^2}\frac{\partial^2 C}{\partial z^2}, \tag{6.12}$$

where $w(r)$ $(\equiv w_H/w_N/w_B)$ is the longitudinal velocity of the fluid, $\frac{d\widetilde{p}}{d\widetilde{z}}$ is the pressure gradient applied along the axis of the tube and $Pe = \frac{\widetilde{R}_3^3 \widetilde{q}_0}{4\widetilde{\mu}_N \widetilde{D}_m}$ is the Peclet number, which measures the relative characteristic time of the diffusion process to the convection process.

6.3.2 Initial and Boundary Conditions

6.3.2.1 Initial Condition (IC)

A uniform distribution of the solute is assumed at the beginning and the distribution of the concentration at the beginning of the diffusion process is reported as below.

$$C(0, z, r) = \psi(z)X(r), \tag{6.13a}$$

with

$$\psi(z) = \frac{\delta(z)}{d^2 Pe}, \tag{6.13b}$$

and

$$X(r) = \begin{cases} 1, & 0 < r \leq d, \\ 0, & d < r \leq 1, \end{cases} \tag{6.13c}$$

where $\delta(z)$ is Dirac delta function.

6.3.2.2 Boundary Conditions (BCs)

The boundary conditions (BCs) signifying a first order heterogeneous irreversible reaction at the tube wall and a finite concentration in the system at any instant of time are given by

$$\frac{\partial C}{\partial r}(t,z,1) = -\beta C(t,z,1), \tag{6.14a}$$

$$C(t,\infty,r) = \frac{\partial C}{\partial z}(t,\infty,r) = 0, \tag{6.14b}$$

$$C(t,z,0) = \text{finite}, \tag{6.14c}$$

where β is the non-dimensional wall absorption parameter or first-order reaction rate representing the rate of loss on the tube wall.

6.3.3 Diffusion Coefficients and Mean Concentration

The solution of the equation (6.12) with the help of the initial and boundary conditions $(6.13)-(6.14)$ has been obtained using Sankarasubramanian and Gill [2] approach to finally obtain the diffusion coefficients and mean concentration. The solution expression for the exchange coefficient $M_0(t)$ is obtained as

$$M_0(t) = -\frac{\sum_0^\infty A_k \alpha_k J_1(\alpha_k) e^{-\alpha_k^2 t}}{\sum_0^\infty \left(\frac{A_k}{\alpha_k}\right) J_1(\alpha_k) e^{-\alpha_k^2 t}}, \tag{6.15a}$$

which is exactly the same as derived in the previous works ([2], [87], [88], [89]) as its computation does not include fluid velocity.

The expression for convection coefficient (M_1) is obtained as

$$M_1 = \frac{-2\alpha_0^2}{(\alpha_0^2+\beta^2)J_0^2(\alpha_0)}\int_0^1 w(r)rJ_0^2(\alpha_0 r)dr. \tag{6.15b}$$

The expression for the dispersion coefficient (M_2) is given by

$$M_2 = \frac{1}{Pe^2} - \frac{4\alpha_0 J_1(\alpha_0)}{(\alpha_0^2+\beta^2)J_0^2(\alpha_0)}\int_0^1 (w(r)+M_1)g_1(r)rJ_0(\alpha_0 r)dr. \tag{6.15c}$$

The expression for the mean concentration (C_M) of the solute is obtained as

$$C_M(t,z) = \frac{1}{2Pe\sqrt{\pi T}}\text{Exp}\left(\eta - \frac{z_1^2}{4T}\right). \tag{6.15d}$$

The detailed description of the solution method and derivation of the diffusion coefficients as well as mean concentration has been provided in Chapter 1 (1.5.3). All the integrations involved in the expressions of convective coefficient $(-M_1)$, dispersion coefficient (M_2) and mean concentration (C_M) are evaluated in MATHEMATICA 10.0.2 software using numerical integration.

6.4 Results and Discussion

An effort has been made to understand the impact of a porous layer near the tube wall on solute dispersion in the circulation of yield-stress fluid flowing through a tube with wall absorption. The impact of various parameters like porous layer parameters (k, λ_1, β_S) and viscosity parameters (K, m) on solute dispersion process has been analyzed and it is observed that these parameters significantly affect the solute dispersion process. In the absence of a porous layer near the wall and variable nature of viscosity, this model reduces to the work of Ramana and Sarojamma [88] representing the case of the single-fluid model (SFM) with constant viscosity. A comparative study has also been done between the two-fluid model (TFM) with and without a porous layer near the tube walls in the present work. The thickness of the intermediate region $(R_1 < r \leq R_2)$ is taken as 25% of the whole plasma layer width ([3], [62], [66]). The range of the core, intermediate and porous regions are $0 < r \leq R_1$, $R_1 < r \leq R_2$ and $R_2 < r \leq 1$, respectively. We have taken the thickness of core and plasma regions as h_1 and h, respectively and $h_1 + h = 1$. Therefore, the typical estimates for core, intermediate and porous regions radii are $R_1 = 1-h$, $R_2 = 1-\frac{3h}{4}$ and 1, respectively. The impact of the porous layer and viscosity parameters on flow variables like velocity, flow rate, and flow impedance has been discussed in detail in previous work ([49]).

The range of values of various parameters are taken from the previous studies to perform the graphical analysis and comparison of our result has been made with the previous works. The range of values of various parameters with their resources are given in Table 6.1.

Values of parameters		
Parameters	Values	Resources
Peclet number Pe	$10-10^4$	[89]
Permeability k	$(0,\infty)$	[98], [158], [49]
Plasma layer thickness h	0.015-0.050	[31], [28], [49]
Power-law index n	0.90-1.10	[91], [28], [49]
Steady pressure gradient p_s	1-10	[91], [28], [49]
Stress-jump parameter β_S	$-1 < \beta_S < 1$	[68]
Viscosity index m	0.0-3.0	[47], [49]
Viscosity parameter K	0.00-0.90	[47], [49]
Viscosity ratio parameter λ_1	1.0-1.5	[124],[122]
Wall absorption parameter β	$0.01 \leq \beta \leq 100$	[87], [111], [112], [36]
Yield stress Θ	0.00-0.10	[87], [91], [36]

Table 6.1: The range of parameters appropriate for flow through narrow tubes with their resources

6.4.1 Convective Coefficient

The effect of a thin porous layer on the convective coefficient $(-M_1)$ is discussed through various porous medium parameters in Figure 6.2 and Figure 6.3. Decay in convective coefficient $(-M_1)$ is observed with viscosity ratio parameter λ_1 in Figure 6.2, signifying that a reduced porosity obstructs the flow of plasma in the peripheral layer resulting in a reduced convective coefficient $(-M_1)$. The impact of variable viscosity is more significant in the case of higher wall absorption $(\beta = 100)$. A comparative study of viscosity ratio parameter λ_1 affecting the convective coefficient $(-M_1)$ for four different fluids is depicted in Figure 6.3 by taking different peripheral layer thickness h. It is evident that the reduction rate of convective coefficient $(-M_1)$ with λ_1 is significantly larger for high plasma layer thickness

h as for a thick porous layer, the effect of porosity will have a relatively more significant effect on convective coefficient. The convective coefficient is least for Herschel-Bulkley (HB) fluid and most for Newtonian fluid (NF) and an increased h leads to a significant increase in the decay rate of convective coefficient as a thicker porous layer near the wall have a significant impact of porosity parameter on velocity and hence the convective coefficient.

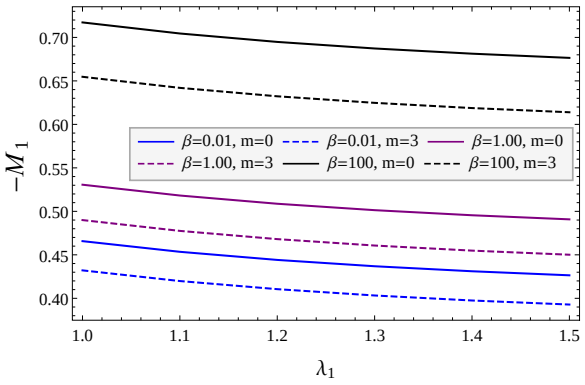

Figure 6.2: Impact of wall absorption parameter β and viscosity index m on convective coefficient $(-M_1)$ varying with viscosity ratio parameter λ_1. $K = 0.2, h = 0.05, \beta_S = 0.1, k = 5, \Theta = 0.10, p_s = 1, n = 0.95$)

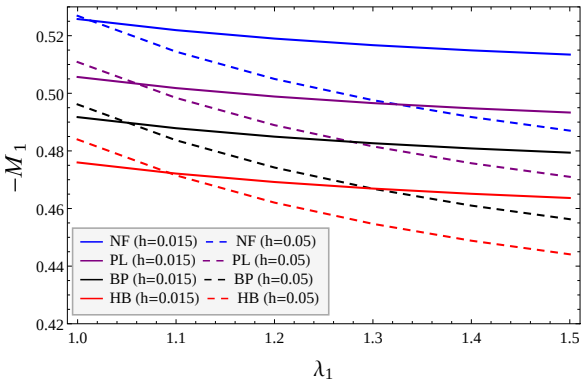

Figure 6.3: Impact of plasma layer thickness h on convective coefficient $(-M_1)$ varying with viscosity ratio parameter λ_1. $(K = 0.2, m = 3, \beta_S = 0.1, k = 5, p_s = 1, \beta = 1.0)$

The effect of steady-state pressure gradient p_s and hence the effect of pressure-driven flow on convective coefficient $(-M_1)$ is discussed in Figure 6.4. An increasing pressure gradient p_s leads to a significant rise in the convective coefficient $(-M_1)$ due to the rise in fluid velocity. The growth rate of the convective coefficient increases with an increase in the reactive nature of the wall which agrees with the previous studies of Nagarani *et al.* [87], and Ramana and Sarojamma [88]. However, for varying nature of viscosity, a slight decay in convective coefficient $(-M_1)$ is observed which is due to a rise in obstruction against the flow. It is also perceived that the varying nature of viscosity reduces the growth

rate of convective coefficient with pressure gradient and this decay in growth rate is more significant for highly reactive walls ($\beta = 100$).

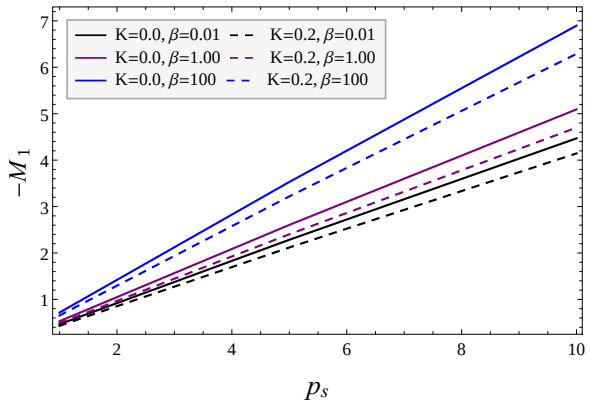

Figure 6.4: Impact of wall absorption parameter β and viscosity parameter K on convective coefficient $(-M_1)$ varying with pressure gradient p_s. $(m = 3, h = 0.05, \beta_S = 0.1, k = 5, \Theta = 0.10, n = 0.95, \lambda_1 = 1)$

Figure 6.5 reveals the increasing nature of convective coefficient $(-M_1)$ with Herschel-Bulkley fluid (HB) parameter n for different porous layer thickness but this growth rate slightly decays with higher porous layer thickness near the wall. Similarly, a wider difference in convective coefficient $(-M_1)$ between walls with and without a porous layer is reported owing to increased resistance for plasma flow in the peripheral region. Another observation of a higher convective coefficient is reported for higher plasma layer thickness h owing to a higher plasma layer thickness resulting in a higher flow rate.

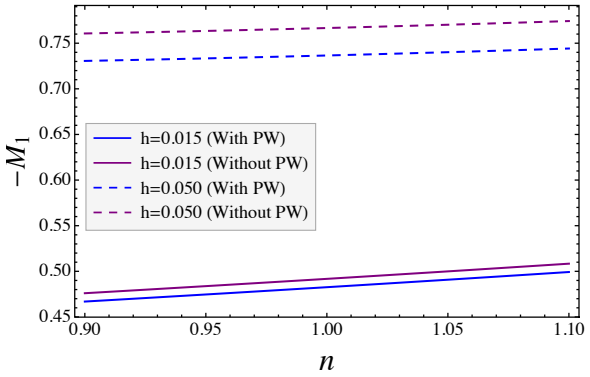

Figure 6.5: Impact of plasma layer thickness h on convective coefficient $(-M_1)$ varying with Herschel-Bulkley fluid parameter n. $(m = 3, K = 0.2, \beta_S = 0.1, k = 5, \Theta = 0.10, \beta = p_s = \lambda_1 = 1)$

A slight increase in convective coefficient $(-M_1)$ is observed with a rise in permeability (k) of the porous layer near the wall, which is due to smoother flow of plasma in the porous layer (Table 6.2).

k	m=0, β=0.01	m=3, β=0.01	m=0, β=1.00	m=3, β=1.00	m=0, β=100	m=3, β=100
0.5	0.465416	0.431794	0.530309	0.489636	0.716915	0.654389
1.0	0.465561	0.431939	0.530454	0.489781	0.717060	0.654534
3.0	0.465697	0.432075	0.530590	0.489917	0.717196	0.654670
5.0	0.465737	0.432115	0.530630	0.489957	0.717236	0.654710
7.0	0.465757	0.432135	0.530650	0.489977	0.717257	0.654731
9.0	0.465770	0.432148	0.530663	0.489991	0.717270	0.654744

Table 6.2: Impact of viscosity index m, wall absorption parameter β and permeability in porous region k on convection coefficient $(-M_1)$. $(K = 0.2, \Theta = 0.10, n = 0.95, p_s = \lambda_1 = 1, h = 0.05, \beta_S = 0.1)$

k	m=0, β=0.01	m=3, β=0.01	m=0, β=1.00	m=3, β=1.00	m=0, β=100	m=3, β=100
0.5	0.465416	0.431794	0.530309	0.489636	0.716915	0.654389
1.0	0.465561	0.431939	0.530454	0.489781	0.717060	0.654534
3.0	0.465697	0.432075	0.530590	0.489917	0.717196	0.654670
5.0	0.465737	0.432115	0.530630	0.489957	0.717236	0.654710
7.0	0.465757	0.432135	0.530650	0.489977	0.717257	0.654731
9.0	0.465770	0.432148	0.530663	0.489991	0.717270	0.654744

Table 6.3: Impact of viscosity index m, wall absorption parameter β and permeability in porous region k on convection coefficient $(-M_1)$. $(K = 0.2, \Theta = 0.10, n = 0.95, p_s = \lambda_1 = 1, h = 0.05, \beta_S = 0.1)$

It is also apparent that an increase in the viscosity index contributes to substantial decay in convective coefficient $(-M_1)$, which is the same for high as well as low permeability of

the porous layer. A slight decay in convective coefficient $(-M_1)$ is observed with the stress-jump parameter β_S and this decay is relatively higher for thicker porous layer near the wall indicating that deposition of thick layer near the wall significantly affects the convective coefficient $(-M_1)$ in the tube (Table 6.3).

6.4.2 Dispersion Coefficient

Axial dispersion $(M_2 - 1/Pe^2)$ is significantly affected by the viscosity index m as evident from Figure 6.6 for all the range of β $(0.01 - 100)$. For the low and moderate range of β (0.01 and 1.00), the axial dispersion demonstrates a slight increase with λ_1 showing that a low porosity layer near the wall contributes towards a slight rise in axial dispersion $(M_2 - 1/Pe^2)$ if the wall is not highly reactive. However, in the case of a highly reactive wall $(\beta = 100)$, the axial dispersion slightly decays with λ_1. For all ranges of β, the varying nature of viscosity contributes towards significant decay in axial dispersion, which may be attributed to decay in velocity and flow rates.

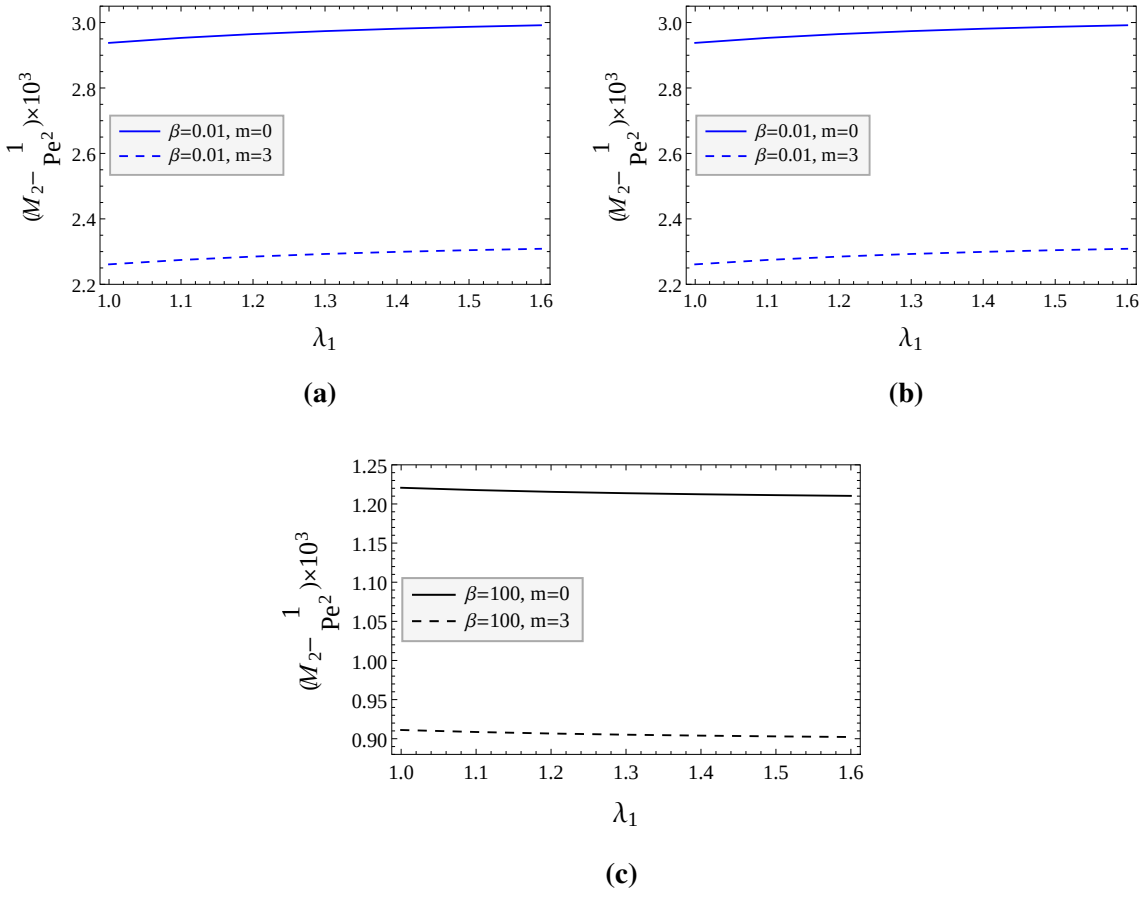

Figure 6.6: Impact of wall absorption parameter on dispersion coefficient $(M_2 - 1/Pe^2)$ varying with viscosity ratio parameter λ_1 **(a)** $\beta = 0.01$, **(b)** $\beta = 1.00$ and **(c)** $\beta = 100$. $(K = 0.2, h = 0.05, \Theta = 0.10, p_s = 1, \beta_S = 0.1, k = 5, n = 0.95)$

Figure 6.7 denotes the comparative variation of axial dispersion with λ_1 for four different fluids using different porous layer thickness. As evident a thin porous layer has an almost negligible effect on axial dispersion for all four fluids but as the thickness is increased, a slight growth in axial dispersion with rising λ_1 is observed. This indicates that a reduced porosity slightly assist the axial dispersion for higher plasma layer thickness. Further, a significant difference in dispersion coefficient between yield-stress (BP and HB) and non yield-stress (NF and PL) fluids is observed for all plasma layer thickness.

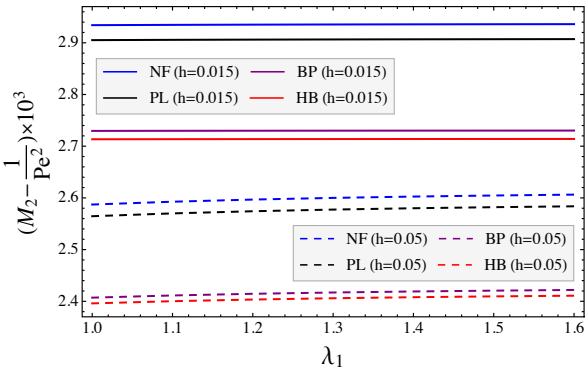

Figure 6.7: Impact of plasma layer thickness h on dispersion coefficient $(M_2 - 1/Pe^2)$ varying with viscosity ratio parameter λ_1. $(K = 0.2, m = 3, \beta_S = 0.1, k = 5, p_s = \beta = 1)$

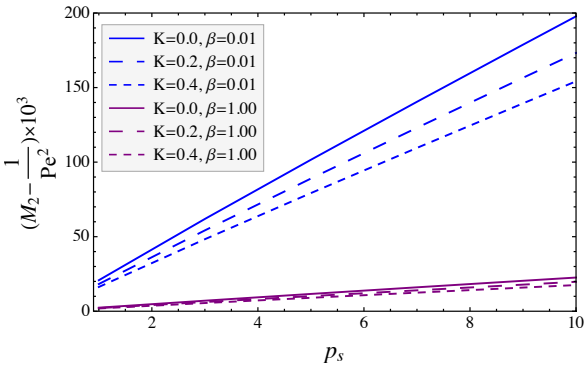

Figure 6.8: Impact of wall absorption parameter β and viscosity parameter K on dispersion coefficient $(M_2 - 1/Pe^2)$ varying with pressure gradient p_s. $(m = 3, h = 0.05, \beta_S = 0.1, k = 5, \Theta = 0.10, n = 0.95, \lambda_1 = 1)$

Figure 6.8 suggests that like the convective coefficient $(-M_1)$, the axial dispersion $(M_2 - 1/Pe^2)$ also increases with a rise in pressure gradient p_s and the increasing growth rate is significantly reduced for varying viscosity model as well as for absorbing walls with moderate reactivity compared to low reactive walls. It is further observed that the effect of varying viscosity on axial dispersion is relatively more significant for less reactive walls. As observed from the previous works of Nagarani *et al.* [87], Ramana and Sarojamma [88], Rana and Murthy [89], the dispersion coefficient significantly reduces for reactive walls.

Unlike the convective coefficient $(-M_1)$, the axial dispersion $(M_2 - 1/Pe^2)$ shows reduction with increased peripheral layer thickness. The reduction in the axial dispersion $(M_2 - 1/Pe^2)$ further grows with the inclusion of porous layer near the wall (Figure 6.9). This variation remains same for shear thinning and shear thickening fluids, exhibiting a slight ease in axial dispersion for shear thinning fluid.

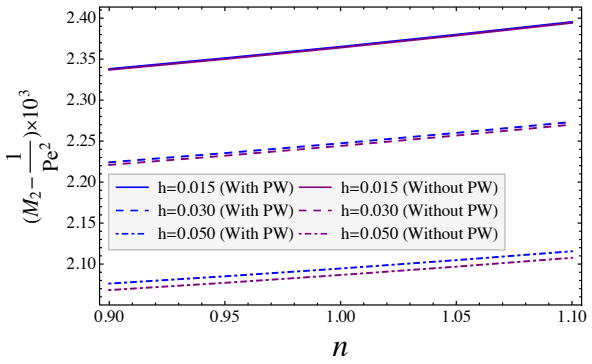

Figure 6.9: Impact of plasma layer thickness h on dispersion coefficient $(M_2 - 1/Pe^2)$ varying with HB fluid parameter n. $(m = 3, K = 0.2, \beta_S = 0.1, k = 5, \Theta = 0.10, \beta = p_s = \lambda_1 = 1)$

k	m=0, β=0.01	m=3, β=0.01	m=0, β=1.00	m=3, β=1.00	m=0, β=100	m=3, β=100
0.5	20.7697	18.2348	2.38418	2.08942	1.31168	1.14144
1.0	20.7690	18.2342	2.38414	2.08938	1.31169	1.14146
3.0	20.7685	18.2336	2.38410	2.08935	1.31171	1.14147
5.0	20.7683	18.2334	2.38409	2.08934	1.31171	1.14148
7.0	20.7682	18.2333	2.38409	2.08933	1.31171	1.14148
9.0	20.7681	18.2333	2.38408	2.08933	1.31172	1.14148

Table 6.4: Impact of viscosity index m, wall absorption parameter β and permeability in porous region k on dispersion coefficient $(M_2 - 1/Pe^2) \times 10^3$. $(K = 0.2, \Theta = 0.10, n = 0.95, p_s = \lambda_1 = 1, h = 0.05, \beta_S = 0.1)$

Table 6.4 reveals the effect of permeability on axial dispersion for reactive walls. An almost negligible decay in axial dispersion is reported with rising permeability. However, a significant decay is reported for varying viscosity model. Also, as observed from the previous studies of Nagarani *et al.* [87], Ramana and Sarojamma [88], Rana and Murthy [89], the axial dispersion shows decay with rising wall absorption parameter.

6.4.3 Mean Concentration

Time-dependent concentration profile C_M for different viscosity index m and viscosity ratio parameter λ_1 is depicted in Figure 6.10:(a). Increment of both the viscosity index m and viscosity ratio parameter λ_1 lead to a significant decay in mean concentration. A delayed and reduced peak of mean concentration is observed for higher m and λ_1 showing that the varying nature of viscosity and the porosity of porous layer near the wall affect the mean concentration with time. However, for variation with axial distance z the rising viscosity index leads to a rise in mean concentration. The justification for this comes from the time variation of mean concentration showing that for a low time the concentration profile is slightly different and the same is reflected in Figure 6.10:(b). It is also evident that an increasing viscosity index and viscosity parameter results in an early peak (lesser z) but an almost negligible change in peak is observed for reduced porosity of layer near the wall.

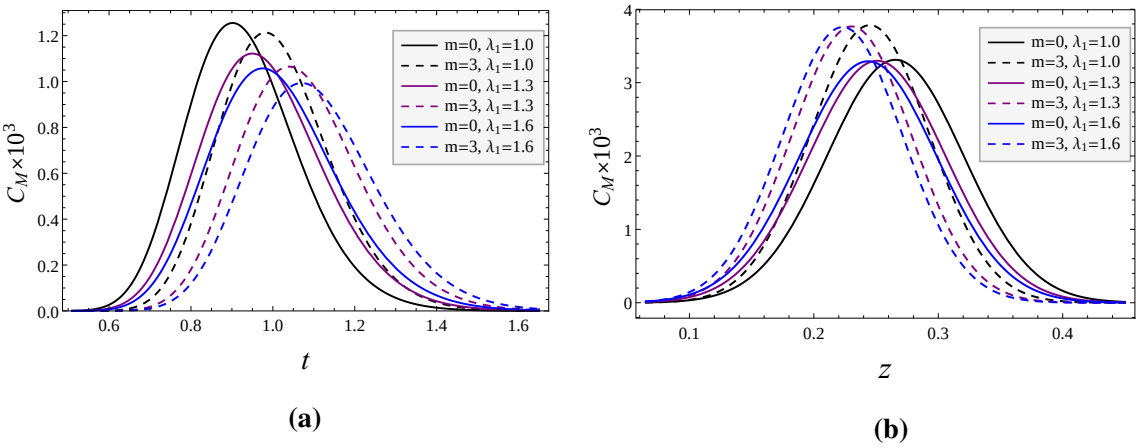

Figure 6.10: Impact of viscosity index m and viscosity ratio parameter λ_1 on mean concentration C_M varying with respect to **(a)** time t $(z = 0.5)$ and **(b)** axial distance z $(t = 0.5)$. $(K = 0.2, \beta = 1.00, h = 0.05, Pe = 10^3, \Theta = 0.10, p_s = 1, \beta_S = 0.1, k = 5, n = 0.95)$

Figure 6.11:(a) reveals a significantly reduced and delayed peak of mean concentration C_M with rising viscosity parameter K emphasizing the effect of varying nature of viscosity on the dispersion process. A similar observation of mean concentration profile with longitudinal direction z for different viscosity parameter K and viscosity ratio parameter λ_1 is reported in Figure 6.11:(b) for which the justification is the same as that of Figure 6.10:(b).

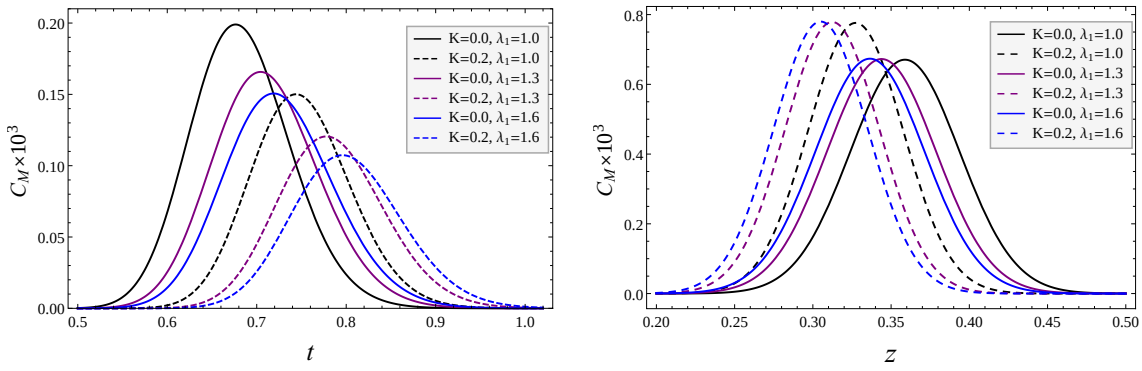

(a) **(b)**

Figure 6.11: Impact of viscosity parameter K and viscosity ratio parameter λ_1 on mean concentration C_M varying with respect to **(a)** time t $(z = 0.5)$ and **(b)** axial distance z $(t = 0.5)$. $(m = 3, \beta = 100, h = 0.05, Pe = 10^3, \Theta = 0.10, p_s = 1, \beta_S = 0.1, k = 5, n = 0.95)$

A time-dependent concentration profile C_M for different m and z shows that a larger time is required to attain peak as we move away from the point of solute injection which matches with previous studies (Figure 6.12:(a)). A noteworthy observation is that the time taken for the solute dispersion process increases and peak in C_M decreases between constant and varying viscosity model significantly as we move away from the point of injection. So, a shift and decay in peak of mean concentration between constant and varying viscosity is observed as we move away from point of injection.

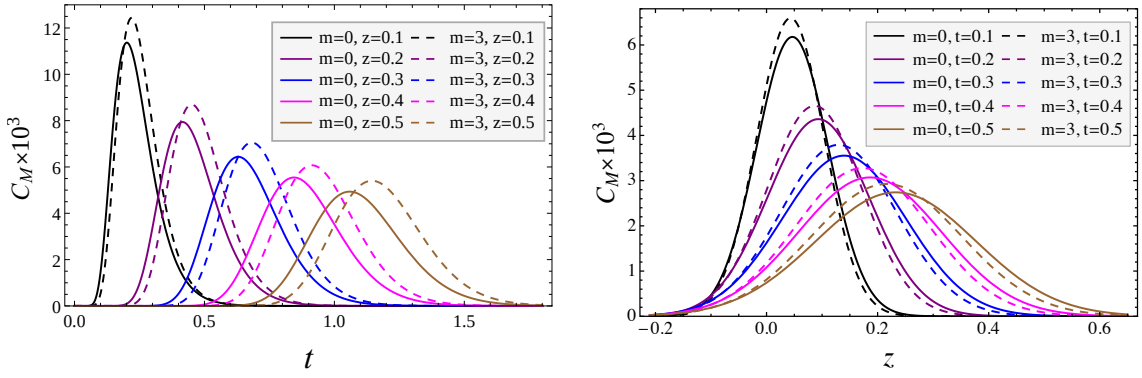

(a) **(b)**

Figure 6.12: Impact of viscosity index m on mean concentration C_M varying with respect to **(a)** time t for different values of axial distance z and **(b)** axial distance z for different values of time t. $(K = 0.2, h = 0.05, \Theta = 0.10, p_s = \lambda_1 = 1, \beta_S = 0.1, k = 5, n = 0.95, Pe = 10^3, \beta = 0.01)$

A similar observation is reported for variation of C_M with longitudinal distance for different times (Figure 6.12:(b)). For a larger time, the peak of C_M is shifted. The mean concentration curve along axial distance shows that initially the peak of mean concentration appeared almost at the same location (same z) for constant and varying viscosity cases but a

slight shift in peak position is observed with the progress of time in the dispersion process. Furthermore, a larger time leads to farther spread of solute in the axial direction for constant and varying viscosity cases which agrees with previous works of Nagarani *et al.* [87], Ramana and Sarojamma [88], Rana and Murthy [89].

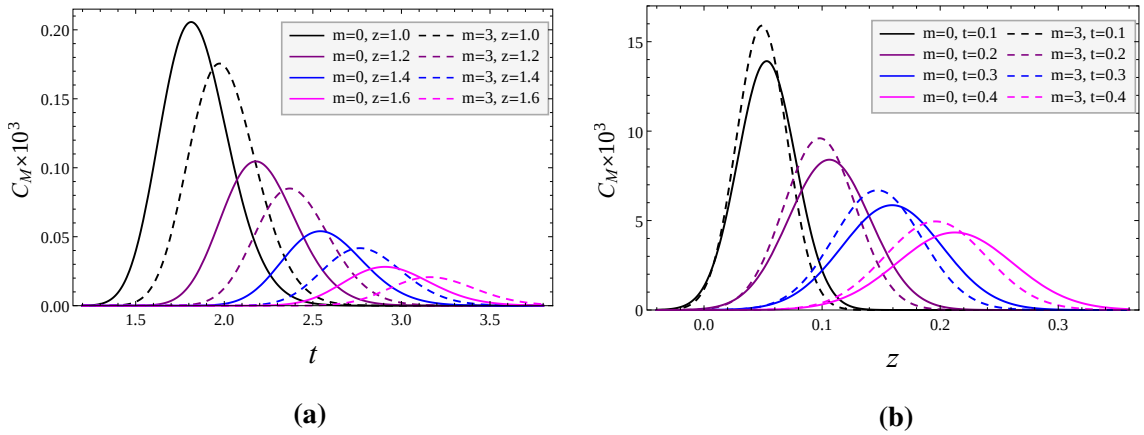

(a) **(b)**

Figure 6.13: Impact of viscosity index m on mean concentration C_M varying with respect to **(a)** time t for different values of axial distance z and **(b)** axial distance z for different values of time t. ($K = 0.2, h = 0.05, \Theta = 0.10, p_s = \lambda_1 = 1, \beta_S = 0.1, k = 5, n = 0.95, Pe = 10^3, \beta = 1.00$)

A similar analysis has been done for a tube with a reactive wall where a slightly delayed peak is observed for a reactive wall for the varying viscosity case. For a highly reactive wall, the solute dispersion process is completed relatively quicker along with the axial distance. A higher mean concentration is observed for varying viscosity relative to constant viscosity for low β.

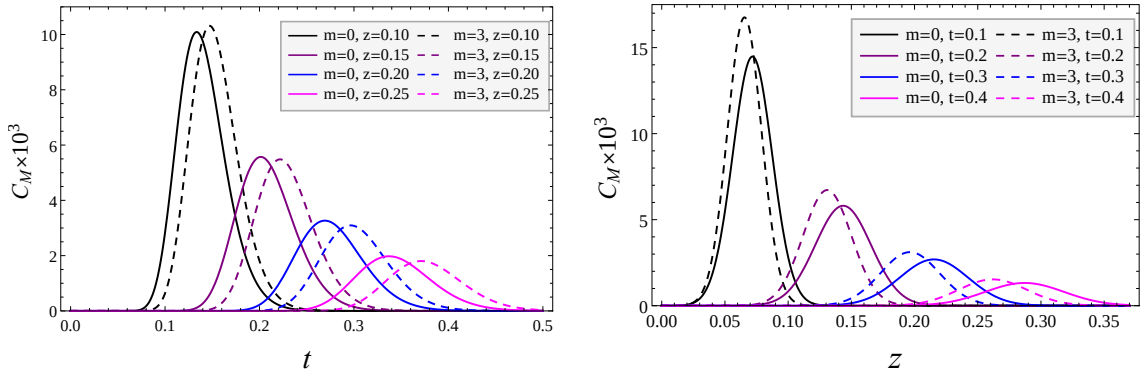

(a) **(b)**

Figure 6.14: Impact of viscosity index m on mean concentration C_M varying with respect to **(a)** time t for different values of axial distance z and **(b)** axial distance z for different values of time t. ($K = 0.2, h = 0.05, \Theta = 0.10, p_s = \lambda_1 = 1, \beta_S = 0.1, k = 5, n = 0.95, Pe = 10^3, \beta = 100$)

A noteworthy observation is that near the point of solute injection, the mean concentration is higher for varying viscosity in comparison to constant viscosity model and this pattern reverses as we move away from the point of injection (Figure 6.13-6.14). Figure 6.13 also depicts a significant decay and shift in the peak of mean concentration between constant and varying viscosity models for a relatively larger time. Unlike the less and intermediate reactive walls (Figure 6.12:(a) and 6.13:(a)), the peak of mean concentration C_M for varying viscosity model is higher than constant viscosity model for highly reactive walls (Figure 6.14:(a)) near the point of solute injection. However, this trend reverses as we move away from the point of solute injection (increasing z).

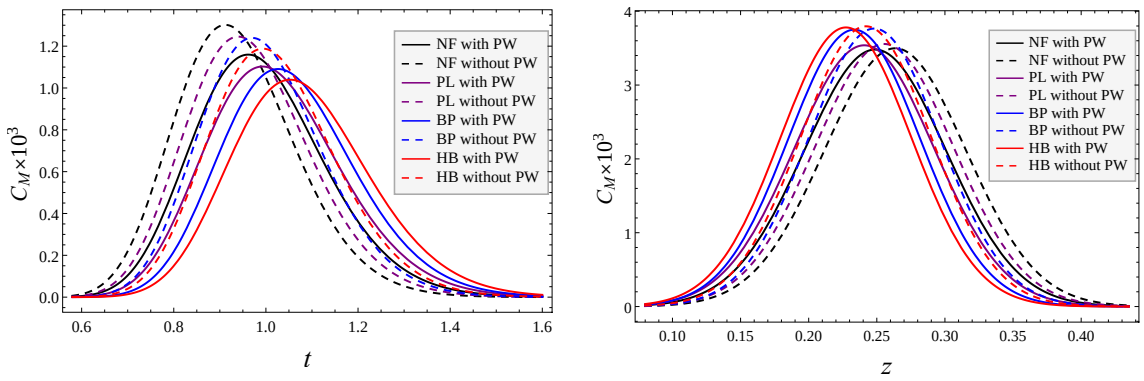

Figure 6.15: Mean concentration C_M varying with respect to **(a)** time t $(z = 0.5)$ and **(b)** axial distance z $(t = 0.5)$ between with and without porous region near the walls. $(K = 0.2, h = 0.05, \beta_S = 0.1, m = 3, n = 0.90, k = 5, \Theta = 0.10, p_s = \beta = 1, \lambda_1 = 1.3, Pe = 10^3)$

A comparative study of present work with previous works (dispersion through a tube with no porous layer near the wall) is discussed in Figure 6.15. For all four fluids, the C_M for the tube with a porous layer near the tube wall is significantly less than C_M for a tube without a porous layer near the boundary. It is also perceived that the viscoelastic nature reduces the mean concentration C_M which is evident from Figure 6.15:(a) showing a consistently decaying mean concentration C_M from Newtonian fluid to Herschel-Bulkley fluid. An important observation is that the inclusion of a porous layer near the wall contributes to a reduced and delayed peak of C_M relative to that of the tube without a porous layer near the wall for all four fluids. Apart from that, a delayed peak is reported for viscoelastic fluids in comparison to NF. However, for small z, the Herschel-Bulkley fluid shows a higher C_M relative to NF and an early peak of C_M is reported for tubes with porous walls in comparison to tubes without porous walls (Figure 6.15:(b)).

The mean concentration slightly rises with increasing permeability owing to a smoother flow of plasma in the peripheral region (Table 6.5). Although the growth rate slightly reduces for highly reactive walls.

k	m=0, β=0.01	m=3, β=0.01	m=0, β=1.00	m=3, β=1.00	m=0, β=100	m=3, β=100
0.5	0.490829	0.319880	0.337616	0.229289	0.0902226	0.0508794
1.0	0.491268	0.320222	0.337883	0.229512	0.0903063	0.0509460
3.0	0.491682	0.320545	0.338135	0.229722	0.0903852	0.0510087
5.0	0.491802	0.320639	0.338208	0.229783	0.0904081	0.0510269
7.0	0.491865	0.320687	0.338246	0.229814	0.0904201	0.0510364
9.0	0.491905	0.320719	0.338271	0.229835	0.0904277	0.0510425

Table 6.5: Impact of viscosity index m, wall absorption parameter β and permeability in porous region k on mean concentration $(C_M \times 10^3)$. $(K = 0.2, \Theta = 0.10, n = 0.95, p_s = \lambda_1 = 1, h = 0.05, \beta_S = 0.1, t = z = 0.5, Pe = 10^3)$

β_S	K=0.0, h=0.015	K=0.2, h=0.015	K=0.0, h=0.03	K=0.2, h=0.03	K=0.0, h=0.05	K=0.2, h=0.05
-0.9	0.326551	0.0143416	0.233528	0.0088705	0.142586	0.0044259
-0.5	0.325980	0.0143106	0.231852	0.0087920	0.139642	0.0043135
-0.3	0.325696	0.0142953	0.231024	0.0087533	0.138207	0.0042589
0.3	0.324849	0.0142493	0.228575	0.0086389	0.134039	0.0041012
0.5	0.324569	0.0142341	0.227771	0.0086014	0.132694	0.0040506
0.9	0.324009	0.0142039	0.226180	0.0085273	0.130069	0.0039520

Table 6.6: Impact of viscosity parameter K, plasma layer thickness h and stress jump parameter β_S on mean concentration $(C_M \times 10^6)$. $(m = 3, \Theta = 0.10, n = 0.95, p_s = \lambda_1 = 1, k = 5, \beta = 1.0, Pe = 10^3, t = z = 0.5)$

Further, a rising stress-jump parameter slightly decays the mean concentration for various porous layer thickness (Table 6.6). However, this decay rate slightly reduces for varying viscosity model. So, we conclude that a relative slipping at the fluid-porous interface slightly affects the mean concentration.

The time profile of mean concentration depicts a higher C_M for shear-thinning fluids, which gradually enhances with steady pressure gradient p_s (Figure 6.16:(a)). It is also perceived that the dispersion process lasts slightly longer for shear thickening fluids. However, along axial variation, the mean concentration decays with rising steady pressure gradient p_s (Figure 6.16:(b)). A remarkable observation is that as we move away from the point of injection, the peak of mean concentration for shear thickening fluids become relatively higher than shear-thinning fluids. This further results in a relatively delayed peak of mean concentration for shear-thinning fluids.

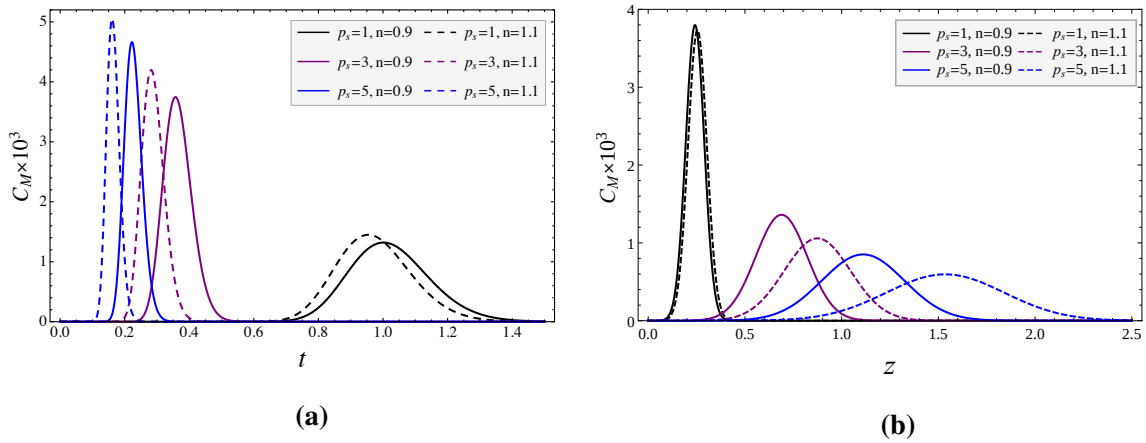

Figure 6.16: Impact of pressure gradient p_s and HB fluid parameter n on mean concentration C_M varying with respect to with **(a)** time t $(z = 0.5)$ and **(b)** axial distance z $(t = 0.5)$. $(K = 0.2, h = 0.05, \beta_S = 0.1, m = 3, k = 5, \Theta = 0.10, \beta = 1, \lambda_1 = 1.0, Pe = 10^3)$

6.5 Conclusions

Solute dispersion analysis for two-fluid model of blood flowing through a tube with a porous layer near the boundary has been done using a generalized dispersion model with emphasis is being given to varying nature of viscosity in the central region containing non-Newtonian fluid. The important findings of the present study are:

1. The convective coefficient and axial dispersion are significantly affected by the porosity of the porous layer, viscosity index, viscosity parameter, Herschel-Bulkley fluid parameter and the thickness of the porous layer near the wall.

2. The mean concentration depends upon, the varying nature of viscosity as well as the parameters determining thickness and porosity of the porous layer near the wall.

3. The mean concentration is higher for shear-thinning fluids and the dispersion process lasts slightly longer for shear-thickening fluids.

4. A comparative study shows a significant difference in the mean concentration for flow-through tubes with and without a porous layer near the wall.

So, any process involving solute dispersion such as drug delivery to a specific tissue or physiological system may be significantly affected in case there is a deposition of a porous layer at the wall which is a physically realistic situation as suggested by Secomb *et al.* [3].

Chapter 7

Conclusions and Research Prospects

7.1 Conclusions

The present study is a novel approach to investigate the mechanical aspects of blood microcirculation by depicting it as an axially symmetric unidirectional, fully developed, steady, laminar flow of an incompressible two-fluid. Considering the viscosity's dependence on hematocrit or temperature in different scenarios, the effects of variable viscosity on flow variables and diffusion coefficients have been examined. The influence of the microstructure of erythrocytes on microcirculation and transport phenomena has been examined. The presence of endothelial glycocalyx layer (EGL) in close proximity to the vessel wall has been taken into account, and the impact of the permeable properties of the vessel wall on hemodynamic and transport properties has been investigated. A comparative analysis has been conducted with existing literature, revealing that obtained findings are consistent with prior research.

The primary conclusions are found to be:

1. Most of the important flow variables are significantly affected by the microlevel parameters (N and n), which includes a significant reduction in velocity, flow rate Q_S and hematocrit H_T while the same leads to growth in flow resistance λ_s and Fåhræus effect Fe. The heat transfer parameters such as Grashof number Gr, thermal conductivity ratio K_0vand radiation parameter N_1 significantly affect the hematocrit H_T and Fåhræus effect Fe.

2. The viscosity index α rises for less viscous core fluid and results into the growth of velocity profile, the higher velocity in plug core region and higher flow rate of fluid. But the flow impedance is observed to be reduced in less viscous core fluid.

3. The mean concentration depends upon, the varying nature of viscosity as well as the parameters determining thickness and porosity of the porous layer near the wall. The

mean concentration is higher for shear-thinning fluids and the dispersion process lasts slightly longer for shear-thickening fluids. A comparative study shows a significant difference in the mean concentration for flow-through tubes with and without a porous layer near the wall.

7.2 Noteworthy Contributions

The study offers following noteworthy contributions to the existing understanding of the subject.

1. Microlevel parameters (N and n) have a significant impact on the diffusion coefficients and mean concentration in both the formulations (NS and NCS). Specifically, a higher coupling parameter N leads to a delay in the diffusion process. A rising Hartmann number H leads to decay in diffusion coefficients as well as time profile of mean concentration showing a clear impact of the magnetic field on the diffusion process.

2. Relatively higher diffusion coefficients (convective and dispersion coefficients) are reported for no-couple stress formulation in comparison to no-spin condition at the fluid-fluid interface. For no-couple stress formulation, the peak in the time profile of mean concentration appears relatively earlier in comparison to the no-spin formulation.

3. All the diffusion coefficients and mean concentration are significantly affected by the thermal buoyancy forces Gr, thermal conductivity ratio K_0 and varying viscosity parameter α. The time to complete diffusion process is significantly lesser under the dominance of thermal buoyancy forces (i.e. higher Grashof number Gr). These outcomes suggest that transportation of nutrients to physiological system or drug delivery to tissues under medical treatment involving slightly high temperature are severely affected.

4. The impact of Forchheimer number on flow quantities is slightly visible for small Darcy number however, it is negligible in case of large Darcy number. This effect is more significant for a thick endothelial glycocalyx layer adjacent with the wall.

5. All the flow variables except the flow resistance assume relatively higher values for flow through microvessels without an EGL adjacent with the wall in comparison to the flow through microvessels with an EGL adjacent with the wall owing to absence of the Brinkman and nonlinear Forchheimer resistance of the porous medium.

7.3 Research Constraint

The study has certain limitations that should be acknowledged.

1. The curvature of micro vessel has not been taken into account. Microvessel curvature may compromise brain blood flow and oxygenation, leading to cognitive impairment in neurodegenerative conditions. The mechanics of different physiological and pathological processes may be revealed by studying microvessel curvature. It may assist find vascular disease therapy targets.

2. Plaque accumulation in arteriosclerosis may roughen artery walls, reducing blood flow and increasing the risk of clot formation. The impact of rough vessel walls on microcirculation and transport phenomena has not been investigated in the present study.

3. Hypertension may cause the smooth muscle layer of the artery wall to become hypertrophied and lose its flexibility, raising blood pressure and risk of cardiovascular disease. However, Marfan syndrome may make artery walls excessively elastic, causing aneurysms and other structural problems. Although, the elastic nature of microvessel has significant influence on microcirculation, the influence of microvessel elasticity remains unexamined.

4. Obtained results should be experimentally validated for further applications to various medical treatments of diseases related to the physiological systems.

Although there may be limitations to the research work, the findings can still provide valuable insights and contribute to the existing body of knowledge in the field. These limitations can serve as opportunities for future research and improvement to build upon the current findings.

7.4 Research Prospects

In regard of the study presented and above mentioned constraints, the following research prospects arises

1. An analytical study for solute dispersion in the two-fluid model for blood microcirculation through straight or slightly curved microvessels should be done to examine the impact of roughness and elasticity of vessel walls.

2. Solute dispersion of electroosmotic blood flow through straight or slightly curved microvessels can be studied under different pathological conditions.

3. The mass transport process in microcirculation of blood throgh straight or slightly curved microvessels with linear reversible and irreversible reactions at the vessel wall should be studied.

4. Blood microcirculation through microvessels with non circular cross section under various circumstances can be examined.

5. Center Manifolds and Hypocoercivity approach can be applied to gain a rigorous understanding of solute dispersion process in flow of blood through straight or slightly curved microvessels under two fluid model framework.

6. The machine learning approach can be utilised to investigate the microcirculation and transport phenomena in cardiovascular system.

" I may not have reached where I intended to,
but I think I have ended up where I needed to be."

— Douglas Adams

Bibliography

[1] J. A. Ochoa-Tapia and S. Whitaker, "Momentum transfer at the boundary between a porous medium and a homogeneous fluid- i", Theoretical development, International Journal of Heat and Mass Transfer **38**, 2635–2646 (1995).

[2] R. Sankarasubramanian and W. N. Gill, "Unsteady convective diffusion with interphase mass transfer, proceedings of the royal society of london", Series A, Mathematical and Physical Sciences **333**, 115–132 (1973).

[3] T. W. Secomb, R. Hsu, and A A. R. Pries, "Model for red blood cell motion in glycocalyx-lined capillaries", American Physiological Society **274**, H1016–H1022 (1998).

[4] A. R. Pries, T. W. Secomb, and P. Gaehtgens, "The endothelial surface layer", European Journal of Physiology **440**, 653–666 (2000).

[5] G. J. Tortora and B. Derrickson, *Principles of anatomy and physiology* (John Wiley & Sons, Inc., 2009).

[6] V. V. Li, "Design of a thermal diffusion sensor for noninvasive assessment of skin surface perfusion and endothelial dysfunction", PhD thesis (Massachusetts Institute of Technology, 2008).

[7] T. Britannica, edited by E. of Encyclopaedia (Encyclopedia Britannica).

[8] S. P. Sutera and R Skalak, "The history of poiseuille's law", Annual Review of Fluid Mechanics **25**, 1–20 (1993).

[9] Y. Fung and B. Zweifach, "Microcirculation: mechanics of blood flow in capillaries", Ann. Rev. Fluid Mech **3**, 189–210 (1971).

[10] S. Gauri, "Evaluation of potential dna sources and need of dna analysis for personalized medicine in microfluidic device", Open International Journal of Informatics **7**, 111–123 (2019).

[11] T. Ariman, "On the analysis of blood flow", Journal of Biomechanics **4**, 185–192 (1971).

[12] G. Bugliarello and J. W. Hayden, "High-speed microcinematographic studies of blood flow in vitro", Science **138**, 981–983 (1962).

[13] T. Ariman, M. A. Turk, and N. D. Sylvester, "Microcontinuum fluid mechanics- a review", International Journal of Enginnering Science **11**, 905–930 (1973).

[14] T. Ariman, M. A. Turk, and N. D. Sylvester, "Applications of microcontinuum fluid mechanics", International Journal of Enginnering Science **12**, 273–293 (1974).

[15] A. C. Eringen, "Simple microfluids", International Journal of Engineering Science **2**, 205–217 (1964).

[16] A. C. Eringen, "Theory of micropolar fluids", Journal of Mathematics and Mechanics **16**, 1–18 (1966).

[17] A. C. Burton, *Physiology and biophysics of the circularion* (Year Book Medical Publishers, Chicago, 1965).

[18] Y. C. Fung, "Biomechanics", Applied Mechanics Review **21**, 1–20 (1968).

[19] R. Devanathan and S. Parvathamma, "Flow of micropolar fluid through a tube with stenosis", Medical & Biological Engineering & Computing **21**, 438–445 (1983).

[20] K. Mekheimer and M. A. Kot, "The micropolar fluid model of blood flow through a tapered artery with a stenosis", Acta Mechanica Sinica **24**, 637–644 (2008).

[21] D. Srinivasacharya and M. Shiferaw, "Magnetohydrodynamic flow of a micropolar fluid in a circular pipe with hall effects", ANZIAM Journal **51**, 277–285 (2009).

[22] D. Y. Khanukaeva, A. Filippov, P. Yadav, and A. Tiwari, "Creeping flow of micropolar fluid parallel to the axis of cylindrical cells with porous layer", European Journal of Mechanics / B Fluids **76**, 73–80 (2019).

[23] D. Y. Khanukaeva, A. Filippov, P. Yadav, and A. Tiwari, "Creeping flow of micropolar fluid through a swarm of cylindrical cells with porous layer (membrane)", Journal of Molecular Liquids **294** (2019).

[24] P. G. Siddheshwar and S. Manjunath, "Unsteady convective diffusion with heterogeneous chemical reaction in a plane-poiseuille flow of a micropolar fluid", International Journal of Engineering Science **38**, 765–783 (2000).

[25] W. H. Herschel and R. Bulkley, "Konsistenzmessungen von gummi-benzollösungen", Kolloid-Zeitschrift **39**, 291–300 (1926).

[26] G. P. Galdi, R. Rannacher, A. M. Robertson, and S. Turek, *Hemodynamical flows: modeling, analysis and simulation*, Vol. 37 (Birkhauser Verlag, Basel- Boston–Berlin, 2008).

[27] G. Bugliarello and J. Sevilla, "Velocity distribution and other characteristics of steady and pulsatile blood flow in fine glass tubes", Biorheology **7**, 85–107 (1970).

[28] A. Tiwari and S. S. Chauhan, "Effect of varying viscosity on two-fluid model of blood flow through constricted blood vessels: a comparative study", Cardiovascular Engineering and Technology **10**, 155–172 (2019).

[29] J. Aroesty and J. F. Gross, "Pulsatile flow in small blood vessels i", Casson theory, Biorheology **9**, 33–43 (1972).

[30] J. B. Shukla, R. S. Parihar, and S. P. Gupta, "Effects of peripheral layer viscosity on blood flow through the artery with mild stenosis", Bulletin of Mathematical Biology **42**, 797–805 (1980).

[31] V. P. Srivastava and M. Saxena, "Two-layered model of casson fluid flow through stenotic blood vessels: applications to the cardiovascular system", Journal of Biomechanics **27**, 921–928 (1994).

[32] D. S. Sankar and U. Lee, "Two-phase non-linear model for the flow through stenosed blood vessels", Journal of Mechanical Science and Technology **21**, 678–689 (2007).

[33] D. S. Sankar and U. Lee, "Two-fluid casson model for pulsatile blood flow through stenosed arteries: a theoretical model", Communications in Nonlinear Sciences and Numerical Simulation **15**, 2086–2097 (2010).

[34] A. E. Medvedev and V. M. Fomin, "Two-phase blood-flow model in large and small vessels", Doklady Physics **56**, 610–613 (2011).

[35] P. Chaturani and V. S. Upadhya, "On micropolar fluid model for blood flow through narrow tubes", Biorheology **16**, 419–428 (1979).

[36] S. Debnath, A. P. Saha, B. S. Mazumder, and A. K. Roy, "Dispersion phenomena of reactive solute in a pulsatile flow of three-layer liquids", Physics of Fluids **29** (2017).

[37] J. Rana and P. V. S. N. Murthy, "Unsteady solute dispersion in small blood vessels using a two-phase casson model, proceedings of the royal society of london", Series A, Mathematical and Physical Sciences **473**, 427 (2017).

[38] M. M. Lih, *Transport phenomena in medicine and biology*, 1^{st} (John Wiley, New York, 1975).

[39] R. Bali and U. Awasthi, "Effect of a magnetic field on the resistance to blood flow through stenotic artery", Applied Mathematics and Computation **188**, 1635–1641 (2007).

[40] G. C. Shit, M. Roy, and M. A. Sinha, "Modelling of blood flow through a tapered overlapping stenosed artery with variable viscosity", Applied Bionics and Biomechanics **11**, 185–195 (2014).

[41] S. Nadeem, N. S. Akbar, and M. Hameed, "Peristaltic transport and heat transfer of a mhd newtonian fluid with variable viscosity", International Journal for Numerical Methods in Fluids **63**, 1375–1393 (2010).

[42] K. Mekheimer and Y. A. Elmaboud, "Simultaneous effects of variable viscosity and thermal conductivity on peristaltic flow in a vertical asymmetric channel", Canadian Journal of Physics **92**, 1541–1555 (2014).

[43] G. C. Shit and S. Majee, "Peristaltic flow of blood and heat transfer with variable viscosity under magnetic and vibration environment", Journal of Magnetism and Magnetic Materials **388**, 106–115 (2015).

[44] S. Majee and G. C. Shit, "Numerical investigation of mhd flow of blood and heat transfer in a stenosed arterial segment", Journal of Magnetism and Magnetic Materials **424**, 137–147 (2017).

[45] N. S. Akbar, D. Tripathi, and O. A. B*é*g, "Variable-viscosity thermal hemodynamic slip flow conveying nanoparticles through a permeable-walled composite stenosis artery", The European Physical Journal Plus **132**, 294 (2017).

[46] T. Elnaqeeb, N. A. Shah, and K. Mekheimer, "Hemodynamic characteristics of gold nanoparticle blood flow through a tapered stenosed vessel with variable nanofluid viscosity", BioNanoScience **9**, 245–255 (2019).

[47] J. C. Misra and S. K. Ghosh, "Flow of a casson fluid in a narrow tube with a side branch", International Journal of Engineering Science **38**, 2045–2077 (2000).

[48] R. Ponalagusamy and R. T. Selvi, "Blood flow in stenosed arteries with radially variable viscosity", peripheral plasma layer thickness and magnetic field, Meccanica **48**, 2427–2438 (2013).

[49] A. Tiwari and S. S. Chauhan, "Effect of varying viscosity on a two-layer model of the blood flow through porous blood vessels", The European Physical Journal Plus **134**, 41 (2019).

[50] A. Tiwari and S. S. Chauhan, "Effect of varying viscosity on two-fluid model of pulsatile blood flow through porous blood vessels: a comparative study", Microvascular Research **123**, 99–110 (2019).

[51] A. Tiwari and S. S. Chauhan, "Effect of varying viscosity on two-layer model of pulsatile flow through blood vessels with porous region near walls", Transport in Porous Media **129**, 721–741 (2019).

[52] A. Ogulu and A. R. Bestman, "Deep heat muscle treatment- a mathematical model - i", Acta Physica Hungarica **73**, 3 (1993).

[53] A. Ogulu and T. M. Abbey, "Simulation of heat transfer on an oscillatory blood flow in an indented porous artery", International Communications in Heat and Mass Transfer **32**, 983–989 (2005).

[54] J. Prakash and A A. Ogulu, "Study of pulsatile blood flow modeled as a power law fluid in a constricted tube", International Communications in Heat and Mass Transfer **34**, 762–768 (2007).

[55] A. J. Chamkha, "Non-darcy fully developed mixed convection in a porous medium channel with heat generation/absorption and hydromagnetic effects", Numerical Heat Transfer: Part A: Applications **32**, 653–675 (1997).

[56] A. J. Chamkha, T. Grosan, and I. Pop, "Fully developed free convection of a micropolar fluid in a vertical channel", International Communications in Heat and Mass Transfer **29**, 1119–1127 (2002).

[57] A. J. Chamkha, T. Grosan, and I. Pop, "Fully developed mixed convection of a micropolar fluid in a vertical channel", International Journal of Fluid Mechanics Research **30**, 251–263 (2003).

[58] K. Hooman and A H. Gurgenci, "Theoretical analysis of forced convection in a porous-saturated circular tube: brinkman-forchheimer model", Transport in Porous Media **69**, 289–300 (2007).

[59] F. Selimefendigil, M. A. Ismael, and A. J. Chamkha, "Mixed convection in superposed nanofluid and porous layers in square enclosure with inner rotating cylinder", International Journal of Mechanical Sciences **124–125**, 95–108 (2017).

[60] C. Desjardins and B. R. Duling, "Microvessel hematocrit: measurement and implications for capillary oxygen transport", American Physiological Society **252**, H494–H503 (1987).

[61] C. Desjardins and B. R. Duling, "Heparinase treatment suggests a role for the endothelial cell glycocalyx in regulation of capillary hematocrit", American Physiological Society **258**, H647–H654 (1990).

[62] A. A. Hill and B. Straughan, "Poiseuille flow in a fluid overlying a porous medium", Journal of Fluid Mechanics **603**, 137–149 (2008).

[63] N. C. Sacheti, P. Chandran, B. S. Bhatt, and R. P. Chhabra, "Steady creeping motion of a liquid bubble in an immiscible viscous fluid bounded by a vertical porous cylinder of finite thickness", Advanced Studies in Theoretical Physics **2**, 243–260 (2008).

[64] S. Deo, A. N. Filippov, A. Tiwari, S. Vasin, and V. Starov, "Hydrodynamic permeability of aggregates of porous particles with an impermeable core", Advances in Colloid and Interface Science **164**, 21–37 (2011).

[65] A. Tiwari and S. Deo, "Pulsatile flow in a cylindrical tube with porous walls: applications to blood flow", Journal of Porous Media **16**, 335–340 (2013).

[66] C. Boodoo, B. Bhatt, and D. Comissiong, "Two-phase fluid flow in a porous tube: a model for blood flow in capillaries", Rheology Acta **52**, 579–588 (2013).

[67] B. D. Sharma and P. K. Yadav, "Two-layer mathematical model of blood flow in porous constricted blood vessels", Transport in Porous Media **120**, 239–254 (2017).

[68] S. Jaiswal and P. K. Yadav, "A micropolar-newtonian blood flow model through a porous layered artery in the presence of a magnetic field", Physics of Fluids **31**, 071901 (2019).

[69] M. Dejam, H. Hassanzadeh, and Z. Chen, "Shear dispersion in combined pressure-driven and electro-osmotic flows in a channel with porous walls", Chemical Engineering Science **137**, 205–215 (2015).

[70] M. Dejam, H. Hassanzadeh, and Z. Chen, "Shear dispersion in combined pressure-driven and electro-osmotic flows in a capillary tube with a porous wall", AIChE Journal **61**, 3981–3995 (2015).

[71] M. Dejam, H. Hassanzadeh, and Z. Chen, "Shear dispersion in a capillary tube with a porous wall", Journal of Contaminant Hydrology **185**, 87–104 (2016).

[72] M. Dejam, H. Hassanzadeh, and A Z. Chen, "Reduced-order model for chemical species transport in a tube with a constant wall concentration", The Canadian Journal of Chemical Engineering **96**, 307–316 (2018).

[73] Z. Kou and M. Dejam, "Dispersion due to combined pressure-driven and electro-osmotic flows in a channel surrounded by a permeable porous medium", Physics of Fluids **31**, 056603 (2019).

[74] G. Q. Chen, Z. Wu, and L. Zeng, "Environmental dispersion in a two-layer wetland: analytical solution by method of concentration moments", International Journal of Engineering Science **51**, 272–291 (2012).

[75] M. Shamsi, A. Sedaghatkish, M. Dejam, M. Saghafian, M. Mohammadi, and A. Sanati-Nezhad, "Magnetically assisted intraperitoneal drug delivery for cancer chemotherapy", Drug delivery **25**, 846–861 (2018).

[76] M. Dejam, "Hydrodynamic dispersion due to a variety of flow velocity profiles in a porous-walled microfluidic channel", International Journal of Heat and Mass Transfer **136**, 87–98 (2019).

[77] H. K Chang and L. F. Mockros, "Blood-gas transfers in an axial flow annular exchanger", American Institute of Chemical Engineers Journal **17**, 397–401 (1971).

[78] G. Taylor, "Dispersion of soluble matter in solvent flowing slowly through a tube, proceedings of the royal society of london", Series A, Mathematical and Physical Sciences **219**, 186–203 (1953).

[79] R. Aris, "On the dispersion of a solute in a fluid flowing through a tube, proceedings of the royal society of london", Series A, Mathematical and Physical Sciences **235**, 67–77 (1956).

[80] W. N. Gill and R. Sankarasubramanian, "Exact analysis of unsteady convective diffusion, proceedings of the royal society of london", Series A, Mathematical and Physical Sciences **316**, 341–350 (1970).

[81] H. C. Brinkman, "A calculation of the viscous force exerted by a flowing fluid on a dense swarm of particles", Flow, Turbulence and Combustion **1**, 27 (1949).

[82] D. S. Sankar and A. K. Hemalatha, "Pulsatile flow of Herschel–Bulkley fluid through stenosed arteries— A mathematical model", International Journal of Non-Linear Mechanics **41**, 979–990 (2006).

[83] B. D. Sharma and P. K. Yadav, "A two-layer mathematical model of blood flow in porous constricted blood vessels", Transport in Porous Media **120**, 239–254 (2017).

[84] A. W. Bush, *Perturbation methods for engineers and scientists* (CRC Press, Boca Raton, 1992).

[85] A. H. Nayfeh, "Problems in perturbation", in 2^{nd} *ed*, edited by N. Y. Wiley (1993).

[86] W. E. Boyce and R. C. DiPrima, *Elementary differential equations and boundary value problems*, 7^{th} (Wiley, John & Sons, 2017).

[87] P. Nagarani, G. Sarojamma, and G. Jayaraman, "Effect of boundary absorption in dispersion in casson fluid flow in a tube", Annals of Biomedical Engineering **32**, 706–719 (2004).

[88] B. Ramana and G. Sarojamma, "Unsteady convective diffusion in a herschel-bulkley fluid in a conduit with interphase mass transfer", International Journal of Mathematical Modelling & Computations 0 **2**, 159–179 (2012).

[89] J. Rana and P. V. S. N. Murthy, "Unsteady solute dispersion in non-newtonian fluid flow in a tube with wall absorption, proceedings of the royal society of london", Series A, Mathematical and Physical Sciences **472**, 294 (2016).

[90] D. F. Young, "Fluid mechanics of arterial stenosis", Journal of Biomechanical Engineering **101**, 157–175 (1979).

[91] D. S. Sankar and A K. Hemalatha, "Non-newtonian fluid flow model for blood flow through a catheterized artery- steady flow", Applied Mathematical Modelling **31**, 1847–1864 (2007).

[92] D. S. Sankar and K. Hemalatha, "Pulsatile flow of herschel-bulkley fluid through stenosed arteries - a mathematical model", International Journal of Non-Linear Mechanics **41**, 979–990 (2006).

[93] S. U. Siddiqui, N. K. Verma, S. Mishra, and R. S. Gupta, "Mathematical modelling of pulsatile flow of casson's fluid in arterial stenosis", Applied Mathematics and Computation **210**, 1–10 (2009).

[94] H. Darcy, *Les fontaines publiques de la ville de dijon* (Dalmont, Paris, 1856).

[95] H. C. Brinkman, "A calculation of the viscous force exerted by a flowing fluid on a dense swarm of particles", Applied Scientific Research A **1**, 27–34 (1947).

[96] H. C. Brinkman, "On the permeability of media consisting of closely packed porous particles", Applied Scientific Research A **1**, 81–86 (1947).

[97] J. A. Ochoa-Tapia and S. Whitaker, "Momentum transfer at the boundary between a porous medium and a homogeneous fluid- ii", Comparison with experiment, International Journal of Heat and Mass Transfer **38**, 2647–2655 (1995).

[98] R. K. Dash, K. N. Mehta, and G. Jayaraman, "Casson fluid flow in a pipe filled with a homogeneous porous medium", International Journal of Engineering Science **34**, 1145–1156 (1996).

[99] A. J. Chamkha, "On laminar hydromagnetic mixed convection flow in a vertical channel with symmetric and asymmetric wall heating conditions", International Journal of Heat and Mass Transfer **45**, 2509–2525 (2002).

[100] A. J. Chamkha, "Unsteady laminar hydromagnetic flow and heat transfer in porous channels with temperature-dependent properties", International Journal of Numerical Methods for Heat and Fluid Flow **11**, 430–448 (2001).

[101] A. J. Chamkha, "Double-diffusive convection in a porous enclosure with cooperating temperature and concentration gradients and heat generation or absorption effects", Numerical Heat Transfer: Part A: Applications **41**, 65–87 (2002).

[102] J. C. Umavathi, A. J. Chamkha, A. Mateen, and A. Al-Mudhaf, "Unsteady two-fluid flow and heat transfer in a horizontal channel", Heat Mass Transfer **42**, 81–90 (2005).

[103] R. Ponalagusamy and R. T. Selvi, "Influence of magnetic field and heat transfer on two-phase fluid model for oscillatory blood flow in an arterial stenosis", Meccanica **50**, 927–943 (2015).

[104] J. P. Kumar, J. C. Umavathi, A. J. Chamkha, and I. Pop, "Fully-developed free-convective flow of micropolar and viscous fluids in a vertical channel", Applied Mathematical Modelling **34**, 1175–1186 (2010).

[105] A. J. Chamkha, "Flow of two-immiscible fluids in porous and nonporous channels", Journal of Fluids Engineering **122**, 117–124 (1999).

[106] J. C. Umavathi, A. J. Chamkha, A. Mateen, and A. Al-Mudhaf, "Unsteady oscillatory flow and heat transfer in a horizontal composite porous medium channel", Nonlinear Analysis: Modelling and Control **14**, 397–415 (2009).

[107] J. C. Umavathi, A. J. Chamkha, and K. S. R. Sridhar, "Generalized plain cauette flow and heat transfer in a composite channel", Transport in Porous Media **85**, 157–169 (2010).

[108] A. J. Chamkha, "Unsteady flow of a dusty conducting fluid through a pipe", Mechanics Research Communications **21**, 281–288 (1994).

[109] A. J. Chmakha and M. A. Al-Subaie, "Hydromagnetic buoyancy-induced flow of a particulate suspension through a vertical pipe with heat generation or absorption effects", Turkish Journal of Engineering and Environmental Science **33**, 127–134 (2009).

[110] J. B. Shukla, R. S. Parihar, and S. P. Gupta, "Effects of peripheral layer viscosity on blood flow through the artery with mild stenosis", Bulletin of Mathematical Biology **42**, 797–805 (1980).

[111] J. Rana and P. V. S. N. Murthy, "Solute dispersion in pulsatile casson fluid flow in a tube with wall absorption", Journal of Fluid Mechanics **793**, 877–914 (2016).

[112] J. Rana and P. V. S. N. Murthy, "Unsteady solute dispersion in herschel-bulkley fluid in a tube with wall absorption", Physics of Fluids **28** (2016).

[113] A. K. Roy, A. K. Saha, and S. Debnath, "Effect of multiple reactions on the transport coefficients in pulsatile flow through an annulus", International Communications in Heat and Mass Transfer **110** (2020).

[114] A. Ogulu and T. M. Abbey, "Simulation of heat transfer on an oscillatory blood flow in an indented porous artery", International Communications in Heat and Mass Transfer **32**, 983–989 (2005).

[115] J. C. Misra, A. Sinha, and G. C. Shit, "Flow of a biomagnetic viscoelastic fluid: application to estimation of blood flow in arteries during electromagnetic hyperthermia", a therapeutic procedure for cancer treatment, Applied Mathematics and Mechanics **31**, 1405–1420 (2010).

[116] M. Modather, A. M. Rashad, and A. J. Chamkha, "An analytical study of mhd heat and mass transfer oscillatory flow of a micropolar fluid over a vertical permeable plate in a porous medium", Turkish Journal of Engineering and Environmental Sciences **33**, 245–257 (2009).

[117] E. Magyari and A. J. Chamkha, "Combined effect of heat generation or absorption and first-order chemical reaction on micropolar fluid flows over a uniformly stretched permeable surface: the full analytical solution", International Journal of Thermal Sciences **49**, 1821–1828 (2010).

[118] A. J. Chamkha and A. M. Rashad, "Unsteady heat and mass transfer by mhd mixed convection flow from a rotating vertical cone with chemical reaction and soret and dufour effects", The Canadian Journal of Chemical Engineering **9999**, 1–10 (2013).

[119] M. Ghalambaz, A. J. Chamkha, and D. Wen, "Natural convective flow and heat transfer of nano-encapsulated phase change materials (nepcms) in a cavity", International Journal of Heat and Mass Transfer **138**, 738–749 (2019).

[120] N. S. Shashikumar, B. J. Gireesha, B. Mahanthesh, B. C. Prasannakumara, and A. J. Chamkha, "Entropy generation analysis of magneto-nanoliquids embedded with aluminium and titanium alloy nanoparticles in microchannel with partial slips and convective conditions", International Journal of Numerical Methods for Heat and Fluid Flow **29**, 3638–3658 (2019).

[121] K. A. Ayoubloo, M. Ghalambaz, T. Armaghani, A. Noghrehabadi, and A. J. Chamkha, "Pseudoplastic natural convection flow and heat transfer in a cylindrical vertical cavity partially filled with a porous layer", International Journal of Numerical Methods for Heat and Fluid Flow **30**, 1096–1114 (2020).

[122] A. Tiwari, P. D. Shah, and S. S. Chauhan, "Analytical study of micropolar fluid flow through porous layered microvessels with heat transfer approach", The European Physical Journal Plus **135**, 209 (2020).

[123] S. Whitaker, *The method of volume averaging*, Vol. 13 (Springer Science & Business Media, 1998).

[124] A. Srivastava and N. Srivastava, "Flow past a porous sphere at small reynolds number", Zeitschrift für angewandte Mathematik und Physik ZAMP **56**, 821–835 (2005).

[125] J. R. Keltner, M. S. Roos, P. R. Brakeman, and T. F. Budinger, "Magnetohydrodynamics of blood flow", Magnetic resonance in medicine **16**, 139–149 (1990).

[126] P. A. Davidson and S. A. Berger, "An introduction to magneto-hydrodynamics", Physics Today **55**, 56–57 (2002).

[127] I. Abdullah, N. Amin, and T. Hayat, "Magnetohydrodynamic effects on blood flow through an irregular stenosis", International Journal for Numerical Methods in Fluids **67**, 1624–1636 (2011).

[128] P. K. Yadav and S. Jaiswal, "Influence of an inclined magnetic field on the poiseuille flow of immiscible micropolar–newtonian fluids in a porous medium", Canadian Journal of Physics **96**, 1016–1028 (2018).

[129] P. Kumar Yadav, S. Jaiswal, T. Asim, and R. Mishra, "Influence of a magnetic field on the flow of a micropolar fluid sandwiched between two newtonian fluid layers through a porous medium", The European Physical Journal Plus **133**, 1–13 (2018).

[130] J. B. Shukla, R. S. Parihar, and B. R. P. Rao, "Effects of stenosis on non-newtonian flow of the blood in an artery", Bulletin of Mathematical Biology **42**, 283–294 (1980).

[131] K. Hooman and A H. Gurgenci, "Theoretical analysis of forced convection in a porous-saturated circular tube: brinkman-forchheimer model", Transport in Porous Media **69**, 289–300 (2007).

[132] K. Hooman, "A perturbation solution for forced convection in a porous-saturated duct", Journal of Computational and Applied Mathematics **211**, 57–66 (2008).

[133] A. J. Chamkha, A. S. Dogonchi, and D. D. Ganji, "Magneto-hydrodynamic flow and heat transfer of a hybrid nanofluid in a rotating system among two surfaces in the presence of thermal radiation and joule heating", AIP Advances **9**, 025103 (2019).

[134] J. Raza, F. Mebarek-Oudina, and A. J. Chamkha, "Magnetohydrodynamic flow of molybdenum disulfide nanofluid in a channel with shape effects", Multi discipline Modeling in Materials and Structures **15**, 737–757 (2019).

[135] D. Toghraie, R. Mashayekhi, H. Arasteh, S. Sheykhi, M. Niknejadi, and A. J. Chamkha, "Two-phase investigation of water-al2o3 nanofluid in a micro concentric annulus under non-uniform heat flux boundary conditions", International Journal of Numerical Methods for Heat and Fluid Flow **30**, 1795–1814 (2020).

[136] Y. A. Elmaboud, K. S. Mekheimer, and T. G. Emam, "Numerical examination of gold nanoparticles as a drug carrier on peristaltic blood flow through physiological vessels: cancer therapy treatment", BioNanoScience **9**, 952–965 (2019).

[137] B. D. Sharma, P. K. Yadav, and A. N. Filippov, "Jeffrey-fluid model of blood flow in tubes with stenosis", Colloid Journal **79**, 849–856 (2017).

[138] B. D. Sharma and P. K. Yadav, "A mathematical model of blood flow in narrow blood vessels in presence of magnetic field", National Academy Science Letters **42**, 239–243 (2019).

[139] P. K. Yadav, B. D. Sharma, and A. N. Filippov, "Oscillatory viscoelastic model of blood flow in stenotic artery", Colloid Journal **82**, 617–625 (2020).

[140] P. D. Shah, A. Tiwari, and S. S. Chauhan, "Solute dispersion in micropolar-newtonian fluid flowing through porous layered tubes with absorbing walls", International Communications in Heat and Mass Transfer **119**, 104724 (2020).

[141] A. Tiwari, P. D. Shah, and S. S. Chauhan, "Unsteady solute dispersion in two-fluid flowing through narrow tubes: a temperature-dependent viscosity approach", International Journal of Thermal Sciences **161**, 106651 (2021).

[142] A. K. Saini, S. S. Chauhan, and A. Tiwari, "Creeping flow of jeffrey fluid through a swarm of porous cylindrical particles: brinkman-forchheimer model", International Journal of Multiphase Flow **145**, 103803 (2021).

[143] A. H. Mahmoudi and K. Hooman, "Effect of a discrete heat source location on entropy generation in mixed convective cooling of a nanofluid inside the ventilated cavity", International Journal of Exergy **13**, 299–319 (2013).

[144] F. Garoosi, S. Garoosi, and K. Hooman, "Numerical simulation of natural convection and mixed convection of the nanofluid in a square cavity using buongiorno model", Powder Technology **268**, 279–292 (2014).

[145] M. Sharan, B. Singh, and A P. Kumar, "Two-layer model for studying the effect of plasma layer on the delivery of oxygen to tissue using a finite element method", Applied Mathematical Modelling **21**, 419–426 (1997).

[146] H. Fujiwara, T. Ishikawa, R. Lima, N. Matsuki, Y. Imai, H. Kaji, M. Nishizawa, and T. Yamaguchi, "Red blood cell motions in high-hematocrit blood flowing through a stenosed microchannel", Journal of Biomechanics **42**, 838–843 (2009).

[147] M. K. D. Manshadi, M. Saadat, M. Mohammadi, M. Shamsi, M. Dejam, R. Kamali, and A. Sanati-Nezhad, "Delivery of magnetic micro/nanoparticles and magnetic-based drug/cargo into arterial flow for targeted therapy", Drug delivery **25**, 1963–1973 (2018).

[148] M. Shamsi, M. Saghafian, M. Dejam, and A. Sanati-Nezhad, "Mathematical modeling of the function of warburg effect in tumor microenvironment", Scientific Reports **8**, 8903 (2018).

[149] A. Sarkar and G. Jayaraman, "The effect of wall absorption on dispersion in annular flows", Acta Mechanica **158**, 105–119 (2002).

[150] A. Sarkar and G. Jayaraman, "The effect of wall absorption on dispersion in oscillatory flow in an annulus: application to a catheterized artery", Acta Mechanica **172**, 151–167 (2004).

[151] P. Nagarani, G. Sarojamma, and G. Jayaraman, "Exact analysis of unsteady convective diffusion in casson fluid flow in an annulus- application to catheterized artery", Acta Mechanica **187**, 189–202 (2006).

[152] P. Nagarani, G. Sarojamma, and G. Jayaraman, "Effect of boundary absorption on dispersion in casson fluid flow in an annulus: application to catheterized artery", Acta Mechanica **202**, 47–63 (2009).

[153] M. Dejam, "Dispersion in non-newtonian fluid flows in a conduit with porous walls", Chemical Engineering Science **189**, 296–310 (2018).

[154] M. Dejam, "Derivation of dispersion coefficient in an electro-osmotic flow of a viscoelastic fluid through a porous-walled microchannel", Chemical Engineering Science **204**, 298–309 (2019).

[155] Y. A. Elmaboud and K. Mekheimer, "Unsteady pulsatile flow through a vertical constricted annulus with heat transfer", **67**, 185–194 (2012).

[156] A. Tiwari, P. D. Shah, and S. S. Chauhan, "Solute dispersion in two-fluid flowing through tubes with a porous layer near the absorbing wall: model for dispersion phenomenon in microvessels", International Journal of Multiphase Flow **131**, 10338 (2020).

[157] J. C. Chato, "Heat transfer to blood vessels", Journal of Biomechanical Engineering **102**, 110–118 (1980).

[158] A. Tiwari and S. Deo, "Pulsatile flow in a cylindrical tube with porous walls: applications to blood flow", Journal of Porous Media **16**, 335–340 (2013).

[159] S. Shaw, P. V. S. N. Murthy, and P. Sibanda, "Magnetic drug targeting in a permeable microvessel", Microvascular Research **85**, 77–85 (2013).

[160] G. S. Beavers and D. D. Joseph, "Boundary conditions at a naturally permeable wall", Journal of Fluid Mechanics **30**, 197–207 (1967).

[161] A. Bhattacharyya and G. P. Raja Sekhar, "Stokes flow inside a porous spherical shell: stress jump boundary condition", Zeitschrift für angewandte Mathematik und Physik ZAMP **56**, 475–496 (2005).

List of Publications

The following works included in this thesis in chapter form have been published/ communicated in the following journals:

1. A. Tiwari, **P.D. Shah** and S.S. Chauhan, Analytical study of Micropolar fluid flow through porous layered microvessels with heat transfer approach, *European Physical Journal Plus* 135 (2020) 209. (SCI, IF- 3.758)
(https://doi.org/10.1140/epjp/s13360-020-00128-x)

2. A. Tiwari, **P.D. Shah** and S.S. Chauhan, Solute dispersion in two-fluid flowing through tubes with a porous layer near the absorbing wall: Model for dispersion phenomenon in microvessels, *International Journal of Multiphase Flow* 131 (2020) 103380. (SCI, IF- 4.044)
(https://doi.org/10.1016/j.ijmultiphaseflow.2020.103380)

3. **P.D. Shah**, A. Tiwari and S.S. Chauhan, Solute dispersion in Micropolar-Newtonian fluid flowing through porous layered tubes with absorbing walls, *International Communications in Heat and Mass Transfer* 119 (2020) 104724. (SCI, IF- 6.782)
(https://doi.org/10.1016/j.icheatmasstransfer.2020.104724)

4. A. Tiwari, **P.D. Shah** and S.S. Chauhan, Unsteady solute dispersion in two-fluid flowing through narrow tubes: A temperature-dependent viscosity approach, *International Journal of Thermal Sciences* 161 (2021) 106651. (SCI, IF- 4.779)
(https://doi.org/10.1016/j.ijthermalsci.2020.106651)

5. S.S. Chauhan, **P.D. Shah**, and A. Tiwari, Analytical Study of the Effect of Variable Viscosity and Heat Transfer on Two Fluid Flowing through Porous Layered Tubes, *Transport in Porous Media* 142 (2022) 641. (SCI, IF- 3.610)
(https://doi.org/10.1007/s11242-022-01765-9)

Conferences / Workshops

1. Seven day workshop on **Theory and Simulation of Hyperbolic PDEs arising in Mathematical Biology and Fluid Flow** organized by Department of Mathematics, Bits Pilani, Pilani Campus, India during 05-11 January 2019.

2. Two day workshop on **Research Methodology** jointly organized by the Departments of Huminities and Social Sciences, Economics & Finance, and Management, Bits Pilani, Pilani Campus, India during 23-24 February 2019.

3. **Academic Writing** jointly organised by Department of Mathematics, BITS Pilani, Pilani Campus, India in collabration with Society for Industrial and Applied Mathematics (SIAM) on 04 November 2019.

4. Article entitled "Solute Dispersion in Viscoelastic Fluid Flow through Tubes with a Porous Layer Near Absorbing Wall" presented at International Conference and 22^{nd} Annual Convention of Vijnana Parishad of India on **Advances in Operations Research, Statistics and Mathematics (AOSM 2019)** organised by Department of Mathematics, BITS Pilani, Pilani Campus, India during 28-30 December 2019.

5. Five day virtual FDP on **Data Analytics Tools for Real-World Problems**, organized by Division of Mathematics, School of Advanced Sciences, Vellore Institute of Technology, Chennai, India during 01-05 May 2023.

6. Article entitled "Mathematical Assessment of Electrokinetic Blood Microcirculation through Curved Microvessels" at **International Conference on Differential Equations and Controll Problems (ICDECP23)**, IIT Mandi, India during 15-17 June 2023.

7. Article entitled "Analysis of Pressure-Driven Electrokinetic Blood Microcirculation through Microvessels" presented at 2^{nd} International Conference on **Mathematical Modelling and Simulation in Physical Sciences (MMSPS)**, Sardar Vallabhbhai National Institute of Technology (SVNIT), Gujarat, India during 23-24 June 2023.

Brief Biography of the Candidate

Mr. Pallav Shah earned his Bachelor's degree in Mathematics from Gujarat University. He then pursued his Master's degree in Mathematics at Sardar Patel University and did a project entitled "Futures Markets and Futures Options," supported by UGC-BRS during his M.Sc. He also holds M.Phil. in Mathematics from Saurashtra University. He was declared successful in Joint CSIR-UGC Test for Junior Research Fellowship and Eligibility for Lectureship (NET) under the Eligibility for Lectureship category and qualified for GATE in the subject Mathematical Sciences. After completing his graduate studies, he served in various teaching positions and gained teaching experience for more than five years. He then decided to pursue his doctoral degree at BITS Pilani, where he is currently an Institute Fellow and conducting research on the Mathematical analysis of blood in microcirculation under the guidance of Dr. Ashish Tiwari.

Brief Biography of the Supervisor

Dr. Ashish Tiwari is an Associate Professor in the Department of Mathematics, Birla Institute of Technology and Science Pilani, Pilani Campus, Rajasthan. He has completed his Master of Science (M. Sc. in Mathematics) in 2003 and received his Doctor of Philosophy (D. Phil) in 2010 from the University of Allahabad, Prayagraj, Uttar Pradesh. After that, he joined as an Assistant Professor in the Department of Mathematics at Birla Institute of Technology and Science Pilani, Pilani Campus, Rajasthan in December 2011. His research interests are in the area of flow through porous media, creeping flow, heat transfer, dispersion process, and physiological fluid flow. He has published 25 research articles in reputed international journals. Mr. Satyendra Singh Chauhan has completed and four students are currently persuing Ph.D. under the guidance of Dr. Ashish Tiwari. He was also the principal investigator of 2 major projects entitled “Modeling of cardiovascular flows and influence of magnetic field on circulation" (SR/FTP/MS-038/2011) and another one is an Indo-Russian project entitled “Flow through a membrane modeled of porous cylindrical particles using particle-in-cell approach" under DST-RFBR in collaboration with Prof. A.N. Filippov, Gubkin Russian State University, Moscow, Russia (INT/RUS/RFBR/P-212).

॥ अंतः अस्ति प्रारंभः ॥

अंत से ही एक नई शुरुआत होती है।

"The end is the beginning."